DOKUZ EYLÜL UNIVERSITY
GRADUATE SCHOOL OF NATURAL AND APPLIED
SCIENCES

MICROSTRUCTURAL CHARACTERIZATION AND MECHANICAL PROPERTY DETERMINATION OF OVERLAP FRICTION STIR WELDING OF ALUMINUM AND COPPER

by
Aysun Tunç ÖNOL

March, 2010
İZMİR

MICROSTRUCTURAL CHARACTERIZATION AND MECHANICAL PROPERTY DETERMINATION OF OVERLAP FRICTION STIR WELDING OF ALUMINUM AND COPPER

A Thesis Submitted to the
Graduate School of Natural and Applied Sciences of Dokuz Eylül University
In Partial Fulfillment of the Requirements for the Degree of Master of Science
in
Mechanical Engineering, Mechanics Program

by
Aysun Tunç ÖNOL

March, 2010
İZMİR

M.Sc THESIS EXAMINATION RESULT FORM

We have read the thesis entitled **"MICROSTRUCTURAL CHARACTERIZATION AND MECHANICAL PROPERTY DETERMINATION OF OVERLAP FRICTION STIR WELDING OF ALUMINUM AND COPPER"** completed by **AYSUN TUNÇ ÖNOL** under supervision of **ASSISTANT PROFESSOR EMİNE ÇINAR YENİ** and we certify that in our opinion it is fully adequate, in scope and in quality, as a thesis for the degree of Master of Science.

Supervisor

(Jury Member)   (Jury Member)

Prof.Dr. Cahit HELVACI

Director

Graduate School of Natural and Applied Sciences

ACKNOWLEDGMENTS

MICROSTRUCTURAL CHARACTERIZATION AND MECHANICAL PROPERTY DETERMINATION OF OVERLAP FRICTION STIR WELDING OF ALUMINUM AND COPPER

ABSTRACT

The purpose of this study, aluminum alloy 1050 and pure copper plates have been welded as dissimilar alloy overlap joints by using Friction Stir Welding (FSW) with three different welding speeds and keeping other parameters constant in order to investigate mechanical and microstructural properties and determine the optimum welding speed. The aim is to examine the effect of the welding speeds on microstructural and mechanical properties, and mechanical tests were carried out on the welded areas of the parts. Tensile shear tests of the joints utilized to obtain for determining stress distribution. The best mechanical properties joint has been obtained at the higher welding speed.

ALÜMİNYUM VE BAKIRIN BİNDİRME SÜRTÜNME KARIŞTIRMA KAYNAĞINDA MİKROYAPI KARAKTERİZASYONU VE MEKANİK ÖZELLİKLERİN BELİRLENMESİ

ÖZ

Bu çalışmanın amacı, 1050 alüminyum alaşımı ve saf bakır levhaların farklı alaşımların bindirme kaynağı olarak Sürtünme Karıştırma Kaynak (SKK) yöntemiyle üç değişik kaynak hızı kullanılarak ve diğer parametreler sabit kalarak kaynaklanması ve buna bağlı olarak mekanik ve mikroyapı özelliklerinin araştırılması ve en uygun kaynak hızının belirlenmesi olarak hedeflenmiştir. Kaynakla birleştirilmiş bölgelerde kaynak hızının mikroyapı ve mekanik özelliklerde meydana getirdiği değişikliklerin etkisi mekanik testler yardımıyla değerlendirilmiştir. Gerilme dağılımı, kaynağın çekme testleri kullanılarak elde edilmiştir. En iyi mekanik özelliklere sahip kaynak yüksek kaynak hızında elde edilmiştir.

Anahtar sözcükler: Sürtünme Karıştırma Kaynağı, Bindirme kaynağı, 1050 Alüminyum alaşımı, Saf bakır, Kaynak hızı, Farklı alaşım malzemeleri

CONTENTS

CHAPTER ONE
INTRODUCTION

1.1 Friction Stir Welding

The friction stir welding (FSW) technique is a solid state joining process, recently invented by The Welding Institute (TWI) of UK in 1991 (Mishra & Mahoney, 2007, p.1) under research funded partly by the National Aeronautics and Space Administration (NASA) (Payton, 2002). FSW joins two pieces of sheet or thin plate by mechanical means. The process is solid-state in nature and relies on forging of the welding zone to operate by generating frictional heat between rotating tool and the sheets to produce to joint (Lee & Jung, 2003). The basic concept of the process is weld by rotating tool as a result of combination of frictional heating and plastic deformation. Figure 1.1 shows schematically three-dimensional friction stir welding process (Mishra & Ma, 2005).
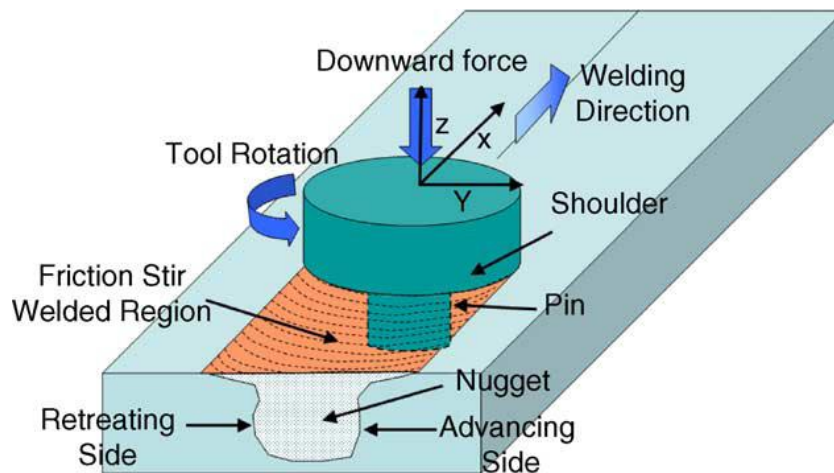
Figure 1.1 Schematic drawing of friction stir welding (Mishra & Ma, 2005).

First, the tool is rotated between 180 to 300 revolutions per minute, depending on the thickness of the material. The pin tip of the tool is forced into the material under 5,000 to 10,000 pounds per square inch (775 to1550 pounds per square centimeter or about 35-70 MPa) of force. The pin continues rotating and moves forward at a rate of 3.5 to 5 inches per minute (8.89 to 12.7 centimeters per minute) (NASA, 2001).
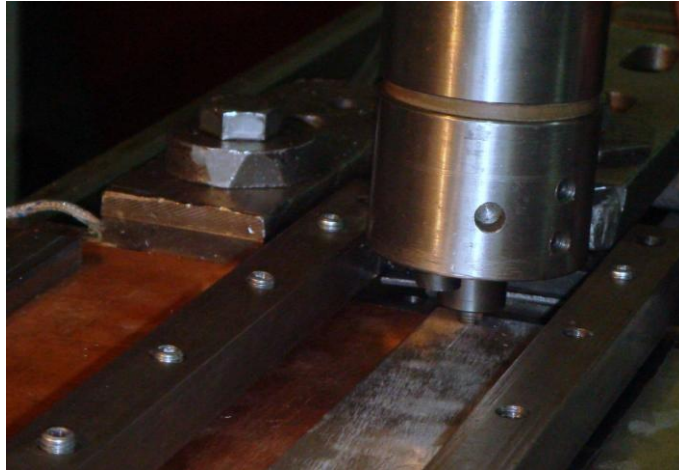
Figure 1.2 The rotating pin is inserted into abutting edges for overlap joint.

A non-consumable friction stir welding tool of hardened steel or carbide consists of a shoulder, normal to the axis of rotation of the tool, and a pin. The shoulder diameter is relatively larger than pin diameter to prevent highly plasticized material from being expelled from the joint. It also controls the depth of the pin and helps to create additional frictional heating above the workpiece surfaces and minimizes the formation of gaps in the welding area. The rotating pin is inserted into the abutting edges of the workpieces up to the intimate contact between the tool shoulder and work surface and moved in the welding direction as shown in Figure 1.2 (Ulysse, 2002). When the tool is moved along the abutting edges, the localized heating softens the material which makes it flow around the pin and a combination of tool rotations and translations lead to movement of material from the front of the pin to back of the pin, where the workpieces compound together to weld (Mishra & Ma, 2005).

The plastic or solid state of the result of this process has created a high-quality mechanical property and a very fine microstructural bond surfaces, additionally, the tool axis is generally tilted 2° or 3° vertically for eccentricity gets the hydromechanically incompressible plasticized material to flow easily around the pin as shown in Figure 1.3 (Campbell, 2006).

The highest temperature reached is about 0.8 of the melting temperature. Only 5% of the heat created by FSW flows into the tool and the rest of it flows thru the workpieces which has a thermomechanically affected zone (TMAZ) and a heat affected zone (HAZ) is shown in Figure 1.4 (Campbell, 2006).
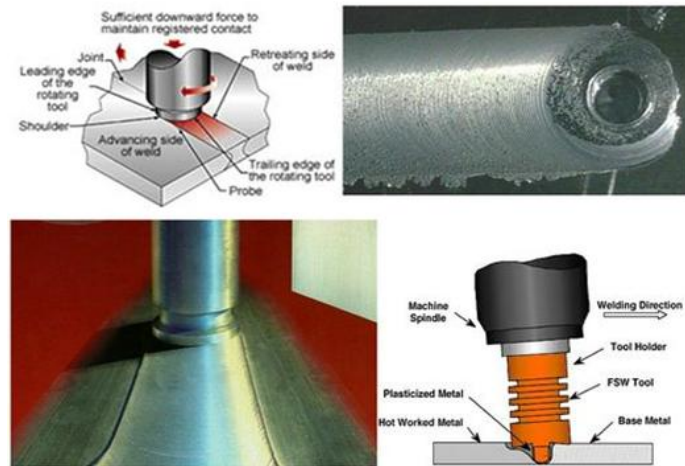
Figure 1.3 A very fine grain microstructural bond of FSW and eccentricity of the tool (loxin2002).

1.1.1 Friction Stir Welding Process Parameters

Friction stir welding consists of composite material movement and plastic deformation. The metallurgical problems related with the friction stir welding process can be cleared by choosing suitable friction stir welding parameters. The friction stir welding process parameters are a joint design, tool geometry, and welding parameters which are rotational speed, traverse speed, travel angle, work angle and plunge rate. These parameters apply important effect on the material flow pattern and temperature distribution, by affecting the microstructural changing of material (Mishra & Ma, 2005 and Padmanaban & Balasubramanian, 2008).

The tensile properties of the joints produced with different welding conditions demonstrated the lowest tensile strength and ductility at the lowest rotational speed for a given traverse speed. When the rotational speed increased, the strength and elongation improved, reaching a maximum before falling again at high rotational

speeds. Besides, while the rotational speeds increase, the heat input also increases. Thus, the tool rotational speed must be optimized to reach maximum tensile properties in FSW joints. When the welding speed increases, the width of the strained zone and the amount of the maximum strain decrease and the location of the maximum strain progressively shifts to the retreating side from the advancing side of the joint. On the other hand, when the welding speed is increased, the ultimate tensile strength reduces significantly (Babu, Elangovan, Balasubramanian, & Balasubramanian, 2008).
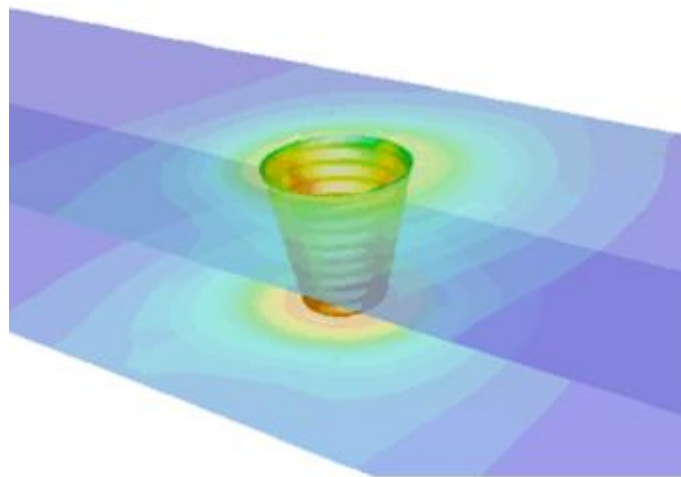
Figure 1.4 Temperature contours around the tool and inside the workpiece (Google Images).
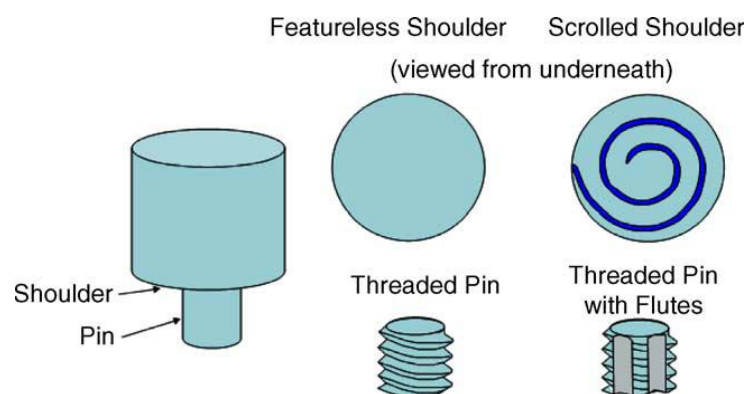
Figure 1.5 Schematic drawing of the FSW tool (Mishra & Ma, 2005)

The top surface of the weld formation presented weak plasticization and consolidation of the material under the pressure of the tool shoulder for low axial

force. Thus, the axial force must be optimized to reach maximum tensile properties. Pin profile is an important role in material flow and controls the welding parameters of the FSW process. The characterization of the weld can be described by nugget and flow contours, almost spherical in shape in friction stir welding area. These contours are dependent on the tool design, the welding parameters and the process conditions used (Baba et al., 2008).
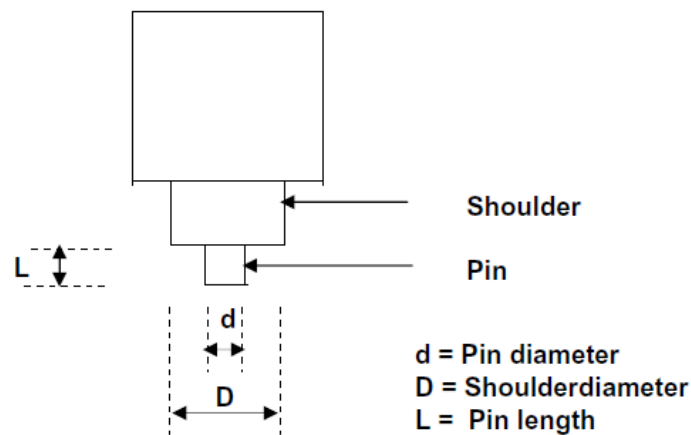
Figure 1.6 Schematic drawing of shoulder diameter, pin diameter and length (Padmanaban & Balasubramanian, 2008)

1.1.1.1   Friction Stir Welding Tool Geometries

The tool geometry is the most important part of the friction stir welding process development. FSW tool has two parts that are shoulder and pin as shown in Figure 1.5. Designing of these parts are critical role for welding quality. The main functions of the tool are localized heating and material flow. When the tool is plunged into the workpiece, the friction between pin and workpiece are created the heating. Another heat resource is deformation of material. The functions of the pin is deforming the material around the tool and generating heat. But, the main heat generation of friction is started between the shoulder and workpiece, when the tool shoulder touches the workpiece. The second function of the tool shoulder prevents material expulsion from welding area and assists material movement around the tool. The plasticized material which is trapped by shoulder that moves along the weld is extruded from the

leading to the trailing side of the tool, to produce a smooth surface finish. Additional functions of the tool is stirring and moving material. A concave shoulder and threaded cylindrical pins is preferred in industrial usage (Colegrove & Shercliff, 2005 and Padmanaban & Balasubramanian, 2008).
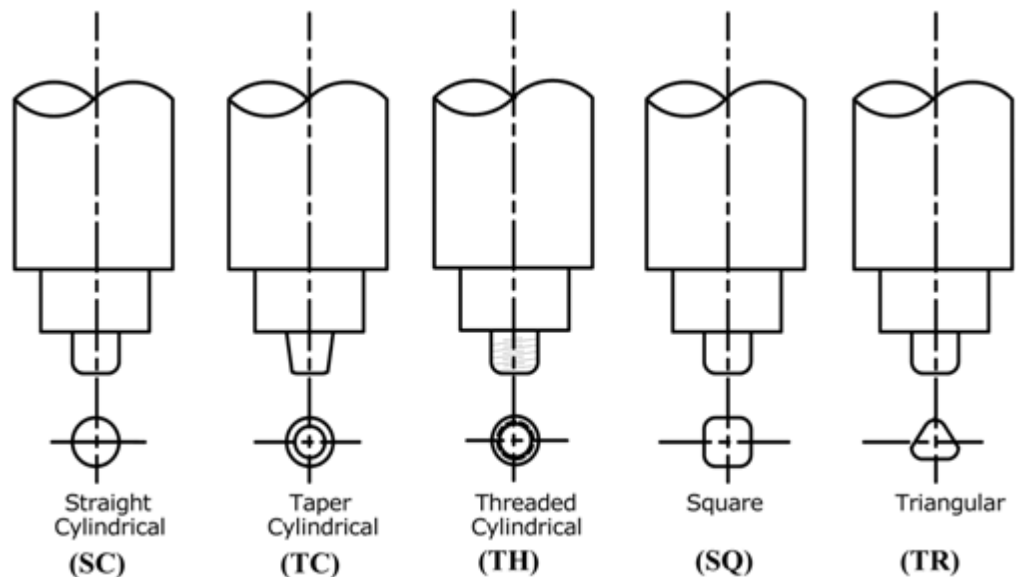
Figure 1.7 Schematic drawings of different types of tool pin profiles; SC-Straight cylindrical, TC-Taper cylindrical, TH-Threaded cylindrical, SQ-Square, TR-Triangular (Babu et al., 2008).
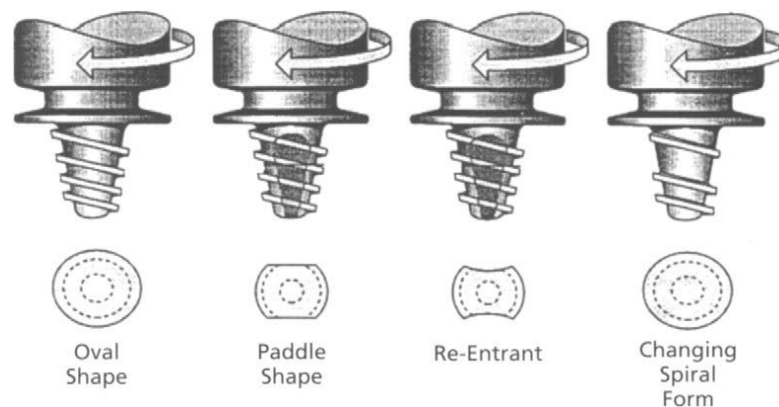
Figure 1.8 Sample FSW tool geometries, source: TWI (Campbell, 2006).

Dissimilar materials and variation of thicknesses of workpieces are necessary different pin profiles. As shown in Figure 1.6, the shoulder diameter, the shoulder profile, the pin length, the pin diameter and the pin profile that are important

parameters deciding the welding speed and quality of the welding, can be compound infinite numbers of tool design. The tool material is another important parameter in the choosing suitable tool for a particular application. About 70-90% of the material that is moved by welding is below the melting point temperature. It is important that the tool material should have enough strength at that temperature if not the tool can twist and break (Padmanaban & Balasubramanian, 2008).

There are different types of tool pin profiles, some examples for that straight cylindrical, taper cylindrical, threaded cylindrical, square, and triangular as shown in Figure 1.7. In addition to this, new tool geometries have been recently developed to improve quality of joining is shown samples in Figure 1.8.
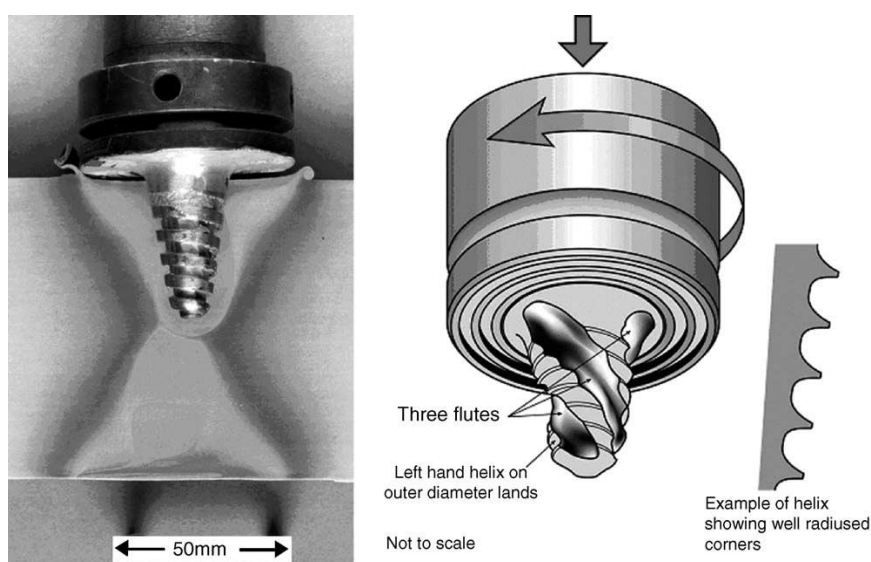
Figure 1.9 Worl[TM] and MX Triflute[TM] tools developed by TWI, UK (Copyright@ 2001, TWI Ltd) (Thomas et al., 2001).

Some complex features tool geometries have been developed to material flow, stirring effect and lower process loads. Whorl[TM] and MX Triflute[TM] tools developed by TWI are shown in Figure1.9. Thomas, Nicholas, & Smith (2001) identified that pins for both tools are shaped as a frustum that relocate less material than a cylindrical tool of the same diameter. The Whorl[TM] reduces the relocated material volume by about 60%, while the MX Triflute[TM] reduces the relocated material volume by about

70%. These tools are assumed that to reduce welding force, enable easier flow of plasticized material, facilitate the downward augering effect, and increase the interface surface between the pin and the plasticized material, therefore increasing heat generation. The major factor determining the superiority of the whorl pins over the conventional cylindrical pin type probe is the ratio of the swept volume during rotation to the volume of the pin itself, This is a ratio of the ''dynamic volume to the static volume'' that is essential in providing a sufficient flow path. Usually, this ratio is 1.1:1 for conventional cylindrical pin, 1.8:1 for the Whorl^{TM} and 2.6:1 for the MX Triflute^{TM} pin (when welding 25 mm thick plate) with similar root diameters and pin length (Thomas et al., 2001).
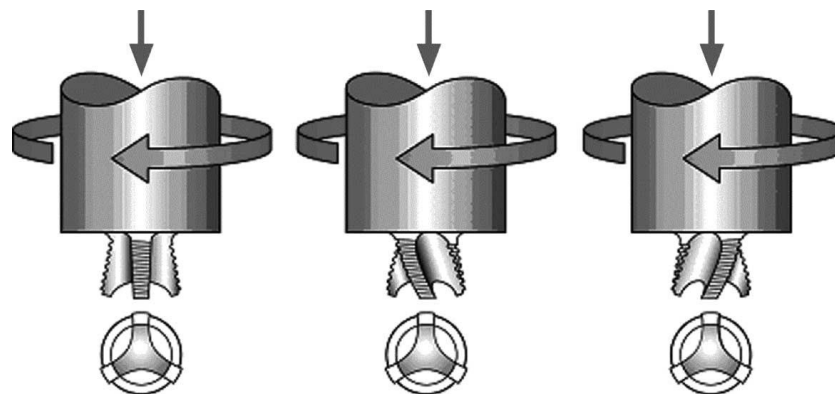
Figure 1.10 Flared-Triflute^{TM} tools developed by TWI, UK: (a) neutral flutes, (b) left flutes, and (c) right hand flutes (Mishra & Ma, 2005)

Mishra & Ma (2005) discussed complex tool geometries. Standard cylindrical threaded pin caused extreme thinning of the top of the workpiece, producing significantly lowered bend properties for lap welding. Besides, the width of the weld interface and the angle at which the notch meets the edge of the weld is also important for applications where fatigue is of main problem, for lap welds. The tool pin geometries were developed for improving quality of lap welding. Flared-Trifute^{TM} with the different types of the flute lands as shown in Figure 1.10. A-skew^{TM} has axis being slightly inclined to the axis of machine spindle as shown in Figure 1.11. The Flared-Trifute and the A-skew tools designed the idea of increasing the ratio between of the swept volume and static volume of the pin, thus improving

the flow path around and underneath the pin, increase the welding region because of flared-out flute lands in the Flared-Trifute pin and the skew action in the A-skew pin, offer an improved mixing action for oxide fragmentation and diffusion at the weld interface. Moreover, an orbital forging action is provided at the root of the weld because of the skew action. As a result the weld quality in this region is improved. When the conventional threaded pin is compared to Flared-Trifute and A-skew pins, the results show in over 100% improvement in welding speed, about 20% reduction in axial force, extensively increased welding region (190–195% of the plate thickness for Flared-Trifute and A-skew pins, 110% for conventional threaded pin), and a reduction in upper plate thinning by a factor of>4. Moreover, these tool geometries are improving the properties of the FSW joints. Flared-Trifute pin reduced drastically the angle of the notch turn over at the overlapping plate/weld interface, although A-skew pin produced a negligible turn down at the outer regions of the overlapping plate/weld interface. Thomas & Dolby (2002) indicated that Flared-Trifute and A-skew pins are useful for lap, T, and similar welds where joining interface is vertical to the machine axis.
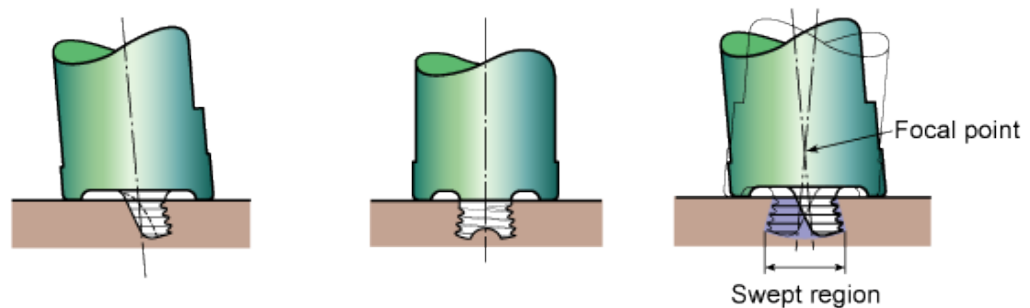
Figure 1.11 A-Skew tool developed by TWI, UK: (a) side view, (b) front view, and (c) swept region encompassed by skew action (Thomas & Dolby).

Additionally, TWI was designed different shoulder profiles to appropriate various materials and conditions as shown in Figure 1.12. These shoulder profiles enhance the coupling between the tool shoulder and the workpieces by capturing plasticized material within special re-entrant features. The tool shape should be simple to reduce production cost of the tool and strong to stir enough welding pieces.

1.1.1.2   Friction Stir Welding Parameters

Rotational speed, traverse speed, travel angle, work angle and plunge rate are friction stir welding parameters of the process which is related technical necessity of the machine.
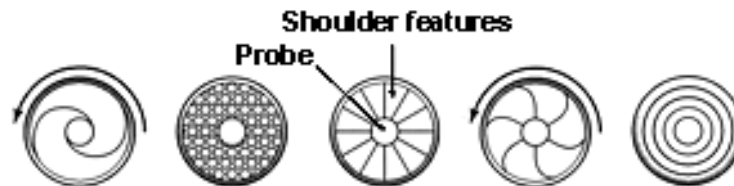
Figure 1.12 Tool shoulder geometries, viewed from underneath the shoulder (Copyright © 2001, TWI Ltd) (Thomas et al., 2001).

1.1.1.2.1   Friction Stir Welding Rotational Speed. The main function of the tool rotational speed is stirring and mixing the material around the rotating pin. Increasing rotational speed generate higher temperature due to increasing frictional heat and high quality stirring and mixing of material. The main heating is come from friction between shoulder and workpiece. Additionally, increasing in rotational speed commonly decreasing the required welding force. But, reducing in welding force is not precisely related to increasing in rotational speed.

1.1.1.2.2   Friction Stir Welding Transverse Speed. Tool transverse speed is along the line of joint. Transverse speed of the tool is moved the stirred material from the front to the back of the pin. Increasing in travel speed increases the required welding force.

1.1.1.2.3   Friction Stir Welding Travel (Tilt) Angle. Another important process parameter is travel angle or the angle of spindle or tool tilt with respect to workpiece surface. An appropriate travel angle along the welding path insures which the tool shoulder is hold the stirred material by threaded pin and the material should move sufficiently from the front to the back. Increasing in travel angle increases the required welding force. Moreover, the process should be kept certain limits to avoid

flash generation. According to TWI the ideal travel angles should be used between 1.5˚ to 3˚ for similar thickness materials, to have good quality welding process. Otherwise, it should be constant process or the machine is required to improve rigidity and data. The minimum welding force, highest travel speed and minimum flexibility of the machine can be seen by using 0˚ travel angle. Over the range of forces is admissible weld quality due to the more sensitive process. If the forces are too low, generate surface or create internal gaps. If the forces are too high, cause flash to be generated. For this reason, the machine rigidity and data must be higher for 0˚ travel angle.

1.1.1.2.4   Friction Stir Welding Work Angle. The work angle has little effect on machine requirements, but five or more axis machine is useful for a nonzero work angle.
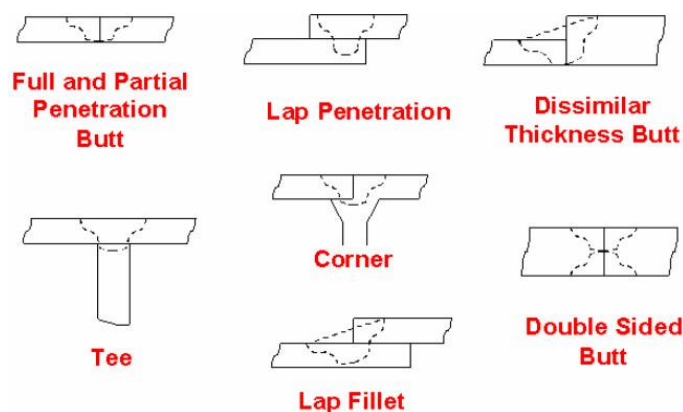
Figure 1.13 Joint configurations for friction stir welding (Friction Stir Link Inc.).

1.1.1.2.5   Friction Stir Welding Plunge Rate. Plunge rate which is also named as target depth is the injection depth of pin into the workpieces is an important process parameter for generating good quality welds with even tool shoulders. The injection depth of pin is directly related with the pin length. When the injection depth is not too deep, the tool shoulder does not contact the original workpiece surface. Hence, rotating shoulder cannot move the stirred material sufficiently from the front to the back of the pin, as a result of this creation of welds contains with inner channel or

surface groove. Meanwhile the injection depth is too deep, the tool shoulder plunges into the workpiece creating excessive flash. In this situation, a concave weld is produced, leading to local thinning of the welded plates. Meanwhile the plunging operation, the plunge rate is affected the force. The plunge rate can be set for friction stir welding, because of no controlling factor in maximum force. On the other hand, the plunge rate is precisely affected welding force for friction stir spot welding. Increasing in plunge rate increases the required welding force.

1.1.1.3   *Friction Stir Welding Joint Design*

The workpieces can be weld many different joint design configurations that are mainly square butt joint, lap joint, dissimilar thickness butt joint, T-butt joint, corner, lap fillet and double sided butt joint as shown in Figure 1.13 (Friction Stir Link Inc.). The most conventional usage of joint configurations for friction stir welding is butt and lap joints. No special preparation is needed for friction stir welding of butt and lap joints. Many other joint configurations can be developed by combination of butt and lap joints. On the other hand, classic tee fillet joint configuration cannot be easy as many fusion welding applications. In this case, the workpiece should be redesign to use the benefits of the friction stir welding.
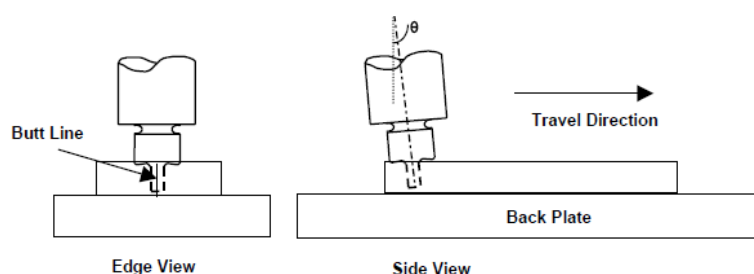
Figure 1.14 Schematic view of tool and workpieces are tilted with respect to each other (Khaled, 2005)**.**

1.1.1.3.2   Butt Joints. A simple square butt joint means that is two workpieces or plates with same thickness are placed on a rigid backing plate and fixed tightly to prevent the abutting joint faces from being forced apart is shown in Figure 1.13. The

welding tool is rotated to a designated speed and tilted with respect to the workpiece normal, as schematically shown in Fig.1.14. The tool is slowly plunged into the workpiece material at the butt joint line, until the tool shoulder is in close contact with the upper surface of the plates and the pin is a short distance from the backing plate, and then traversed. Initial plunging of the tool is required high forces which should be carefully applied for not splitting in butt joint configuration. The apparatus also help to prevent the workpieces from spreading apart or lifting during welding. The development of the thermal fields for preheating and softening the material along the joint line is obtained by applying a downward force to maintain the contact for a short dwell time. At this moment, a lateral force is applied in the direction of welding (travel direction) and the tool is forcibly traversed along the butt line, up to it arrives at the end of the weld. The tool should be withdrawn by rotating when the welding is reached to end. When the pin is removed from workpiece, as we mentioned before it leaves a keyhole at the end of the weld. Semi circular wave is tracked from shoulder contact. (Mishra & Ma, 2005 and Khaled, 2005).
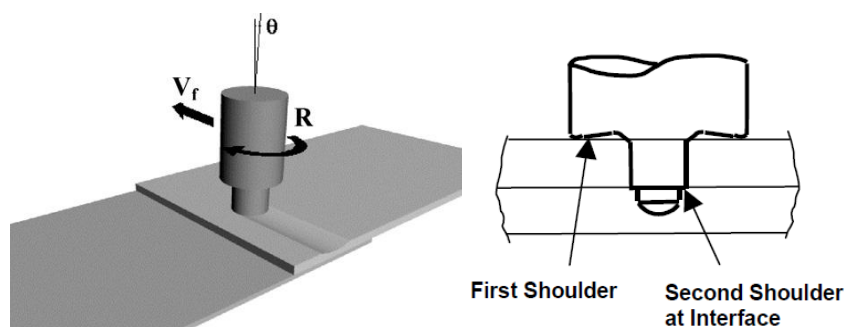
Figure 1.15 Sketches of the FSW process of lap joints (Buffa, et al., 2009 and Khaled, 2005).

Khaled (2005) explained this tool movement deeply as, when the tool is moved in the direction of welding, the leading edge of the pin forces the plasticized material from on either side of the butt line to the back of the pin. The material is actually moved from the leading edge of the tool to the trailing edge of the pin and the result of the intimate contact of the shoulder and the pin form material. There are some opinions that the stirring motion tends to divide oxides on the faying surfaces, allowing bonding between clean surfaces. Besides, if it is necessary to complete full

closure of the root, the pin has to pass very nearby to the backplate, because the deformation below the pin is limited, and around the pin surface. To stick in mind an open root is known lack of penetration is a possible failure point. The tool axis and the workpiece normal are tilted about each other by a small angle θ which is generally in the 2-4˚ range as shown in Figure 1.14. The tilt angle can be obtained by tilting either the tool or the workpieces. This tilting compresses the material behind the tool; however, performing nonlinear welds and limiting the welding speed are disadvantages. In addition, it is recommended that a small-diameter hole is predrilled in the butt line to reduce the forces acting on the welding tool for steel and other high melting alloys during the plunge. Moreover, protect workpiece from low joint strengths at the weld start and end regions, use run-on run-off tabs is helpful solution.
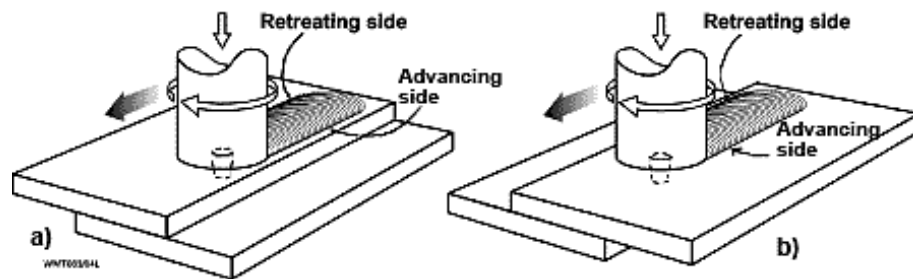
Figure 1.16 Lap weld joint configuration: a) Advancing side near the top sheet edge (ANE), b) Retreating side near the top sheet edge (RNE) (Thomas et al., 2004).

1.1.1.3.2   Overlap Joints. The same operational principles considered above for butt joints also apply to lap welds, with some exceptions. As shown in Figure 1.15, a simple lap joint, two lapped workpieces or plates are fixed on a backing plate (Buffa, Campanile, Fratini & Prisco, 2009). A rotating tool which is rather small tilt angle (Ɵ) is vertically plunged through the upper plate and into the lower plate and traversed along desired direction for joining the two plates. On the contrary to butt welds, lap welds need out of plane stirring, across the interface of the two workpieces or more being welded. Another difference between a tool for butt joint and lap joint is the preface of a second shoulder, located at the interface between the two workpieces being welded as shown in Figure 1.15. Pre-drilling is not always required for lap joint (Khaled, 2005). Thomas, Nicholas, Staines, Tubby & Gittos (2004)

researched mechanical properties of different lap weld joint configurations which were advancing side near the top sheet edge (ANE) and retreating side near the top sheet edge (RNE) as shown in Figure 1.16. They concluded that 'RNE' joint configuration lap welds Figure 1.16a were slightly better than 'ANE' configuration lap welds Figure 1.16b. On the contrary, with a longer probe length and/or slower travel speed 'ANE' type joint lap configuration had better fatigue performance than the 'RNE' joint lap configuration.

The tool pin must penetrate entirely though the thickness of the top workpiece, and continue through some thickness of the bottom workpiece. The end of the pin end passes very close to the bottom of the lower plate. However, the effect of the penetration distance into the lapped lower plate on the mechanical properties of the joint can be overestimated. The notches between the interface surface of the workpiece are possible sites for crack initiation and, also, they have a profound effect on mechanical properties. Generally, the lap joints are not as strong as butt joints, but they have sufficient static and fatigue properties to replace fastened joints (Khaled, 2005). In aeronautic industry, overlap welding is extensively preferred in the assembled parts and products.

Buffa et al. (2009) mentioned to improve the mechanical resistance of the obtained FSW lap joints, the geometrical characteristics of the tool and in particular to the diameter of the pin has a great importance. In fact, a large tool pin diameter is required to expand as much as possible the welded surface. Additionally, a large tool shoulder diameter is required to spread the heat flux created by the frictional forces work.

1.1.1.3.3 T-butt Joints. Friction stir welding has been also used to prepare T-joints Figure 1.13. Khaled (2005) described a T-joint could be viewed as a special lap joint. A specially designed rotating pin is inserted with a tilt angle into the clamped blanks and then it is moved all along the welding direction in FSW of T-joints. The attained knowledge on FSW process of butt joints is not immediately

applicable to the T-joints. Because, the surface to be welded is vertical in butt joints, whereas it is horizontal in T-joints and placed at the bottom of the top plate to be welded. Fratini, Buffa & Shivpuri (2008) explained the welding of T-joints as ''in transparency'' which requires the building of an appropriate clamping fixture designed to fix the stringer under the skin during the FSW process as shown in Figure 1.17. Such as, fixture is described by two radii, one for each side of the joints, corresponding to the radii between skin and stringer in the final welded part (corner-fillets). In point of fact, such radii must be filled by the flowing material during the FSW process. Therefore, an actual forging process is needed to force the sheet and the stringer material in fulfilling the radii of the clamping fixture, resulting in the radii of the T-joint. The surfaces of individual parts and those of the clamping fixture should be finished with grinding operations, to obtain good quality and repeatability of the welding operations. Designing with T-joints is challenging, because it must be taken carefully to prevent compression failure of the web which is vertical plate and the notches on either side of the weld are potential crack initiation regions.
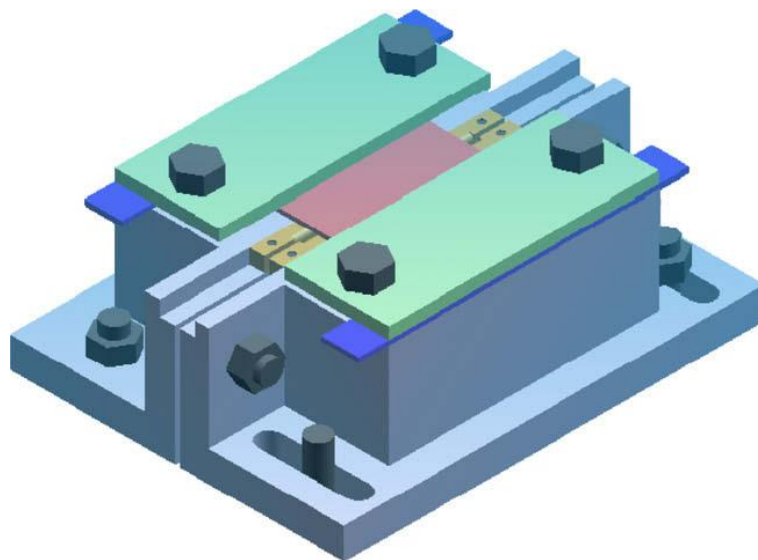
Figure 1.17 Sketch of the used clamping fixture for T-joints (Fratini et al., 2008).

T-geometries are very critical in several departments of the transportation industries: components and in particular panels frequently require straightening parts

usually welded in transparency, specifically, through T-joints, on the panel surface. Likewise, the aircraft applications where skins and stringers are welded together, corrosion occurrence have to be accurately researched in order to maximize the operating life of the joints (Fratini et al., 2008).

Consequently, the most effective set of operating and geometrical parameters that optimize the FSW of butt joints will not in all probability perform for the T-joints. Especially, the tool geometries together with the tool feed rate and rotating speed must be resolved for T-joints in order to get an effective material flow and bonding conditions during the FSW process. Besides, the plastomechanics of the two processes are completely different (Fratini et al., 2008).

1.1.1.3.4   Fillet and Other Joint Types. In FSW fillet joints are probably needed for some engineering applications. FSW has been also used to produce spot joints with and without the end keyhole. Spot welds can be applied both the butt and lap type joints. A corner joint is in the form of a special butt joint (butt configuration) or a special lap joint (rabbet configuration). Additionally, hem joints can be produced by using FSW.

1.1.1.4   Optimization of Friction Stir Welding Process Parameters

1.1.1.4.1   Effect of Rotational Speed. Babu et al. (2008) researched optimizing friction stir welding parameters for AA2219 aluminum alloy joints. They revealed a decrease in tool rotation speed reduces the area of the weld zone and affects the temperature distribution in the weld zone. Reducing heat input situation resulted in lack of stirring and yielded drop joint strength. In addition, a higher rotational speed initiates excessive release of stirred materials to top surface, which occur defects in the weld zone.

Normally, the base metal microstructure contains elongated grains but FSW region grain size depends on the welding parameters. Babu et al. (2008) studied,

where the grain size was found to increase with the increase of the tool rotation speed, because of the higher heat input. The average grain size of the stir zone of the welded joints grows with rotational speed. However, increasing in average grain size causes a lower hardness value and resulted in weaker tensile properties.

They also observed coarsening of precipitates at high speeds compared to the base material. In the stirred zone, higher temperatures are reached during welding. Hence, the coarsened precipitates even begin to dissolve in the stir zone. The number of particles in the stir zone is less than that in the parent material. Besides, particles would suffer more fragmentations at high rotational speeds. The microstructural distrubutions affected the mechanical properties. In the microstructure of the friction stir welded zone obvious variations were observed with softening because of recrystallization by the dynamic recrystallization process, and the elongated grains of the base material are changed into equiaxed fine grain structure. The higher hardness and superior tensile properties were resulted of a defect-free friction stir processed (FSP) region with smaller grain size and very fine, homogeneous particles distribution.

Recently, Balasubramanian (2007) studied effect of friction stir welding parameters for five different grades of aluminum alloys, i.e. AA1050, AA6061 AA2024, AA7039 and AA7075 using different combinations of process parameters. The weld quality (defective or defect free) were checked by macrostructural analysis. He found out empirical relationships between base metal properties and tool rotational speed and welding speed, respectively. The developed empirical relationships can be practically used to produce the FSW process parameters to fabricate defect free welds. In this study, twenty-five joints (5 base metals×5 tool rotational speeds) were fabricated to investigate the effect of tool rotational speed on FSP zone quality. 75 mm/min welding speed and 8 kN axial force were kept constant while varying the tool rotational speeds that were 600, 700, 800, 900, 1100, 1200, 1300, 1400, 1500 and 1600 rpm, but only five tool rotational speeds were chosen for each material depend on material properties. Therefore, macrostructure of the FSW

joints obtained at different tool rotational speeds were magnified by using optical microscope as shown in Figure 1.18. Defect free welds in AA1050 aluminum alloy produced with a rotational speed of 900 rpm of the five rotational speeds used as shown in Figure 1.18d. In the same way, a rotational speed of 1100 rpm in AA6061 as shown in Figure 1.18i, 1200 rpm in AA2024 as shown in Figure 1.18m, 1300 rpm in AA7039 as shown in Figure 1.18s and 1500 rpm in AA7075 as shown in Figure 1.18x alloys produced defect free joints.
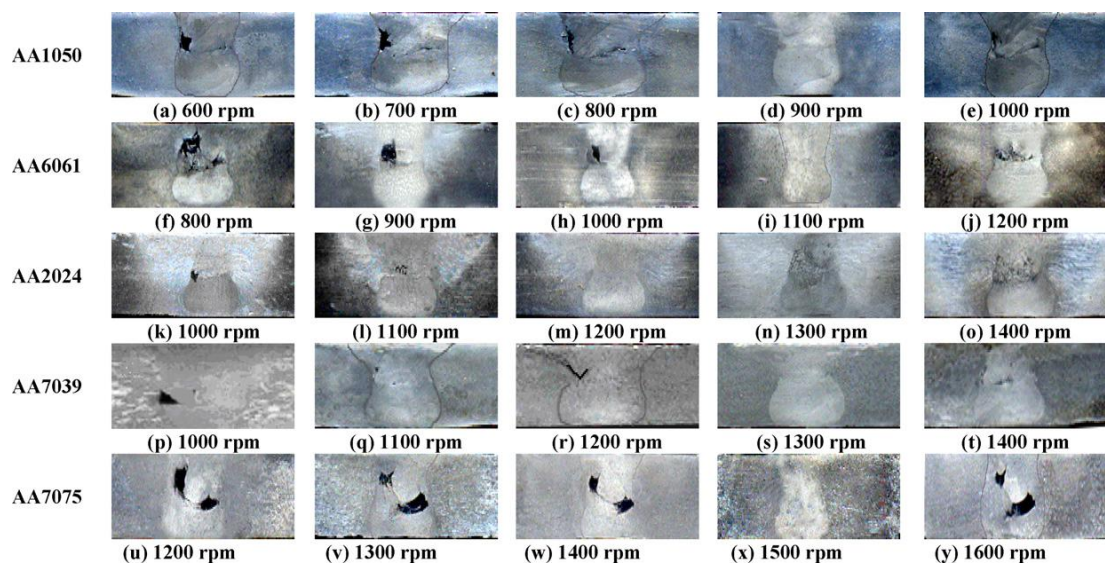
Figure 1.18a-y Effect of tool rotational speed on macrostructure of aluminum alloys (welding speed = 75 mm/min and axial force = 8 kN) (Balasubramanian, 2007).

1.1.1.4.2 Effect of Welding Speed. Babu et al. (2008) also studied optimization of the welding speed. He obtained the joints fabricated using lower and higher welding speeds 0.25 mm/s and 1.25 mm/s and exhibited significant variations in tensile properties compared to the joints fabricated using a welding speed of 0.75 mm/s. The joints tensile properties fabricated at a welding speed of 0.75 mm/s show superior performance than the other joints.

Grain growth and grain coarsening can be observed as a result of higher heat input at lower welding speeds. The weld region grains demonstrated to contain many subboundaries at the lower welding speed. During FSW, the subgrain size was

observed to increase with increasing heat input. Statically, dynamically recrystallized grains were examined to expand during the cooling of the thermal cycle, after the tool has passed. So, the larger heat input affects in larger grains with a lower density of dislocations and subboundaries in the stir zone (Babu et al., 2008).

He also observed abrupt change in the grain size of the friction stir processed (FSP) zone was observed in some joints which were fabricated with higher welding speeds. Normally, FSW higher welding speeds results in shorter exposure times at higher temperatures. That's why, he concluded a welding speed of 0.75 mm/s produced finer grains in the FSP region of the AA2219 alloy than experimented other welding speeds, which resulted in superior tensile properties for the joints.
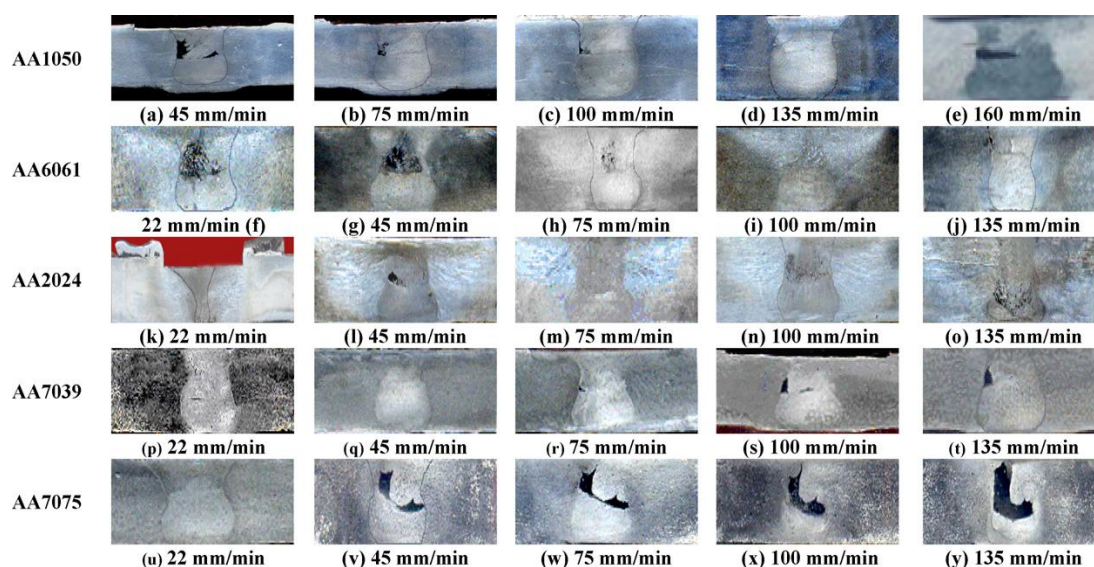
Figure 1.19a-y Effect of welding speed on macrostructure of aluminium alloys (tool rotational speed = 1200 rpm and axial force = 8 kN) (Balasubramanian, 2007).

In section 1.1.1.4.1, research of Balasubramania (2007) has been mentioned about effect of rotational speed in friction stir welding. In the second part of his study, he also researched effect of the welding speeds (or transverse speeds) to same alloys with constant 1200 rpm rotational speed and 8 kN axial force while varying the welding speeds which were 22, 45, 75, 100, 135, 160 mm/min, but only five welding speeds chosen due to material properties. Macrostructure views magnified by the

optical microscope of the FSW joints obtained at different welding speeds were shown in Figure 1.19. The result of the study, defect free welds in AA1050 aluminum alloy obtained by using a welding speed of 135 mm/min as shown in Figure 1.19d of the five welding speeds used. Likewise, a welding speed of 100 mm/min in AA6061 as shown in Figure 1.19i, 75 mm/min in AA2024 as shown in Figure 1.19m, 45 mm/min in AA7039 as shown in Figure 1.19q and 22 mm/min in AA7075 as shown in Figure 1.19u alloys produced defect free joints.

1.1.1.4.2   Effect of Axial Force. The effect of axial force has been researched by Babu et al. (2008). He compared the obvious variations in tensile properties were found in the joints fabricated using lower and higher axial forces of 8 kN and 16 kN to the joints fabricated using an axial force of 12 kN. Regardless of tool profiles, the joints fabricated with an axial force of 12 kN have demonstrated superior tensile properties with respect to the other joints.

Babu et al. (2008) found out the elongated grains of the base material were partially changed into equiaxed grains in the FSP region owing to insufficient forging pressure and friction heat, at the lower axial force level. Grain growth and grain coarsening were observed because of higher heat input and tremendous forging pressure at the higher axial force level. Therefore, the axial force of 12 KN produced smaller grains in the FSP region along with finer strengthening precipitates in the AA2219 alloy joints might be the reason for the higher tensile properties of the joints fabricated using these axial force levels.

Kumar and Kailas (2007) investigated the influence of axial load of the friction stir welded joint. They increased the axial load is continuously varied by linearly the interference between the tool shoulder and the surface of the base material. The aluminum alloy 7020-T6 which is the nominal chemical composition is Zn – 4.63 wt%, Mg – 1.3 wt% and rest aluminum used as the base material. An optimal axial load found as the defect-free weld with joint efficiency of 84% due to softening of the HAZ. Welding speed, tool rotation speed and backward tool tilt angle were kept

constant at 80 mm/min, 1400 rpm and 2˚ respectively with a frustum shaped pin profile. They observed the material flow in the top portion of the weld nugget reaches the advancing side base material and makes the bonding, when the axial load was increased from 6 to 7.4 kN as shown in Figure1.20a–f. For this reason, when the axial load was lower than 6.8 kN the there was a defect in the weld because of not enough coalescence of transferred material. As a result, the welded samples fractured in the weld nugget zone because of the defect in the weld nugget. The welds produces at axial loads above 7.4 kN fractured away from the weld. Moreover, they reported the initial elongated grain structure of the base material was transformed in to fine recrystallized equiaxed grains and the recrystallized grain size in the weld nugget increased when the axial load increased. Besides, the defect free aluminum alloy 7020-T6 weld was obtained by be 8.1 kN, as the optimal axial load.

1.1.1.4.2   Effect of Pin Profiles. The joints fabricated using the square pin profiled tool which one of the five pin profiles as shown in Figure 1.7 used, exhibit the highest tensile strength of the AA2219 joints. The triangular pin profiled tool conducted approximately same tensile properties those of the square pin, followed by high to low performance by the threaded, taper and straight cylindrical pins. The main reason for higher properties obtained from the use of a tool pin with flat faces, like square and triangular pins, the reason for those tools with non-circular profiles allow plasticized material to pass around the probe. Flat faces pin profiles also were associated with eccentricity of which the rotating object is related to dynamic orbit. The amount of the eccentricity is depending on the friction stir welding process characteristics (Babu et al., 2008).

The path for the flow of plasticized material from the leading edge to the trailing edge of the rotating tool is the result of the relationship between the static volume and swept volume. The static volume to swept volume ratio is equal to 1 for straight cylindrical, 1.09 for tapered cylindrical, 1.01 for threaded cylindrical, 1.56 for square and 2.3 for triangular pin profiles. Besides, the triangular and square pin profiles generate a pulsating stirring action in the material flow (Babu et al., 2008).
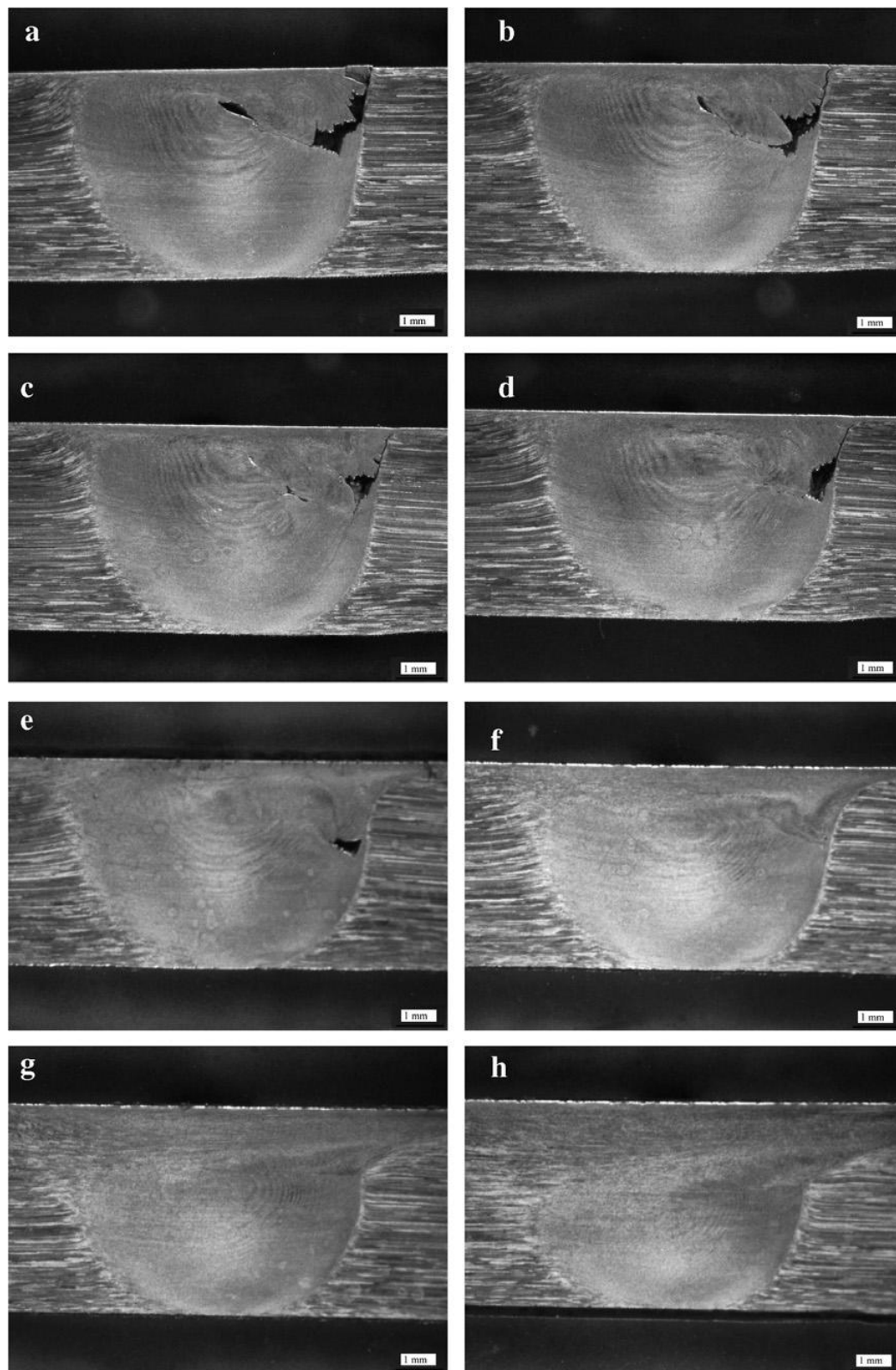
Figure 1.20 The macrographs show the evolution of a defect-free FSW as function of axial load. The welds (a–h) are produced at axial load of 4.0, 4.6, 5.3, 6.0, 6.7, 7.4, 8.1 and 8.8 kN, respectively (Kumar & Kailas, 2008).
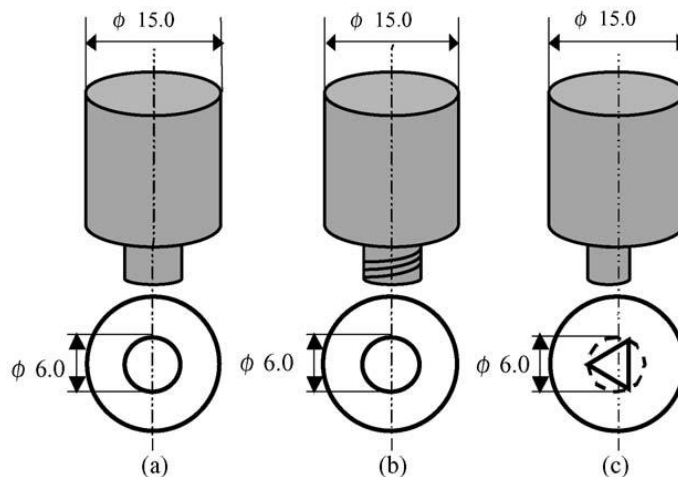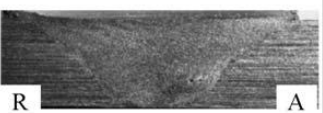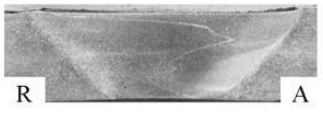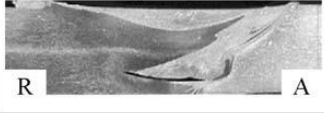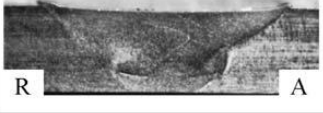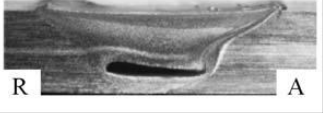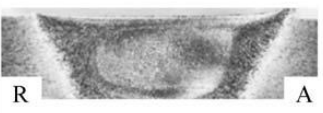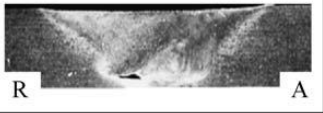
Figure 1.21 FSW tool shape: (a) column without threads, (b) column with threads, (c) triangular prism (Fujii et al., 2005).

Fujii, Cui, Maeda & Nogi (2005) investigated the effect of tool shape on mechanical properties and microstructure of friction stir welded aluminum alloys. Three types of the tool profiles were used as shown in Figure 1.21, as the simplest shape tool with a columnar probe without threads, the ordinary shape tool with a columnar probe with threads and the triangular prism shape probes to obtain the optimal tool design which was affecting the mechanical properties of welded as similarly 1050-H24, 6061-T6 and 5083-O aluminum alloy plates. The triangular prism shape probe was used as its simple profile and it could be expected the simulate the material flow similar to up-to date FSW tools such as MX Triflute[TM] or Trivex[TM]. The best mechanical properties were obtained with 1050-H24 whose deformation resistance is very low, a columnar tool without threads produces weld. They found that, when deformation resistance was relatively low and tool shape effects were negligible on the microstructures and mechanical properties of 6061-T6. The weldablity was significantly affected by the rotation speed for 5083-O whose deformation resistance is relatively high. The tool shape for a low rotation speed 600 rpm did not greatly affect the microstructures and mechanical properties of the joints. Additionally, in tool design should be considered the following features, as simple a shape as possible to reduce the cost and sufficient stirring effect to produce sound welds.
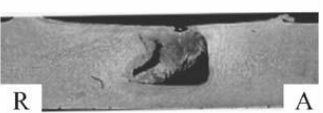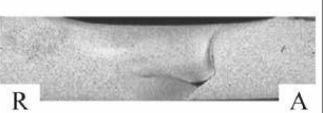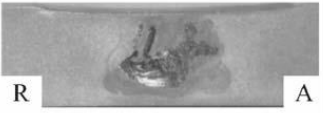
Figure 1.22 Macrostructure of cross section of AA1050-H24 FSW joints (Fujii et al., 2005).

Figure 1.23 Macrostructure of cross section of AA6061-T6 FSW joints (Fujii et al., 2005).

Figure 1.24 Macrostructure of cross section of AA5083-O FSW joints (Fujii et al., 2005).

Fujii et al. (2005) The macrostructures in the cross section of the friction stir welded joints of the 1050-H24 aluminum alloy at various welding speeds with a constant 1500 rpm rotational speed as shown in Figure 1.22. The weld zone using the tool without threads was similar to that using the tool with threads when the welding speed was equal to or below 300 mm/min with the revolutionary pitch is equal to or smaller than 0.2 mm/r. On the other hand, a crack or defect was more easily formed in the joints using the tool with threads than that using the tool without threads when the welding speed was greater than 300 mm/min with the revolutionary pitch was greater than 0.2 mm/r. The defects located in almost all the joints for the triangular prism tool, except, the defects became very small for the welding speed was from 300 mm/min to 500 mm/min with the revolutionary pitch was from 0.2 mm/r to 0.33 mm/r.

The macrostructures in the cross section of the friction stir welded joints of the 6061-T6 aluminum alloy at various welding speeds with a constant 1500 rpm rotational speed as shown in Figure 1.23. Defect free FSW joints were obtained for most of the FSW conditions.

The macrostructures in the cross sections of the friction stir welded joints of the 5083-O aluminum alloys at various rotation speeds with a constant 100 mm/min welding speed as shown in Figure 1.24. Serious defects were easily formed in the joints using the two column tools (circular ones) when a higher the rotation speed was 1500 rpm, whereas only small defects were formed in the joints using the triangular prism tool, means the triangular prism tool was the best . The column tool with threads can produce a sound weld as amount the triangular prism tool below the mid rotational speed 800 rpm. In addition, to obtain the defect-free FSW joints, the rotation speed should be decreased below the low rotational speed 600 rpm for all the tool profile types, especially best result was obtained with column with threads (Fujii et al., 2005).

Scialpi, De Filippis & Cavaliere (2006) studied the effect of different shoulder geometries on the mechanical and microstructural properties of a friction stir welded

6082-T6 aluminum alloy. They observed that shoulder with combination of fillet and cavity produced good joints for thin sheets.

Elangovan & Balasubramanian (2006) studied effect of tool pin profile and tool rotational speed on the formation of friction stir processing zone in AA2219 aluminum alloy and they concluded square pin profiled tool produced defect free FSP region, irrespective of rotational speeds.
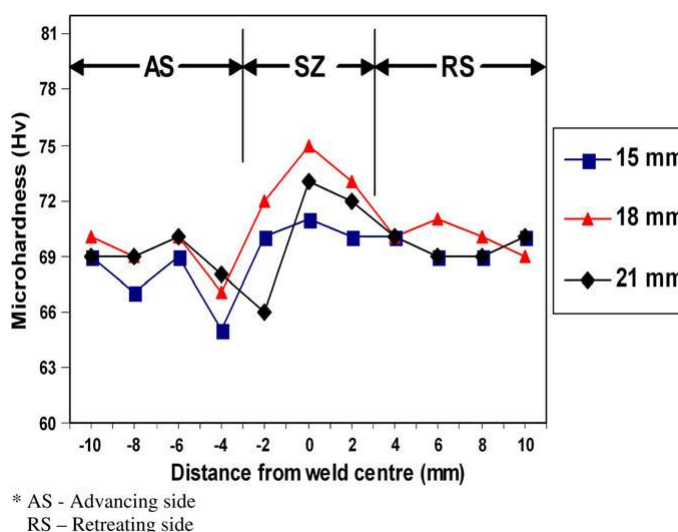
Figure 1.25 Effect of shoulder diameter on hardness (Padmanaban & Balasubramanian, 2008).

Boz & Kurt (2003) indicated that high pitch threaded tools turned like a drill rather than a stirrer and compelled the weld metal outward in the form of chips and the best joining was obtained for low pitch threaded tools.

Padmanaban & Balasubramanian (2008) experimented shoulder diameter and found out the joint fabricated with 18mm shoulder diameter demonstrated superior tensile properties compared to the joints fabricated other 15mm and 21mm shoulder diameters as shown in Figure 1.25.

The ultimate relation between material flow and result of microstructure of welds are varies for each tool which is the most important effect of the material flow.

Padmanaban and Balasubramanian (2008) also examined mild steel, stainless steel, armour steel, high carbon steel and high speed steel and found out the joint fabricated with high carbon steel tool showed superior tensile properties compared to the joints fabricated by other tool materials as shown in Figure 1.26.

* AS - Advancing side
  RS – Retreating side
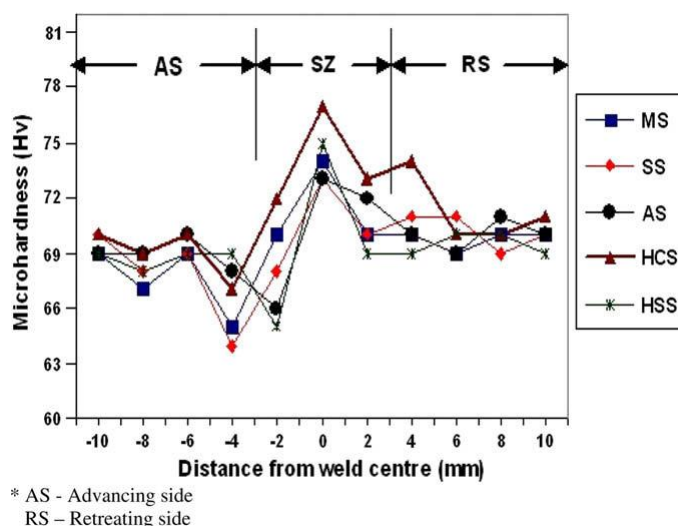
Figure 1.26 Effect of tool materials on hardness; MS-mild steel, SS-stainless steel, AS-armour steel, HCS-high carbon steel, HSS-high speed steel (Padmanaban & Balasubramanian, 2008).

1.2.1.1   *Numerical Control of Process Parameters*

Numerical methods are required to investigate the mechanism of controlling of welding parameters. Zang, Z., & Zang, H. W. (2008) qualitatively analyzed the effect of welding parameters including the rotating speed and the welding speed on the weld quality through the discussions on material flow patterns under different welding parameters by adopting a fully coupled thermo-mechanical model to predict the material deformations and temperature histories in the friction stir welding process. Numerical results pointed out that the maximum temperature in the FSW process can be raised with the increase of the rotating speed. The increase of the welding and rotational speed can cause the increase of the efficient input power for FSW system. They concluded the reason for the formation of the weld fash in FSW as the material particles on the top surface did not enter into the wake and just pile up

at the border of the wake at the retreating side. The friction stir weld quality can be improved by both the increase of the rotating speed and the decrease of the welding speed due to the increase of the stirring effect of the welding tool. However, increasing the rotating speed bring about the weld fash. Simultaneously, the rotating speed must be increased, while the welding speed is rising to prevent any possible welding defects such as void. The maximum temperature increased to 418.7˚C when welding speed was 2.363mm/s and rotational speed was 240rpm and the temperature distribution and its corresponding stress distribution the friction stir weld was shown in Figure 1.27a.More distribution results obtained for maximum temperature 425.9˚C and 443.3˚C with respectively welding and rotational speeds are 2.363mm/s, 375rpm and 3.363mm/s, 400rpm as shown in Figure 1.27b-c. The increase of the residual stress results obtained the simultaneous increase of the rotating and the translating speeds of the welding tool.
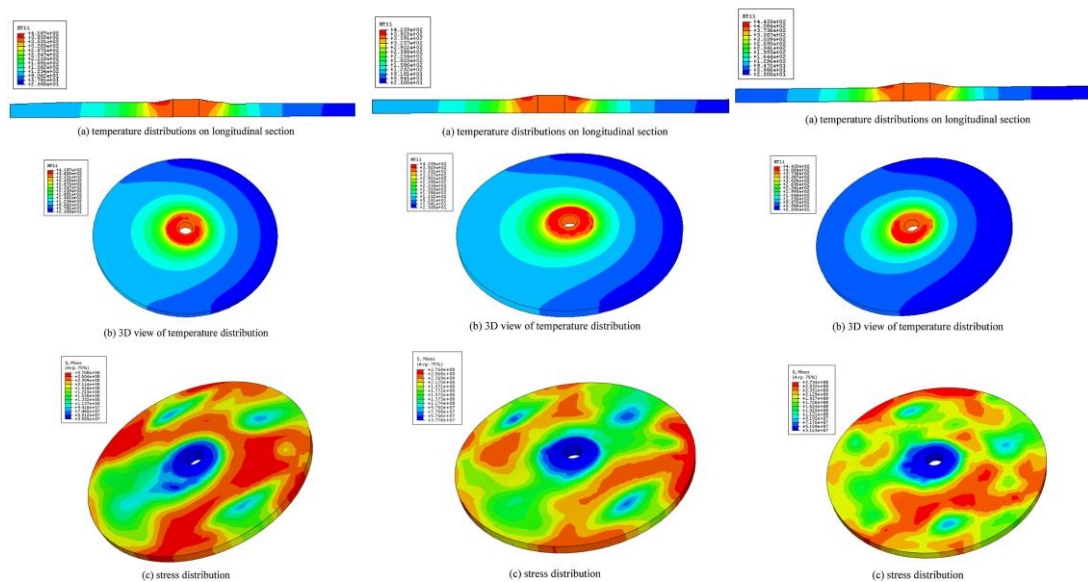
Figure 1.27 Temperature and stress distributions a) when $\upsilon = 2.363$mm/s and $\omega = 240$ rpm, b) when $\upsilon = 2.363$mm/s and $\omega = 375$ rpm, b) when $\upsilon = 3.363$mm/s and $\omega = 400$ rpm (Zang &Zang, 2008).

1.2 Friction Stir Welding Process Modeling

The scientific understanding of mechanical and physical phenomena of the friction stir welding depends on the tool design, joint geometry, the translation and

rotation speeds, the applied pressure and the characteristics of the material being joined. The performance of the FSW joints efficiency is appraised by avoiding defects in the microstructural area, improving microstuctural and property changes in the deformed and heat-affected areas and residual stress. (Mishra & Mahoney, 2007, p.187). Analytical or numerical methods can be used for process modeling. Numerical modeling can be easily use finite element, finite difference, or finite volume methods for complex modeling.

1.2.1 Material Flow

Modeling the material flow in friction stir welding is a complex process. But, it is important to understand the material flow to get better result for weld structure. As shown in Figure 1.28, metal flow is affected by design of tool, interface contact conditions of tool and workpiece, process conditions like speeds, torque and forces and temperature of the process.

The temperature near the rotating pin and workpiece interface constrains the thermally softened and below the melting point. The thermally softened material is rotational flow and vertical flow direction around the pin is stirred and forced down by the threads. When the rotational motion of the pin and its translation motion are in the same direction, the side of the weld is called advancing side. If the rotational and transverse motions are opposite direction, the welding side is called retreating side (Guerra, Schmidt, McClure, Murr, & Nunes, 2002).

Several recent studies about material flow during friction stir welding have been investigated such as a marker insert tracer (MIT) technique studied by Seidel & Reynolds (2001), using a faying surface tracer and pin frozen in a place during welding studied by Guerra et al. (2002), steel shot tracer technique and stop action technique studied by Colligan (1999) and another method is monitoring with Al-SiC and Al-W composite markers was studied by London, Mahoney, Bingel, Calabrese, Bossi & Waldron (2003).
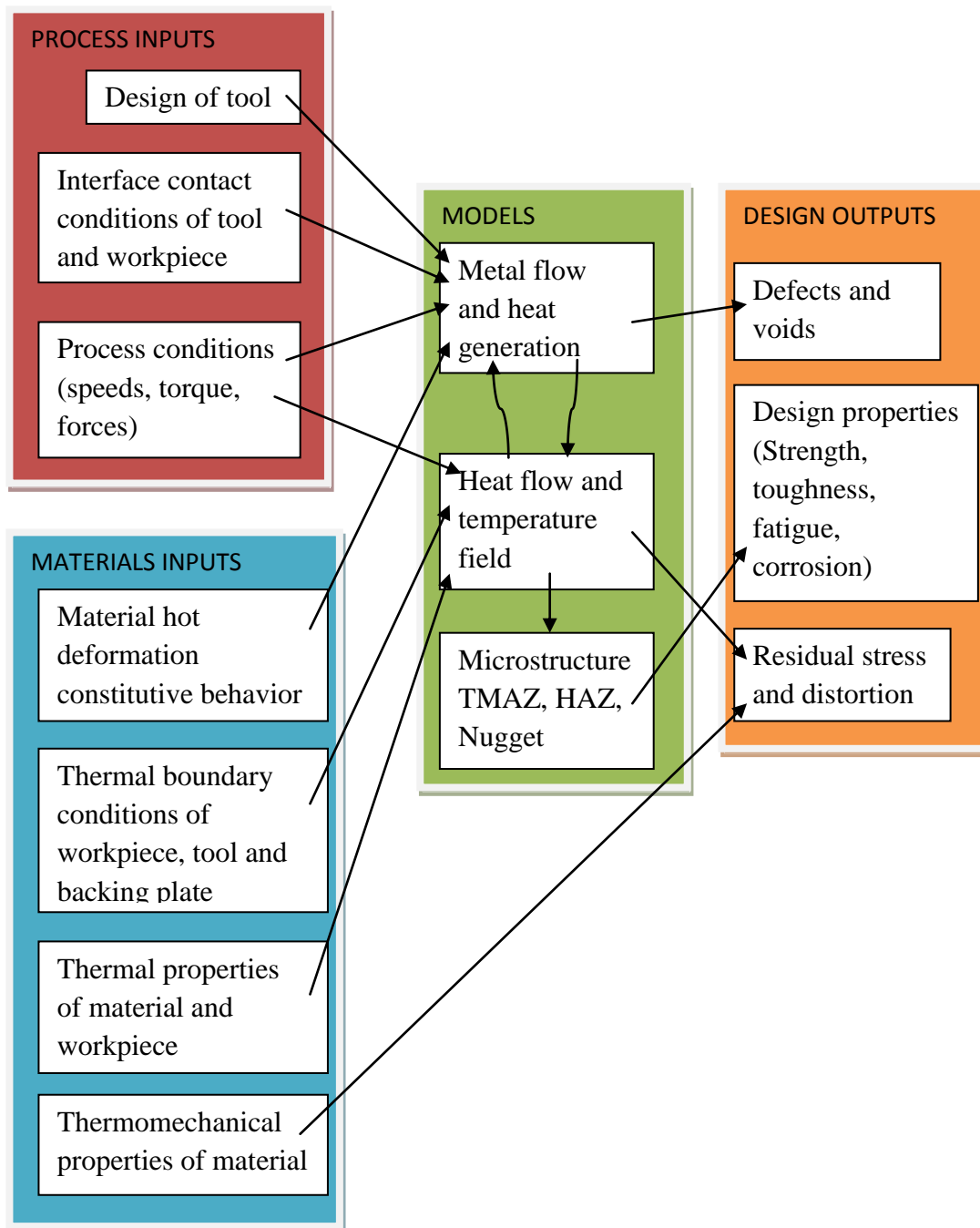
Fig 1.28 Sketch of the friction stir welding physical interactions of the design inputs and outputs.

Guerra et al. (2002) research was concluded that; material on the advancing side of the weld gets into rotational area that stirs and moves around the pin. This highly deformed material creates arc-shaped appearances behind the pin. On the other hand, material that never rotates around the pin on the retreating side was carried along and fills in material on the retreating side of the pin wake. Advancing side and retreating

side have very different thermomechanical actions and properties. The wash and washback of the threads cause a big vertical or vortex movement of the material within the rotational zone. The vortex flow, rotational and translational motion of the pin shaped formed an unwound helical trajectory material entering in this zone. Around upper 1/3 of the top of the weld moved under the influence of the shoulder rather than the threads on the pin. The clockwise or counter-clockwise direction of the pin affects weld by the interface between the material moving in the upper zone and the lower thread prominent zone.
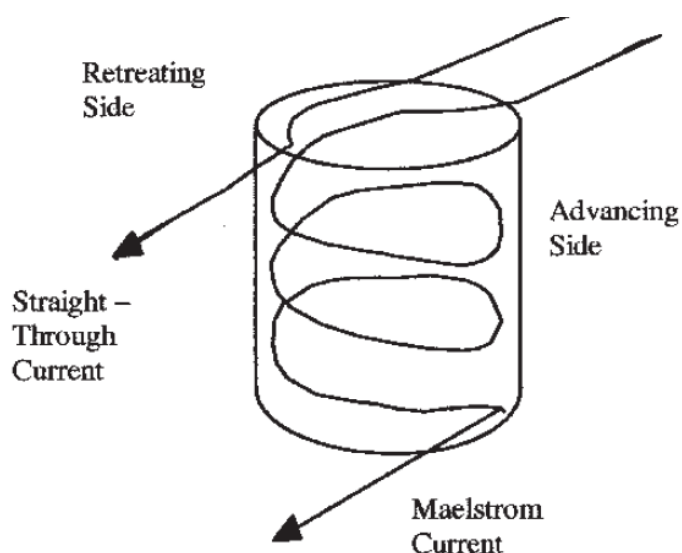
Figure 1.29 The two material flow currents resulting from superimposed incompressible flow fields (Schneider & Nunes, 2004).

Schneider and Nunes (2004) investigated whether the banding on the transverse and lateral sections of a friction stir weld may be the result of two different and distinct metal currents flowing around the FSW pin tool, as shown schematically in Figure 1.29. The proposed current flows would enforce a different thermomechanical processing on their relevant metal flow currents. Different microstructures can be obtained as a result of variations in thermomechanical processing. The metal on the retreating side of the weld was picked up at the front of the tool and deposited directly behind the tool with a minimum residence in the rotational region around the tool, in the suggested model. This was named as the "straightthrough" flow. A gradual radial influx of metal at the top of the pin was become to blocked the weld

material from the advancing side of the pin resides long enough in the rotational flow around the tool. The threads on the pin caused the radial influx of metal was part of a ring-vortex circulation (for instance, a smoke-ring with the pin in the center). The circulations force the blocked metal down the pin. A whirlpool pattern or "maelstrom" flow which emerges further down the pin as the circulation begins to move outward was obtained from accumulation of the rotation around the pin with this downward flow. The direction of the threads in reverse inverts the direction of the maelstrom flow from downward to upward along the pin.
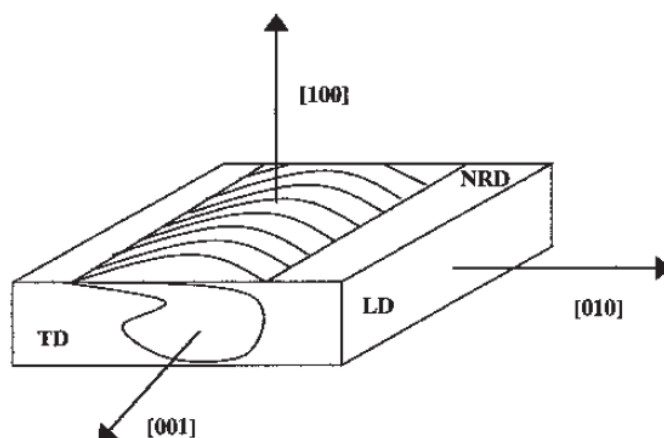
Figure 1.30 Nomenclature of orientation of data analyized from the OIM images (Schneider & Nunes, 2004).

Crystallographic data were taken from the transverse cross section of the weld placing the FSW nugget. The data analyzed by using the nomenclature is shown on the image in Figure 1.30.

The complex flow field around a FSW tool can be divided into three simple parts as shown in Figure 1.31. These component fields are incompressible flows. The first of the flow components, a surface of velocity discontinuity is a plug of metal in rigid body rotation separated from the rest of the weld metal by a cylindrical shearing surface. The second flow components are a homogeneous and isotropic flow field equal and opposite to the tool traverse velocity. The third flow component is a ring vortex flow field surrounding the tool and carrying metal up on the outside, in at the

shoulder, down on the inside, and out again on the inferior regions of the pin (Schneider & Nunes, 2004).
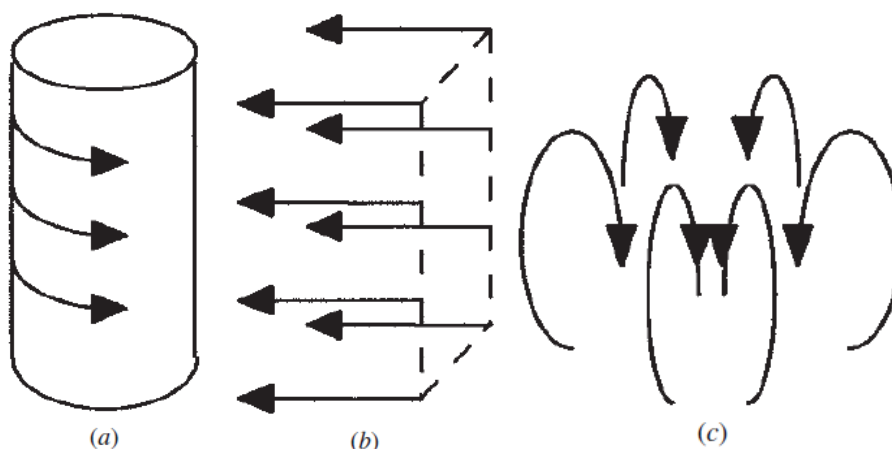
Figure 1.31 Three incompressible flow fields of the friction stir weld: (*a*) rigid body rotation, (*b*) uniform translation, and (*c*) ring vortex (Schneider & Nunes, 2004).

1.2.1.1 *Flow Visualization by FSW of Dissimilar Materials*

The friction stir weld joining which was initially applied for joining aluminum alloys has now rapidly expanded its applications to join steel, titanium, nickel and other high temperature alloys. This technique provides main advantages compared to the conventional fusion processes as it offers lesser workpiece deformation and improved mechanical properties because of the solid-state joining of metals. Dissimilar material joining by friction stir welding process is currently used in product industries like the aircraft, aerospace, marine shipbuilding, transportation, electronics industries, power generation, petrochemical, chemical, nuclear and the process industry like natural gas (Soundararajan, 2006, p.iv)

Several friction stir weld flow of dissimilar metals studies have been used for visualizing the complex flow phenomenon. Li, Murr & McClure (1999) studied the complex flow patterns developed in friction stir welding of Al 2024 to Al 6061. The flow patterns are observed by differential etching of the two aluminum alloys.

Insertion layers of these two dynamically recrystallized alloys creates complex vortex, whorl and swirl features characteristic of chaotic-dynamic mixing.

Watanabe, Takawama, Kimapory & Hotte (2003), have analyzed the joining of steel to aluminum alloy by "interface-activated adhesion welding" induced by friction stir welding. A rotating pin inserted into the aluminum is pushed toward the faying surface of the steel, and as a result, the rubbing motion of the rotating pin mechanically removed the oxide film from the faying surface. Heat generation of friction of a rotating tool shoulder adheres to the activated faying surface of the steel results aluminum in a fluid-like plastic state, therefore, joining between steel and aluminum successfully welded. In spite of that, a small amount of intermetallic compound was observed at the upper region of the weld caused by higher heat generated at the interface between the tool shoulder and the top surface of the welded workpieces, other than interface between steel and aluminum alloy.
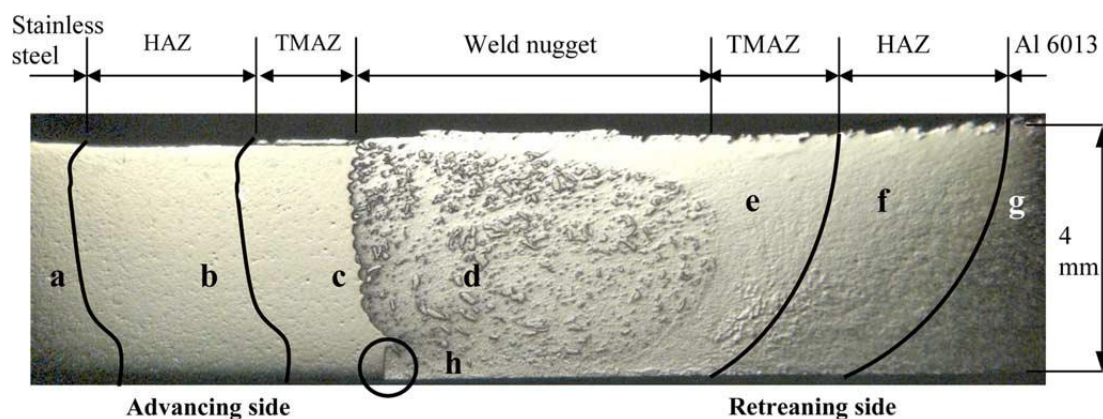
Figure 1.32 Macroscopic overview of the cross-section of the friction stir welded Al 6013-T4 alloy to X5CrNi18-10 stainless steel (Uzun et al., 2004).

Uzun, Donne, Argagnotto, Ghidini & Gambaro (2004) carried out joining of dissimilar Al 6013-T4 alloy and X5CrNi18-10 stainless steel as shown in Figure 1.32. They reported that aluminum slightly diffuses in stainless steel interface between stainless steel and Al alloy of weld nugget; however Fe, Cr and Ni diffuse very little into Al alloy. The diffuse transition between stainless steel particles and Al alloy is mistakable in the weld zone.

McLean, Powell, Brown & Linton (2003) carried out a preliminary investigation for joining a magnesium alloy to an aluminum alloy by friction stir welding. The study has shown that localized melting of aluminum during the welding process can formed a brittle intermetallic compound along the joint interface.

Another investigation for joining aluminum and magnesium alloys has studied by Chen & Nakata (2007). They examined that Al-Si and Mg-Al-Zn alloys were lap joined using friction stir welding, the pin without contacting the lower surface of the Mg-Al-Zn alloy sheet. Two sheets were joined through conversion zone which composed of intermetallic compounds Al12Mg17, Al3Mg2 and Mg2Si at the joint interface. The joint strength was improved by using a lower welding speed results no visible welding cracks in the joint.
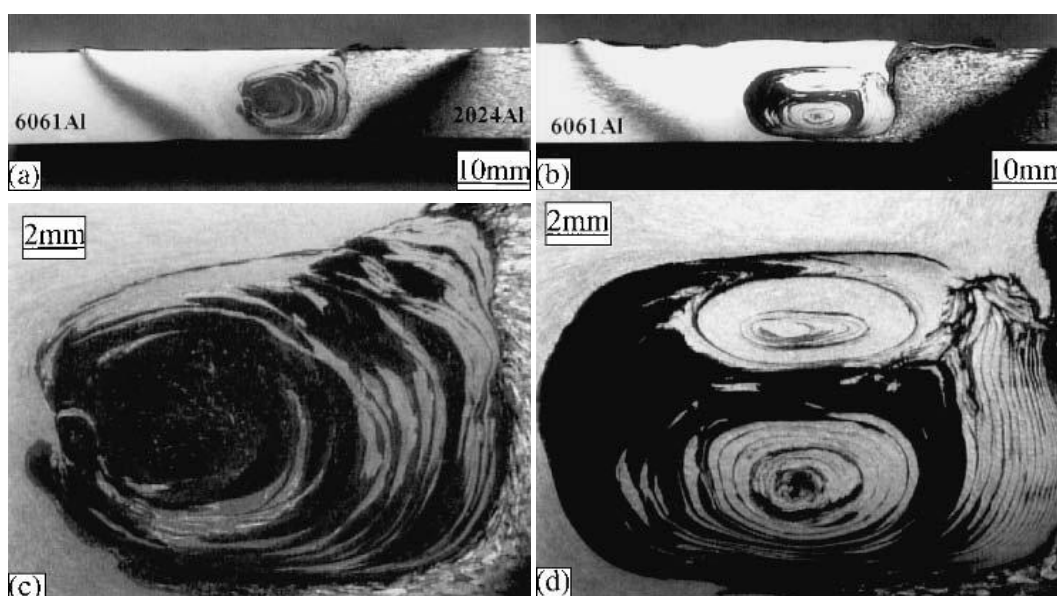
Figure 1.33 Effect of the welding speed on material flow and mechanical mixing in a dissimilar weld of 6061-Al to 2024-Al alloys at rotational speed of 637 rpm: (a) 57 mm/min; (b) 229 mm/min; (c) high magnification of (a); (d) high magnification of (b) (Ouyang & Kovacevic, 2001).

Chen & Nakata (2008) also examined Al-Si alloy and pure titanium for lap joining using friction stir welding. They concluded cast aluminum alloy sheet with a composition of Al-Cu- Zn-Mn-Fe-Mg-Si and pure titanium can be successfully lap joined by using friction stir welding. TiAl$_3$ formed at the interface. These formations

were related welding speed and as a result of this, mechanical properties of joint were affected.
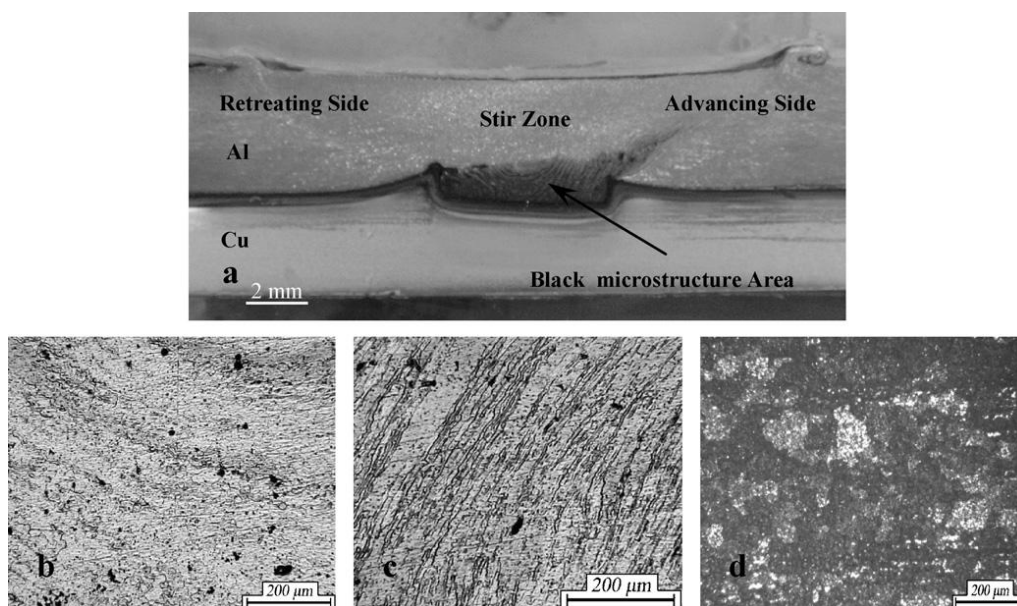
Figure 1.34 Micrographs of different areas in Al–Cu joint produced at welding and rotational speeds of 95 mm/min and 1180 rpm, respectively: (a) overall view of the joint, (b) fine equiaxed grains in stir zone of aluminum, (c) elongated Al grains in the TMAZ, and (d) Al in the HAZ in the advancing side (Abdollah-Zadeh et al., 2007).

Ouyang & Kovacevic (2001) examined the material flow behavior in friction stir butting welding of 2024Al to 6061Al workpieces. The mechanically mixed region characterized by the relatively dispersed particles of different alloy constituents, the stirring-induced plastic flow region consisting of alternative vortex-like lamellae of the two Al-alloys and unmixed region consisting of fine equiaxed grains of the 6061-Al alloy were revealed three different regions in the nugget zone of dissimilar aluminum alloys in the welded zone. The study has shown that the contact between different layers is intimate in the welds, but the mixing is far from complete. Nonetheless, the bonding between the two aluminum alloys was complete. Additionally, the mechanical mixing of the material in the dissimilar welds becomes more uniform, if the rotational speed becomes faster, and the single or multiple cells of the material flow with the alternative lamellae of different alloy constituents becomes rounder and more complete. A higher rotational speed results the return flow of the material more momentum to penetrate wider and mix more

homogeneously, although this means the return flow has to travel a longer distance and at a higher velocity into the center of the nugget. Figure 1.33 shows the effect of 57mm/min and 229mm/min welding speeds on the material flow and mechanical mixing in the dissimilar 6061-Al to 2024-Al welds at rotational speed of 637 rpm.

Abdollah-Zadeh, Saeid & Sazgari (2008) studied microstructural and mechanical properties of friction stir welding 1060 aluminum alloy and pure copper plates for lap joining. They found out that moving of material from the retreating side to advancing side at the top surface of the weld results in vertical flow of material about the longitudinal axis of the weld. As a result of this the plate interface transverse section of a AL-Cu joint could be transported vertically as shown in Figure 1.34a and the strength of the lap weld would be affected. The microstructure of the aluminum stir region was described by equiaxed fine grains as shown in Figure 1.34b. Elongated grains and layers regions in TMAZ are shown in Figure 1.34c. The slightly coarser grains than grains in stir area, which are in HAZ on the advancing side is shown in Figure 1.34d. They also observed a black area which consists of intermetallic compounds of Al_4Cu_9, AlCu and Al_2Cu near to Al/Cu interface and extended toward the advancing side of the joints with increasing the travel speed to reach the aluminum surface at the highest travel speed. Aluminum and copper can be successfully lap joint by producing friction stir welding.

One of the latest studies was done by Liu, Shi, W. Wang, X. Wang & Zhang (2008) about joining copper T2 and aluminum 5A06 dissimilar materials by friction stir welding. Their analysis showed that Cu and Al were closely combined in the Al side, and formed a mixed structure. But, the Cu and Al showed a lamellar alternating structure characteristic.

1.2.1.2   *Material Flow Modeling*

The material flow during friction stir welding is complicated process. There are many factors such as tool geometry like pin and shoulder design and relative

dimensions of pin and shoulder; welding parameters like rate of tool rotation and direction of the rotation (clockwise or counterclockwise), transverse speed, plunge depth and spindle angle; types of material; temperature of the work plates. The material flow is combination of the various uncontrolled deformation processes in the nugget zone. A number of studies have been performed to model the materials flow during friction stir welding using by analytical, numerical, thermal-mechanical, material constitutive behavior, mixed zone, single slip surface and extrusion zone. On the other hand, the first studies were the 2-D flow around the pin at near the surface rather than the full 3-D flow which has better computational efficiency benefits, if it has been accurately modeled. Below efforts were different examples of basic physics of the material flow during friction stir welding and also helped to understand phenomenon of material flow.

1.2.1.2.1   Analytical Flow Modeling. By pretending a basic view of the flow pattern and tool/workpiece interface status have been tried out for analytical flow modeling method in friction stir welding, instead of assuming tool forces, torques or heat generation. Stewart, Adams, Nunes & Romine (1998) considered two material flow theories that are a mixed-zone flow modeling and a single slip surface modeling. In the mixed-zone model, the material in the plastic zone moves in a vortex system with an angular velocity of the tool at the interface of the tool and workpiece. The angular velocity reaches to zero at the boundary of the plastic zone. In the single slip surface model, the main rotational slip happens at a contracted slip surface outside the interface of the tool and workpiece. Using a limited region of slip appeared more consistent with experimental measurement by predictions of the thermal field, the force and the weld region shape (Mishra & Mahoney, 2007, Chap.10).

1.2.1.2.2   Numerical Flow Modeling. Numerical friction stir welding flow modeling can be expressed like other processes used for friction welding, extrusion, machining, forging, rolling and ballistic impact. There are different computational codes for friction stir welding numerical flow modeling known finite element, finite

volume method or shock wave physics codes. The most popular analysis is used for computational fluid dynamics as known CFD which accepts material flowing is viscous fluid flow instead of solid plasticity (Mishra & Mahoney, 2007, Chap.10).

Numerical flow models can use Eulerian or Lagrangian formulation or a hybrid of these two formulations that is arbitrary Lagrangian-Eulerian (ALE) for the mesh design as for heat flow analyses, however, the difference is important. In a Lagrange analysis, the mesh is attached to the material, but the material itself deforms, so this causes the mesh deformation. Before mesh distortion causes to breakdown of the analysis, a fine mesh in the deforming regions and frequently remeshing are necessary for best result.

The CTH code that is a three-dimensional code capable of solving time-dependent equations of continuum mechanics and thermodynamics is a software system developed by Sandia National Laboratories, to model multidimensional, multi-material, large deformation, strong shock wave physics. One-dimensional rectilinear, cylindrical, and spherical meshes; 2-D rectangular and cylindrical meshes; and 3-D rectangular meshes simulations are available. CTH code simulation has a two-step Eulerian solution scheme is used with these meshes. The first one is a Lagrangian simulation in which the cells distort to follow the material motion. The second one is a remeshing where the distorted cells are mapped back to the Eulerian mesh (Mishra & Mahoney, 2007, Chap.10).

Xu, Deng, Reynolds & Seidel (2001) expressed to simulate the friction stir welding process by using two finite element models which are the slipping interface model and the frictional contact model. The simulation predictions of the material flow pattern depended on these finite element models carefully considering with an experimentally found pattern.

Seidel and Reynolds (2002) developed a two-dimensional friction stir welding process model based on the fluid mechanics and handles the solid state material

transport during welding as a laminar, viscous flow of a non-Newtonian fluid past a rotating circular cylinder, where the friction stir welding tool was represented by pin only. Eulerian flow formulation has been used for modeling. CFD code FLUENT was used to simulate the friction stir welding process.

Colegrove & Shercliff (2003) modeled an application of the two-dimensional metal flow in friction stir welding of the computational fluid dynamics (CFD) code by FLUENT. They studied a quantitative method of comparing the flow around the different tool shapes. They found out a slip model where the interface conditions were controlled by the local shear stresses. Therefore two different interface conditions can exist simultaneously on different parts of the pin; stick condition and slip condition. The slip condition has a significant effect on total material flow when compared with the stick condition assumption.
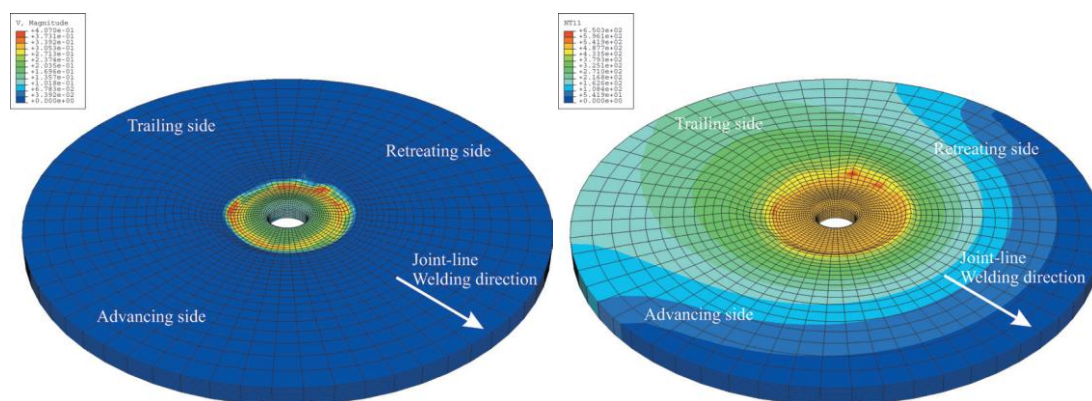
Figure 1.35 Three-dimensional FE model results. Matrix shown for the entire local model. a) Magnitude of velocity vector after 10.0s, b) Temperature field after 10.0s (Schmidt & Hattel, 2004).

Colegrove & Shercliff (2005) also modeled 3-dimensional metal flow around a threaded tool in friction stir welding by using computational fluid dynamics CFD code modeling by FLUENT. The threaded tool that was ranked 2.5˚ away from the direction of travel model was compared a normal threaded tool and normal unthreaded tool. All the models suggested that the material in line with the deformation zone was swept around the retreating side of the pin. The amount of material swept around the pin accumulated at locations closer to the shoulder. On the

other hand, the experimental observation showed that the size of the deformation zone was less than computational values.

1.2.1.2.3   Thermo-mechanical Flow Modeling. The heat generation around tool interface comes from viscous dissipation and friction and conduction bring about thermal rise away from the tool interface, however at the interface, the loop is closed by temperature dependence of the viscosity and friction conditions. The most of the heat generation occurs in a thin layer close to tool. The thermal problem can be solved by imposing the heat flux at the tool and workpiece interface when the heat input estimation can be measured or estimate independently. Then, the result of the thermal area is imposed on a flow model. The thermal and flow models can be analyzed sequentially much faster than fully coupled analysis that needs to converge on temperature and flow areas that are spatially self-consistent with the heat generation and conduction (Mishra & Mahoney, 2007, Chap.10).

Schmidt & Hattel (2004) developed fully coupled thermo-mechanical three-dimensional FE model in ABAQUS/Explicit by using the arbitrary Lagrangian-Eulerian formulation and Johnson-Cook material law in friction stir welding. The compressibility of the model has been covered by including the elastic response of the aluminum matrix. The contact forces are modeled by Coulomb's Law of friction, creating the contact condition very solution dependent. Moreover, separation between the workpiece and tool was not omitted as the most of the other models. The material is forced to keep contacting with the tool in all other models. Figure 1.35 shows the temperature and magnitude of the velocity vector after 10s respectively, for the workpiece matrix in the local model. They did not observe any void formation.

1.2.1.2.4   Metallurgical Flow Modeling. The resultant microstructure and metal flow features of a friction stir welding approximately similar to hot worked microstructure of typical aluminum extrusion and forging suggested by Arbegast (2003). Thus, the FSW process can be modeled as a metalworking process in terms

of five conventional metal working zones: (a) preheat, (b) initial deformation, (c) extrusion, (d) forging, and (e) post heat/cool down Figure 1.36. The frictional heating of the rotating tool and adiabatic heating increase temperature because of the deformation of material in the preheat zone in front of the pin. The thermal properties of material and the traverse speed of the tool control the size and heating rate of this zone. When material is heated above the critical temperature and the amount of stress exceeds above the critical flow stress of the material, an initial deformation zone forms by each the tool movement forward. As shown in Figure 1.37, the material is pushed to upper into the shoulder zone and lowers into the extrusion zone. In the swirl zone, a small amount of material is captured near the pin tip where a vortex flow pattern forms. Material flows around the pin from the front to the rear in the extrusion zone. The material from the front of the tool is forced into the cavity left by the forward moving pin under hydrostatic pressure conditions in the forging zone. The material is kept in the cavity by aiming tool shoulder that also applies a downward forging force. Where the tool leaves the welded area is the post heat/cool zone. The material is cooled passive or forced cooling conditions in the post heat/cool zone. This flow model is included relationship between tool geometry, operating parameters, and flow stress of the materials being joined. Moreover, the results of calculated temperature, width of the extrusion zone, strain rate, and extrusion pressure are consistent with experimental observations (Mishra & Ma, 2005).

1.2.2 Temperature Distribution Of Friction Stir Welding

Understanding the heat generation between the tool and the workpiece at the interface is the most important issue for successful FSW process. It is important to obtain information about temperature distribution during FSW, because the temperature distribution within and around the stirred zone directly influences the microstructure of the welds, such as grain size, grain boundary character, coarsening and dissolution of precipitates, and resultant mechanical properties of the welds. The heat flux must keep the maximum temperature in the workpiece high enough so that

the pin can be easily stirred the well enough softened material. On the other hand, maximum temperature should not exceed the melting temperature of the materials to does not melt. The maximum temperature generated by FSW process ranges from 80% to 90% of the melting temperature of the welding material (Mishra & Ma, 2005 and Chao, Qi, & Tang, 2002).
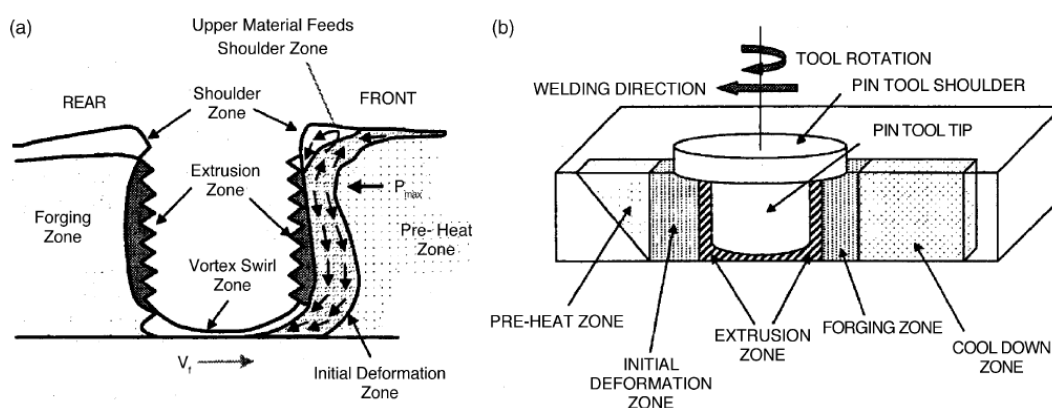
Figure 1.36 a) Metal flow patterns, b) metallurgical processing zones developed during FSW (Mishra & Ma, 2005).
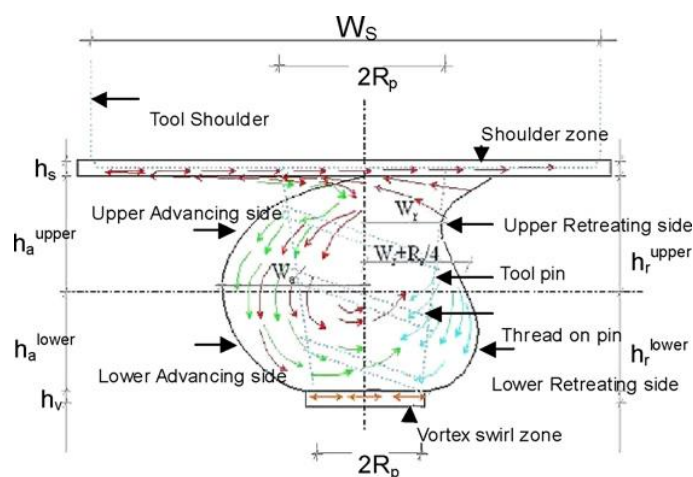
Figure 1.37 Model of metal flow pattern in friction stir welding (Rajesh et al. 2007).

The friction and the deformation process in the friction stir welding is primary cause of the heat flux. This heat is transmited to both the tool and the workpiece. The amount of the heat conducted into the workpiece determines an accurate FSW process, the quality of the weld, shape of the weld, micro-structure of the weld, and

also the residual stress and the workpiece distortion. The amount of the heat is absorbed by the tool is effects the life of the tool and the capability of the tool for the joining process. For example, if the material is not soft enough, the friction could cause to breakage of the pin of the tool, because of insufficient heat. Thus, understanding the heat transfer situation of the FSW process is extremely important, for improving the process. Moreover, the cost of the production process is related the energy consumption of the friction stir welding (Chao et al., 2002).

The temperature distribution within the workpiece during the friction stir welding can be researched by analytical models and experimental methods. Chao & Qi (1999), modeled the heat generation comes from the assumption of sliding friction, where Coulomb's law is used to estimate the shear or friction force at the interface. Besides, the pressure at the tool interface is assumed to be constant, by means of that enabling a radially dependent surface heat flux distribution as a demonstration of the friction heat generated by the tool shoulder, even though probe surface heat generation is neglected. Chao et al. (2002) formulated heat transfer of the friction stir welding as a form of two boundary value problems. The qualification of physical values of the process the temperatures in the workpiece and the tool are measured during FSW. The heat flux generated from the friction to the workpiece and the tool was determined by using the measured transient temperature fields' finite element numerical analyses.

Frigaad, Grong & Midling (2001) developed numerical three-dimensional heat flow model for friction stir welding of age hardenable aluminum alloy by using method of finite differences. The pressure cannot exceed the actual flow stress of the material at the operating temperature by adjustment of the friction coefficient at elevated temperatures.

Colegrove, Painter, Graham & Miller (2000) estimated the heat generation distribution for tools with a threaded probe by using an advanced analytical estimation of the heat generation. The fraction of heat generated by the probe is

estimated to be as high as 20%. This means that the analytical estimated probe heat generation contribution is not negligible.

Zahedul, Khandkar & Kahn (2001) modeled the heat transfer for overlap friction stir welding with the finite element method by using a moving heat source. Song & Kovacevic (2002) introduced a model that is moving coordinate to reduce the difficulty of modeling the moving tool in a three-dimensional heat transfer model for friction stir welding. The model was included the heat input from the tool shoulder and the tool pin. A non-uniform grid mesh is generated by the finite difference method was used in solving the control equations. The calculated and experimental results were concurrent. The preheating the workpiece is beneficial to increase the temperature of the workpiece in front of the tool pin, making the material easy to be welded during the friction stir welding and the calculation result also shows that. Preheating is also protected the tool from being worn out. In addition to this, a higher initial temperature in the workpiece during FSW can be approached by using an insulated backing plate to reduce the heat loss or by applying the laser to assist preheating the workpiece during FSW (Kohn, Greenberg, Makover & Munitz, 2002).

Schmidt, Hattel & Wertet (2003) established an analytical model for heat generation by friction stir welding, based on different assumptions of the contact condition between the rotating tool surface and the workpiece. The flexibility of this model to include the heat generation and material flow were characterized by the contact conditions at the interface, and are described as sliding, sticking or partial sliding/sticking and tool design e.g. conical surfaces and threads. The sliding condition yields a proportional relationship between the plunge force and heat generation. On the other hand, the sticking condition must be presented at the tool/matrix interface.

Chen & Kovacevic (2003) were studied the thermal history and thermomechanical process in the butt-welding of aluminum alloy 6061- T6 for a three-dimensional model based on finite element analysis. The model includes the mechanical reaction

of the tool and thermomechanical process of the welded material. The heat source incorporated in the model affects the friction between the material and the probe and the shoulder. In order to build a quantitative framework to understand the dynamics of the FSW thermomechanical process, the thermal history and the evolution of longitudinal, lateral, and through-thickness stress in the friction stirred weld are simulated numerically.
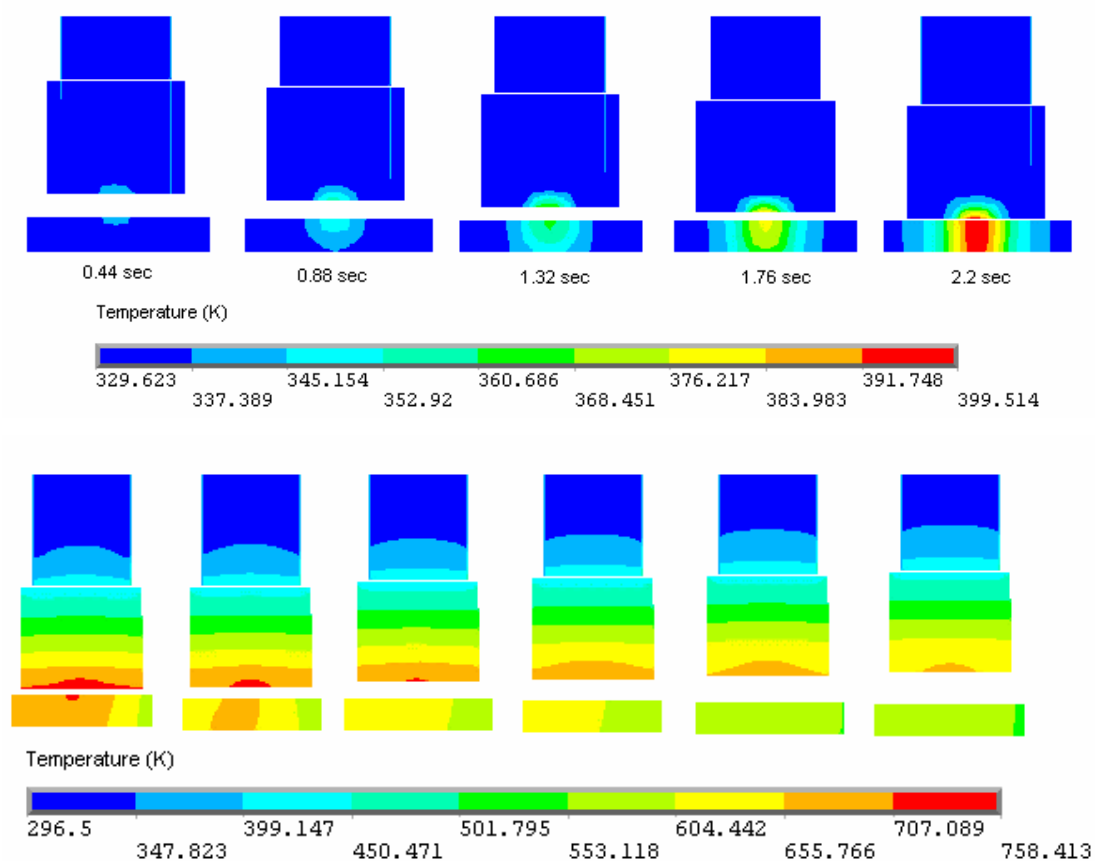
Figure 1.38 Temperature-time history for tool and workpiece during, a) tool pin penetration and, b) tool pullout (V = 5.5 mm/s, ω = 344 rpm) (Soundrarajan, 2006).

The moving heat sources of the shoulder and the probe are represented as moving the heat generation of the nodes in each computational time step in modeling the temperature history. The mechanical effect of the shoulder in the mechanical model has comparatively a bigger contact surface of the shoulder and the workpiece is expected to contribute a large part of the mechanical stress, mainly in the up-half part of the weld.
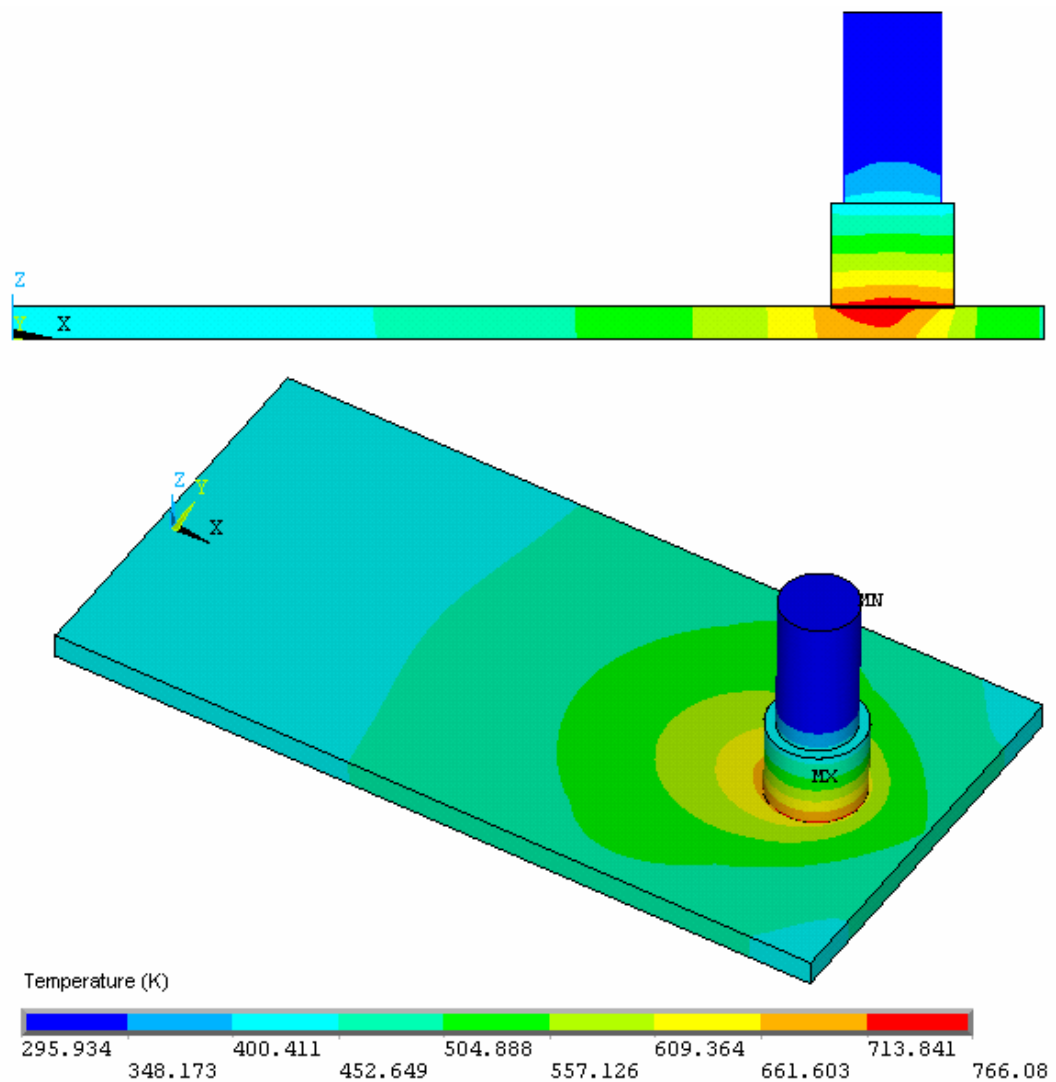
Figure 1.39 Calculated temperature field distribution for the integrated tool workpiece model (V = 5.5 mm/s, ω = 344 rpm) (Soundrarajan, 2006).

The temperature gradient is large around the welding zone and therefore, it seriously changes the materials properties. As a means to increase the precision of the mechanical solution, the thermal and mechanical solutions are coupled: the temperature data at each increment time was used to evaluate the mechanical properties and the thermal parameters. The highest temperature was observed in the center of the welding region extending down from the crown surface to the pin root side, but the rotation of the shoulder and pin contributes the highest heat flux in this region. The results of study show that the maximum temperature gradients in longitudinal and lateral directions are located just beyond the shoulder edge.

Moreover, the longitudinal residual stress is greater than the lateral residual stress at the top surface of the weld (Chen & Kovacevic 2003).

Khandkar, Khan & Reynolds (2002) proposed to study a three-dimensional thermal model that was the transient temperature distributions during the friction stir welding of aluminum alloys. They introduced a torque based heat input model, where the torque/power known from experiments is used in the expression for the heat source. The numerical results of the analyses have also been presented to study the effects on the thermal profiles of (i) different heat transfer conditions at the bottom of the workpiece, (ii) backing plates of different material means different conductivities, and (iii) different contact gap conductances at the interface between workpiece and backing plate.

Recently, Soundrarajan (2006) researched thermo-mechanical finite element model with adaptive boundary conditions and two-dimensional process model of local heat transfer and material flow using CFD for joining similar and dissimilar materials by friction stir welding. Theoretically, the convection heat-transfer coefficients of the surfaces exposed to air can be determined using Newton's law of cooling. Contact conductance depends on the pressure at the interface and has a non-uniform variation. The actual pressure distribution along the interface is dependent on the thermal stress from local temperature and non-linear stress-strain state. As a result, applying an adaptive contact conductance can make the model more strong for process parameter variations. He used a finite element thermo-mechanical model with mechanical tool loading considering a uniform value for contact conductance for predicting the stress at the workpiece and backing plate interface. These pressure distribution contours were used for defining the non-uniform adaptive contact conductance and so, the thermal history and stresses in the workpiece were predicted by repeating the simulation. In this model, the FSW process is divided into the following three phases: (a) the penetration phase, (b) the welding phase and (c) the tool pull-out phase. During the penetration and pullout of the pin, the cross-sectional views of the calculated temperature contours in the workpiece and tool at different

times as shown in Figure 1.38. At the end of the process, the longitudinal view of calculated temperature filed distribution along the joint line was shown in Figure 1.39.
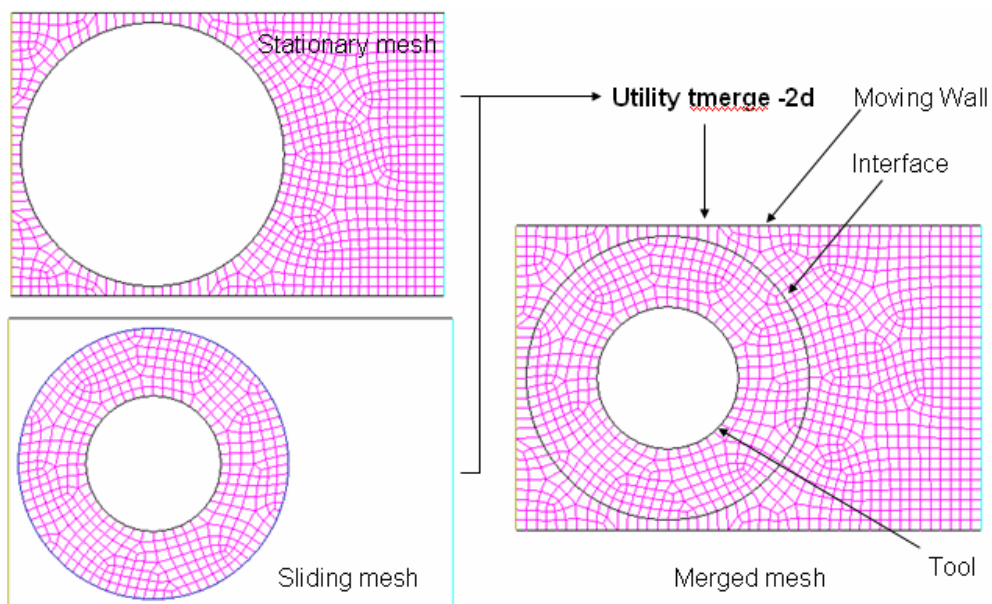
Figure 1.40 Mesh structure – merging stationary and sliding meshes (Soundrarajan, 2006).

He used the sliding mesh capability of FLUENT to predict the time-dependent flow across a two-dimensional tool pin. Stationary and sliding meshes were created separately. As the time progresses, the sliding mesh was rotated with the angular velocity used for the experimentation. The meshes were joined together using a t-merge utility which merges two meshes into a single mesh as shown in Fig. 1.40. The sliding mesh was given an angular velocity and time step used was 0.1 sec was used in the current model. The computed temperature contours lines as shown in Figure 1.41.

Soundrarajan (2006) firstly developed a thermal model to predict the temperature contours. The viscosity values are input as piecewise linear temperature dependent and the steady state material flow streamlines were generated based on the obtained temperatures. Then he solved the model for transient flow and the obtained velocity

vectors of the material flow after various time intervals. He summarized most important characteristics of the model as follows:

(i) Temperature dependent material properties incorporated in the models using piecewise linear in the material property specifications, (ii) User-defined Function is used to define the heat generation in the model, (iii) Sliding mesh is used for considering the angular velocity of the tool rotation, (iv) Viscosity values are determined for a range of temperature based on the thermal model and applied in the material flow model, (v) 2-D CFD models have been developed to predict the thermal field and material flow near the tool matrix, (vi) 2-D model of the flow around a rotating tool pin is used to gain better understanding of the process, (vii) Sliding mesh is used for modeling the tool rotation in the transient model, (viii) The results of the flow simulation compared with post-weld marker experimental results. The model predicts a similar pattern.
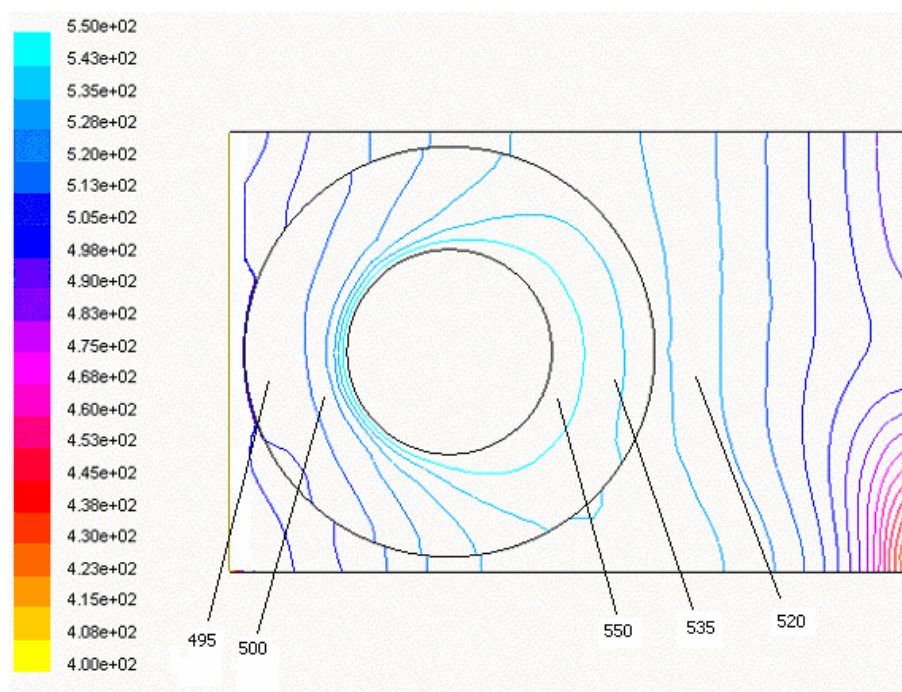
Figure 1.41 Computed temperature contours (Soundrarajan, 2006).

Hwang, Kang, Chiou & Hsu (2007) studied to explore experimentally the thermal histories and temperature distributions in a workpiece during a friction stir welding

(FSW) process involving the butt joining of aluminum 6061-T6 for different types of thermocouple layout in the workpiece were devised to measure at different locations on the workpiece. Regression analyses are used by the least squares method to predict the temperatures at the joint line. As a result of this, the temperatures inside the pin can be regarded as a uniform distribution and that the heat transfer starts from the rim of the pin to the edge of the workpiece. They found a second-order polynomial curve to best fit the experimental temperature values in the width direction of the workpiece. The temperatures on the advancing side are slightly higher than those on the retreating side. The workpiece material stick on the pin and shoulder was the result of the too high temperature, and larger grain sizes of the micro-structure in the welds may also be obtained.

Another new reseach was done by Schmidt & Hattel, (2007) proposed the basic elements of the thermal modeling of friction stir welding as well as to clarify some of the uncertainties in the literature regarding the different contributions to the heat generation. A new thermal pseudomechanical model in which the temperature-dependent yield stress of the weld material controls the heat generation was also presented. Both the friction coefficient under the assumption of sliding and the material yield shear stress under the assumption of sticking are the major unknown parameters in these expressions. These parameters can be obtained either by measuring or assuming. But, in this study they measured these key values experimentally. In practice, this is what has been done during experiments where tool forces and torque have been measured, from which the average friction coefficient and yield shear stress are estimated.

In Schmidt & Hattel's (2007) method is based on a high degree of knowledge regarding the plastic behavior of the workpiece material at elevated temperature, i.e. that the yield stress suddenly decreases when the temperature approaches the solidus temperature, above which the material acts as a fluid. Therefore, the material close to the tool/matrix interface reduces negligible amount of heat generation if it exceeds the solidus temperature, allow the material to recover its strength by reducing the

temperature level. Accordingly, a self-stabilizing effect creates at a temperature level below the solidus temperature. In spite of this, dissimilar material laws used in flow models, the strain rate dependence do not contain the model. The model demonstrates very beneficial results as compared to existing more classical thermal models of FSW as well as compared to experimental measurement of temperatures. So the reliability and the applicability of pure thermal models have been extended to a new stage.
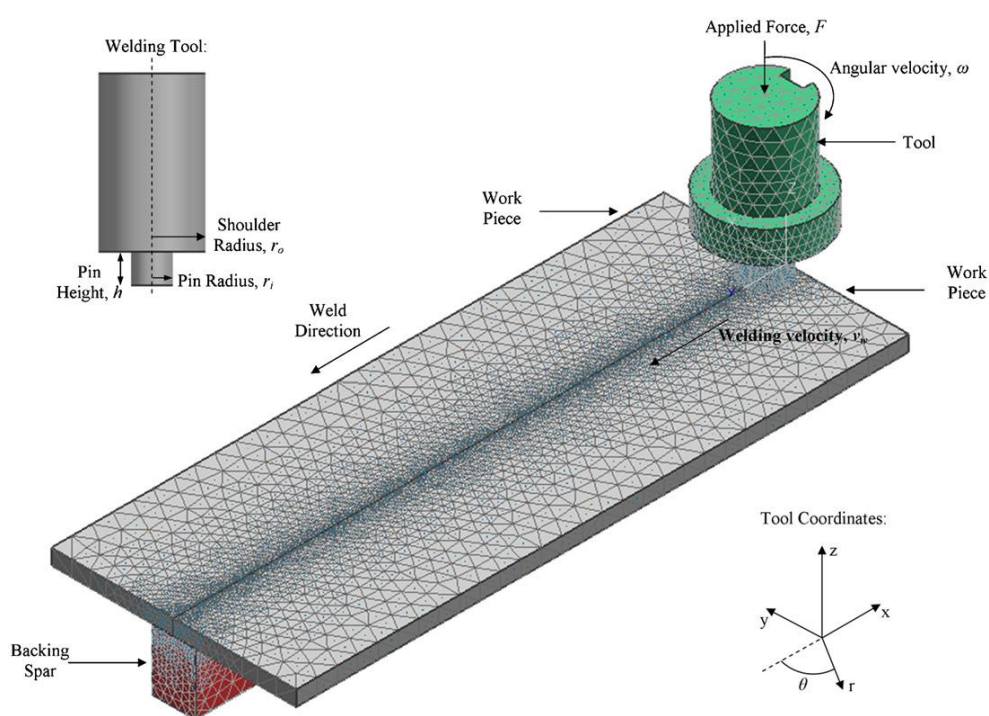
Figure 1.42 Finite element model of FSW, tool coordinate system and tool geometry (Hamilton, Sommers & Dymek, 2008).

Lastly, Hamilton, Dymek & Sommerset (2008) and Hamilton, Sommers, & Dymek (2008) are presented two studies. First one, Hamilton, Dymek & Sommerset (2008) proposed to develop that utilizes a new slip factor which is derived from an empirical, linear relationship observed between the ratio of the maximum welding temperature to the solidus temperature and the welding energy based on the energy per unit length of weld for a thermal model of friction stir welding. The maximum welding temperature over a wide range of energy levels was successfully predicted

by the thermal model but under predicts the temperature for low energy levels for which heat from plastic deformation dominates. The relationship between the temperature ratio and energy level is characteristic of aluminum alloys that share similar thermal diffusivities were supported by this thermal model. In this model was introduced a scaling factors that partitions the heat generation between plastic deformation and friction. Because, aluminum alloys with similar thermal diffusivities reveal the same relationship between the ratio of the maximum welding temperature and solidus temperature and the welding energy, the maximum welding temperature of an alloy may be approximated from the characteristic curves generated by the thermal model if the thermal diffusivity, welding parameters and tool geometry are known. Figure 1.42 shows the finite element model of friction stir welding tool coordinate system and tool geometry.
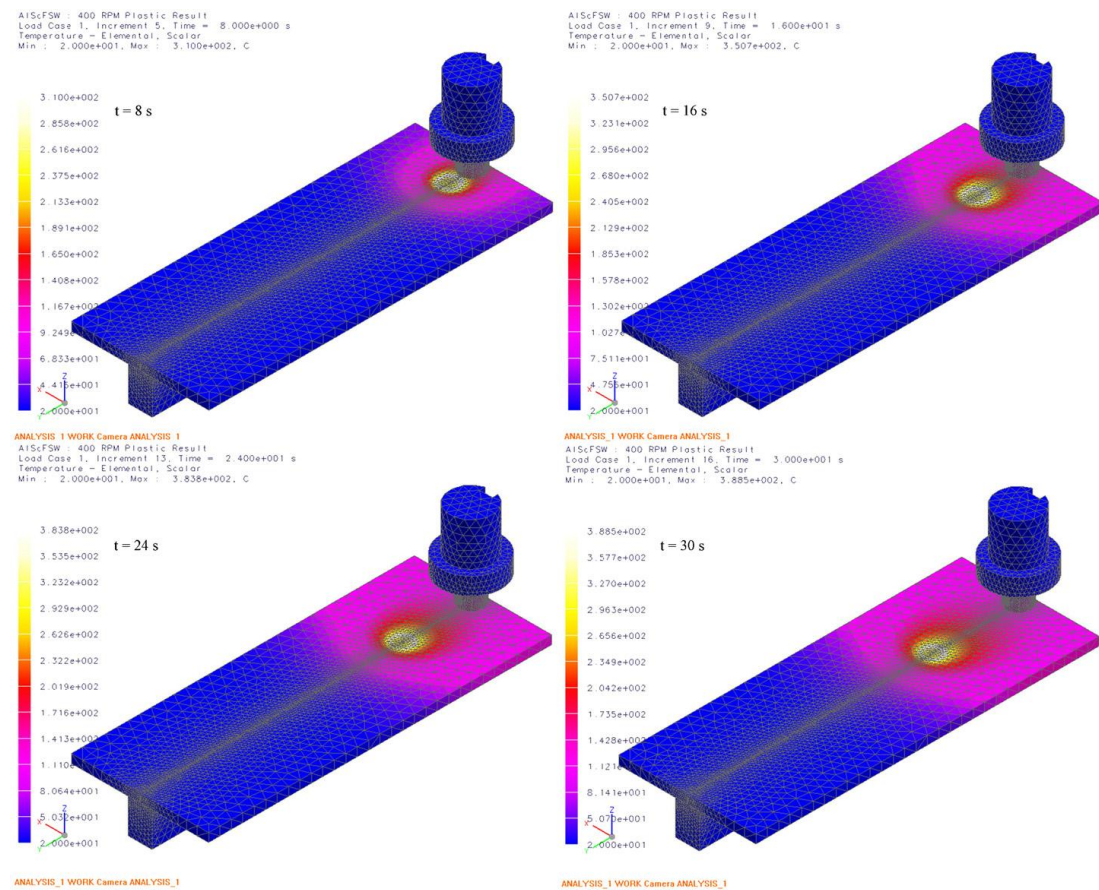
Figure 1.43 Temperature distributions during FSW as predicted by the thermal model at four subsequent times (Hamilton, Sommers & Dymek, 2008).

Second study, Hamilton, Sommers & Dymek (2008) proposed that an energy-based formulation of the Johnson–Cook plasticity model which was derived from an empirical, linear relationship observed between the ratio of the maximum welding temperature to the solidus temperature of the alloy and the welding energy in order to account for heat generation due to plastic deformation for a thermal model of friction stir welding. The thermal model successfully predicts the maximum welding temperatures and temperature distributions over the energy range investigated for the Sc-modified Al–Zn–Mg–Cu alloy extrusions joined by friction stir welding at keeping all the welding parameters constant except tool rotation rate. The thermal model accurately predicts the maximum weld temperatures and temperature profiles at the higher energy weld conditions, with the incorporation of heat generation due to plastic deformation. The model under-predicts the maximum weld temperatures under the tool shoulder at the lower energy welds where plastic deformation contributes a larger portion to the total heat generation. Figure 1.43 shows the thermal distribution in the workpiece at various elapsed times during the simulation
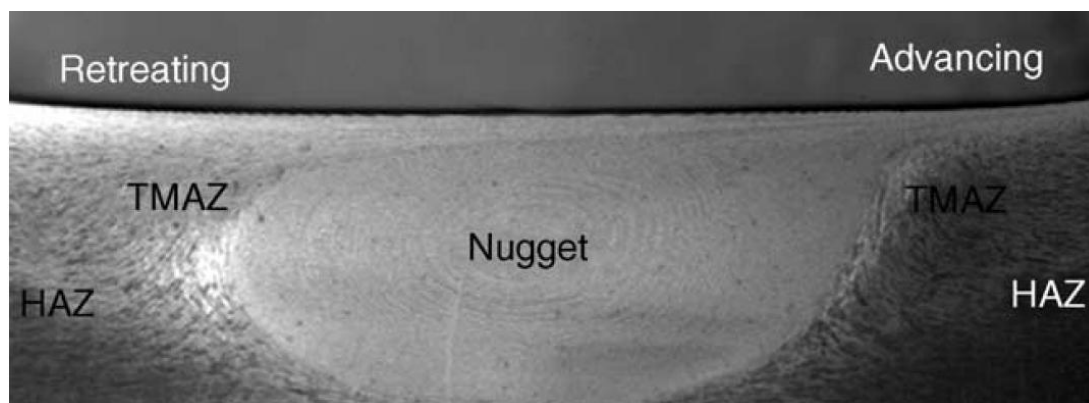
Figure 1.44 A typical macrograph showing various microstructural zones in FSP 7075Al-T651 (standard threaded pin, 400 rpm and 51 mm/min) (Mishra & Ma, 2005).

1.3 Microstructural Evaluation

The microstructural distributions produced during the friction stir welding of aluminum alloys are dependent on so many factors like alloy composition, alloy temper, welding parameters, gage of the welded plate and other geometric effects. Recrystallization and development of texture within the stirred zone and also,

precipitate dissolution and coarsening within and around the stirred zone are result of the contribution of intense plastic deformation and high-temperature exposure within the stirred zone during FSW/FSP. The microstructural characterization of grains and precipitates has three distinct zones which are stirred (nugget) zone, thermo-mechanically affected zone (TMAZ), and heat-affected zone (HAZ), have been identified as shown in Figure 1.44. The result of the mechanical properties of welding affected the microstructrual changes in various zones (Mishra & Ma, 2005).
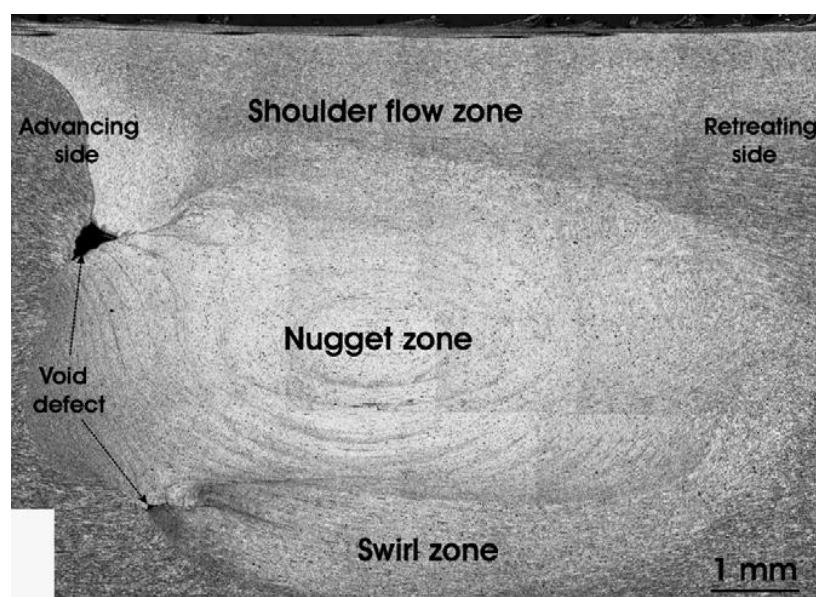
Figure 1.45 A transverse cross-section of a weld plate showing the top zone, Nugget zone and the swirl zone (Chen, Pasang & Qi, 2007).

1.3.1 Nugget Zone (NZ)

The plastic deformation and recrystallization of the fine-grained microstructural of weld metal by stir action and frictional heat was usually occurred during the friction stir welding. This region is known as weld nugget or nugget zone or sometimes named as dynamically recrystallized zone (DXZ). Onion ring structure that is the most prominent features has been observed most of the stir welding process. The peak temperature and the quenching rate from that temperature are two variables that determine the properties of material in the nugget zone.

Chen, Pasang & Qi (2007) studied the flow of the shear layer around the tool pin and how it deposits into the cavity at the trailing end of the pin to form the weld nugget zone during friction stir welding. An alternative experimental technique was used to "freeze" the tool pin which was done by naturally breaking the pin during FSW and hence the tool pin can be embedded in the workpiece.
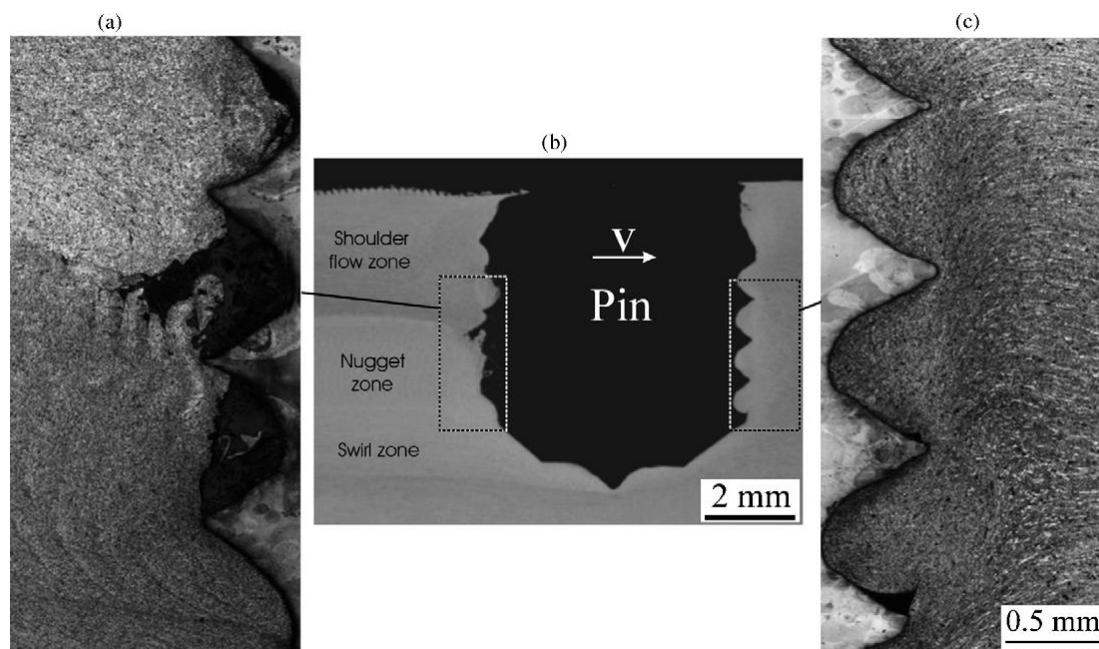
Figure 1.46 Longitudinal cross-section of another weld plate with the broken pin embedded, sectioning along the mid-section of the pin (sectioning plan normal to the plate). (a and c) are higher magnification micrographs taken in locations as indicated in (b) (Chen, Pasang & Qi, 2007).

A shoulder flow zone, a nugget zone with a ring/layer structure, and a swirl zone are three different zones which is a typical transverse cross-section of the welds shown as in Figure 1.45. Seidel and Reynolds (2001) were explained the major features of characterizations of the nugget zone region is as plastically deformed, a fine relatively equiaxed, recrystallized grain structure and outside of the nugget on either side a second region or swirl zone is as deformed with less extension, depending on the alloy, may or may not show signs of recrystallization and last one, shoulder flow zone which is above the nugget zone is as its formed when the rotational tool shoulder passes over the weld, not symmetric about the centerline of the weld.

Another weld sample with a broken pin embedded with longitudinal cross-section that is sectioning through the broken pin is shown in Figure 1.46 (Chen, Pasang & Qi, 2007). When the vertical rotation does not appear to have more than 3–4˚, the pin may have been seen a little pressed forward after the breaking of the pin although the overall characteristic has been affected insignificantly. Filling behind the tool pin to form the Nugget zone (through lamellarly deposition) is importantly ahead of the top shoulder flow zone filling (through forging action of the shoulder) in during FSW. The flow that bring about forming the Nugget zone stopped, when a pin broke during FSW. Still, the top shoulder zone continued to be filled and forged forward and downward direction since the pin shoulder continued rotating and moving forward after the pin broke. Therefore, the top shoulder flow zone has widened and the Nugget zone material would also be pressed forward slightly.
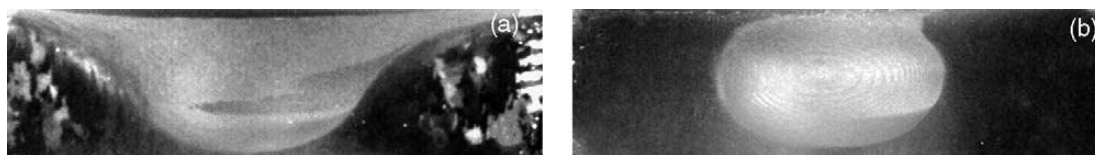
Figure 1.47 Effect of processing parameter on nugget shape in FSP A356: (a) 300 rpm, 51 mm/min and (b) 900 rpm, 203 mm/min (standard threaded pin) (Mishra & Ma, 2005).

1.3.1.1   *Shape of Nugget Zone*

The various shapes of nugget zone have been observed as depending on processing parameter, tool geometry, temperature of workpiece, and thermal conductivity of the material. Fundamentally, nugget zone can be categorized into two types, basin-shaped nugget that widens near the upper surface and elliptical nugget. The formation of basin-shaped nugget was reported by Sato, Kokawa, Enomoto, & Jogan (1999) and Sato, Urata & Kokawa (2001)for 6063Al-T5 plate on friction stir welding. They proposed that the upper surface experiences extreme deformation and frictional heating by contact with a cylindrical-tool shoulder during FSW, by means of that resulting in generation of basin-shaped nugget zone. Conversely, Rhodes, Mahoney, Bingel, Spurling & Bampton (1997) and Mahoney, Rhodes, Flintoff,

Spurling, & Bingel (1998) reported elliptical nugget zone in the weld of 7075Al-T651.

Recently, a study on the effect of FSP parameters on joint's microstructure and properties on joint's of cast A356 suggests that with identical tool geometry, it is possible to generate the basin-shaped nugget zone at lower tool rotation rate of 300–500 rpm while elliptical nugget zone was generated at higher tool rotation of >700 rpm, as shown in Fig 1.47 (Mishra & Ma, 2005). By changing processing parameters, different nugget shapes can be obtained with same tool geometry.
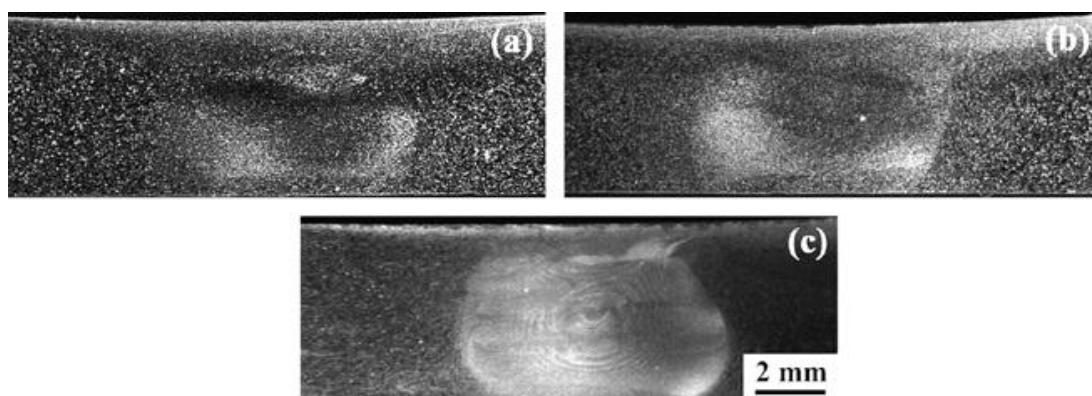
Figure 1.48 Cross-section macrographs of FSW copper joints: (a) 800 rpm, (b) 600 rpm, (c) 400 rpm (the advancing side is on the right) (Xie, et al., 2007).

Xie, Ma & Geng (2007) investigated the properties of a nugget zone in friction stir welded pure copper. They found out that defect-free pure copper welds were achieved under low heat input conditions of 400–800 rpm for a traverse speed of 50 mm/min. In this study, they worked less input than previous reports. This indicates that sound welds can be achieved under relatively low heat input conditions for copper which is also difficult to weld by conventional fusion welding processes because of its thermal diffusivity, which is about 10 to 100 times higher than in many steels and nickel alloys. The typical cross-sectional macrographs of the FSW copper weld are shown in Figure 1.48, while the nugget zone at 600 and 800 rpm did not show a clear outline, an elliptical-shaped nugget zone with obvious onion rings was observed at 400 rpm, and there was a clear boundary between the nugget zone and the thermomechanically affected zone.

Reynolds (2000) reported the relationship between nugget size and pin size. He noted that the nugget zone was relatively larger than the pin diameter, except at the bottom of the weld where the pin tapered to a hemispherical termination. In addition to this, if the pin diameter increases, the nugget obtained a more rounded shape with a maximum diameter in the middle of the weld.
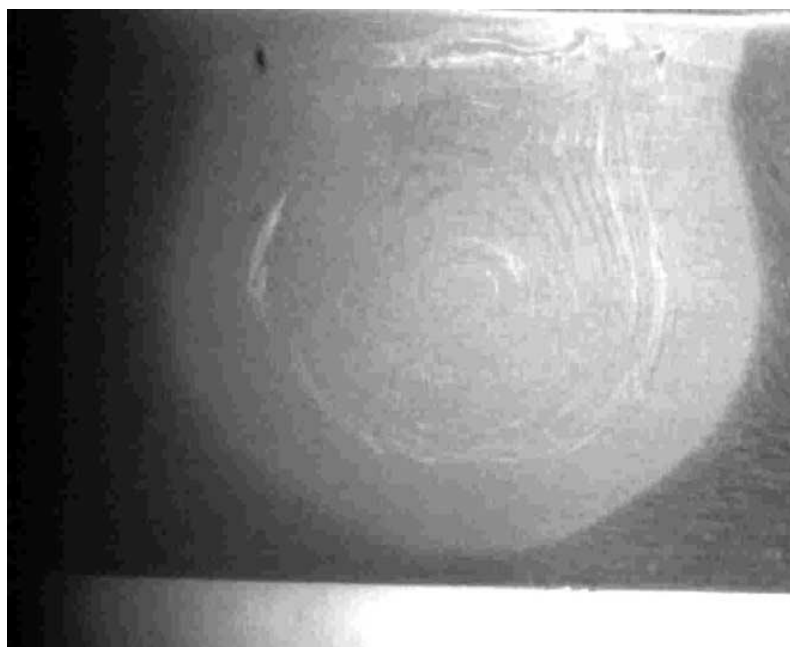
Figure 1.49 Onion rings in the cross-section of a FSW (Krishnan, 2001).

Hartawan, Thoe, Ng, Wu, & Liu (2009) demonstrated feasibility of butt welding aluminum, in particular marine grade aluminum 5083 plate. They proved the strong and sound joint strength of almost the same strength of its base material (91-95%) as an advantage of this welding technique. The basin-shaped nugget was expected at comparatively lower value of rpm speed of 300 rpm, while the exact transitional range of values for the nugget to change in shape may remain different.

1.3.1.1.1   Onion Ring Formation in Friction Stir Welding. The most important characterization of the most of the friction stir welding process is onion rings formation. When you look at the cross-section of the friction stir welding, onion rings can be easily observed as shown in Figure 1.49. These swirl patterns of the onion rings are in a plane 90° to the rotation plane of the tool.

Biallas, Braun, Donne, Staniek & Kaysser (1999) investigated the formation of onion rings was attributed to the reflection of the material flow nearly at the imaginary walls of the patterns that would be formed in the case of regular milling of the metal. The induced circular motion causes circles that shrink in radius and form the tube system. Threadgill (1999) precisely reported that the onion ring formation was associated with the forward motion of the tool in one revolution. On the other hand, there wasn't any discussion about explanation and the formation process affecting the properties of the weld.
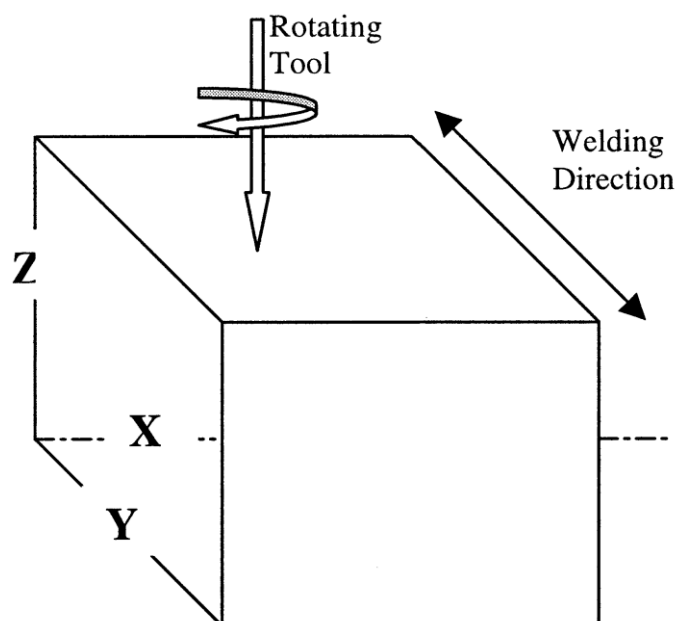
Figure 1.50 Scheme for the various pictures presented later in this work (Krishnan, 2001).

Krishman (2001) examined 6061Al and 7075Al alloys formation of onion rings by using different friction stir welding parameters. Schematic view of his work is as shown in Figure 1.50. He studied that the formation of onion ring is found to be geometric effect in the welded zone due to the fact that cylindrical sheets of material are extruded throughout each rotation of the tool and the cutting through the section of the material produces an 'Onion Rings' structure. The tool appears to wait for a very short time to generate frictional heat and form a cylindrical shaped material

around to the retreating side of the joint. The spacing between the rings has been found to be equal to the forward motion of the tool in one rotation.
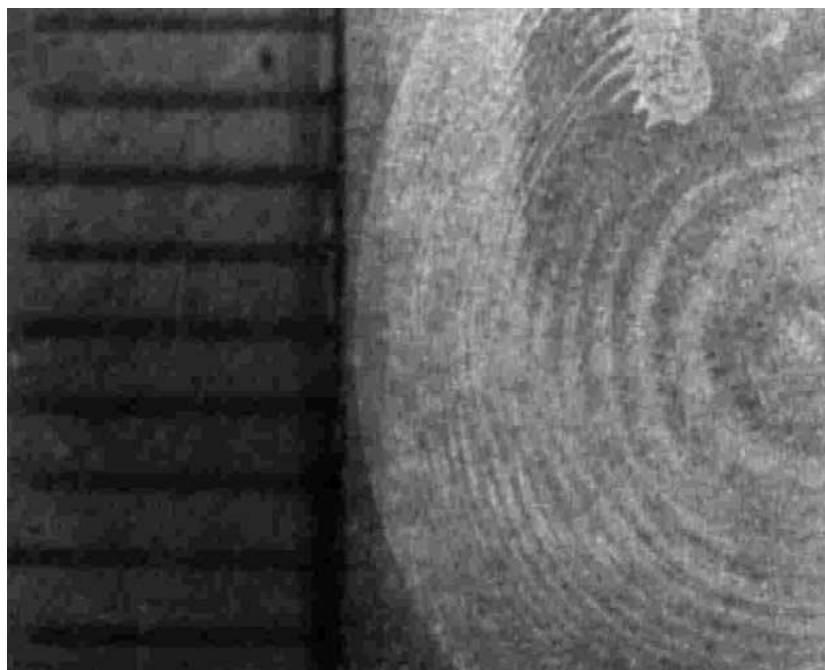
Figure 1.51 Picture of half of the cross-section (*XZ* plane) showing onion rings; 400 rpm, 120 mm/min (Krishnan, 2001).
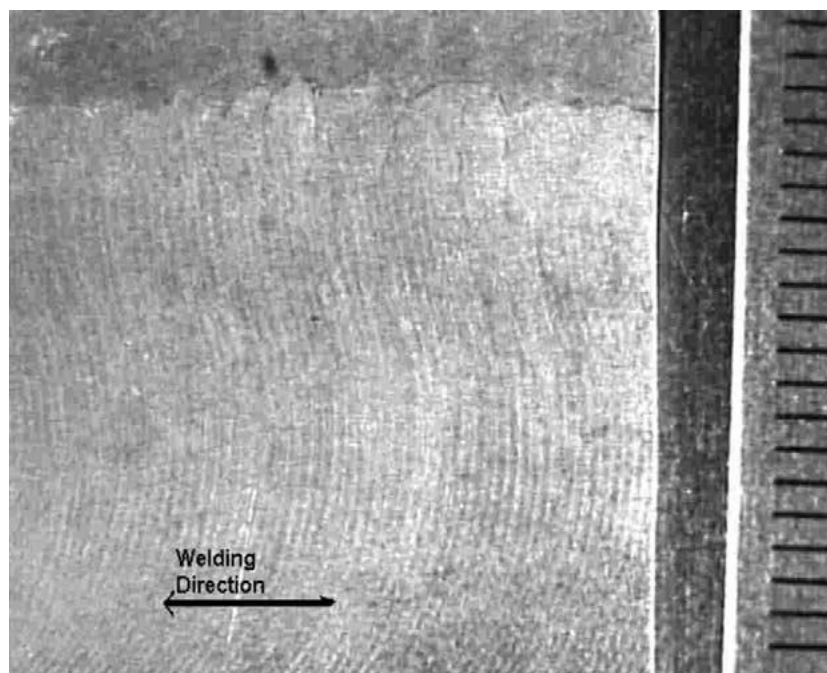
Figure 1.52 Picture of the section from side (*ZY* plane) showing lines curving away from the welding direction, 400 rpm, 120 mm/min (Krishnan, 2001).
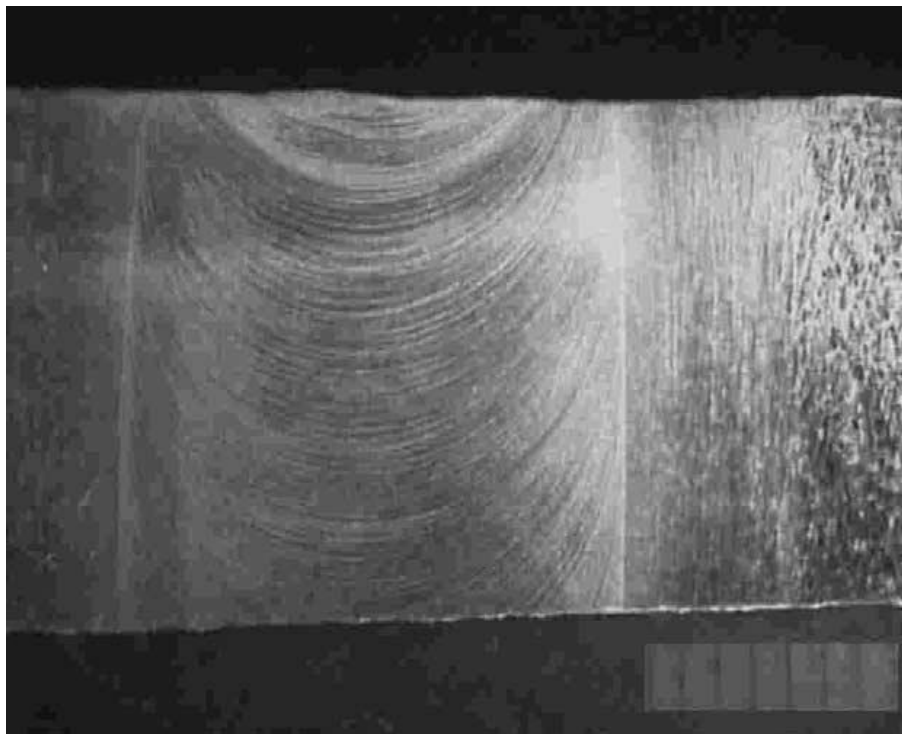
Figure 1.53 Picture showing semicircular features from a section of XY plane cut half way from the Z axis; 400 rpm, 120 mm/min (Krishnan, 2001).

The major part of the onion ring structure which is in the XZ plane is that in the center the size of the light regions are wider and they become narrower as we move forward the outside rings as shown in Figure 1.51. The side view (*ZY* plane) consists of regularly spaced curved lines as shown in Figure 1.52. A region on top surface corresponds to what was compressed by the shoulder. The lines in the centre are curved away from the welding direction. The XY plane picture shows semicircular rings as shown in Figure 1.53. Figure 1.54 shows schematically the combination of the XY-XZ-YZ planes curves.

1.3.1.2 *Grain Size*

Aluminum alloys show a variety of grain size, grain morphologies and crystallographic textures. The texture and grain structure are not totally affected in the most deformed region by the beginning condition, whereas, the texture and grain structure of aluminum alloy may have a major effect on its properties. Tool

geometry, composition of workpiece, temperature of the workpiece, vertical pressure that are FSW/FSP parameters and active cooling exert important influence on the size of the recrystallized grains in the FSW/FSP materials. Most of the studies mentioned that the dynamic recrystallization during FSW/FSP results in generation of fine and equiaxed grains in the nugget zone. The typical recrystallized grain size can be ranged the micron and ultra fine grained (UFG) microstructures (average grain size <1 mm) by using external cooling or special tool geometries in the FSW/FSP aluminum alloys.
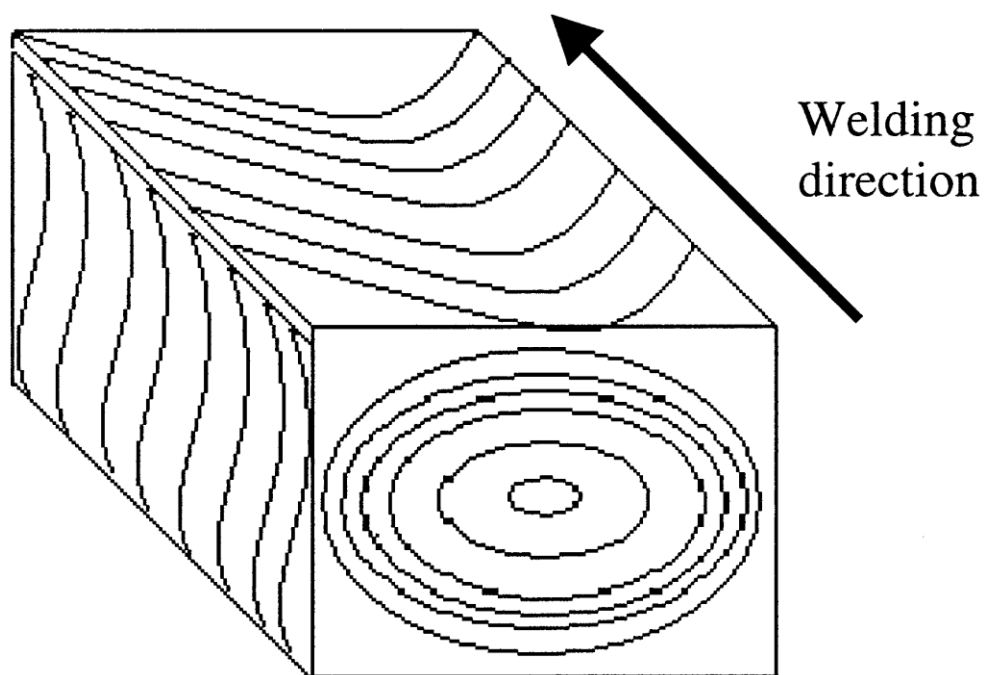
Figure 1.54 Schematic of the various microstructural features in a FSW (Krishnan, 2001).

Murr, Liu & McClure (1998) studied residual microstructures, including dynamic recrystallization and grain growth structures that is producing an average grain size reduction from the base plate by 10 times within the actual weld zone and a wide range of precipitation phenomena associated with a friction stir welding in a thin 6061-T6 aluminium plate, besides, a significant reduction in the dislocation density which leads to considerable softening in contrast to the workpiece.
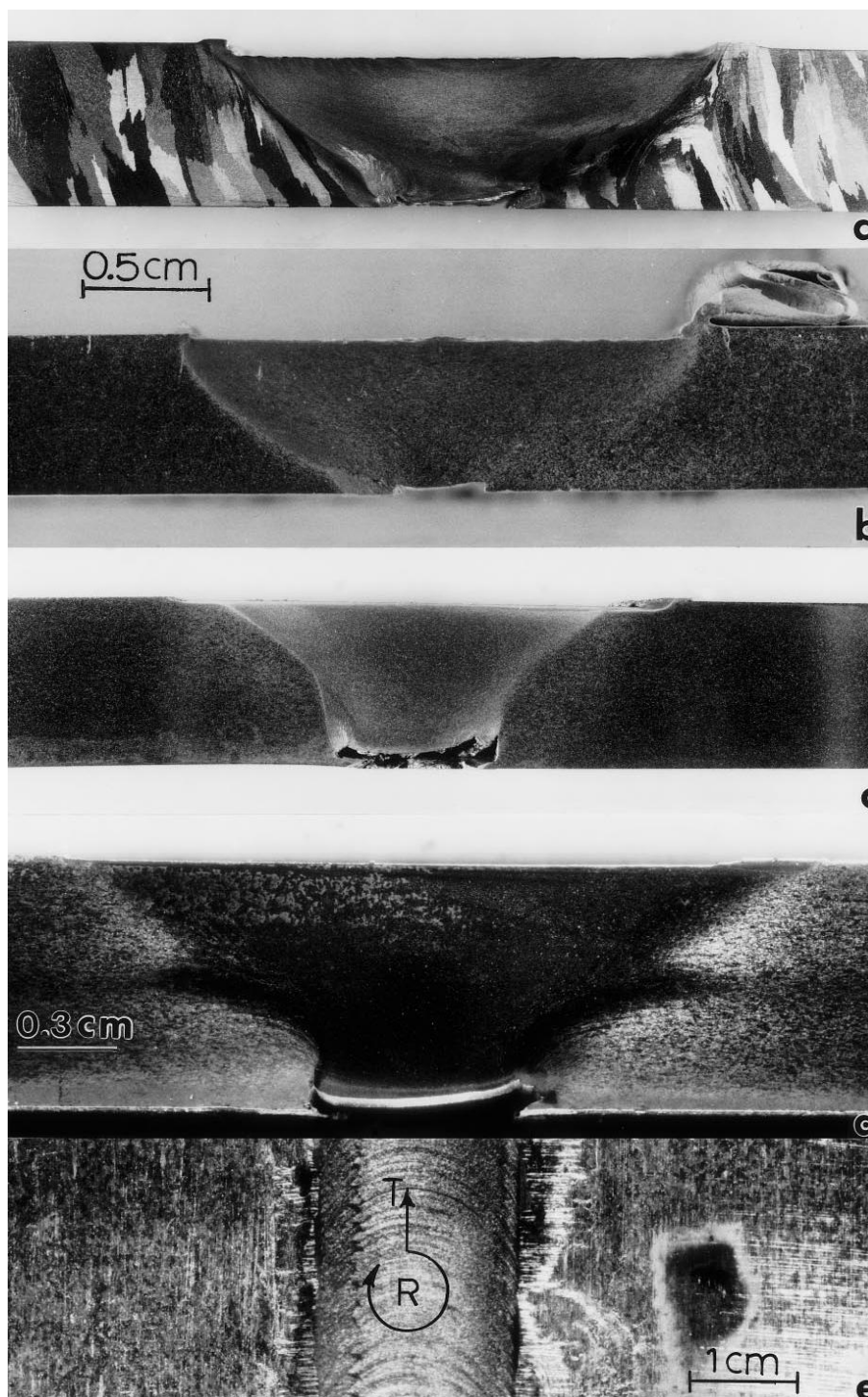
Figure 1.55 a–e Examples of weld zone cross sections in FSW aluminum alloy work pieces. a) Columnar-grained (cast) 1100 aluminum (R=400 rpm; T=1 mm/s), b) Modified 1100 aluminum (R=400 rpm; T=2 mm/s), c) 6061-T6 aluminum (R=300 rpm; T=0.5 mm/s), d) 6061-T6 aluminum (R=400 rpm; T=2 mm/s), e) Upper surface view for d. (Magnification is the same in a, b and c) (Murr et al., 1998).
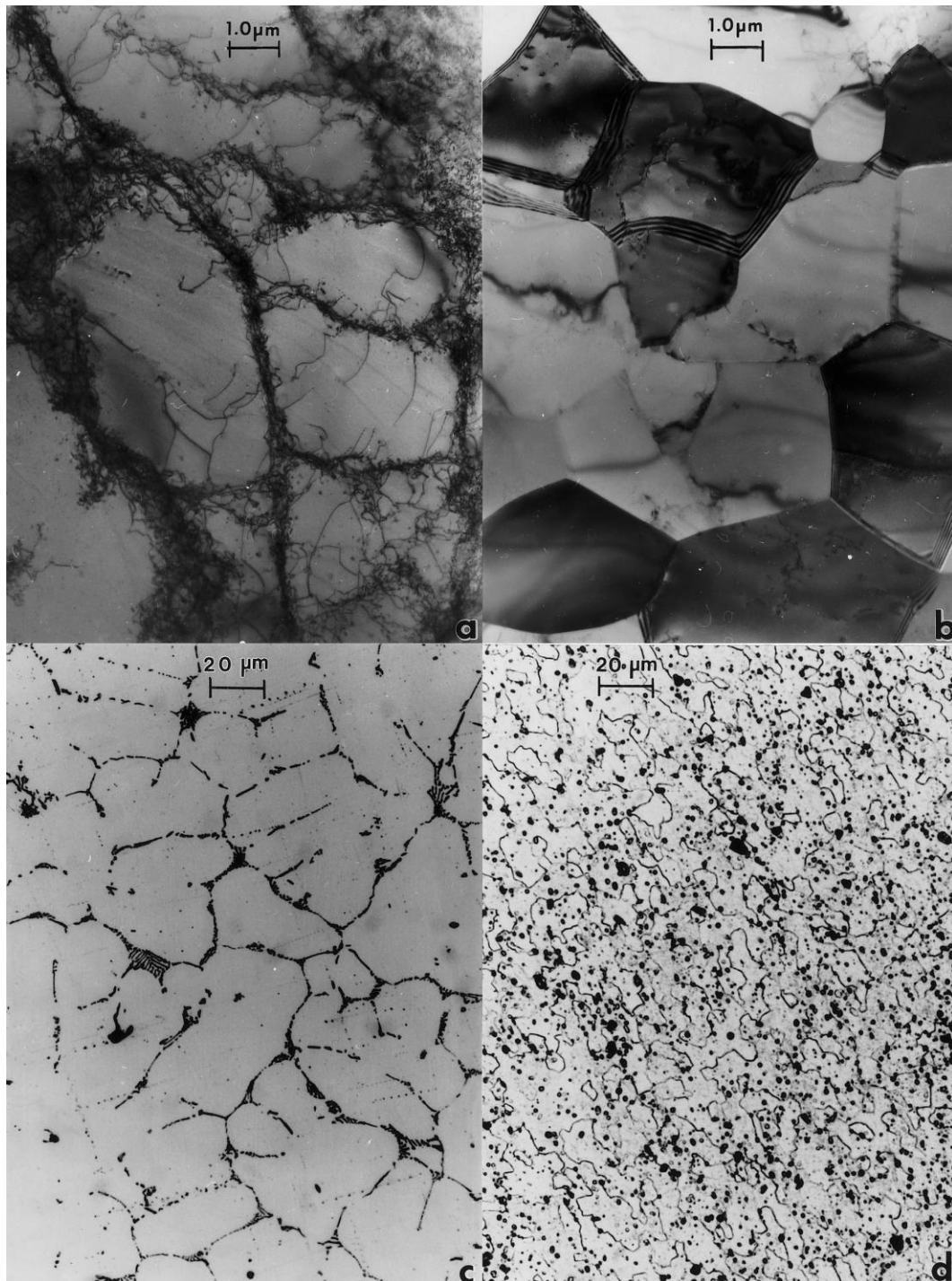
Figure 1.56 a–d Microstructural comparisons in the work piece and in the weld (FSW) zone center, a) TEM bright-field image showing dislocation cell structure within columnar grains in the 1100 aluminum work piece, b) TEM image showing recrystallized grain structure in the 1100 aluminum weld, c) Equiaxed, dendritic cell structure characterizing the modified 1100 aluminum (cast) work piece, d) Modified 1100 aluminum weld zone microstructure. Note magnifications in corresponding and comparative views are the same (Murr et al., 1998).

Figure 1.57 a–d Microstructural comparisons in the 6061-T6 Al work piece and weld zone, a) Work piece grain structure showing precipitates, b) TEM bright-field image of the microstructure in a Note dense (diffuse) dislocation cell structure, c) Weld zone recrystallized grain structure, d) TEM image showing typical dislocation structure in the recrystallized weld zone. Note that comparative image magnifications a and c and b and d are the same (Murr et al., 1998).

Murr et al. (1998) investigated the microstructures of friction stir welding 1100 aluminum alloy and 6061aluminium alloy controllable dynamic recrystallization by

utilizing transmission electron microscopy (TEM). Friction-stir welding of 6061 aluminum to copper produced a complex, interface microstructure which was also dominated by dynamic recrystallization. Some typical weld cross-sections for the three different alum inum alloys examined in this investigation at specific conditions indicated as shown in Figure 1.55. They revealed the weld zones are very continuous and contain no porosity for the most part. As illustrated on comparing the views presented in Figure 1.56 and Figure 1.57, the weld zone microstructures all represent some degree of dynamic recrystallization. These microstructural features provide a compelling sense of extreme plastic deformation which characterizes the FSW process overall, when viewed in contrast to the macrostructures illustrated for the weld cross-sections in Figure 1.55.

When the original work piece microstructure shown in Figure 1.55a for the 1100 aluminum shows initial, large columnar grains which provide a dramatic contrast with the FSW compared the 1100 aluminum and the compositionally-modified 1100 aluminum FSW microstructural variations shown in Figure 1.56 and Figure 1.57. As Figure 1.56b shows dynamically recrystallized grains having a size proportionate with the original dislocation cells, Figure 1.56a and Figure 1.56b provide even more microscopic difference where Fig. 1.56a shows dislocation cell structures characteristic of the matrix within the columnar grains in Figure 1.55a.

The dynamic recrystallization of the microdendritic, equiaxed cell structure of the work-piece can be shown in Figure 1.56c and d, but also the homogeneous redistribution of this microdendritic structure, within the recrystallized FSW zone. The dynamic recrystallization produced a significant reduction in the dislocation density of the 6061-T6 Al work-piece as shown in Figure 1.56, reliable with the microstructural implications of Figure 1.56a and Figure 1.56b. On the other hand, this feature becomes complicated by the dominance of the homogeneously re-distributed formations in Figure 1.56d. Finally, they reported the weld zone microstructures vary, but all of them were dominated by dynamic recrystallization: smaller, equiaxed grains than the workpiece which present a reduced dislocation

density and a redistribution of particulates in the work piece or a wide range of precipitation phenomena were observed in the weld zone and the transition region from the weld zone to the workpiece.

Benavides, Li, Murr, Brown & McClure (1999) compared the residual grain sizes and microstructures in 2024 Al friction stir welding at room temperature about 30°C and low temperature about -30°C which was obtained by pouring liquid nitrogen over the experimental base plates. The friction stir welding of 2024 Al alloy starting temperature was 30°C, and maximum weld zone temperature was 330°C and grain size of about 10 μm, on the other hand, when the starting temperature was -30°C, the maximum weld zone temperatures did not exceed 140°C and grain size shrank to about 0.8 μm .

Kwon, Saito & Shigematsu (2002) used a tool which has sharpened pin in the shape of cone means of smaller contact area with the workpiece to decrease the amount of frictional heat generated during single phase of FSP of 1050Al. The maximum temperature proportionally increased from about 190 to 310 ∘C with increase in the tool rotation speed from 560 to 1840 rpm recorded in the FSP zone at a tool rotation rate of 560 rpm and a traverse speed of 155 mm/min, which resulted in grain size of 0.5 mm.

Ma, Mishra & Mahoney (2002) investigated microstructural evolution of 7075Al during FSP and the stability of the fine grain microstructure during high-temperature heat treatment. Both FSP parameter sets and the post-FSP heat treatment of the microstructural changes in 7075Al are shown in Figure 1.58. Figure 1.58a shows the parent metal microstructure consisted of large elongated pancake shaped grains typical of a hot rolled structure. Figure 1.58b and Figure 1.58c show fine and equiaxed grains of the microstructure characterization in the stirred zone. The average grain size was 7.5 and 3.8 μm for processing parameters of 4 ipm/400 rpm and 6 ipm/350 rpm, respectively. Figure 1.50d shows a highly deformed structure between the parent material and stirred zone. The grains in the FSP zone coarsened

slightly, after heat treatment at 490 °C for 1 h, as shown in Figure1.58e and Figure 1.58f. The mean grain size increased to 9.1 and 5.9 μm for the two FSP conditions of 4 ipm/400 rpm and 6 ipm/ 350 rpm, respectively. This revealed relatively stable grain growth in the fine grain microstructure locations.
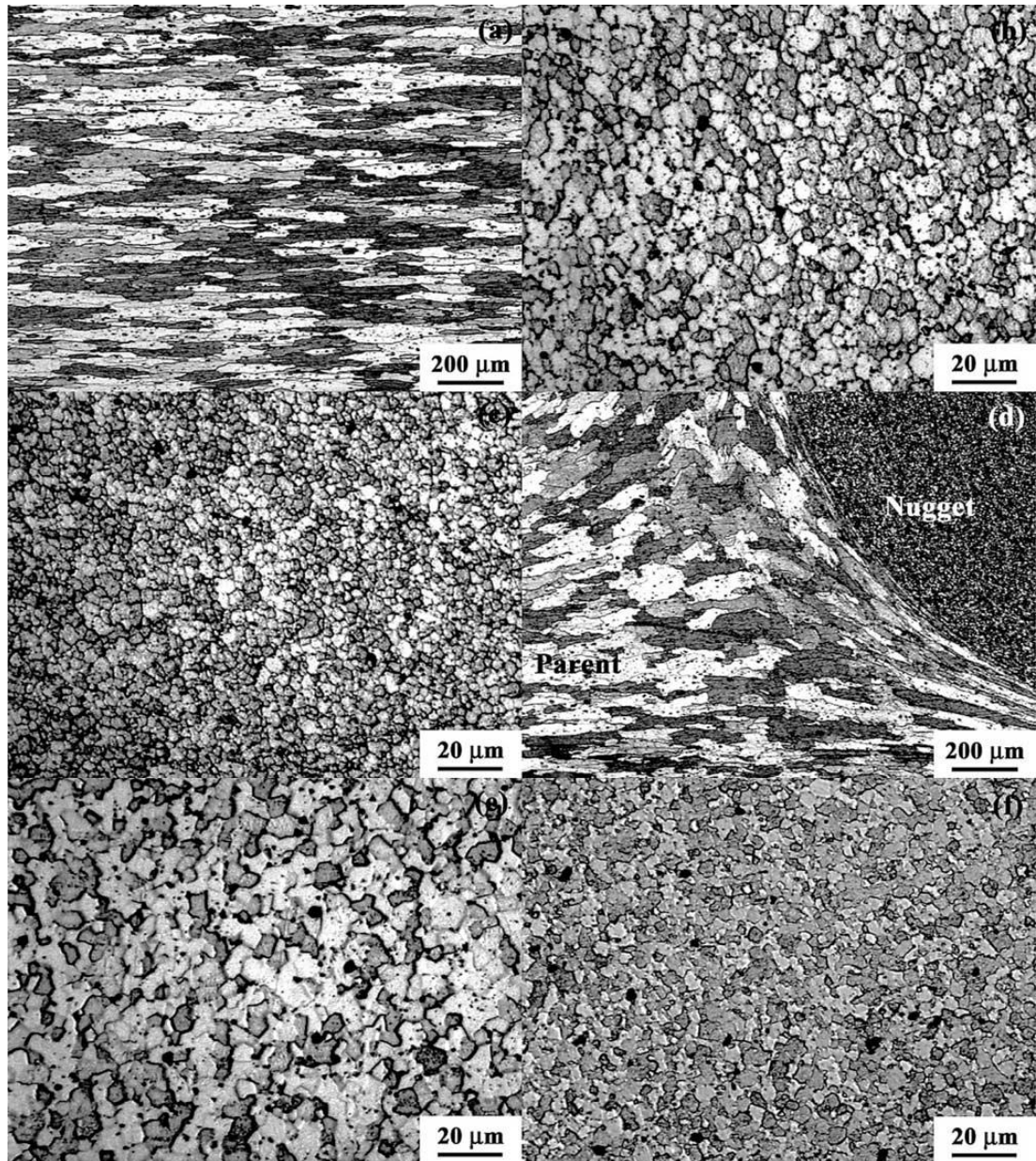
Figure 1.58 Optical micrographs showing grain structure of, a) parent zone, b) FSP zone, 4 ipm/400 rpm, c) FSP zone, 6 ipm/350 rpm, d) transition zone, 4 ipm/400 rpm, e) FSP zone, 4 ipm/400 rpm after heat treatment at 490 °C/1 h, and f) FSP zone, 6 ipm/350 rpm after heat treatment at 490 °C/1 h (Ma et al., 2002).

Sato, Urata & Kokawa (2002) examined the aluminum alloys 6063-T5 and T4 in friction stir welding at tool rotation speed of 800, 1220, 2450 rpm, and the distributions of the microstructure. The maximum temperature of the welding thermal cycle was reached by increasing the tool rotational speed. The recrystallized grain size of the weld enlarged exponentially with increasing maximum temperature.
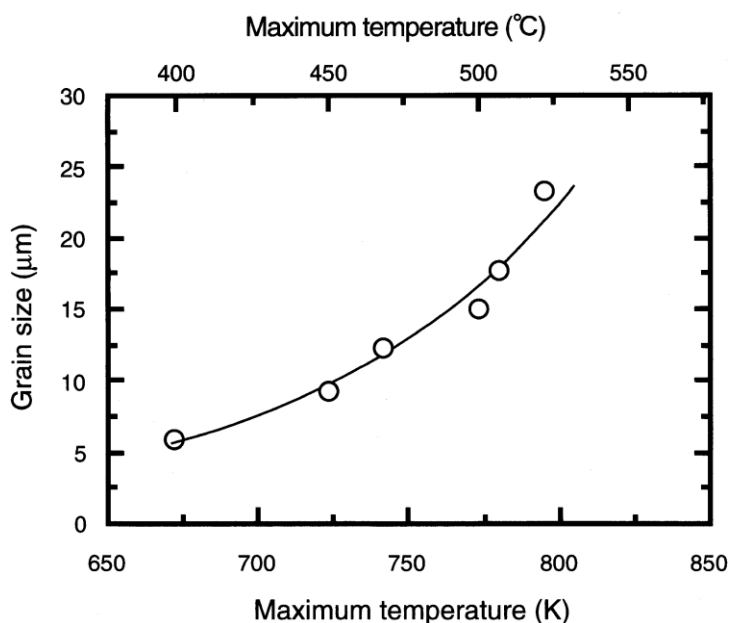
Figure 1.59 Relationship between the grain size and the maximum temperature of the welding thermal cycle (Sato et al, 2002)

The fine-grained microstructure often resulted in excellent mechanical properties in the welds of nonheat-treatable Al alloys because of recrystallization arising from both frictional heating and plastic flow during the welding in the Al alloys. The grain sizes of the stir zone were about 5.88, 9.21, and 17.75 μm, respectively, the tool rotational speed of 800, 1220, and 2450 rpm welds. The diagram in Figure 1.59 shows the relation between temperature and grain size.

Li, Trillo & Murr (2000) reported the FSW of aluminum alloy 2024 to high-purity silver, especially the characterization of residual microstructures in contrast to those of the starting, base metal microstructures. They interested particularly the recrystallization and grain growth behavior of the silver in contrast to the aluminum

alloy 2024. They compared the base plate grain structures with the corresponding FSW zone grain structures in regions which do not exhibit extensive intercalations and intercalation flow patterns. The silver base plate grain size of 10 μm increases to around 90 μm in the FSW zone, in contradiction of the aluminum alloy 2024 where the average base plate grain size decreases from around 35 μm to an average, equiaxed grain size of 5 μm in the FSW zone. Actually, the residual, recrystallized silver grains in the FSW zone are so much larger than the base plate grains, and contain extensive, coherent heat treated Al and silver, which provides compelling corroboration of the very fast grain growth kinetics in silver at relatively low temperatures. The study demonstrated the ability to friction-stir weld 2024 aluminum alloy to pure silver at 30˚C room temperature and at -30˚C by submerged in liquid nitrogen. While dynamic recrystallization provides a mechanism for these two base metals to flow and intercalate in complex patterns within the weld zone, the silver has a propensity for very fast recrystallization and grain growth, and the residual grain size within the weld zone, especially in large, isolated silver regions, is much larger than the silver base metal grain size. Indeed, silver regions within the weld zone exhibit larger grain sizes at starting temperatures of -30˚C is an important consequence.

Rhodes, Mahoney, Bingel & Calabrese (2003) studied the fine-grained structure in friction stir processed 7050 aluminum by using a rotating-tool plunge and extract technique. Initial sizes of newly recrystallized grains are on the order of 25–100 nm. These grains then grow to a size equivalent to that found in friction stir processed aluminum, 2–5 μm, after heating 1– 4 min at 350– 450 ˚C. Including severe deformation of the preexisting sub-grains, the rotating tool has introduced severe deformation in the starting grain structure. Externally, the surface of the aluminum plate was cooled with a chilled mixture of ethylene glycol and alcohol in the starting structure. Heat generation was result of the rotation speed by rotating tool and the external cooling rate. Recrystallization of the deformed aluminum occurs at slower cooling rates and/or faster tool rotation speeds.
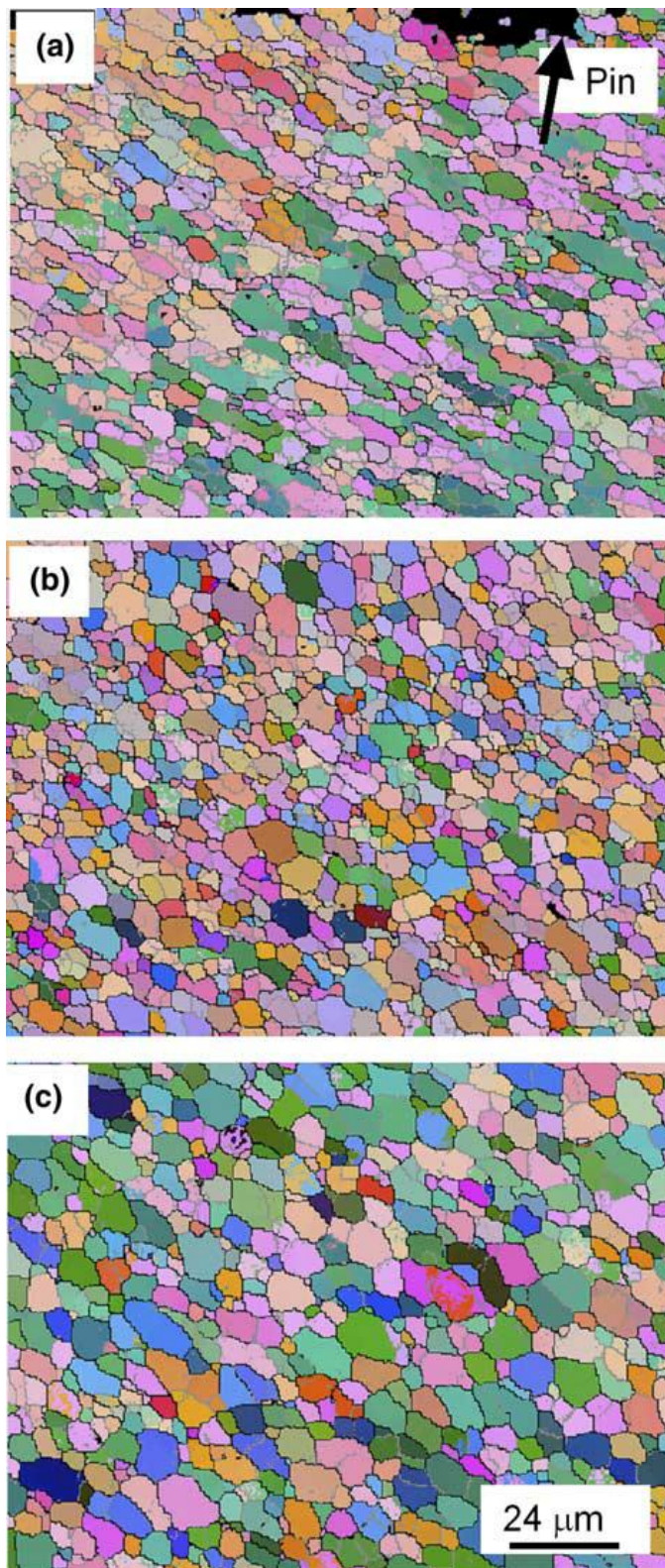
Figure 1.60 EBSD maps showing the nugget grain structure at weld center a) immediately behind the pin, b) 0.5 mm behind the pin and c) 2 mm behind the pin (Prangnell et al., 2005).

Prangnall and Heason (2005) analyzed the grain structure in the nugget behind the 'stopped tool' along the weld centerline by using electron back scattered diffraction (EBSD). The thermal exposure will increase with distance behind the pin, due to the trailing thermal field, since the welding process was quenched. In Figure 1.60, the nugget grain structures along the trailing weld centerline were compared from next to the tool's surface and at 0.5 and 2 mm behind the pin. It can be seen in Figure 1.60a that the grain structure immediately behind the pin is not as recrystallised in appearance and is comprised of fine elongated fibrous grain fragments with a significant proportion of low angle boundaries. 1 mm behind the pin a more equiaxed grain structure was observed as shown in Figure 1.60b, and far behind the pin a similar equiaxed grain structure was again seen, but the grains are significantly coarser as shown in Figure 1.60c. They also noted that there was some variability within the material immediately close to the pin surface which has seen the least recrystallised as shown in Figure 1.60a. It is also difficult to determine on the grain structure of the material at the tool surface due to the effect of the deceleration of the tool and simultaneous quenching.

The grain size decreases with distance off the weld-zone centerline. However, the grain size within the weld zone tends to increase close to the top of the weld zone and these approaches roughly to temperature variation within the weld zone. This means that the difference in temperature profile and heat dissipation in the nugget zone caused such a variation in grain size from bottom to top of the weld nugget. As the bottom of workpieces is in contact with the backing plate, the maximum temperature is lower and the thermal cycle is shorter compared to the nugget top. The grain growth results in smaller recrystallized grains with the combination of lower temperature and shorter excursion time at the nugget bottom. If the plate thickness increases, the temperature difference between bottom and top of the weld nugget increases, and resulting in increased difference in grain size.

1.3.1.3   Recrystallization Mechanism

Dynamic recrystallization (DRX) and / or dynamic recovery (DRV) is the term dynamic signifies that the process is coincident with deformation in the friction stir welding. As the tool passes away, the welded volume will cool to ambient temperature at a net rate that is controlled by the surrounding workpiece and atmosphere, the back plate in butt joints, as well as by the back heating by the tool. Some tempering / aging can take place due to back heating during cooling, and, additionally, static recrystallization (SRX) and recovery (SRV) is the term static signifies that no deformation is involved. Furthermore, the recrystallization and recovery processes are complicated and are not controlled only by temperature, but also by the strain and strain rate. On the other hand, several mechanisms have been proposed for dynamic recrystallization process in aluminum alloys, such as discontinuous dynamic recrystallization (DDRX), continuous dynamic recrystallization (CDRX), and geometric dynamic recrystallization (GDRX).

Etter, Baudin, Fredj & Penelle (2006) mentioned that these three types of dynamic recrystallization are likely to produce new grains in the weld nuggets: (i) discontinuous dynamic recrystallization (DDRX), which occurs by nucleation and growth of new grains; (ii) continuous dynamic recrystallization (CDRX), which involves the formation of arrays of low angle boundaries and a gradual increase in the boundary misorientations during hot deformation, finally leading to new grain development; (iii) geometric dynamic recrystallization(GDRX), occurs when the wavy boundaries present during hot deformation impinge, as a result of the compression of their spacing with strain causing the fibrous grains to break up into shorter lengths. These three mechanisms lead to grain refinement.

McNelley, Swaminathan & Su (2007) studied two models to interpret microstructure and microtexture data for two aluminum alloys during friction stir welding. Dynamic recovery (DRV) occurs quickly during hot working of metals of high stacking fault energy such as aluminum. On the other hand, discontinuous

dynamic recrystallization (DDRX) occurs in metals of moderate to low stacking fault energy during hot deformation. Dislocation-free grains form at sites such as prior grain boundaries, deformation band interfaces or boundaries of newly recrystallized grains in DDRX. The newly formed grains deform as they grow, and the increase of stored strain energy in the new grains may decrease the driving force for their continued growth, however, increase the frequency of initiation of new grains. The geometric dynamic recrystallization (GDRX) may be observed as the strain increases during DRV when the separation of prior boundaries approaches the subgrain size.

Su, Nelson, Mishra & Mahoney (2002) investigated microstructural of FSW 7050Al-T651 aluminum. They reported that, the original base metal grain structure is completely eliminated and replaced by a very fine equiaxed grain structure in the DXZ during the friction stir welding. Depending on the microstructural observations, they suggested that the dynamic recrystallization in the nugget zone can be considered a CDRX on the basis of dynamic recovery. Subgrain growth related with absorption of dislocation into the boundaries is the CDRX mechanism. Repeated absorption of dislocations into subgrain boundaries is the dominant mechanism for growing the misorientation between adjacent subgrains during the CDRX.

Recently, Prangnell and Heason (2005) carried out some experiments to observe the grain structure formation during the friction stir welding by using stop action technique which means to stop the tool and immediately quenching the work piece in an Al-2195 plate welded under typical conditions. The higher temperature latter phases of this refinement process were closely reminiscent of geometric dynamic recrystallisation seen in high strain hot torsion experiments. The recrystallized grain structures which were observed by electron back scattered diffraction (EBSD), magnified formation of bands of ultrafine nugget grain size by GDR related mechanism at elevated temperatures as shown in Figure 1.61. Moreover, within the nugget zone appear showed. In very-high strain hot torsion test, although the scale is finer and the boundaries do not appear as classically wavy in the friction stir welds due to the higher strain rate and larger density of pinning particles.
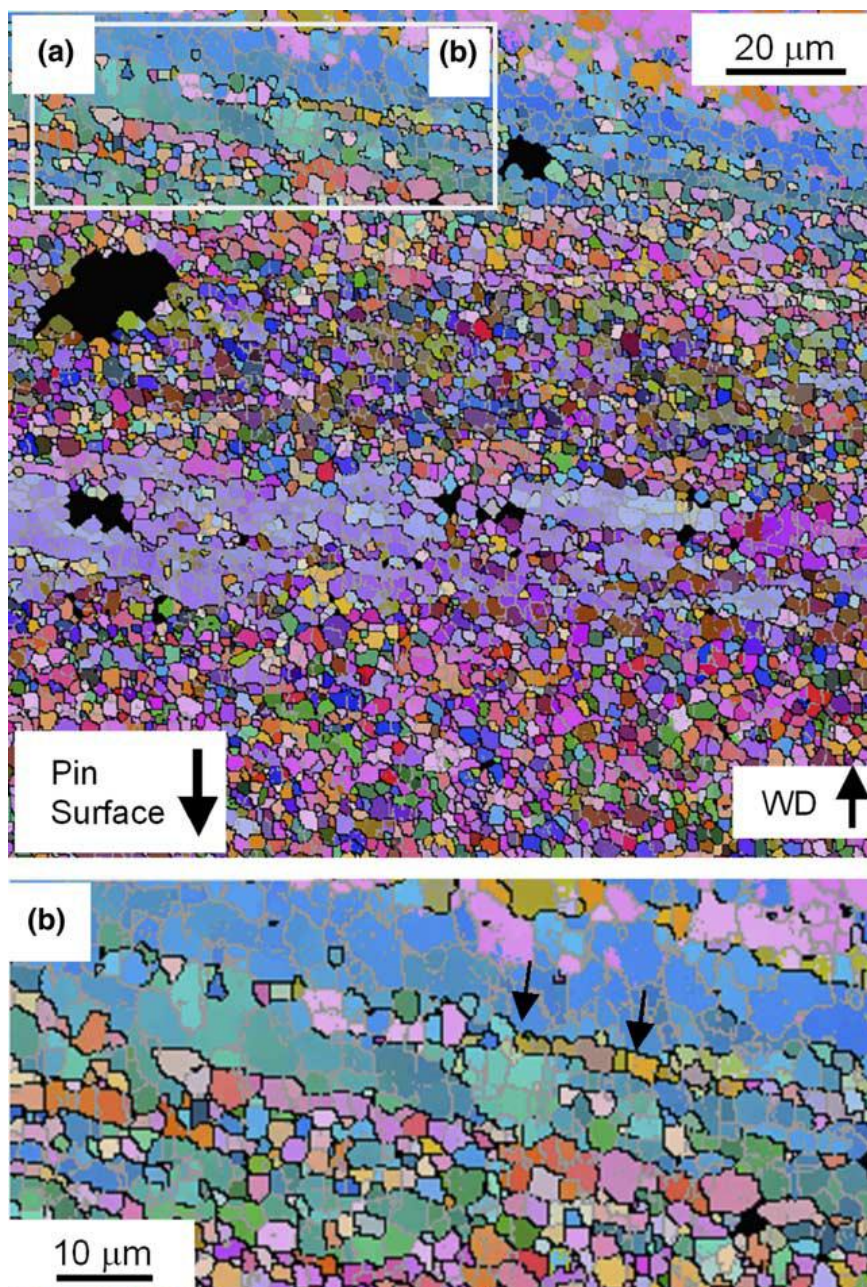
Figure 1.61 a) High resolution EBSD map from ahead of the tool showing the formation of bands of ultrafine nugget scale grains by a GDR related mechanism, b) highlighted at a higher magnification in (Prangnell & Heason, 2005).

1.3.1.4   *Precipitate Dissolution and Coarsening*

Precipitates in aluminum alloys can coarsen or dissolve into aluminum matrix depending on alloy type and maximum temperature in heat-affected zone. Sato et al.

(1999) experimented microstructural distribution of 6063 aluminium during friction stir welding. They presented that the hardness profile depended greatly on the precipitate distribution more than the grain size. Dissolution and growth of the precipitates characterized the softened region during the welding. These precipitate distributions were different from those in the base material, which contains a high density of needle shaped precipitates and a low density of β' precipitates.
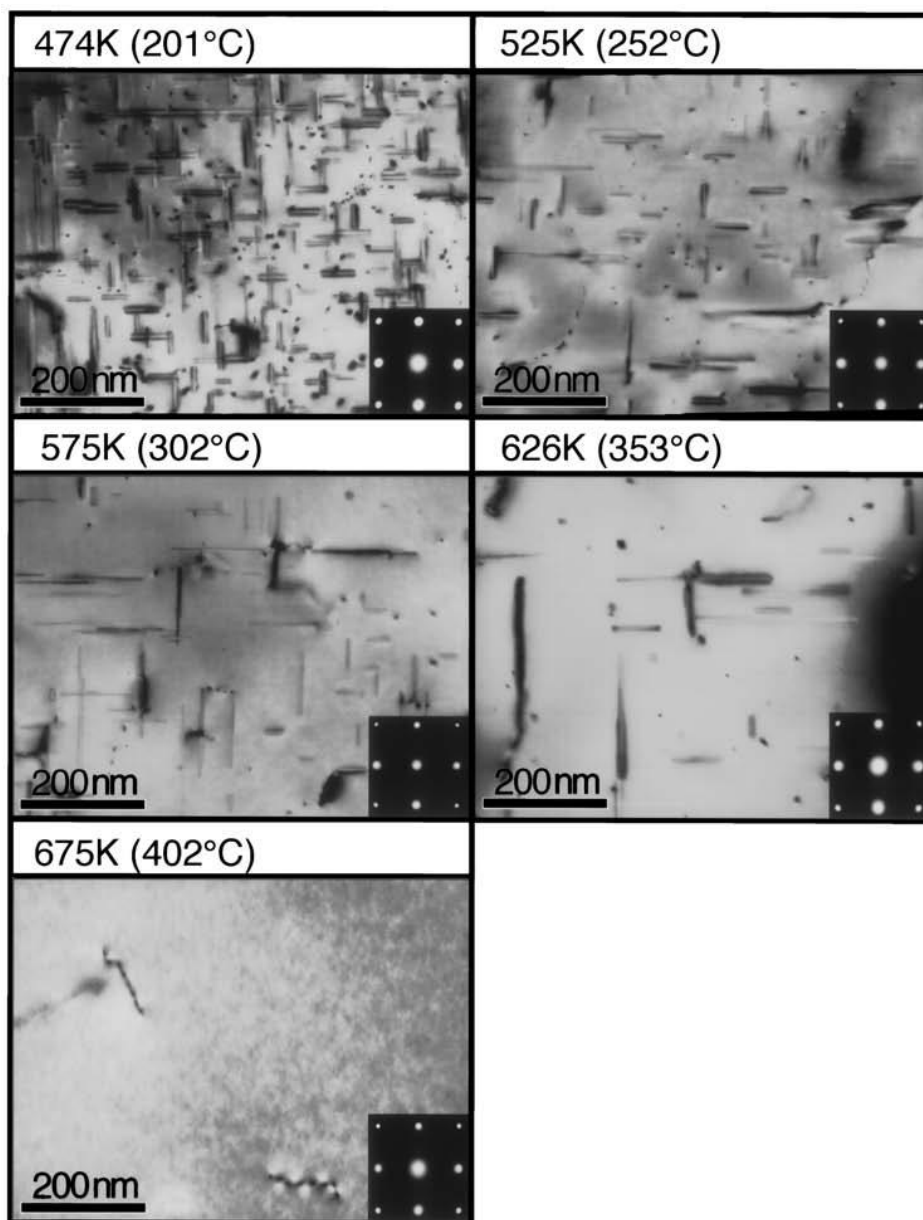
Figure 1.62 TEM micrographs of the specimens experiencing the thermal cycles with peak temperatures of 474, 525, 575, 626, and 675 K. (Sato et al., 1999).
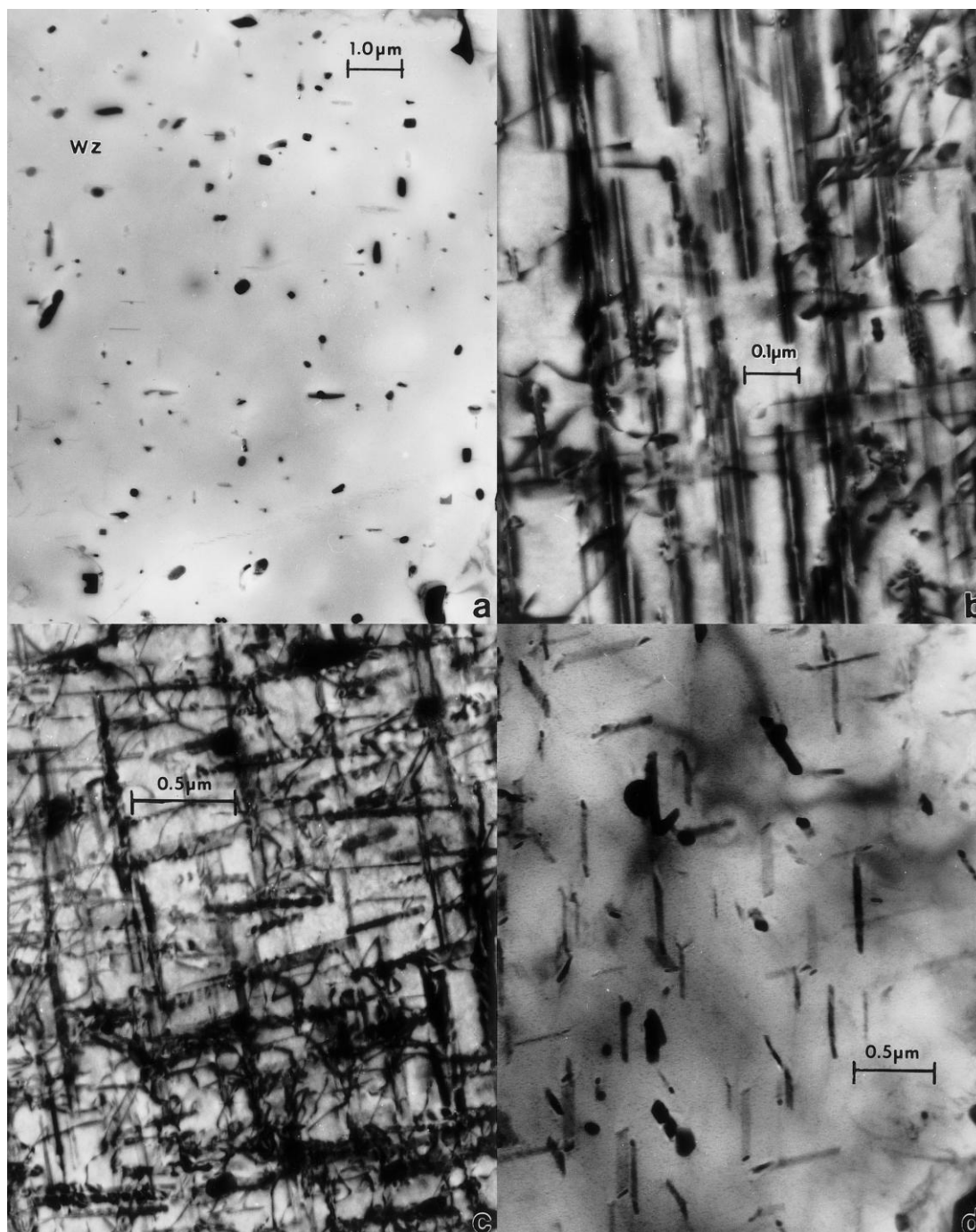
Figure 1.63 a–d Precipitation variations in the weld zone and in the weld transition region (weld/work-piece interface region) for FSW of 6061-T6 aluminum: TEM images, a) Homogeneous, fine precipitates, b) Guinier-Preston-like linear precipitate zones along {100}, c) Widmanstätten-like precipitates intermixed with dislocation loops, spirals, and other dislocation arrays, d) Irregular mixtures of precipitates. Note magnification variations (Murr et al., 1998).

Figure 1.62 shows transmission electron microscopy (TEM) micrographs of the specimens which experienced the simulated thermal cycles for maximum temperatures of 474 K (201 ˚C), 525 K (252 ˚C), 575 K (302 ˚C), 626 K (353 ˚C), and 675 K (402 ˚C). The precipitate distribution was not really affected by peak temperatures, if it was less than 474 K (201 ˚C). The density of needle shaped precipitates decreased with the increase in the maximum temperature the temperature between 525K and 626 K (252 ˚C and 353 ˚C). The most density of the β' precipitates observed at temperature value of 575 K, which is higher than that in the base material. So, some needle-shaped precipitates grow into β' precipitates throughout the thermal cycle with a peak temperature of 575 K (302 8C). Simulated weld thermal cycles with different maximum temperatures indicated that the precipitates are dissolved at temperatures higher than 675 K and that the density of the strengthening precipitate was reduced by thermal cycles lower than 675 K. The precipitate distribution is strongly affected by the thermal hysteresis.

Su et al. (2002) studied the precipitation phenomena in different weld regions. Predominantly, precipitates were intragranular fine η' less than 50 nm with coarser η was precipitates along grain boundaries in the 7050-T651 base alloy. Similarly, a small precipitate-free zone 25 nm in width stays along the grain boundaries.

Murr et al.(1998) and (1999) investigated a wide range of precipitation phenomena associated with a friction-stir-weld in a thin 6061-T6 aluminum plate have been systematically investigated utilizing light metallography and transmission electron microscopy (TEM) as shown in Figure 1.63. This illustration shows that even more complex microstructural issues can be characteristic of more complicated alloy systems like 6061 aluminum where a plethora of precipitation phenomena can occur as a consequence of temperature variations below the melting point which can affect aging conditions requisite for specific precipitate formation. In this studies include a wide range of continuous and discontinuous precipitates consisting of 2.0 nm thick coherent and crystallographically coincident precipitate zones, thin, semi-coherent and non-coherent needles and plates coincident with {110} matrix planes,

in addition to these, complex precipitate shapes intermixed with both homogeneous precipitates and Widmanstatten structures involving crystallographically coincident precipitate needles and thin plates.

Recently, Chen, Feng & Liu (2008) researched precipitate evolution in friction stir welding of 2219-T6 aluminum alloys was characterized in each zone by transmission electron microscopy. Some metastable precipitates overaged to equilibrium phase while others solutionized into the aluminum solid solution in the weld nugget zone and the thermomechanically affected zone. The precipitates coarsened in the heat-affected zone. The weld nugget zone experiences the highest temperature with the maximum value at about 450 °C for all the weld zones.

1.3.1.5   Texture

A variety of properties, including strength, ductility, formability, and corrosion resistance is controlled by texture. The FSW material consists of nugget, TMAZ, HAZ and base material microstructural zones. Each zone has different thermo-mechanical history. The nugget region consists of sub-domains, it makes FSW to more complicate. For instance, the top layer undergoes deformation by shoulder after the pin has passed through. Besides, depending on the tool rotation rate and traverse speed, the nugget region can contain ring pattern or other microstructural variations as mentioned before. The texture information is obtained as microtexture by using orientation imaging microscopy (OIM), which is used to establish the grain boundary misorientation distribution data from same set of experiments.

Sato et al. (2001) analyzed the microtextures in a friction-stir weld of the precipitation-hardened aluminum alloy 6063 by orientation imaging microscopy (OIM) to characterize plastic flow during friction-stir welding. They found out that the base-material plate has a Goss orientation which was known as the typical recrystallized texture in aluminum alloys as shown in Figure 1.64. Except for the upper surface, there is a typical shear texture component with two types of

orientations in the weld center region. The orientations have a pair of common {111} and <110> parallel to the cylindrical pin surface and transverse direction of the plate, respectively. Although it rotates about the plate normal direction, the typical texture piece is also observed around the weld center on the midsection.
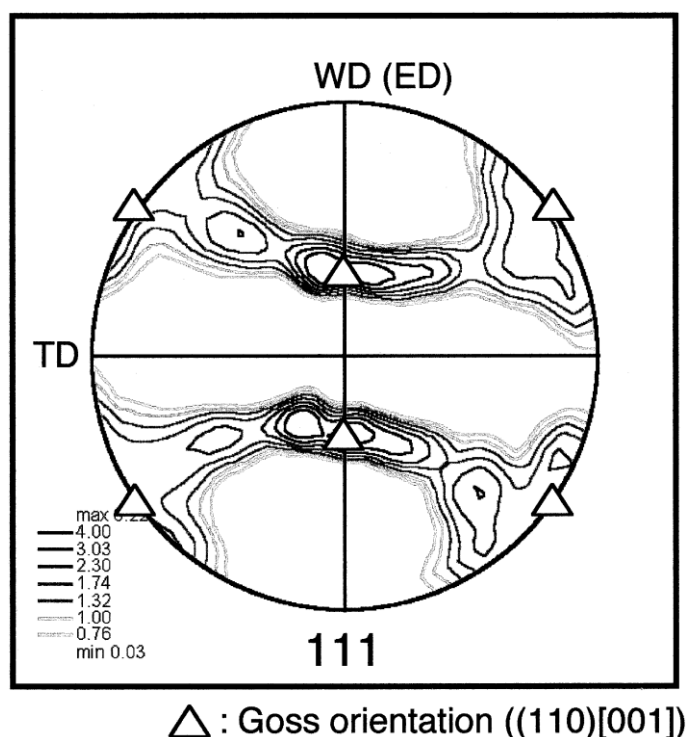
Figure 1.64 (111) pole figures on the C layer of the base material (Sato et al., 2001).

Pole figures of several regions on two cross sections were analyzed by OIM to evaluate the local plastic flow during the welding. The weld cut by using an electro-discharge machine from the cross section (CS) perpendicular to the welding direction (WD) and the midsection of the plate (C layer), as shown in Figure 1.65. Illustrated as solid squares in Figure 1.65 the pole figures were obtained from several regions in the weld zone. The notation "CS(n)" indicates a location n mm in depth from the upper surface of the CS, and the notation "Cn" indicates that the location is n mm away from the weld center on the C layer. Results were exemplified as <111> contour pole figures by OIM. Coordinate axes of pole figures are the welding direction (WD), transverse direction (TD) of the plate, and normal direction (ND), as

shown in Figure 1.65. They labeled the microtextures as {*hkl*}<*uvw*>, where {*hkl*} is the crystallographic plane perpendicular to the WD and <*uvw*> is the crystallographic direction parallel to the ND.
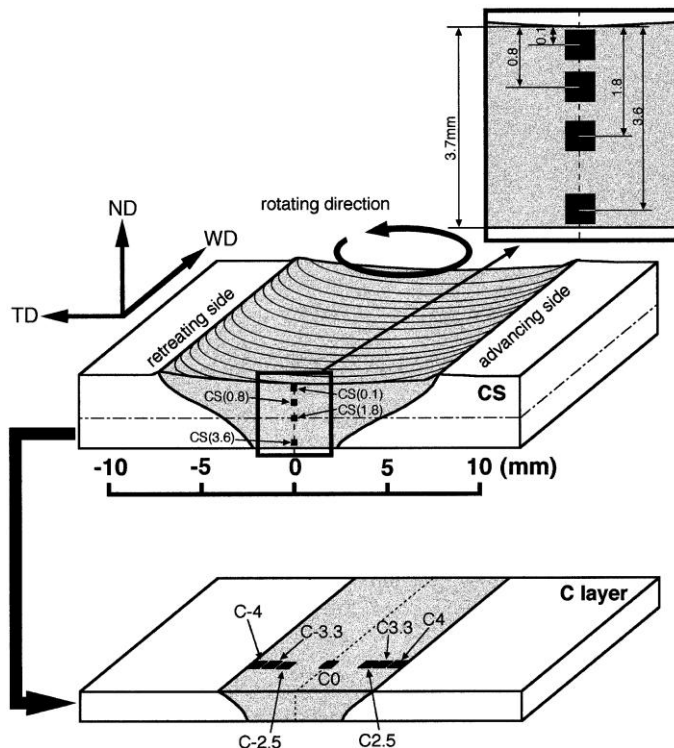
Figure 1.65 Schematic illustrations of the two cross sections (CS: cross section perpendicular to the welding direction, and C layer: the midsection of the plate). Microtextures were obtained from the regions shown by solid squares (Sato et al., 2001)
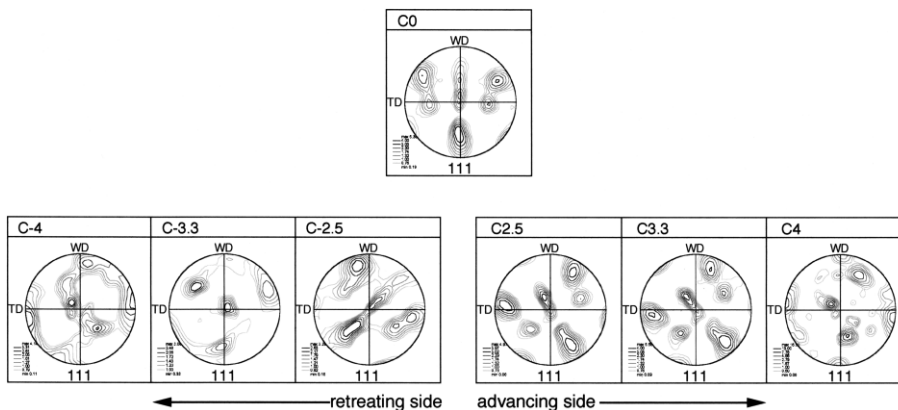
Figure 1.66 <111> pole figures of the C0, C ± 2.5, C ± 3.3, and C ± 4 regions on the C layer in the weld (Sato et al., 2001).
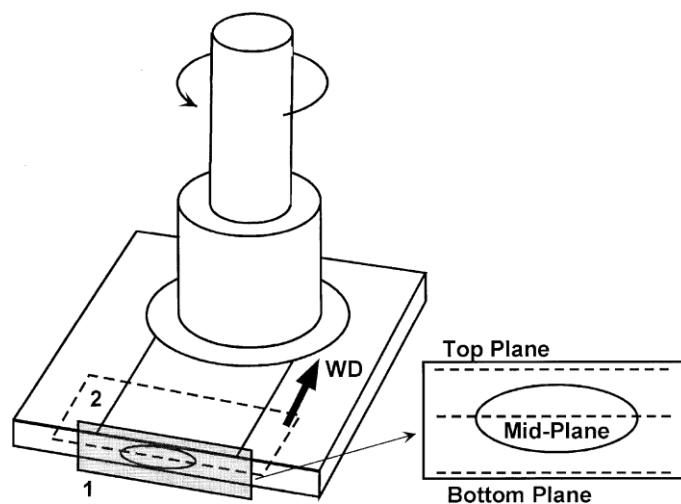
Figure 1.67 A schematic representation of the friction stir welding geometry and the associated analysis planes. Plane 1 (the shaded region) shows the cross section analyzed, and plane 2 indicates the plan-view geometry. Plan-view images were taken at the top, middle, and bottom planes, as indicated in the view on the right (Field et al., 2001).
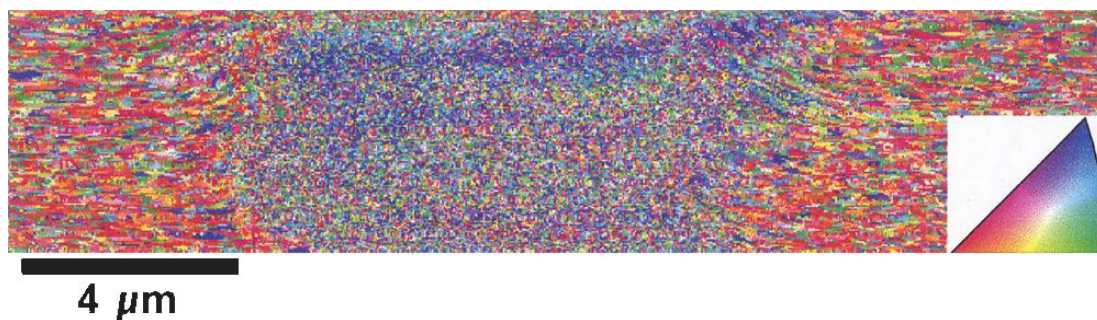
Figure 1.68 A representative orientation image from a complete cross section of 1100 Al joined at 700 rpm and 18 cm/min. The color key shows poles aligned with the normal direction of the plate (Field et al., 2001).

The pole figures at the advancing and retreating sides, microtextures on the midsection (the C layer) as exhibited in Fig 1.66 by OIM. They reported that optical microscopic observations show that fine equiaxed grains occupy the weld center region, and deformed grains exist just outside the weld zone.

Field, Nelson, Hovanski & Jata (2001) investigated heterogeneity of crystallographic texture in friction stir welding of aluminum. A schematic view of

the weld geometry and associated analysis plane is given in Figure 1.67 for this study. The characteristic of local textures through FSWs appears to be fundamentally alloy independent. Some small differences were observed which were not dependent to weld tool rotation and feed rate. They observed the main texture difference as a function of weld parameters was the plane of shearing on the retreating side of the tool as it changed from normal to the tool axis to align with the tool axis at the higher rotation and feed rates. A representative orientation image from complete cross section of 1100 Aluminum joined at 700 rpm and 18 cm/min is shown in Figure 1.68, strong gradients in crystallographic texture can be observed through the stir zone of the weld nugget zone. In order to identify recognizable deformation textures, various zones throughout the weld were isolated and analyzed independently. As a result, the local deformation state responsible for producing the given texture. The most critical textural gradients exist in the center of the weld at the weld floor and along the advancing side (AS) of the tool through the thickness of the plate.
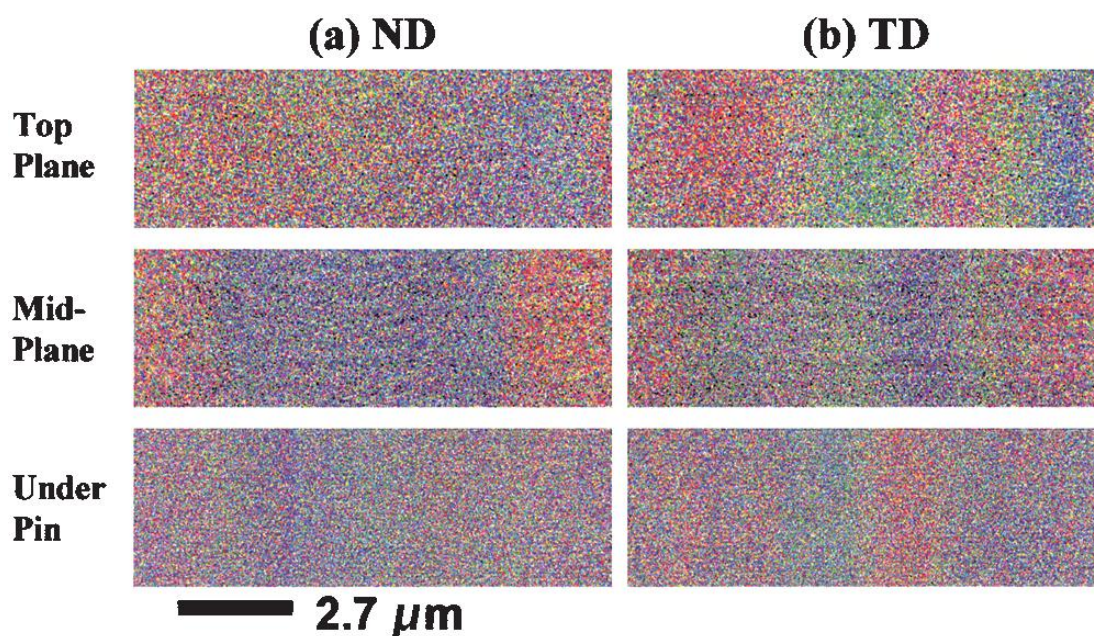
1.69 Plan view orientation images of an FSW joining 1100 Al plates at 700 rpm and 18 cm/min. Column, *a*) colors poles aligned with ND and column, *b*) colors those aligned with TD in the plates. The advancing side is on the right for the top and midplanes and on the left for the bottom plane. Orientations are colored according to the color key shown in Figure 167 (Field et al., 2001).

Orientation images of all three plan-view sections of the 1100 Al weld analyzed, with orientations colored according to the normal direction (ND) of the plates in column (a) and according to the transverse direction (TD) of the plates in column (b) as shown in Fig 1.69.
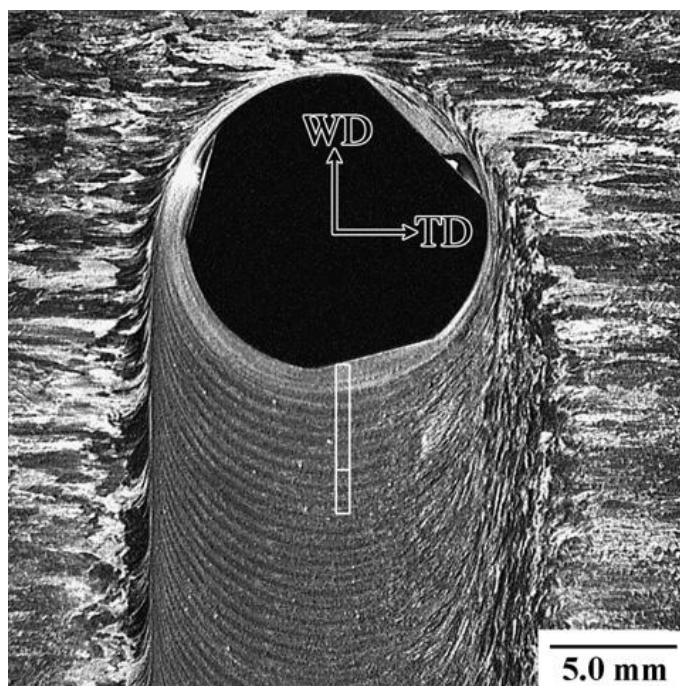
Figure 1.70 Plan view optical macrograph from 10.4 mm below the top surface of the 2195 friction stir weld (Fonda & Bingert, 2007).

Fonda and Bingert (2007) analyzed the textural variations that were produced during FSW of 2195 aluminum. They observed a variation in the crystallographic texture in 2195 aluminum in a friction stir welding. As shown in Figure 1.70, the banded onion ring features appear as arcs similar to the trailing edge of the tool. An electron back scatter diffraction EBSD micrograph along the center of the weld as shown in Figure 1.71 exposes that the banding observed in Figure 1.70 correlates to a periodic variation in the average grain orientation aligned with the plate normal direction. They also examined the crystallographic texture across this region from pole figures (PFs) to orientation distribution functions (ODFs) obtained from 100 μm wide sections along the weld path, as shown in Figure 1.71. In Figure 1.72 shown,

these figures have been rotated respectively by -10˚, -7˚ and -7˚ about the welding direction (WD) up, transverse direction (TD) right and normal direction (ND) out axes to align them with the ideal shear deformation reference frame. They also reported that that there is a periodic variation in the deformation conditions, although the orientation of that deformation field remains relatively constant. Additionally, either the periodically strong interaction with the rotating threads or an eccentricity of the tool itself could increase such an effect during FSW.
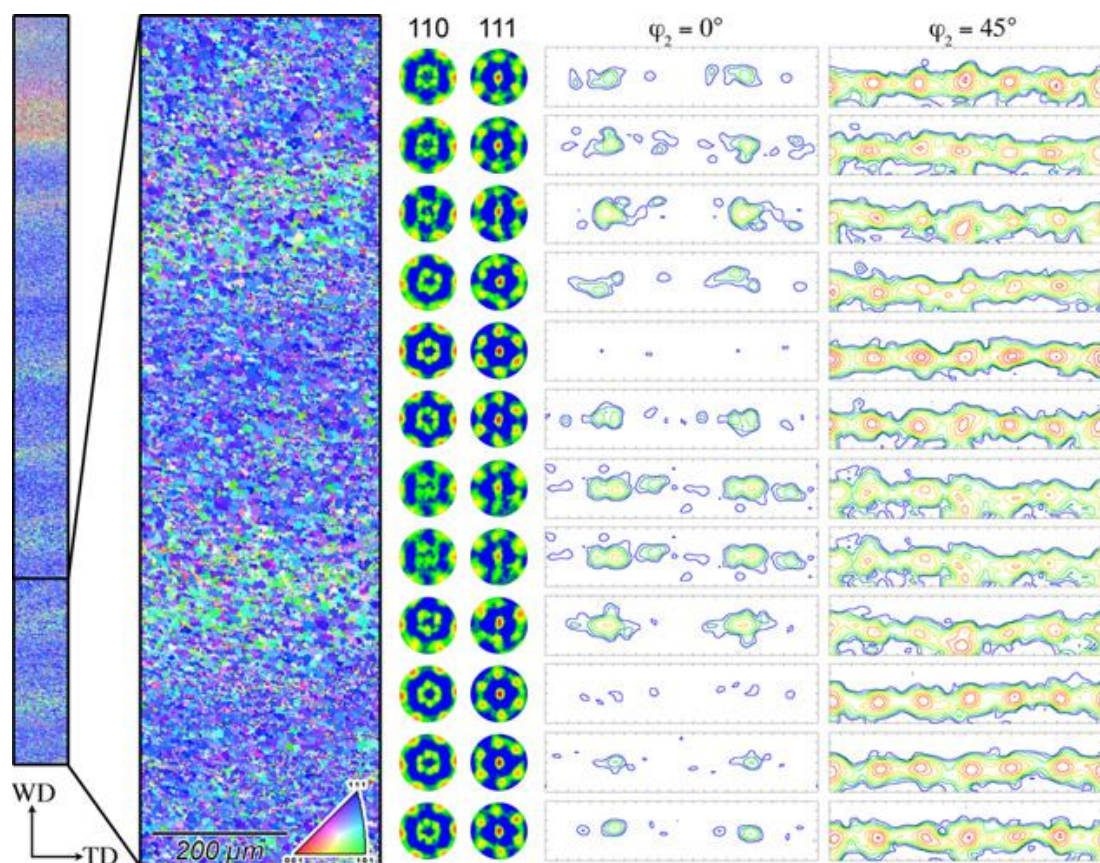
Figure 1.71 Electron backscatter diffraction map of grain orientations along the viewing directions from the indicated regions in Figure 1.70, and texture information (110 and 111 PFs in stereographic projection and u2 = 0_ and u2 = 45_ ODF sections) from 100 lm regions along the vertical welding direction. PF and ODF scales are provided in Figure 1.72. (Fonda & Bingert, 2007)

The material goes through concurrently intense shearing and dynamic recrystallization during FSW. The nucleation of new grains and continuous deformation are main issues to affect the final texture results. Besides, it is important

to separate out the effect of final deformation by shoulder through the forging action after the pin has passed. The final texture significantly influenced by the deformation under shoulder. There is an additional shear deformation component at lower temperature to the recrystallized volume processed by the pin.
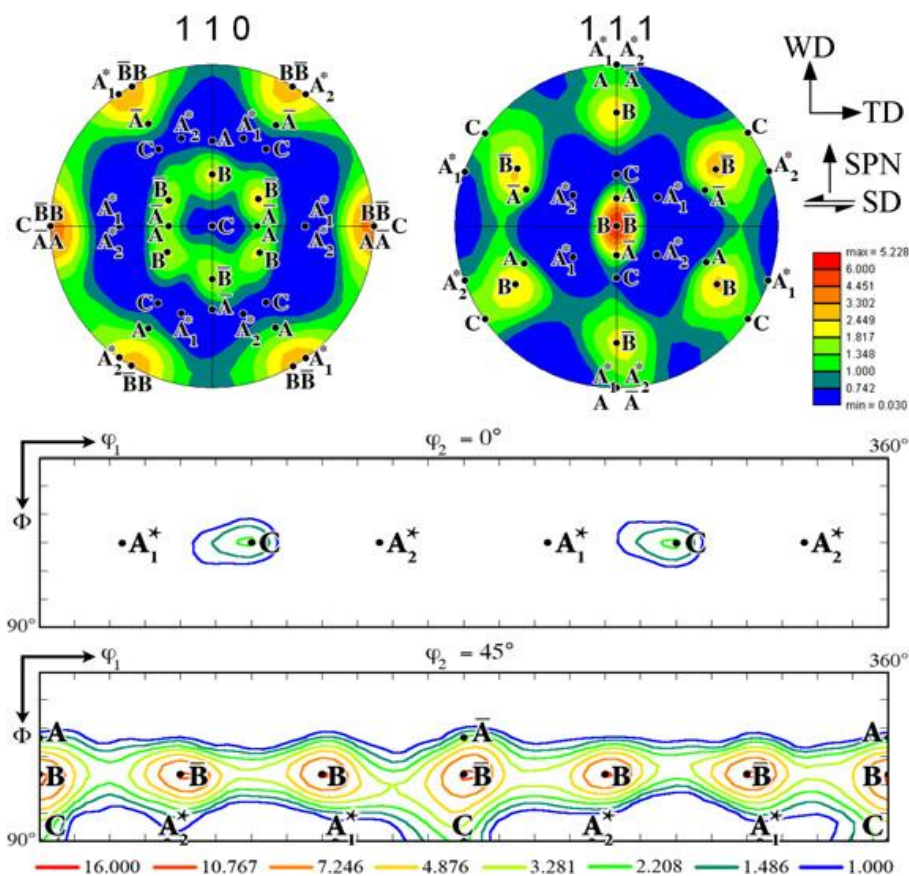
Figure 1.72 Texture results (110 and 111 PFs in stereographic projection and u2 = 0_ and u2 = 45_ ODF sections) from the enlarged EBSD scan shown in Figure 1.71, labeled with the locations of the ideal components of a simple shear texture (Fonda & Bingert, 2007).

1.3.2 Thermomechanically Affected Zone (TAZ)

The thermomechanically-affected zone (TMAZ) lies between the heat-affected zone (HAZ) and weld nugget zone; the grains of the original microstructure are retained in this region, but in a deformed state as shown in Figure 1.32. The top surface of the weld has a different microstructure; the rotating tool shoulder

generates an effect of the shearing. Because, in this region, the parent alloy grain structure becomes both heated and deformed, while it has lesser extent than the weld nugget zone.
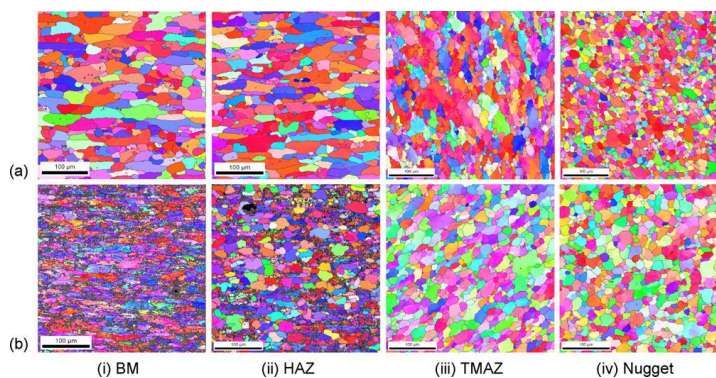
Figure 1.73 SEM/EBSD reconstructed microstructure from the base metal to the nugget for: a) the 5251 O, b) the 5251 H14. High angle boundaries (HAGB) are in black (Etter et al., 2006).
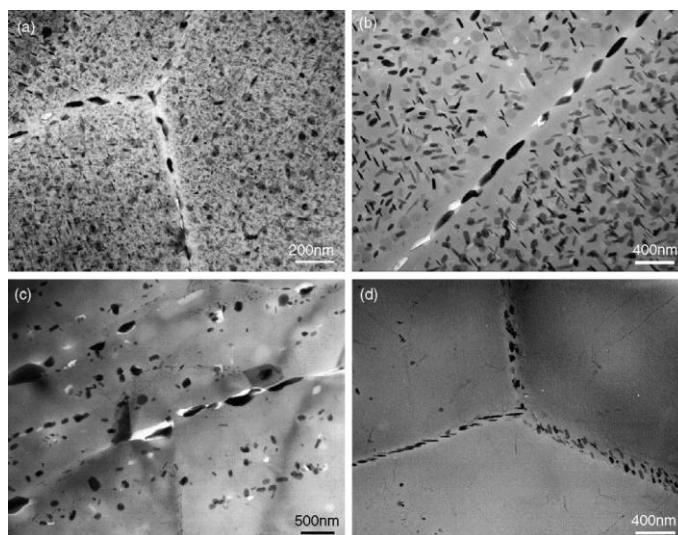
Figure 1.74 Precipitate microstructures in the grain interior and along grain boundaries in: a) base metal, b) HAZ, c) TMAZ near HAZ, and d) TMAZ near nugget zone (FSW 7050Al-T651, tool rotation rate: 350 rpm, traverse speed: 15 mm/min) (Su et al. 2002).

Etter et al. (2006) compared microstructures of aluminum 5251 H14 and aluminum 5251 O each zone which are base material, heat-affected,

thermomechanically-affected and weld nugget by using scanning electron microscopy (SEM) and electron back scattered diffraction (EBSD) as illustrated in Figure 1.73. Recrystallization did not happen in this zone due to insufficient deformation strain. Su et al. (2002) observed dissolution of some precipitates in the TMAZ, as shown in Figure 1.74c and Figure 1.74d, due to high-temperature exposure during FSW/FSP (Sato et al., 1999 and Su et al., 2002). Moreover, the grains in the TMAZ typically hold a high density of sub-boundaries was revealed.

On the other hand, Uzun et al. (2004) have been characterized microstructural area to seven different zones for dissimilar alloys which are aluminum 6013-T4 and X5CrNi18-10 stainless steel by using optical microscopy. These different zones of the microstructure in the welding were reported as follows: (1) base or parent stainless steel, (2) HAZ in the stainless steel at advancing side of weld, (3) TMAZ in the stainless steel at advancing side of weld, (4) weld nugget, (5) TMAZ in the Al alloy at retreating side of weld, (6) HAZ in the Al alloy at retreating side of weld and (7) base or parent Al alloy. Fig 1.75 shows the optical micrograph of these regions indicated as (a)-(h).

1.3.3 Heat Affected Zone (HAZ)

The heat-affected zone (HAZ) is defined as not mechanically deformed, so process occurring in the HAZ is the result only of a temperature transient as shown in Figure 1.32. The heat-affected zone (HAZ) is as in conventional welds. The transient is severest when it is close to the weld center line and reduces in severity far away from the weld. Sometimes, the effect of the transient will be insignificant, depending on the maximum temperature and temporal length of the transient at some distance from the weld. The HAZ will be transitioned to base material. Microstructure of the HAZ can be compared by other zones shown in Figure 1.73. As mentioned by Chen & Kovacevic (2003), the HAZ usually contains a large amount of coarsened grains with relatively lower yield strength than that in the TMAZ and the nugget, which is believed to be the weakest place for the crack initiation in the tests of fatigue performance and tensile strength.
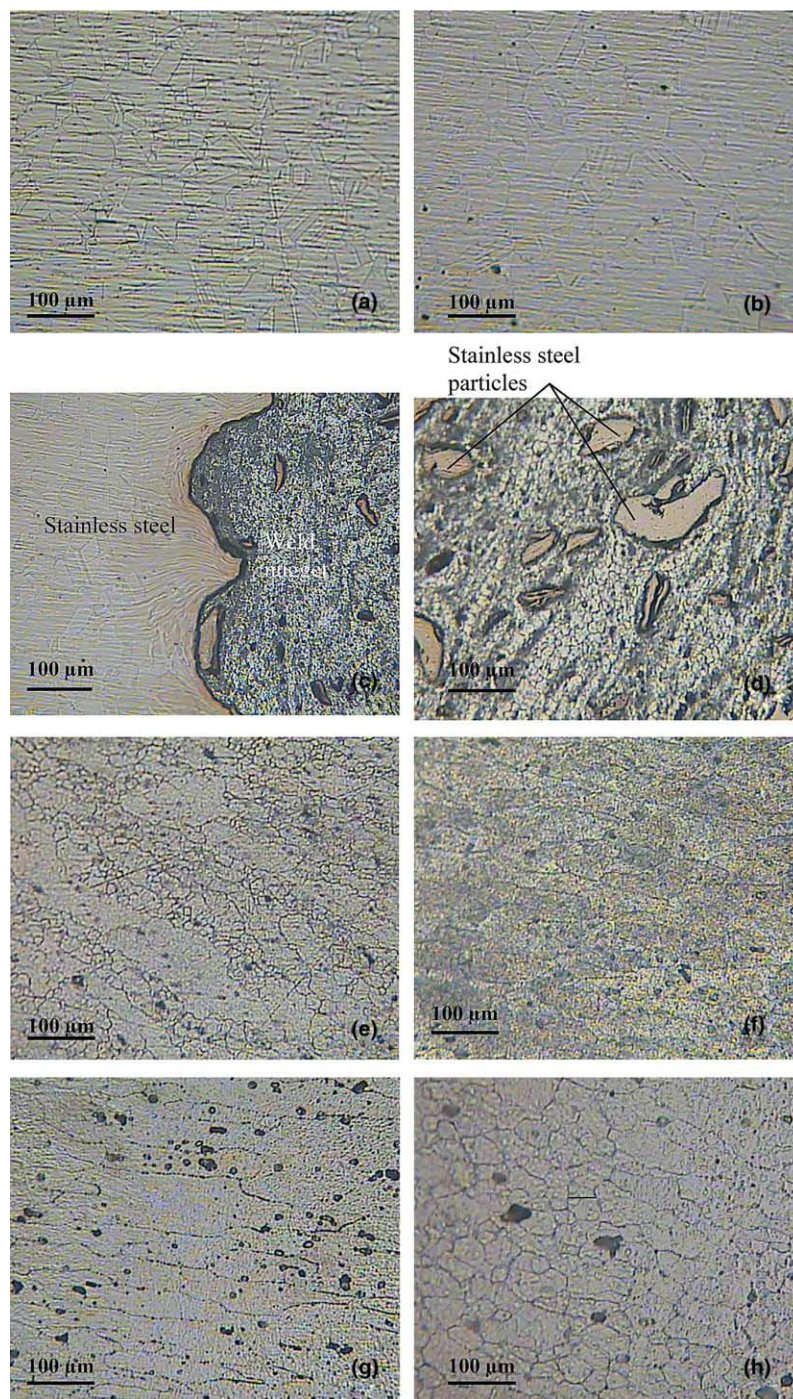
Figure 1.75 Optical microstructures of the ''a–h'' regions shown in Figure 1.32: a) grain structure of base stainless steel, b) HAZ at advancing side, c) TMAZ at advancing side, d) stainless steel particles surrounded by fine equiaxed grains of Al 6013 alloy in the weld nugget, e) TMAZ at retreating side, f) HAZ at retreating side, g) base Al 6013 alloy and h) grain structure of weld root (Uzun et al., 2004).

As Welded

< 100°C   250°C - 300°C   300°C   475°C   Deformed Grains

TMAZ
Dislocation
ρ = Higher

Tensile Fracture

Parent Metal
Dislocation ρ = Modest
10-20nm MgZn$_2$Precipitaes

HAZ   HAZ
Overaged 20-30nm
Mg Zn$_2$ Precipitates

Friction Stir Weld
Recrystallized Fine
Grain Nugget (3-10µm)
Dislocation ρ = Low
No Small Mg Zn$_2$ Precipitates

– 50 to 70nm Mg Zn$_2$ in all Zones with v/o
Maximized in the Low Temperature Region
of the HAZ

HAZ = Heat Affected Zone
TMAZ = Thermal Mechanically Affected Zone

Figure 1.76 Schematic illustration of friction-stir-weld zone microstructures, precipitate distributions, and temperature ranges for 7075 T651 Al (Mahoney et al., 1998).

Mahoney et al. (1998) studied properties of friction stir welding for aluminum 7075 T651and defined the HAZ as a zone experiencing temperature between 250°C and 475°C as illustrated in Figure 1.76.

Recently, Jata, Sankaran & Ruschau (2000) observed dissolution of hardening precipitates in friction stir welding 7050Al-T7451 aluminum alloy; the weld nugget was free of precipitates. They reported that the coarsening of the strengthening precipitates and the precipitate-free zone (PFZ) increases by a factor of 5. Su et al. (2002) get similar results in a detailed TEM examination on FSW 7050Al-T651 as shown in Figure 174b. They observed that a small precipitate free zone (PFZ) was appeared along the grain boundaries.

1.4 Properties of Friction Stir Welding

1.4.1 Residual Stress

It is generally believed that generation of residual stresses in both longitudinal and transverse directions are low in friction stir welds due to low temperature solid-state

process of FSW. But, compared to more compliant clamps used for fixing the parts in conventional welding processes, the rigid clamping arrangements used in FSW exerts a much higher restraint on the welded plates. Thus, the existence of high value of residual stress exerts a significant effect on the postweld mechanical properties, particularly the fatigue crack propagation behaviour. For that reason, it is important to investigate the residual stress distribution in the FSW welds.

James, Mahoney & Waldron (1999) measured residual stress by means of X-ray diffraction $\sin^2\psi$ c method in the FSW 7050Al-T7451, C458 Al–Li alloy, and 2219Al. Donne, Lima, Wegener, Pyzalla & Buslaps (2001) measured residual stress distribution by using the cut compliance technique which are X-ray diffraction, neutron diffraction, and high-energy synchrotron radiation in FSW 2024Al-T3 and 6013Al-T6 welds. Reynolds, Tang, Gnaupel-Herold & Prasket (2003) measured residual stress of 304L stainless steel by neutron diffraction in friction stir welding. Recently, Peel, Steuwer, Preuss & Withers (2003) investigated the residual stress distribution on FSW 5083Al by using synchrotron X-ray diffraction.

The results of these investigations show the residual stress distribution nonhomogeneous in three principle direction. Both longitudinal and transverse residual stresses formed an ''M''-like distribution across the weld. The maximum residual stress value was measured in the HAZ, also, a small amount of compressive stresses observed in the base material which was near to the HAZ as shown in Figure 1.77. The residual stress distribution across the welds observed similarly at the top and root sides of the welds. The residual stress levels were found to be dependent upon the pin diameter, rotational speed and welding speed. The residual stresses in the longitudinal direction were found to be higher than the transverse direction. The residual stress values in all the FSW welds were quite low compared to those generated during fusion welding. The peak tensile residual stress was tested at about 10 mm from the weld centerline, a distance corresponding to the tool shoulder edge. A mild asymmetry in longitudinal residual stress distribution was observed within the nugget zone with about 10% higher stress level on the advancing side. The low

residual stress was attributed to the lower heat input during FSW and recrystallization accommodation of stresses in the FSW welds (Mishra & Ma, 2005).
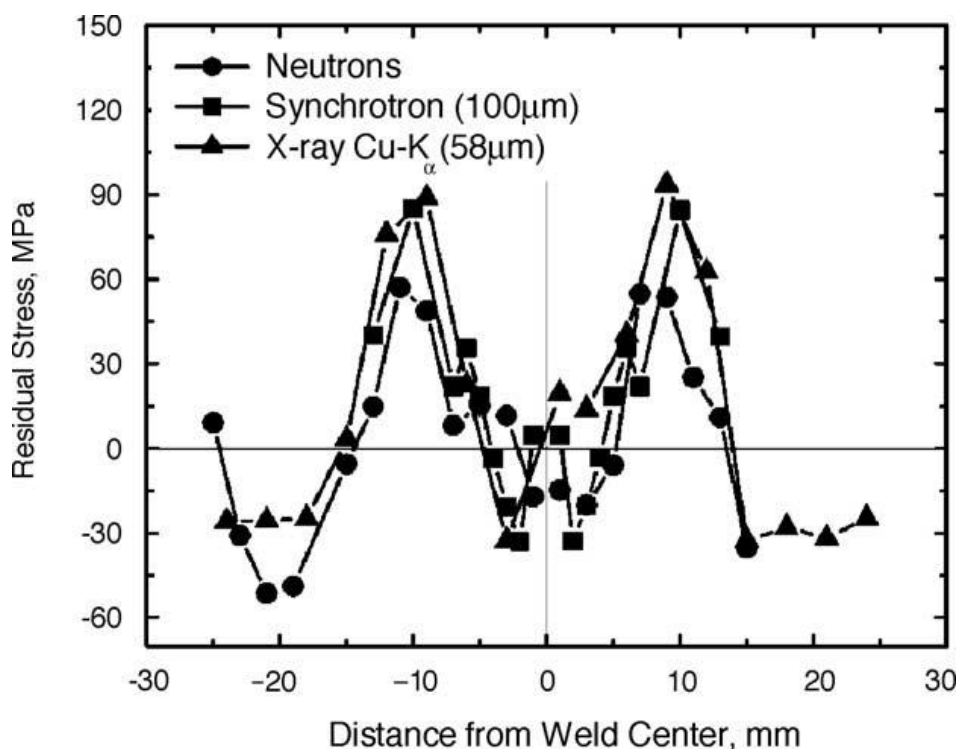
Figure 1.77 Longitudinal residual stress distribution in FSW 6013Al-T4 welds determined by different measurement methods (tool rotation rate: 2500 rpm, traverse speed: 1000 mm/min, tool shoulder diameter: 15 mm) (Mishra & Ma, 2005).

1.4.2 Hardness

Hardness is another mechanical property of the material to discuss in friction stir welding. Aluminum alloys are divided into two groups which are heat-treatable (precipitation-hardenable) alloys and nonheat- treatable (solid-solution-hardened) alloys. Besides, for heat treatable alloys, the FSW temperatures reached within the nugget and parts of the TMAZ will cause at least partial dissolution of the hardening phases. The changing in hardness in the friction stir welds caused different for precipitation-hardened and solid-solution- hardened aluminum alloys. Therefore, FSW creates a softened region around the weld center in a number of precipitation-hardened aluminum alloys (Rhodes et al, 1997, Benavides et al., 1999, and Sato et

al., 1999). Such a softening is caused by grain coarsening and dissolution of strengthening precipitates during the thermal cycle of the FSW could also take place in HAZ.
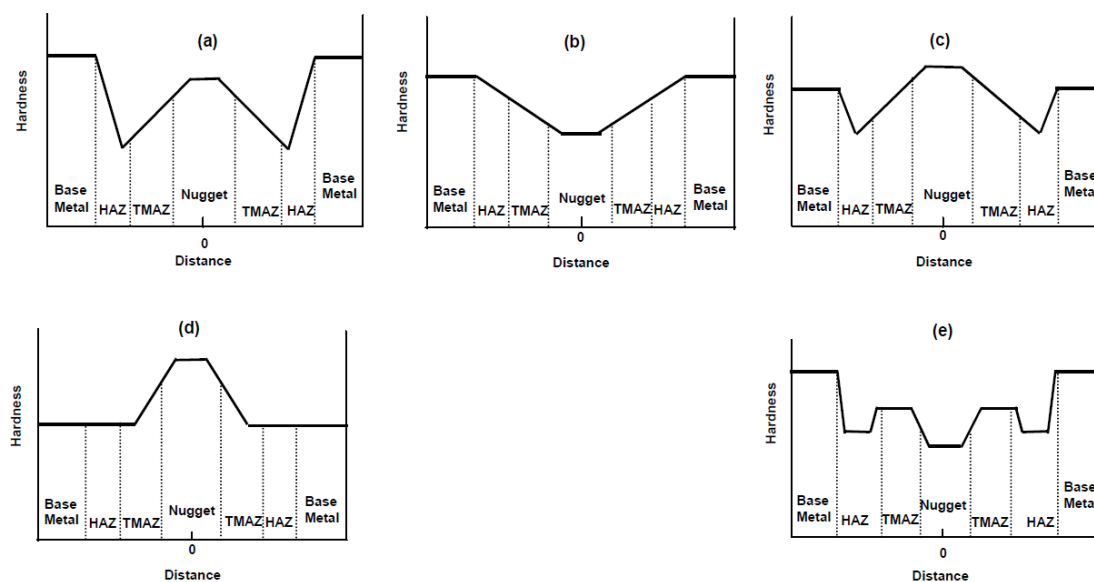
Figure 1.78 Hardness distribution trends across butt joint profiles. Zone boundaries are approximate (Khaled, 2005).

Khaled (2005) gave same example of the hardness distribution curves diagrams for different aluminum alloy in butt joint profiles. The microstructure of the HAZ should transition the base metal into the TMAZ, at the same time; TMAZ should transition the HAZ into the nugget. As shown in Figure 1.78a, the curve just indicated a W-shaped hardness distribution across the joint profile, with minimum in the HAZ around the HAZ / TMAZ interface. The nugget hardness is depending on the alloy and temper, and it could range from just above the HAZ minimum to values approaching that of the base metal. On the other hand, Figure 1.78c hardness distribution is similar the Figure 1.78a, except hardness distributions display nugget hardness values which have reported higher than anywhere else, including the base metal, depending on the welding conditions. The curve as shown in Figure 1.78c has been reported for the vast majority of 2xxx, 6xxx and 7xxx aluminum alloys welds. The hardness distributions of natural or artificial aging of the joints, such as 5083-H131, recrystallization in the nugget, during FSW would eliminate some or all of the

cold work effects. This means that, the non-heat treatable alloys would lead to nugget softening and the development of as welded hardness distributions similar to that illustrated in Figure 1.78b. Conversely is true for the annealed tempers of these alloys, such as 5083-O, where the grain refinement associated with recrystallization, would bring about increasing the nugget hardness and the development of as welded hardness distributions similar to that illustrated in Figure 1.78d. This same type of hardness distribution for 7050 that was resolution heat treated and artificially aged to the -T74 temper as depicted in Figure 1.78e. This curve looks like combination of Figure 1.78b, Figure 1.78c and Figure 1.78d, which means, the resolution heat treatment and aging have obliterated the HAZ minimum, while the grain refinement in the nugget led to some hardening.

He also concluded the asymmetry of the weld zones with respect to the weld centerline and mid-thickness plane, the hardness distribution is expected to vary with depth; that is to say the hardness distribution at the face of the weld would be different from that at mid-thickness or that at the root. Hence, the location of the distribution with respect to some fixed reference, such as mid-thickness, face or root are very important to indicate, when comparing the hardness especially.

Sato, Urata & Kokawa (2001) have investigated the hardness distribution profiles of the aluminum alloy 6063Al-T5 and T4 in friction stir welding at several rotational speeds. They reported that the hardness values in the as-welded condition were reduced around the weld center in the weld of Al alloy 6063-T5 and were distributed homogeneously in the weld of Al alloy 6063-T4. There is not any important difference in the hardness profile for different rotation speeds in these welds, but the softened region widens with increasing rotational speed in the weld of Al alloy 6063-T5. Post-weld aging cause a rise in hardness in most parts of the welds, in spite of this, a small increase in hardness observed at the over-aged regions and the stir zone of the 800 rpm weld. This small increase in hardness in the stir zone was strongly related to the increase in volume fraction of the PFZ caused by the smaller grain size in the 800-rpm weld zone.

Table 1.1 Variation of weld parameters.* Water cooled (Yeni, 2008)

Joint	Rotation Speed (RS) (rev/min)	Welding Speed (WS) (mm/min)	WS/RS ratio
condition A	800	100	0.125
condition B	800	200	0.250
condition C	1250	100	0.080
condition D	1250	200	0.160
condition E	1600	100	0.063
condition F	1600	200	0.125

Yeni (2008) investigated aluminum alloy 7075 (AA 7075) hardness measurements by using three different rotational speeds and two welding speeds which were given in Table 1.1 to determine optimum welding parameters. She made microhardness measurements only for conditions C, D, F and base metal because of conditions A and B visible porosity. The hardness measurements specimens were chosen middle section (3 mm from the top surface). The welding speed was doubled in condition D to respect to condition C, this is the only difference between these two condition and hardness values decreased 100 HV for condition D and 115 HV for condition C at HAZ. This drop in condition D came from increasing welding speed, which means less heat input in condition D because of faster welding speed. Less heat input also caused to decrease yields in the hardness values slightly. Highest harness values have been obtained from condition F. Therefore, increasing rotational speed caused more heat generation and better hardness values.

Recently, Aydin, Bayram, Uğuz & Akay (2008) investigated the different heat-treated-state 2024 Al-alloys were friction stir welded. They tested the Al 2024-W states which were metallurgical state results from a water quench after a solution treatment of the alloy at 510°C for 2.5 h (W state), Al 2024-T4 states which were obtained by keeping the Al 2024-W plates several years of ageing, Al 2024-T6a

states that were produced by keeping Al 2024-W plates at 100˚C for 10h, Al 2024-T6b states obtained same way as Al 2024-T6a, except tempering conditions, that were 190˚C with same time (10h) and Al 2024-O temper was cooled in air after the solution treatment. The microhardness values in the weld zone of the Al 2024-O joint are higher than those in the base material, which means that the weld zone is strengthened by the FSW process. The microhardness values in the 2024-T4 and -T6 (190 ˚C – 10 h) joints are partially higher than those in the 2024-W and -T6 (100 ˚C – 10 h) joints. An appropriate natural or artificial ageing in 2024 Al-alloys has lead to a pre-ageing effect during welding, but in these experiments pre-aging resulted in decrease of mechanical characteristics. In fact, in Figure 1.79 illustrated TMAZ and HAZ have lowest values microhardness trends of FSW joints. As verified by drop in microhardness, hardening precipitates experience a somewhat over-ageing, causing phase transformations and as a result of this, losing general mechanical properties. However, great shear stresses generate by tool motion cause a very fine grain structure generation, which lets a partial recovery. They also reported the hardness profiles greatly depend on the precipitate distribution, only slightly on the grain and dislocation structures in precipitation hardening aluminum alloys.
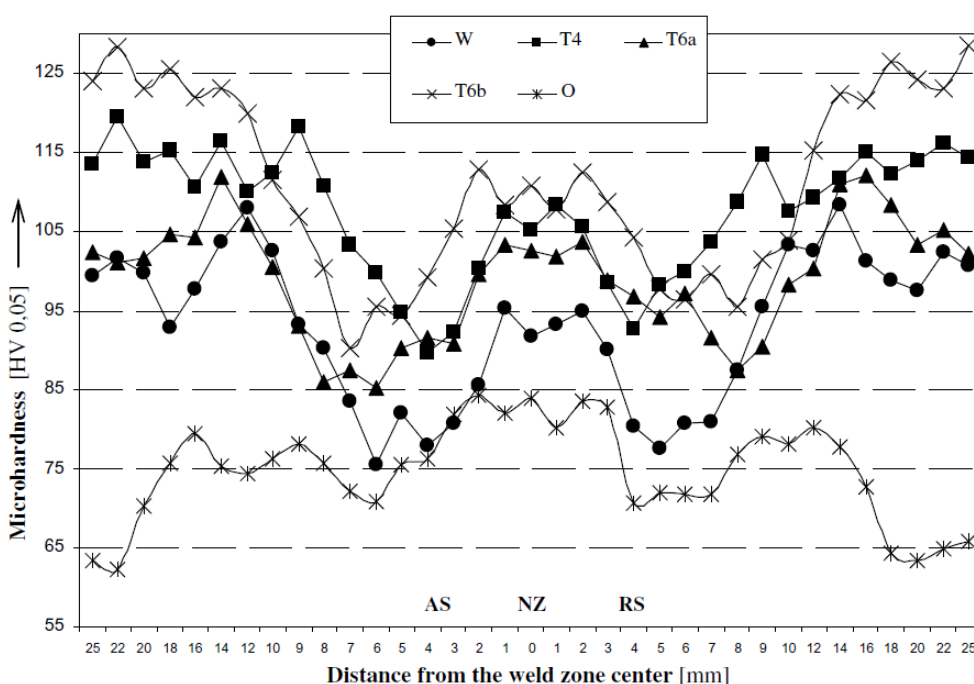
Figure 1.79 Microhardness profiles of the joints across the mid-sections (Aydin et al., 2008)

1.4.3 Mechanical Properties

When FSW is properly applied, the post-weld mechanical properties improved, such as high strength and ductility, fatigue life and fracture toughness. During the early stages of FSW development, the method appeared simple when compared to many conventional welding methods. On the other hand, when the FSW developments were continued, the method complexity was realized. The scientists have demonstrated the post-weld mechanical properties can be a function of: tool travel speed; tool rotational rate; tool design; tool tilt; material thickness; alloy composition; initial material temper; cooling rate; heat sink; test sample size, location and orientation; surface oxides; joint design; post-weld heat treatment; FSW test system; time between FSW and testing, that is, natural aging at room temperature.

1.4.3.1   Strength and Ductility

As Peel et al. (2003) mentioned conventional transverse tensile testing only provides a value for the overall (macroscopic) strain experienced by the sample. Therefore, generally the failure strain of samples cut transverse to the weld direction so as to include both parent and welded material fail at considerably lower strains than would be expected for the parent material.
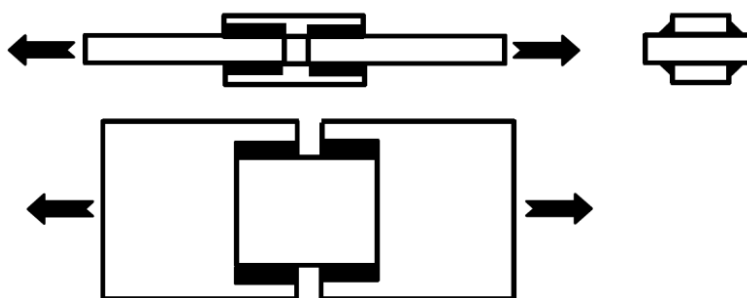
Figure 1.83 The longitudinal fillet weld tension shear specimen. Block
arrows indicate loading direction (Khaled, 2005).

Khaled (2005) explained tensile properties of 2xxx, 5xxx, 6xxx, 7xxx aluminum alloys, multiple aluminum alloys, dissimilar aluminum alloys, magnesium alloys, titanium alloys and copper alloys. Moreover, gave the detailed information about tensile testing. The tensile testing may be transverse or longitudinal, using flat or round specimens for butt joints. Transverse-weld specimens are loaded transverse to the weld direction in transverse testing. Longitudinal-weld specimens are loaded parallel to the weld direction in longitudinal testing.

In general, the tension-shear test is used to generate data for fillet and spot welds. Two basic types of specimen are available, for fillet welds which are the longitudinal-tension-shear specimen as shown in Figure 1.80 and the transverse-tension-shear specimen that may be of the single-lap or double-lap configuration as shown in Figure 1.81. The double-lap transverse-tension-shear test specimen is preferable, because it prevents the bending effects associated with single-lap specimens. Moreover, minimizes data sensitivity to preparation parameters, for example, the gap between the overlapped members. Ultimate shear strength data may be indicated as in psi / ksi, based on fillet throat (where fracture is expected to take place), or in lbs per lineal inch of the fillet weld. There are no data about yield strength or elongation. Commonly, axial fatigue S-N data obtained from the transverse-single lap-tension-shear type of specimen as shown in Figure 1.81a (Khaled, 2005).
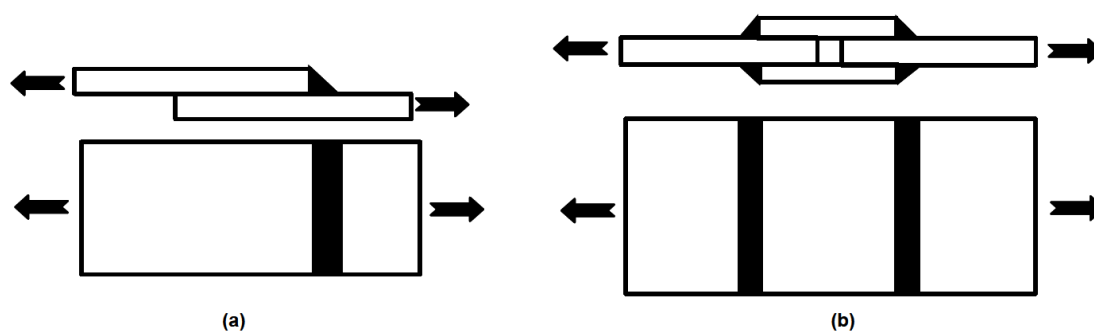
Figure 1.81 The transverse-fillet-weld-tension-shear specimens. Block arrows indicate loading direction, a) Single-lap configuration, b) Double-lap configuration (Khaled, 2005).
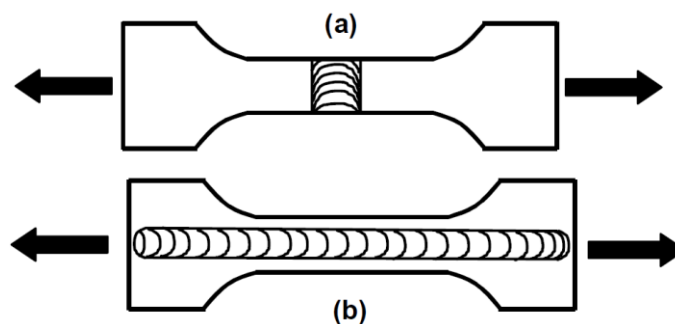
Figure 1.82 Transverse; a) and longitudinal, b) specimens. The specimens may be flat or round. Flat specimens are typical in FSW. Block arrows indicate loading direction (Khaled, 2005).

As shown in Figure 1.82a the transverse-weld specimens can be flat or round. Usually, the flat specimens are more frequently used in FSW work. In transverse specimens, the nugget zone (NZ), heat-affected zone (HAZ) and base metal regions, with their respective microstructures, are all represented along the gage length. Each region should be loaded to the same stress during tensile testing. If the strength of the NZ exceeds that of the base metal, nearly all the plastic deformation occurs outside that NZ, usually in the HAZ. By itself, the test will not give any information about the NZ or any defects in the weld. However, if the NZ is weaker than the base metal, the plastic strain and failure would occur mainly in the NZ. By itself, the test may not reveal undesirable HAZ or base metal characterization that might be present. The elongation is based on the entire gage length (i.e., based on all the regions and microstructures) and, so, the % elongation data can be misleading.

As shown in Figure 1.82b flat longitudinal-weld specimens are used to generate tensile data along the weld. The width of the specimen includes the NZ, HAZ and maybe the base metal. The NZ, HAZ and base metal regions are all strained equally and simultaneously during testing. There are no standards to control the relative lengths of HAZ and base metal to be included in specimen width. As a result, data can be inconsistency. In addition, crack initiation will possibly start any region with poor ductility, typically at low stress levels. Regions with good ductility may carry on loads to strength levels higher than their own. Otherwise, longitudinal test results can be misleading, if the data is not used in combination with transverse test data.

Sometimes, it is better to generate region-specific data. The longitudinal round or flat specimens are necessary to cut out from certain regions, such as the NZ or a specific region thereof (all-weld specimens) or HAZ, Figure 1.83. Typically, specimen dimensions of the selected region need to be size to fit within the envelope. Occasionally, microspecimens (very small specimens) must be used to get the required data. Small and large size specimens' data can be different.
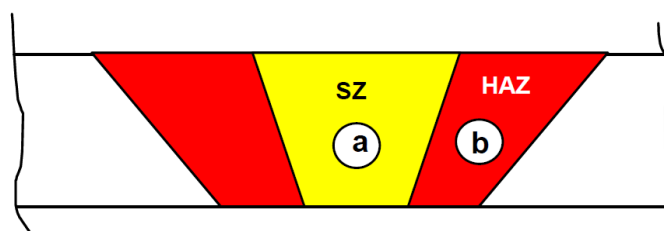
Figure 1.83 Longitudinal specimens. Specimens shown here are round; flat specimens are also used, a) Within the SZ (all weld metal specimens), b) Within the HAZ (Khaled, 2005).

As a result of the offset between the axes of the lapped members bending stresses develop in single-lap-tension-shear testing. The maximum bending tensile stresses occur around the weld joint at the bottom of the top member and at the top of the bottom member as illustrated in, Figure 1.84. Additional intensity obtained by using bending stresses test to generate static (strength) or dynamic (fatigue) data. It is necessary to provide the single-lap test specimens with packing pieces in the grip regions because of balance the offset axes of the lapped details, and minimize bending effects, as shown in Figure 1.85 (Khaled, 2005).
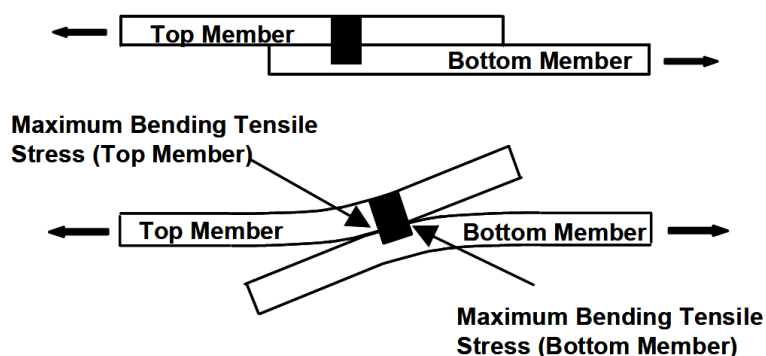
Figure 1.84 Bending in single-lap-tension-shear testing (Khaled, 2005).
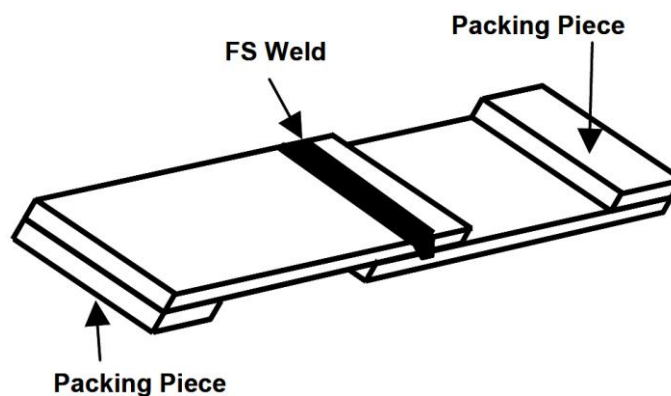
Figure 1.85 Packing pieces in single lap tension shear specimens (Khaled, 2005).

. Generally, a conventional spot weld is tested in tension-shear or in peel. The tension-shear test uses the single- lap specimen for obtaining strength or fatigue data as shown in Figure 1.86. The peel test is used mainly manual means to grip and apply the pealing force in a shop control test as illustrated in Figure 1.87a-c. In only conjunction with spot joints which exist at the interface between the overlapped details obtained by the peel test. Sometimes a special tension-peel test which is not listed among the standard tests used for conventional welds used to generate strength data as shown Figure 1.87d (Khaled, 2005).
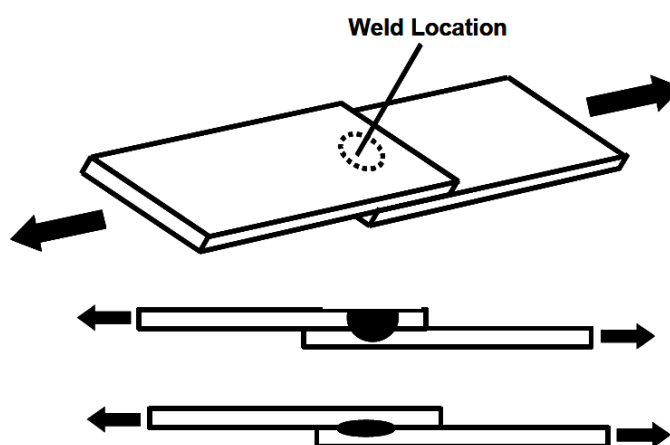
Figure 1.86 Tension-shear testing of spot joints. Block arrows indicate loading direction (Khaled, 2005).

A fundamental problem generating stress combination of the shear and peel is caused by loading in tension-shear testing of single-lap joints. Therefore, the strength

data generated cannot be directly compared to base metal ultimate tensile strength, obtained in a tension test, or seen as pure shear strength, if failure occurs through the weld; this can be occur also tension-peel testing. Conventionally produced joints can be tested in tension-shear in the single-lap configuration without using packing pieces.
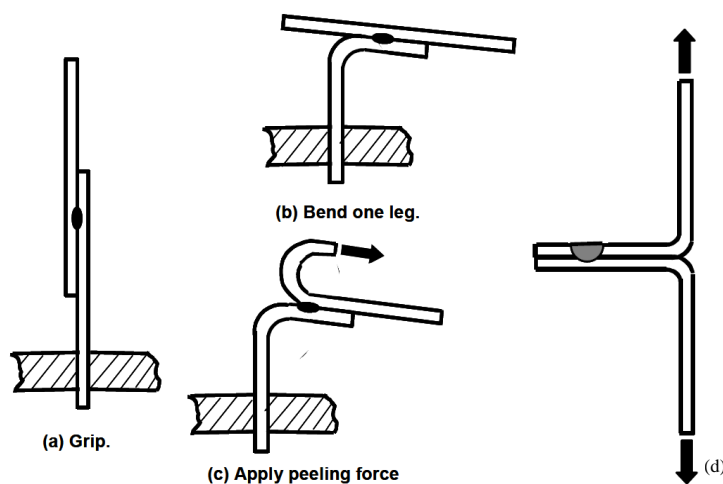
Figure 1.87 a-c) Peel test as shop control means, d) A non-standard tension-peel test. Block arrows indicate direction of loading (Khaled, 2005).

Peel et al. (2003) also concluded as their experimental result the weld properties were dominated by the thermal input rather than the mechanical deformation by the tool. They investigated the effect of different welding speeds on the weld properties. They observed the peak longitudinal stresses increase as the traverse speed increases. This maybe the result of steeper thermal gradients during welding and the reduced time for occurring stress relaxation occur. The tensile stresses appearance observed to be limited to the softened weld zone resulting in a narrowing of the tensile region (and the peak stresses) as the traverse speed increases.

Mahoney et al. (1998) investigated solid-state welds of 7075Al-T651 to determine mechanical properties both in the longitudinal direction that is in the weld nugget, and, transverse direction of the weld the tensile properties. Tensile specimens were excised from the nugget zone in two directions, longitudinal (parallel) and transverse

(normal) to the weld. Longitudinal tensile specimens contained only fully recrystallized grains from the nugget zone, while transverse tensile specimens contained microstructures from all four zones, which are parent material, HAZ, TMAZ, and nugget zone. The longitudinal tensile properties of nugget zone summarized at Table 1.2. Yield and ultimate strengths in the weld nugget decreased, while ductility remained high in the as-welded condition. So that, Mahoney et al. (1998) led a post-weld aging treatment (121˚C/24 h) on the FSW sample for recover the lost tensile strength of the nugget zone. As addition of a post-weld age treatment, has resulted in recovery of a large portion of the tensile yield strength in the nugget, but at the expense of ultimate strength and in particularly ductility. They reported the increase in the yield strength of post-weld samples was attributed to the increase in the volume fraction of fine hardening precipitates, where the drop in the ductility was explained for by both the increase in the hardening precipitates and the development of precipitate-free zones (PFZs) at grain boundaries. Table 1.3 are summarized the tensile properties in transverse orientation of FSW 7075Al-T651.

Table 1.2 Longitudinal tensile properties of weld nugget in friction stir welded 7075Al-T651 at room temperature (Mahoney et al., 1998).

Condition	Yield Strength (MPa)	Ultimate Strength (MPa)	Elongation (%)
Base Metal, T651	571	622	14.5
As-FSW	365	525	15.0
Post-weld age treatment	455	496	3.5

Table 1.3 Transverse tensile properties of weld nugget in friction stir welded 7075Al-T651 at room temperature (Mahoney et al., 1998).

Condition	Yield Strength (MPa)	Ultimate Strength (MPa)	Elongation (%)
Base Metal, T651	571	622	14.5
As-FSW	312	468	15.0
Post-weld age treatment	312	447	3.5
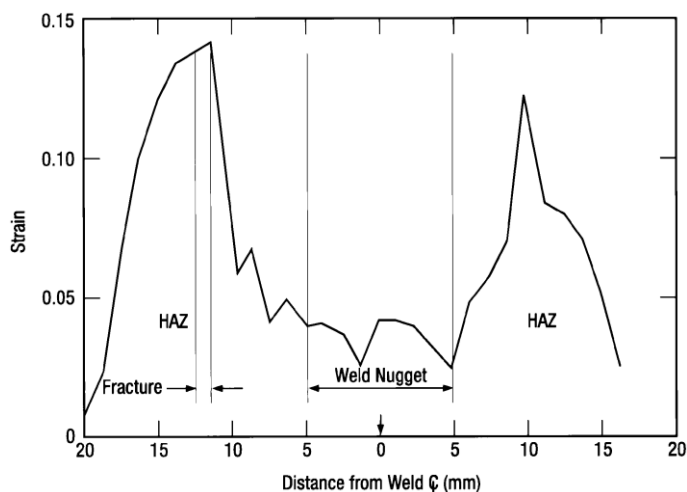
Figure 1.88 Tensile strain distribution within the HAZs and weld nugget of a friction stir weld (Mahoney et al., 1998).

The samples tested in transverse direction showed a significant reduction in both strength and ductility relative to unwelded base metal. Moreover, the strength and ductility observed in transverse orientation are also considerably less than those in longitudinal orientation. The post-weld aging treatment did not re-establish any of the strength to the as-welded condition and additional reduced ductility. Failures occurred as shear fracture in the HAZ in both as-welded and aged conditions. The HAZ has the lowest strength because of significantly coarsened precipitates and the development of the FPZs. Therefore, strain occurs mainly in the HAZ during tension. Figure 1.89 shows the strain distribution across weld and HAZ in the as-welded sample. The weld nugget which has higher strength zone resists deformation more than HAZ. The low-strength HAZ locally elongated to high levels of strain (12–14%), eventually resulting in necking and fracture, whereas the nugget zone experiences only 2–5% strain as illustrated in Figure 1.88. Therefore, resulting in a low strength and ductility along transverse orientation of the weld, fracture always occurred in the HAZ.

Sato & Kokawa (2000) investigated major microstructural factors governing the global tensile properties of a friction-stir-welded joint of 6063 aluminum by estimating distribution of local tensile properties corresponding to local

microstructure and hardness. They reported yield and ultimate tensile strengths of the as-welded material were significantly lower than those of the base material. 6063-T5 Al used as base material. Moreover, the weld was artificially post-weld aged at 448 K (175 °C) for 43.2 ks (12 hours) after examinations of the as-welded weld. Additionally, solution heat treatment (SHT), solution heat treatment and aging (SHTA) were applied to the weld. The SHTA process consisted of SHT at 803 K (530 °C) for 3.6ks (1 hour) followed by quenching in water and subsequent aging at 448 K (175 °C) for 43.2 ks (12 hours). Therefore, tensile properties of the base material, the weld, aged weld, and the SHTA weld as shown in Figure 1.89. It gives an idea about elongation and the strengths are lowest in the as-welded weld. The aged weld has slightly higher strengths than the base material with at the same time improved ductility. The SHTA restored the strengths of the weld to the levels of the base material with almost completely restored ductility.

Yeni (2008) studied the effect of welding parameters on the mechanical properties of friction stir welded AA 7075 at room temperature. The optimum welding parameters determined by applying three different rotational speeds, i.e. 800, 1250 and 1600 rpm and two different welding speeds, i.e. 100 and 200 mm/min. The six different joints obtained. Mismatch ratio that provides a means of comparing the relative strength of the joints was defined as the ratio of the weld metal yield strength to that of the base metal. She also reported joint efficiency which is the ratio of the ultimate condition to that of the base metal percentage, of the conditions A-B where the rotational speed was 36% and 50% lower compared to conditions C-D and E-F, respectively, specified insufficient joint efficiency. Joint efficiency of the higher rotational speeds of 1250rpm and 1600 rpm were similar.

Flat transverse tensile tests results are summarized in Fig 1.90. Condition A and F welding speed to rotational speed (WS/RS) ratio are same that, i.e. 0.125, but sample A yield and ultimate strength results improved 60% by doubling welding and rotational speeds as sample F with improving elongation 6 times. This is the result of higher rotational speed generate higher temperatures due to higher frictional heating

and better stirring and mixing of the material. Another result can be obtained according to Fig 1.90, when the condition D and F are compared, only difference is their rotational speed and result in higher yield strength, but ultimate strength is same. In the study, condition D, E, F ultimate strength are almost same, however there is small improvement in yield strength values condition C, though F. We can conclude that after reaching the peak value for ultimate strength for optimum welding parameters, there no more progress in ultimate strength, only progressing obtained in yield strength and elongation
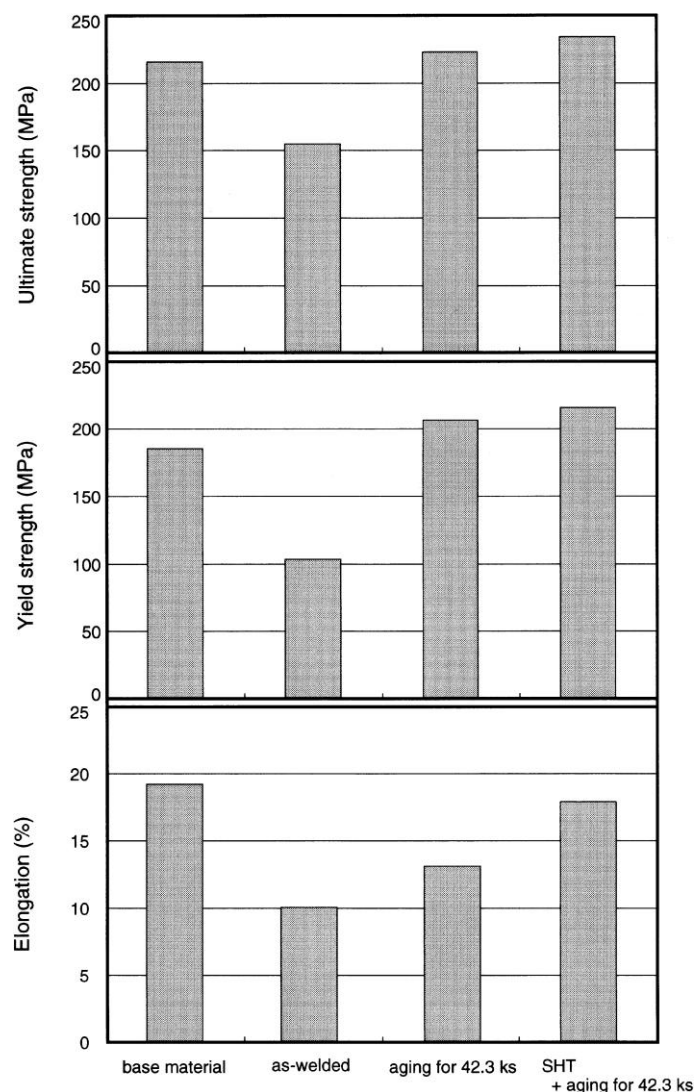
Figure 1.89 Tensile properties of the base material, the as-welded weld, the aged weld, and the SHTA weld (Sato & Kokawa, 2001).
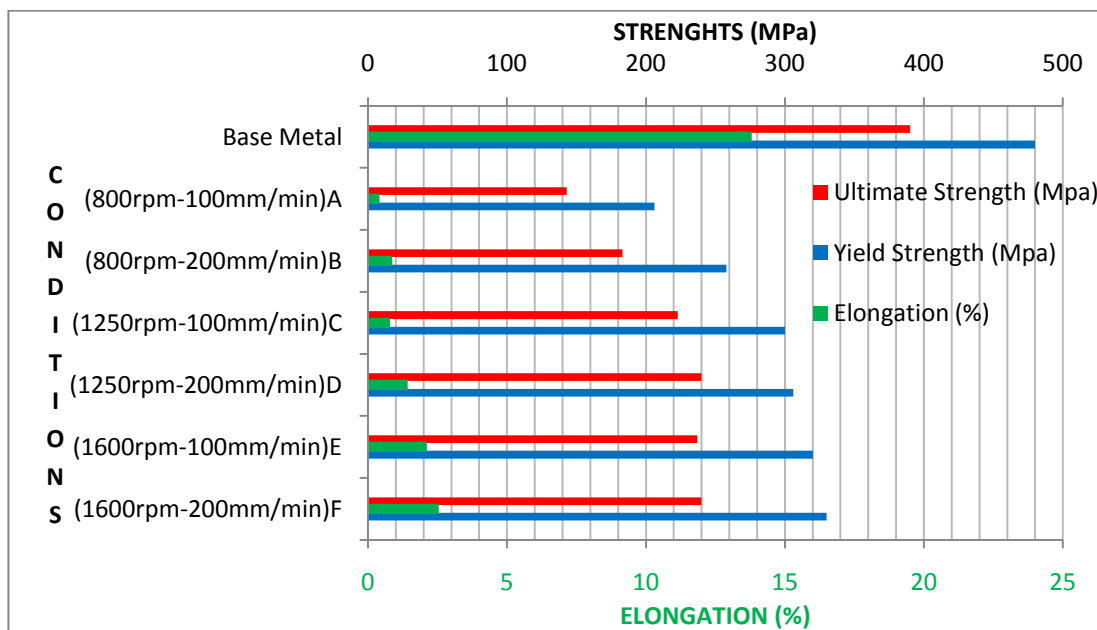
Figure 1.90 Comparison of the tensile properties of the AA 7075 joints.
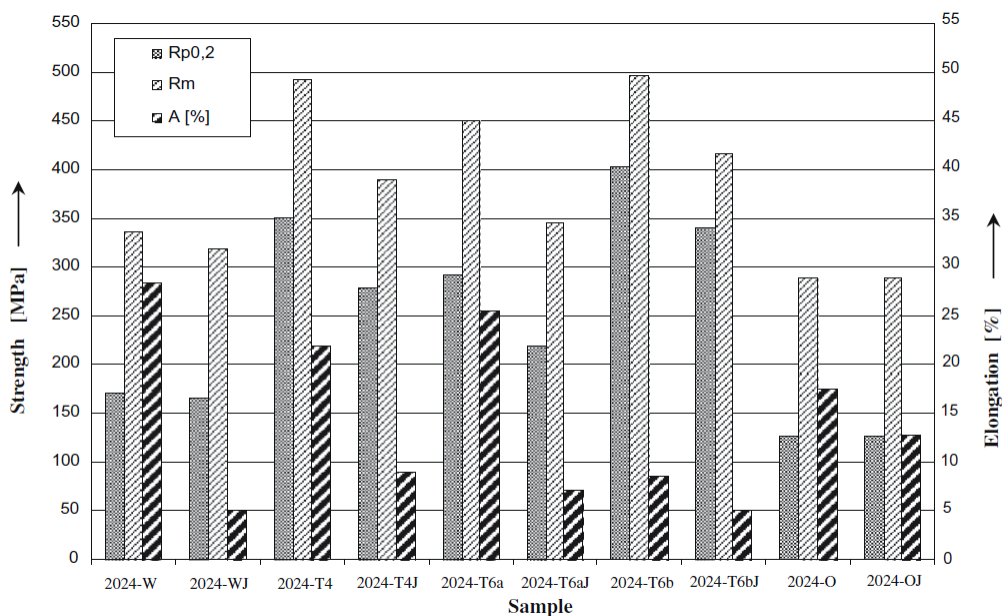
Figure 1.91 Comparison of tensile properties of joints (Aydin et al., 2008).

Most recent study investigated by Aydin et al. (2004) for tensile properties of friction stir welded joints of 2024 aluminum alloys in different heat treated-states. They used aluminum alloys have been discussed in 1.4.2. The tensile properties of the joints have a tendency to increase with the precipitation hardening of the base material. The maximum tensile properties have been obtained in the Al 2024-T6 (100

˚C – 10 h) joint. The Al 2024-O joint weld zone got more strength by the friction stir welding process. The fracture regions were detected near the interface between the nugget and the thermomechanically affected zone for T4 and T6 joints and base material for O joint, expect for W joints were detected near the nugget.

Table 1.4 Tensile properties of the joints (BM: Base material) (Aydin et al. 2004).

Sample	0.2% proof strength, $R_{p0.2}$ (MPa)	Ultimate tensile strength, R_m (MPa)	Elongation, A (%)	Fracture locations of the joints
2024-W (BM)	171	336	28.4	–
2024-T4 (BM)	351	492	21.9	–
2024-T6a (BM) (100 ˚C – 10 h)	293	451	25.5	–
2024-T6b (BM) (190 ˚C – 10 h)	403	496	8.6	–
2024-O (BM)	126	289	17.6	–
2024-W joint	165	318	5	NZ on the AS
2024-T4 joint	279	389	9	The interface between the NZ and the TMAZ on the AS
2024-T6a joint	220	346	7.1	The interface between the NZ and the TMAZ on the AS
2024-T6b joint	341	416	5.1	The interface between the NZ and the TMAZ on the AS
2024-O joint	The same values with 2024-O		12.8	BM

The tensile properties of the joints are shown at Table 1.4 and in Figure 1.91. The tensile properties of each joint are lower than those of the base materials, except for 2024-O joint. The tensile properties of the joints change with the base material conditions. The 2024- W joint has the lowest tensile properties for the joints among the heat treated samples (base materials). The samples which were excised from the 2024-T6b joint have been generated the maximum tensile properties for the joints. The tensile properties of the joints have a tendency to improve with the precipitation hardening of the base material. The tensile properties of the 2024-O joint are equivalent to those of the base material, but it has lower elongation than that of the base material. The heat-treated 2024 Al-alloys joints possess higher yield and tensile strength but a lower elongation than the joint of the 2024-O Al-alloy. The thermal history of the material has mainly affected on mechanical properties, such as, the ductility and strength of defect-free friction stir welds in heat-treatable aluminum alloys. During welding, the coarse scale precipitates within the grains and the grain boundaries are owing to the dissolution of fine scale precipitate zones which affect the tensile properties of the joints. All of the joints demonstrated lower ductility that is the percentage elongation values than their base material as seen in the Table 1.4. The maximum elongation has been obtained in the, on the contrary that 2024-W and T6b joints have the lowest elongation values with 5% and 5.1%, respectively (Aydin et al., 2008).

1.5 Friction Stir Welding Variations

There are some application technologies to improve Friction stir welding, like Friction Stir Processing (FSP), Micro Friction Stir Welding (MFSW), Laser Shock Peening (LSP) of Friction Stir Welding, Thermal Stir Welding (TSW), Ultrasonic Stir Welding Process (USWP), Friction Stir Spot Welding (FSSW), Orbital Friction Stir Welding, Advance Friction Stir Welding (AFSW), Friction Stir Channeling (FSC) and Friction Stir Knead Welding (FSKW), Laser-Assisted Friction Stir Welding (LAFSW), and Double, Twin or Multi-Stir Friction Stir Welding.

1.5.1 Friction Stir Processing (FSP)

Friction stir processing (FSP) was developed by modifying basic principles of FSW. Friction stir processing uses same principles like friction stir welding, but FSP is used to modify the local microstructure and does not join plates together (Mahoney & Lynch (n.d.)). High-strain rate superplasticity was obtained in commercial 7075Al alloy is an example of FSP (Ma, Mishra & Mahoney, 2002). Friction-stir processing (FSP) can locally eliminate casting defects and refine microstructures, by means of that improve strength and ductility, increase resistance to corrosion and fatigue, enhance formability, and improve other mechanical properties.

One more variant of FSW is friction stir processing (FSP), where the friction stir tool is basically traversed through the material. There isn't any joint, in these applications. Considerably, FSP can be used to improve the material properties of castings and wrought material. In castings, porosity can be eliminated by using friction stir processed. Besides, a significant improvement in material properties can be obtained. In other applications, ductility of the material can be improved. In the case of forming and bending material applications can be advantage compare to classical methods by improving lower ductility materials, such as aluminum (Friction Stir Link Inc.).

1.5.2 Micro Friction Stir Welding (MFSW)

Friction stir welding is traditionally joining thicker materials which are difficult to weld. Micro friction stir welding (MFSW) is new application using FSW for thin sheet joining as shown in Figure 1.92. In addition to FSW advantages, butt, lap and spot weld joints can be weld down to 0.3 mm thickness. Some examples of applications of MFSW are innovative thin-wall piping solutions, aerospace thin casings and aluminum bus-bars. According to TWI, example of future possible uses of MFSW are thinner welding, hermetic sealing for packaging, copper cable joints and low distortion flexible sheets (TWI, Micro Friction Stir Welding).

Figure 1.92 Micro friction stir welding (TWI).

1.5.3   Laser Shock Peening (LSP) of Friction Stir Welding

Friction stir welding is caused significantly growth of residual stresses of welded material with respect to fatigue properties and fatigue crack growth process. The residual stress which is generally in the heat-affected zone can reduce advantages of

friction stir welding by causing faster crack initiation and propagation. Laser shock peening (LSP) which is a new surface treatment process was found out to reduce tensile residual welding stress of the plates (Hatamleh, n.d.).

LSP is increasing fatigue properties of the weld where the failure occurs at initiated surface cracks. High-energy laser pulses are exposed at the surface coated with dark paint and water which is used as a thin layer of transparent material. The absorption of laser and paint causes a pressure shock wave with a layer of water. This wave creates a compressive stress layer precisely under the focused laser pulse and increase compressive residual stress.

LSP is a method of treatment for fatigue critical locations without masking, and also there is a chance to repair cracks. LSP supplies smooth surface which has excellent process control and repeatable. Expected one of the future usage of LSP of FSW is space vehicles.

1.5.4   Thermal Stir Welding (TSW)

Thermal stir welding is new improved technology that is joining method used for fusion welding and friction stir welding for dissimilar materials for better joining quality. Thermal stir welding process has totally independent heating and stirring functions of the friction stir welding process. Classic fusion welding apparatus (laser, plasma torch, etc) can be used to initially melt the material. Another way of this is heating material by using induction resistance heating. These apparatus is used to heat material, a separate grinding/extrusion form recrystallizes the result of dendrite matrix structure as it changes from the melted temperature state through the plastic temperature state (NASA, Thermal stir welding).

Each material of the weld joint heat source can be controlled independently. Welding copper and aluminum or stainless steel and titanium plates are good example for joining dissimilar metals for thermal stir welding.

In addition to FSW advantages, thermal stir welding has totally separate heating and stirring forms, also the independent heating process makes easy welding which has higher melting temperatures materials, like steel and titanium. It improves surface finish. It is possible to have higher weld speeds. Application areas for thermal stir welding are in aerospace, automotive, shipbuilding, storage tank, railway, and construction industries.

1.5.5   *Ultrasonic Stir Welding Process (USWP)*

Ultrasonically heated stir welding process that is developed by NASA, uses a new solid state welding device which is similar to friction stir welding process for need to build or repair space-based structures. It uses a rotating pin. On the other hand, the heating source created by ultrasonic energy instead of friction. Hence, ultrasonic stir welding process reduces the requirement power loads which use higher by conventional friction stir welding (NASA's ultrasonic stir welding process for handheld solid state welding).

Benefits of ultrasonic stir welding over the friction stir welding are portability that means it can be used in the field for repair, robotics and tack welding. It can be used different materials, thicknesses, high temperature alloys which are hard to weld and different weld geometries. Reducing plunge force, reduce to power requirements and increase the tool life. A single rotation or rotating speed can be controlled the coupled stir pin and shoulder, shoulder pressure and heat input resulting better control, besides, obtained better quality of surface on the joint and mechanical properties.

1.5.6   *Friction Stir Spot Welding (FSSW)*

Friction stir spot welding (FSSW) is newly developed process using the part of the linear friction stir welding process that is tool is plunged and retracted, without the transverse force as shown in Figure 1.93 (Feng et al., 2005). FSSW creates a spot and

lap welding without bulk melting. FSSW has been developed for aluminum alloys and advanced high-strength steels which have difficulties for welding process. Aluminum alloys can be join relatively low temperatures like 550˚C.

(a) Plunging   (b) Stirring   (c) Drawing out
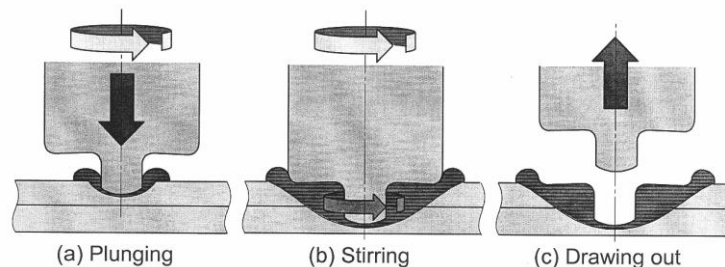
Figure1.94 Principles of FSSW with fixed pin (Feng et al., 2005).

Feng et al. (2005) discussed two types of FSSW process have been developed. The first one is using rigid pin tool geometry. The pin plunged into materials by rotating force for stirring after welding, pin is pulled out, and it leaves a peculiar exit hole in the middle of the joint. The second type is that exquisite relative motions of the pin and shoulder to refill the exit pin hole. The second way is required more processing time, because of, complication of the motion of the tool to refill the gap. The fixed pin tool geometry friction stir spot welding machine and control system is very simple and easy to use for high volume mass productions. The example of the fast process is aluminum alloys welding can be made less than a second. By using FSSW, some of the automotive companies save 90% production energy and 40% of their capital investing instead of using conventional resistance spot welding of aluminum alloys. FSSW can be readily substituted for the resistance spot welding RSW with little or no design modifications.

1.5.7   Orbital Friction Stir Welding

Orbital friction stir welding is another new technique has developed by NASA to use the principal of friction stir welding for different apparatus to join two cylindrical pieces like pipes as shown in Figure 1.94.
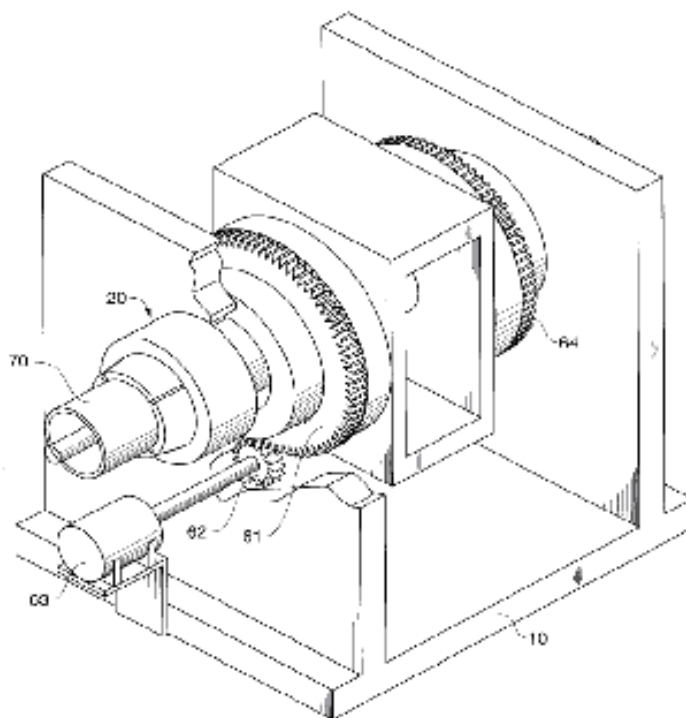
Figure 1.94 The orbital friction stir welding apparatus (NASA).

The Orbital Friction Stir Weld System is comprised of a base frame, a cylindrical clamping mechanism for securing a cylindrical work piece, a weld head, a reaction support, a means for transmitting load from the weld head to the reaction support, and a means for rotating the weld head in conjunction with the reaction support around the longitudinal axes of the clamping mechanisms. Since the cylindrical work piece will probably be in two sections, the cylindrical clamping mechanism must be capable of securing both sections of the work piece. The weld head and the reaction support separate the two pieces of the cylindrical clamping mechanism. The weld head and the reaction support are rotationally mounted to the base frame such that the weld head can rotate completely around the longitudinal axis of the cylindrical clamping mechanism and the reaction support can be maintained in a position diametrically opposed to the weld head. The rollers are mounted on the cylindrical clamping mechanism. They provide the mechanism by which the weld held and the reaction support are rotated around the circumference of the cylindrical work piece. The weld head is movable in a radial direction. The reaction support also has a roller

to facilitate movement of the reaction support around the perimeter of the work piece. The means for transmitting load from the weld head to the reaction support is a radial load bar that is able to rotate and stay aligned with the weld head and the reaction support. Synchronized rotation may be accomplished with a motor and gearing mechanism and with a control mechanism that coordinates the rotation of the radial load bar with the weld head and the reaction support. The means for rotating the weld head in conjunction with the reaction support around the longitudinal axis of the cylindrical clamping mechanism includes a ring gear that is attached to both the weld head and the reaction support and is concentric with the cylindrical clamping mechanism; a drive gear engaged with the ring gear; and a motor for controlling the rotation of the drive gear. A second ring gear connected to a second drive gear and a second motor may be used to rotate the weld head and the reaction support. The motors can also be used to synchronize rotation of the radial load bar with the weld head and reaction support (NASA, orbital friction stir weld system).

Figure 1.95 Retractable pin tool (NASA, Marshall Space Flight Center).

1.5.8 Advance Friction Stir Welding (AFSW)

Advance friction stir welding process is newly developing system using friction stir welding with retractable pin tool as shown in Figure.1.95 (NASA). This tool is

designed because of disadvantages of the FSW which are the requirement for different tool length for each material thicknesses and a pin hole at the end of the weld, that was a reliability concern some items such as pipes, storage tanks and drums. An automatic retractable pin tool motor is controlled by computer which is automatically retracting the pin into the shoulder of the tool at the end of the weld to close the pin hole. The pin angle and length can be adjustable for different material thicknesses with advance friction stir welding tool. Additionally, smooth hole closure is obtained. This product is a flexible system that can be advanced friction stir welding applications for high strength structural alloys. In addition to FSW, advance friction stir welding has some benefits; no hole at the end of the weld, adjustable thickness, welds in all positions and creates straight or complex shape welding ('Friction stir welding technology: adopting NASA's retractable pin tool' and 'Friction stir welding technology').
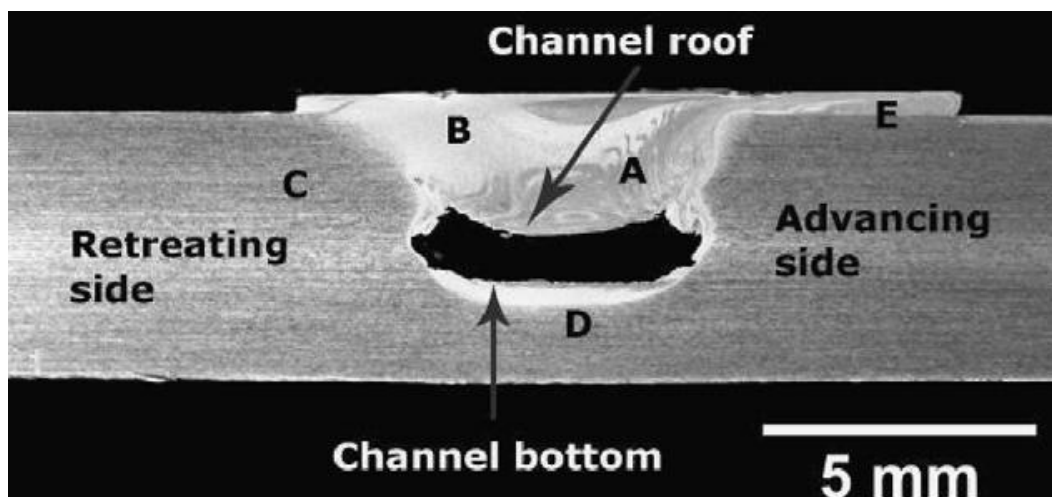
Figure 1.96 Cross-sectional image of a channel showing the different process regions: (A + B) channel   nugget, (C) parent material, (D) channel and (E) material from the channel nugget deposited on the surface (Balasubramania et al., 2008).

1.5.9 Friction Stir Channeling (FSC)

Friction stir channeling is newly innovated technique that uses to manufacture heat exchangers in a single step by using friction stir welding. Friction stir

channeling is generated a friction between tool and workpiece to soften and deform the material as like in friction stir welding but, if the processing parameters and tool shoulder contact is not appropriate throughout this process, it is created a defected which is named as a "wormhole" by Balasubramania, Mishra & Krishnamurthy (2008). Then, if the process is continued, it creates continuous, whole channels in a monolithic plate in a single pass. The fundamental principle of FSC is imperfection of friction stir welding to change into manufacturing process of heat exchanger applications. Choosing suitable processing parameters and reversing the material flow can create a continues hole in a single plate can be obtained. The main features of FSC is that the rotation of the tool is like that the material flow is upwards towards the tool shoulder, and where the material from the base of the pin is placed, the initial difference is provided between the shoulder and plate, and the space between tool shoulder and plate can be adjusted the control the shape, size and solidity of the channel.

The main difference is between FSC and FSW to creation for gap, where the back of the shoulder contact with the plate to make the forging force is necessary to produce welding process without any gap. But, when friction stir channeling is processing, clockwise rotation for right-handed or counter clockwise for left-handed threaded tool is used to generated upward force. For awhile of rotation, plasticized material around the pin and plasticized material around the base of the pin are separated. This separation of the material is proceed upwards by the rotation of the pin and orientation of the threads, and saved on the top of the nugget underneath the tool shoulder. The variations of the parameters that can be controllable, which are effecting the shape and size of the channel, are difference between the tool shoulder and plate, the tool rotational speed, the tool traverse speed and tool design (Balasubramania et al., 2008).

The shape of the channel is looks like ellipse or oval by using friction stir channeling as shown in Figure 1.96. It also shows the cross-section of the channel nugget area. The stir zones are shown as region A and B. Region C is parent material

that is raw l. Region D represents the channel. Finally, region E is showing saved material which is above the original surface of the material, between channel nugget region and tool shoulder. Material must be removed from stir zone to create a channel. Another layer is around the nugget is named as thermo-mechanically affected zone (TMAZ) is meaningless and inexplicit in Figure 1.96 (Balasubramania et al., 2008).

The continuous channel by FSC has ultimate applications in the heat exchanger industry. Balasubramanian studied achievement of continuous and integral channel linear and curved shapes. An increase in traverse speed and decrease the rotational speed expands the channel size. The roughness of the inside channel is significant in the pressure drop in heat exchanger applications.
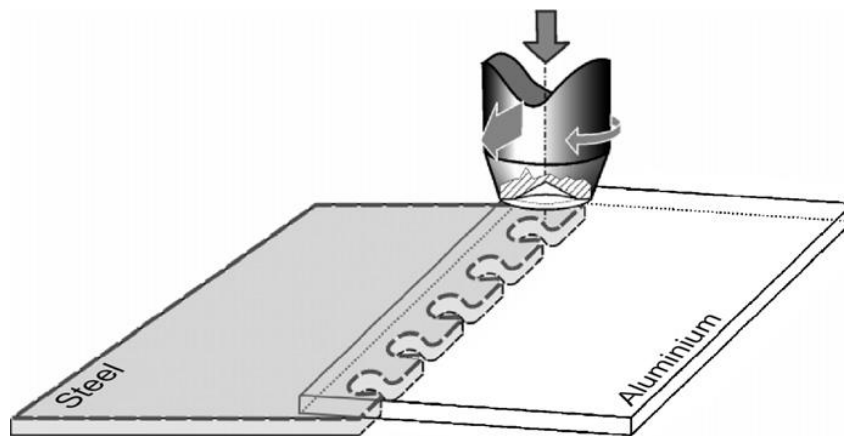
Figure 1.97 Principle of friction stir knead welding (Geiger et al., 2007).

1.5.10 Friction Stir Knead Welding (FSKW)

Friction stir knead welding is a new innovation as joining technique is applied for patent in 2005 Geiger et al. (2007). Figure1.97 shows the principle of the friction stir knead welding process.

Geiger et al. (2007) studied the friction stir knead welding of steel aluminum butt joints. In this study, friction stir knead welding was used to join steel and aluminum

sheets which are around 1 mm thickness. Especially, conventional friction stir welding is not suitable to obtain butt joints for small thicknesses, because of a high distortion of the workpiece. Changing the process parameters for FSW like tool geometry, thermal flux and tool material have failed for small thicknesses. Most of the scientific researches investigate above the 3mm thicknesses by using friction stir welding process.

Friction stir knead welding tool has no pin, as a result of this higher welding speed can be reached. Friction stir welding is still difficult to join for steel applications, by reasons of the high wear of the tool and its slow welding feed. Some of the usage of industrial applications of steel and aluminum should be joined, but they are non-weldable materials conventional ways due to melting problems (Geiger et al., 2007).

Steel and aluminum sheets have studied by Geiger et al. (2007) to join as experimental procedure of friction stir knead welding for butt joint. Beginning of the process, the softer aluminum sheet is put above the steel blank as lap joint position is shown in Figure 1.97. The steel sheet abutting edge is a special contoured shape, while the aluminum sheet is normal linear cutting edge. Probeless friction stir knead welding tool rotates in the normal or little bit tilted angle to the plane of the sheet and is gently pushed into the upper sheet. The frictional heat is occurred because of the tool rotation and at the same time, vertical force that plasticizes the upper plate and kneads into the cavity of the contoured steel plate. In other words, touching surfaces of the aluminum sheet is formed and forged into the steel cavity. However, the other touching surfaces of the steel and aluminum, the upper sheet is formed sideward and cut, as no forging into a free cavity is possible. The higher welding speed can be reached and small distortions realized, due to small effect between tool and blank. Metallographic results of this experiment shows a characteristic deformation of the aluminum in between steel tooth, because of stirring effect time of the friction stir knead welding and a layer of chemical reaction between steel and aluminum. This technique is very useful for joining steel aluminum plates. But, there isn't enough research for friction stir knead welding cutting contour of the sheet.

1.5.11 Laser-Assisted Friction Stir Welding(LAFSW)

Laser-assisted friction stir welding is a new modified technique of the friction stir welding. The principle of the laser-assisted friction stir welding is used a laser beam to heat the welding area instead of using frictional heat and as a result of this, the main function of the tool pin is stir and join the plate is shown in Figure 1.98. Laser beam introduces additional local heat for welding surface of the plates which is the welding area ahead of the pin. By the way, the material around the pin is plasticized and joined the plates as FSW with less mechanical energy and higher speed welds. No extra clamping fixture is necessary due to using laser beam. Since, laser beam is easily increased heat of the material and less force is used to move tool forward. In the industrial usage of LAFSW, laser power that is the amount of energy thru the plates can be accurately controlled by beam steering optics. By using this modification of the friction stir welding, laser energy helps friction stir welding a feasible and cost-efficient, simple and inexpensive process (Kohn et al., 2002 and Feldman, Kohn &Stern, 2006).
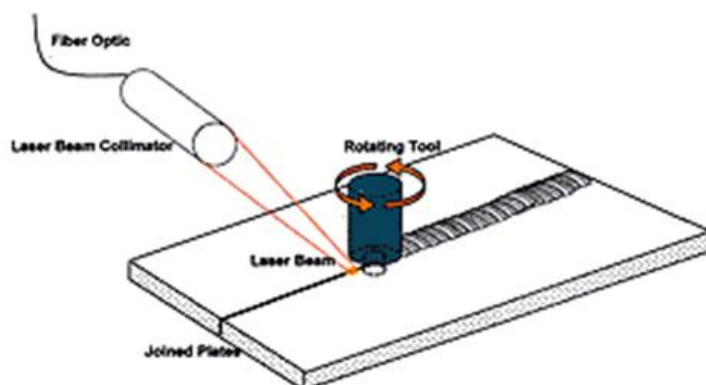
Figure 1.98 The principle of laser-assisted friction stir welding (Kohn, 2002).

1.5.12 Double, Twin or Multi Stir Friction Stir Welding

The simultaneous use of two or more friction stir welding tools acting is the main concept of these techniques. A pair of tools applied on opposite sides of the

workpiece slightly displaced in the direction of travel. The using contra-rotating simultaneous double-sided operation with combined weld passes has definite advantages for instance a decrease in reactive torque and a more symmetrical weld and heat input through-the-thickness. The pins need not touch together however, they should be located adequately close that the softened 'third-body' material around the two pins overlaps near the pin tips to create a full through-thickness weld as shown in Figure 1.99. Furthermore, multi-headed friction stir welding machines designed for some applications to able to increase productivity, reduce side force asymmetry, and reduce or minimize reactive torque as shown in Figure 1.100 (Thomas, Staines, Watts &Norris, 2005).
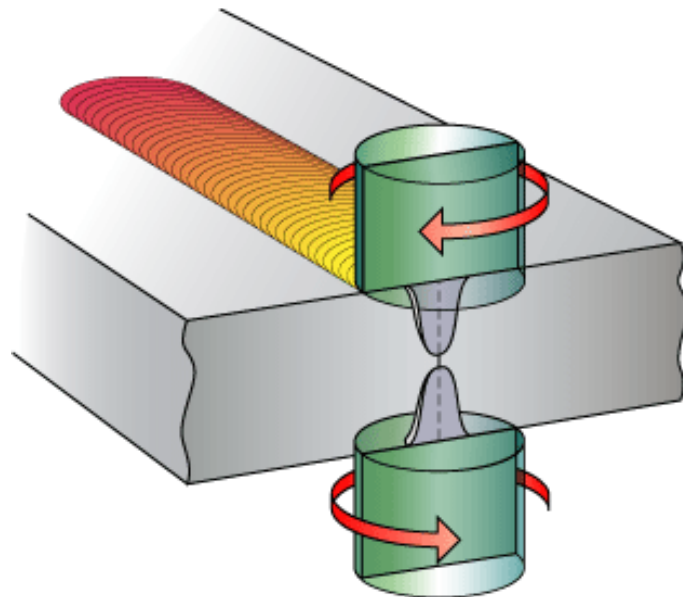
Figure 1.99 Simultaneous double-sided friction stir welding with contra-rotating tools (Thomas et al., 2005).

The two rotating tools one used to preheat and other one used to weld are rotating in the same direction is known as tandem technique. As shown in Figure 1.101a, the Twin-stir TM parallel contra-rotating variant enables defects associated with lap welding to be positioned on the inside between the two welds. As shown in Figure 1.101b, the Twin-stir TM tandem contra-rotating variant can be used to all conventional FSW joints and will decrease reactive torque.
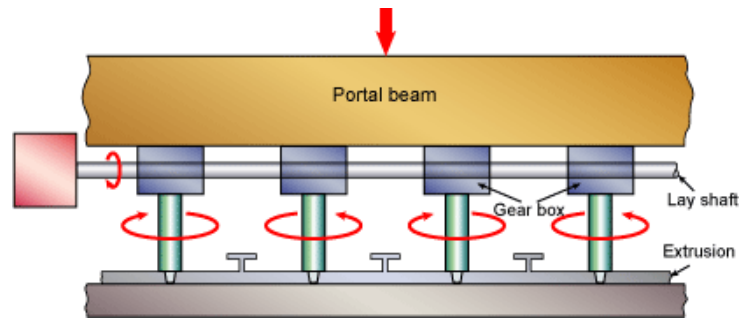
Figure 1.100 Multi-head friction welding machine (Thomas, 2005)
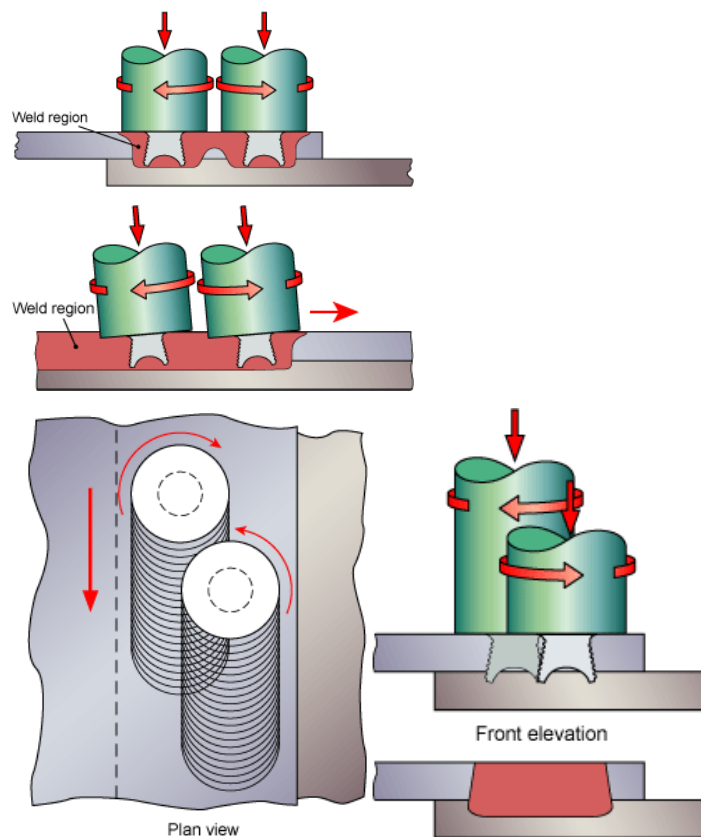
Figure 1.101 a) Parallel side-by-side transverse to the welding direction, b) Tandem in-line with the welding direction, c) Staggered to ensure the edges of the weld regions partially overlap (Thomas et al., 2005).

As shown in Figure 1.101c, the staggered Twin-stir [TM] means that a very wide common weld region can be created. Fundamentally, the tools are located with one in front and slightly to the side of the other in order that the second pin partially overlaps the previous weld region (Thomas, Staines, Watts &Norris, 2005).

Table 1.5 Example of a comparison FSW and GMAW (Defalco, 2006).

	Category	FSW	GMAW
	Arc time	2:25	7:22
	Lifting and clamping	8:05	3:11
TIME	Welding head cold runs	2:25	5:13
	Oxide removal	0:00	6:14
	Welders' protection	0:00	2:00
	Total Prep Time	12:55	24:00:00
	Welding Speed (mm/min.)	2000	750
	Investment Costs $	400	200
	Weld Length	2000	2000
Fixed hourly costs $	Location rent	13	13
	Amortization 4 Yrs	52	26
	Labor costs	30	30
	Energy	1	3
Variable hourly costs $	Welding costs: consumable		2
	Welding costs: gases		2
	Total Cost/h	96	76
	Weld Length/h	11.4	5.47
	Cost/Length	**8.38**	**13.81**

1.6 Advantages and Disadvantages of Friction Stir Welding

Friction stir welding (FSW) is a proven solid-state nonferrous metal joining process without base metal melting, filler metal and shielding gases. Therefore, friction stir welding eliminates most of the ill effects associated with resolidification inherent to conventional fusion welding. Friction stir welding has compared with gas metal arc welding (GMAW) on Table 1.5 by Defalco (2006). He used for comparing a 2-in. hollow profile weld. Even though the FSW capital cost is higher, the cost per length is less than GMAW because of fast welding speeds and low preparation costs.

1.6.1 Advantages of FSW

The many advantages of FSW compared to conventional arc welding with both improved joint properties and performance as (NASA, TWI and Williams, 2001):

- Joining of conventionally non-fusion weldable alloys. All aluminum alloys tested so far have been to be weldable. Because, high temperatures and melting temperatures do not occur in the FSW process. Therefore, fewer problems with porosity, cracking and loss of alloying elements.

- Applicable to varied materials like dissimilar alloys, like Al, Ni, Mg, Ti, Cu, Brass, steel etc. and higher temperature alloys, thicknesses and weld geometries, most of the time it is not possible with conventional welding processes.

- Improving mechanical properties of weldable alloy joints. Excellent joint properties when compared to fusion weldable joint properties. Such as, static properties are usually between 80 and 90 % of those of the base material. Similarly, the fatigue properties are near to those of the base material.

- Less sensitivity to corrosion.

- Portable, that enables use in field repair, robotics and tack welding.

- Lower plunge force.

- High travel speed.

- Energy efficient.

- Welding very thick materials. Can weld aluminum and copper of >50mm thickness in one pass.

- Improving surface finish. No grinding, brushing or pickling required in mass production.

- No filler wire required.

- No shielding gas required.

- No fume or smoke and sparking produced. As a result no toxic welding fumes.

- No noise problem.

- Environmental friendly process.

- Safe process.

- No welder certification required.

- No radiation hazards or high voltage.

- Easy automation and repeatability.

- Low distortion, even in long welds.

- Low shrinkage.

- Some tolerance to imperfect weld preparation (thin oxide layers).

- Welding Preparation not usually required.

- Non-consumable tool and long tool life. One tool can typically be used for up to 1000m of weld length in 6000 series aluminum alloys.

- Welding of wrought materials to castings.

- No spatter.

- Post-weld processes not required.

- Sometimes production costs significantly reduced.

1.6.2 Disadvantages of FSW

The disadvantages of the FSW process are being reduced by intensive research and development. However, there are also some limitations of FSW process compared to conventional welding processes as (NASA, TWI and Williams, 2001):

- Workpieces must be rigidly clamped.

- Backing bar required (except where self-reacting tool or directly opposed tools are used).

- Cannot make joints which required metal deposition (e.g. fillet welds).

- Tool design is limited some materials and thicknesses.

- Process parameters and mechanical property data are only certain alloys and thicknesses.

- For specific zones has problem with corrosion properties, residual stresses and distortion.

- Some applications need further improvement.

- Size and shape of the workpiece.

- Protecting from "keyhole" at the end of the weld, it has to be used a specialty tool.
- A small percentage of the welding industry has been targeted for implementation of FSW.
- Problems if weld gap > 10% material thickness.
- License cost.

Abregast (2006) also indentified some disadvantages of the more extensive FSW applications in US markets.

- Lack of industry standards and specifications.
- Lack of accepted design guidelines and design allowable.
- Lack of an informed workforce.
- The high cost of capital equipment.

CHAPTER TWO
ALUMINUM AND COPPER

2.1 Aluminum Alloys

The main part of the material distribution of the Boeing 777 consists of aluminum alloys as shown in Figure 2.1. There are several of reasons to use aluminum, such as, low cost, light weight metal can be heat treated for high strength levels and can be easily fabricated with lower cost for high performance materials. Aluminum is a high performance material because of high strength to weight ratio, cryogenic properties and fabricability.

Material Distribution for Boeing 777

Aluminum 70%
Composite 11%
Other 1%
Steel 11%
Titanium 7%
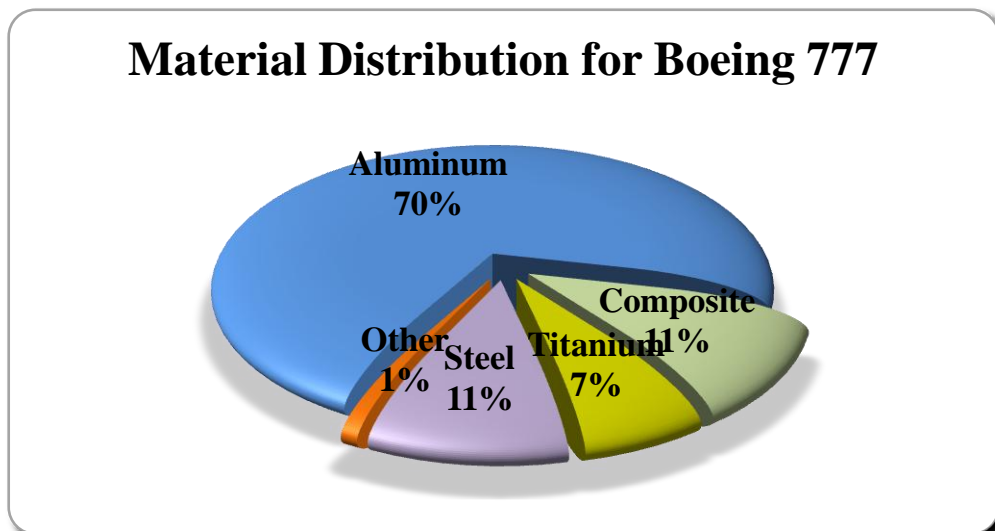
Figure 2.1 Material distribution of a commercial aircraft Boeing 777 (Campbell, 2006).

- High Strength to Weight Ratio: The high strength 2XXX and 7XXX alloys are heavier than titanium and steel alloys with higher strengths. Therefore they have been using for the most important structural material in commercial and military aircraft.

- Cryogenic Properties: Cryogenic property of the aluminum alloys make them ideal for producing fuel tanks for rockets and launch vehicles. This gives the

aluminum alloys durability at low temperatures. Likewise, when the temperature decreases, they become stronger with insignificant ductility losses.

- Fabricability; Aluminum alloys can be formed very easy. Some of the high strength 2XXX and 7XXX series alloys can be formed in a relatively soft state after that they can be heat treated to much higher strength levels.

Furthermore, aluminum is noncorrosive element; therefore it is very suitable for commercial use at food and beverage storage container, high electric and thermal conductivity, high reflectivity and easy for recycling.

A great number of aluminum alloys provide exceptional resistance to corrosion in chemical environments and in atmosphere, because of the result of the oxide film (Al_2O_3) of a naturally occurring tenacious. After the copper, aluminum and some of its alloys have high electrical conductivities.

The main disadvantages of the aluminum alloys are low modulus of elasticity and rather low elevated temperature capability and vulnerability to corrosion. Aluminum alloys modulus of elasticity is around 70-79GPa, it is lower when compared competing metals such as; titanium has 105-120GPa and steel has 200GPa. Generally, aluminum alloys can be used for a high temperature around 200-260C^o for a short time application. But, for long term usage temperatures are very limited around 120-150C^o.

Metallurgically, aluminum is very light weight material with a density of 2.6-2.8g/cm^3 and melting point is 660C^o. Besides, aluminum includes multi slip crystallize structure layers, therefore it is very easy to form of aluminum alloys for fabricated pieces. The copper, magnesium, silicon, zinc and titanium elements have sufficient solid solubility in aluminum to be major alloying elements. Also, chromium, manganese and zirconium are the transition metals with lower solid solubility which normally form compounds that help to control the grain structure.

Aluminum alloys are usually categorized as wrought non-heat treatable alloys, wrought heat treatable alloys and casting alloys.

Wrought aluminum alloys are designated by a four digit numerical. The first digit describes the major alloying class of the series. The second one describes the variations in the original basic alloy which means, if it is a zero (0), it is the original composition, if it is a one (1), it is the first variation, if it is two (2), it is second variation and so forth. Depending upon the level of the added element defines the variations. The third digit describes the specific alloy in the series and same thing for fourth digit. Designation can be summarized for wrought aluminum alloys as shown in Table 2.1.

Table 2.1 Designations for wrought aluminum alloys.

SERIES	MAIN ALLOYING ELEMENT
1XXX	MINIMUM 99.00% ALUMINUM
2XXX	COPPER
3XXX	MANGANESE
4XXX	SILICON
5XXX	MAGNESIUM
6XXX	MAGNESIUM and SILICON
7XXX	ZINC
8XXX	OTHERS
9XXX	UNUSED

The wrought non-heat treatable aluminum alloys are hardened by cold working, except some of the aluminum-silicon series. These alloys include the pure aluminum series (1XXX), the aluminum-manganese series (3XXX), the aluminum-silicon series (4XXX) and the aluminum-magnesium series (5XXX). Not hardened by cold working aluminum-silicon alloys can be hardened by heat treatment.

The wrought heat treatable aluminum alloys can be strengthened by developing precipitation hardening. These alloys include the aluminum-copper series (2XXX), the aluminum-magnesium-silicon series (6XXX), the aluminum-zinc series (7XXX) and the aluminum-lithium series (8XXX). The highest strength level alloys are 2XXX and 7XXX series alloys and mainly used for metallic airframe components. The medium strength level alloys are 2XXX, 6XXX and 7XXX series alloys are classified as being fusing weldable materials while Al-Cu-Mg (2XXX) and Al-Zn-Mg-Cu (7XXX) alloy series are generally higher strength but, they are not fusion weldable materials. The 2XXX series alloys are used for welded fuel tanks for launch vehicles, but not for aerospace structures.

Table 2.2 Designations for casting aluminum alloys

SERIES	MAIN ALLOYING ELEMENT
1XX.0	MINIMUM 99.00% ALUMINUM
2XX.0	COPPER
3XX.0	SILICON with COPPER and/or MAGNESIUM
4XX.0	SILICON
5XX.0	MAGNESIUM
6XX.0	UNUSED
7XX.0	ZINC
8XX.0	TIN
9XX.0	OTHERS

Cast aluminum alloys are designated by four digit numerical system like wrought alloys with little difference. Similarly the wrought aluminum alloy designation, the first digit defines the major alloying element; second and third digit defines the specific alloy. By the forth digit, there is a period. If the forth digit is a zero (0), it means the alloy as cast product. If it is a one (1), it indicates an ingot composition that would be supplied to a casting house. An impurity level of the secondary alloy element can be described by using a prefix letter. It starts from A with an alphabetical order but omits letters I, O, Q and X which is kept for experimental

alloys. Designation can be summarized as cast aluminum alloys as shown in Table 2.2.
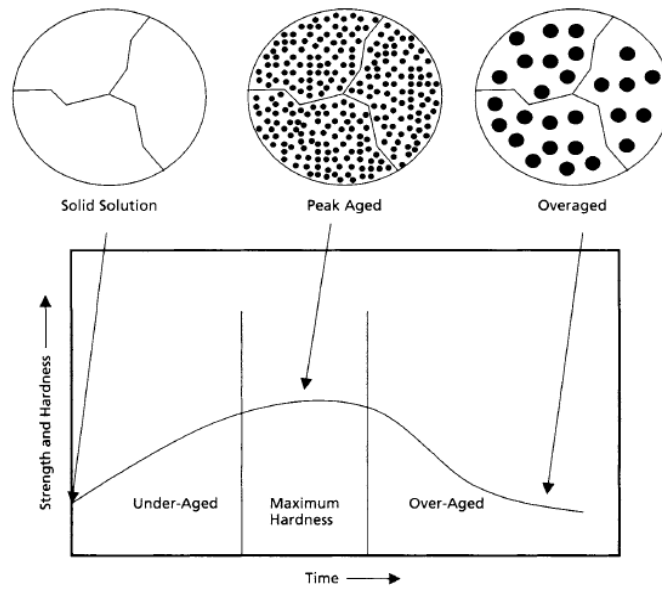
Figure 2.2 Typical aging curve for aluminum alloys (Campbell, 2006). 2005).

It is important the strengthening process by precipitation hardening for high strength aluminum alloys. Precipitation hardening contains three stages:

1. *Solution heat treating:* The aluminum alloy is heated to a temperature which is high enough to put the soluble alloying in solution, before staying at the solution treating temperature for a certain time.

2. *Rapidly quenching to a lower temperature:* The aluminum alloy is quenched to a lower temperature to keep the alloying elements trapped in solution.

3. *Aging:* The alloying elements trapped in solution precipitate to form a uniform distribution of very fine particles which strengthens and hardens the alloy generating obstacles to dislocation movement. Natural aging is

hardening aluminum alloy at room temperature a few days. Artificial aging is hardening aluminum alloys to heat to an intermediate temperature.

Schematically, the progression of the aging process is as shown in Figure 2.2. The strengths and hardness levels of the aluminum alloy has higher values at peak-aged formation than under-aged and over-aged formations. The letter F, O, H, W and T are the temper designations for aluminum alloys with some numbers. The designated letters and numbers are summarized at Table 2.3.

Table 2.3 Temper designation for aluminum alloys (Campbell, 2006).

SUFFIX LETTERS (Basic Treatment Condition)	FIRST SUFFIX DIGIT (Secondary Treatment Used to Influence Properties)	SECOND SUFFIX DIGIT (Residual Hardening)
• **F** - As Fabricated • **O** - Annealed (Wrought products only)		
• **H** - Cold Worked Strain Hardened (Temper-Non--Heat-Treatable Alloys) (**H**xx)	• **1** - Cold Worked Only (H**1**x) • **2** - Cold Worked and Partially Annealed (H**2**x) • **3** - Cold Worked and Stabilized (H**3**x)	• **0** - Annealed (Hx**0**) • **1** - 1/8 Hard (Hx**1**) • **2** - 1/4 Hard (Hx**2**) • **3** - 3/8 Hard (Hx**3**) • **4** - 1/2 Hard (Hx**4**) • **5** - 5/8 Hard (Hx**5**) • **6** - 3/4 Hard (Hx**6**) • **7** - 7/8 Hard (Hx**7**) • **8** - Full Hard (Hx**8**) • **9** - Extra Hard (Hx**9**)

• **W** - Solution Heat Treated
• **T** - Heat Treated Stable (Temper-Heat-Treatable Alloys)
 	
   T1 - Cooled from an Elevated Temperature Shaping Operation + Natural Age
   T2 - Cooled from an Elevated Temperature Shaping Operation + Cold Worked + Natural Age
   T3 - Solution Treated + Cold Worked + Natural Age
   T4 - Solution Treated + Natural Age
   T5 - Cooled from an Elevated Temperature Shaping Operation + Artificial Age
   T6 - Solution Treated + Artificially Aged
   T7 - Solution Treated + Over-aged
   T8 - Solution Treated + Cold Worked + Artificial Aged
   T9 - Solution Treated + Artificial Aged + Cold Worked
   T10 - Cooled from an Elevated Temperature Shaping Operation + Cold Worked + Artificial Aged		

Table 2.4 Chemical composition of some wrought aluminum alloys.

Alloy	Si	Fe	Cu	Mn	Mg	Cr	Zn	Ti	Bi	Ga	Zr	Other	Limits†† Each	Limits†† Total	Al
1060	0.25	0.35	0.05	0.03	0.03	0.03	0.05	0.03	0.03	0.03	0.03	0.03Pb,0.05V	0.03		99.6*
1100	0.95 Si+Fe		0.05-0.2	0.05			0.1						0.05	0.15	99.0*
1050	0.25	0.4	0.05	0.05	0.05			0.05			0.07				99.5*
2004			6.0								0.4				
2014	0.5-1.2	0.7	3.9-5.0	0.4-1.2	0.2-0.8	0.1	0.25	0.15					0.05	0.15	rest
2017	0.5	0.7	4.0	0.7	0.6										
2020	0.4	0.4	4.5	0.55								1.3Li,0.25Cd			
2024	0.5	0.5	3.8-4.9	0.3-0.9	1.2-1.8	0.1	0.25	0.15					0.05	0.15	rest
X2080		0.1			3.7	0.2	1.85				0.2	0.2Li			
2090	0.1	0.12	2.7								0.1	2.2Li			
2091	0.2	0.3	2.1		1.5						0.1	2.0Li			
X2095	0.12	0.15	4.2		0.4		0.25				0.1	1.3Li,0.4Ag			
2219	0.2	0.3	5.8-6.8	0.2-0.4	0.02		0.1	0.02-0.10			0.10-0.25	0.05-0.15V	0.05	0.15	rest
2224	0.12	0.15	4.1	0.6	1.5										
2324	0.1	0.12	4.1	0.6	1.5										
2519	0.2	0.3	5.8		0.2						0.2	0.1V			
3003	0.6	0.7	0.05-0.2	1.0-1.5			0.1						0.05	0.15	rest
3004	0.3	0.7	0.25	1.0-1.5	0.8-1.3		0.25						0.05	0.15	rest
3102	0.4	0.7	0.1	0.05-0.4			0.3	0.1					0.05	0.15	rest
4043	4.5-6.0	0.8	0.3	0.05	0.05		0.1	0.2					0.05	0.15	rest
5052	0.25	0.4	0.1	0.1	2.2-2.8	0.15-0.35	0.1						0.05	0.15	rest
5083	0.4	0.4	0.1	0.4-1.0	4.0-4.9	0.05-0.25	0.25	0.15					0.05	0.15	rest
5086	0.4	0.5	0.1	0.2-0.7	3.5-4.5	0.05-0.25	0.25	0.15					0.05	0.15	rest
5154	0.25	0.4	0.1	0.1	3.1-3.9	0.15-0.35	0.2	0.2					0.05	0.15	rest
5356	0.25	0.4	0.1	0.1	4.5-5.5	0.05-0.20	0.1	0.06-0.20					0.05	0.15	rest
5454	0.25	0.4	0.1	0.5-1.0	2.4-3.0	0.05-0.20	0.25	0.2					0.05	0.15	rest
5456	0.25	0.4	0.1	0.5-1.0	4.7-5.5	0.05-0.20	0.25	0.2					0.05	0.15	rest
6005	0.6-0.9	0.35	0.1	0.1	0.4-0.6	0.1	0.1	0.1					0.05	0.15	rest
6005A†	0.5-0.9	0.35	0.3	0.5	0.4-0.7	0.3	0.2	0.1					0.05	0.15	rest
6013	0.8	0.3	0.8	0.35	1.0										
6060	0.3-0.6	0.1-0.3	0.1	0.1	0.35-0.6	0.5	0.15	0.1					0.05	0.15	rest
6061	0.4-0.8	0.7	0.15-0.4	0.15	0.8-1.2	0.04-0.35	0.25	0.15					0.05	0.15	rest
6063	0.2-0.6	0.35	0.1	0.1	0.45-0.9	0.1	0.1	0.1					0.05	0.15	rest
6066	0.9-1.8	0.5	0.7-1.2	0.6-1.1	0.8-1.4	0.4	0.25	0.2					0.05	0.15	rest
6070	1.0-1.7	0.5	0.15-0.4	0.4-1.0	0.50-1.2	0.1	0.25	0.15					0.05	0.15	rest
6082	0.7-1.3	0.5	0.1	0.4-1.0	0.6-1.2	0.25	0.2	0.1					0.05	0.15	rest
6105	0.6-1.0	0.35	0.1	0.1	0.45-0.8	0.1	0.1	0.1					0.05	0.15	rest
6113	0.8	0.3	0.8	0.35	1.0							0.2O			
6262	0.4-0.8	0.7	0.15-0.4	0.15	0.8-1.2	0.04-0.14	0.25	0.15	0.4-0.7			0.4-0.7Pb	0.05	0.15	rest
6351	0.7-1.3	0.5	0.1	0.4-0.8	0.4-0.8		0.2	0.2					0.05	0.15	rest
6463	0.2-0.6	0.15	0.2	0.05	0.45-0.9		0.05						0.05	0.15	rest
7005	0.35	0.4	0.1	0.2-0.7	1.0-1.8	0.06-0.20	4.0-5.0	0.01-0.06			0.08-0.20		0.05	0.15	rest
7010	0.12	0.15	1.7		2.35		6.2				0.1				
7049	0.25	0.35	1.6		2.45	0.15	7.7								
7050	0.12	0.15	2.3		2.25		6.2				0.1				
7055	0.1	0.15	2.3		2.05		8.0				0.1				
7072	0.7 Si+Fe		0.1	0.1	0.1		0.8-1.3						0.05	0.15	rest
7075	0.4	0.5	1.2-2.0	0.3	2.1-2.9	0.18-0.28	5.1-6.1	0.2					0.05	0.15	rest
7079	0.3	0.4	0.6	0.2	3.2	0.15	4.3								
X7093	0.12	0.15	1.5		2.5		9.0				0.1	0.2O			
7116	0.15	0.3	0.50-1.1	0.05	0.8-1.4		4.2-5.2	0.05		0.03		0.05V	0.05	0.15	rest
7129	0.15	0.3	0.5-0.9	0.1	1.3-2.0	0.1	4.2-5.2	0.05		0.03		0.05V	0.05	0.15	rest
7150	0.12	0.15	2.2		2.35		6.4				0.1				
7475	0.1	0.12	1.6		2.25	0.21	5.7								
8009	1.8	8.65										1.3V, 0.3O			
X8019	0.2	8.3										4.0Ce, 0.2O			
8090	0.2	0.3	1.3		0.9						0.1	2.4Li			

* Minimum

†Manganese plus chromium must be between 0.12-0.50%.

††This column lists the limits that apply to all elements, whether a table column exists for them or not, for which no other limits are specified.
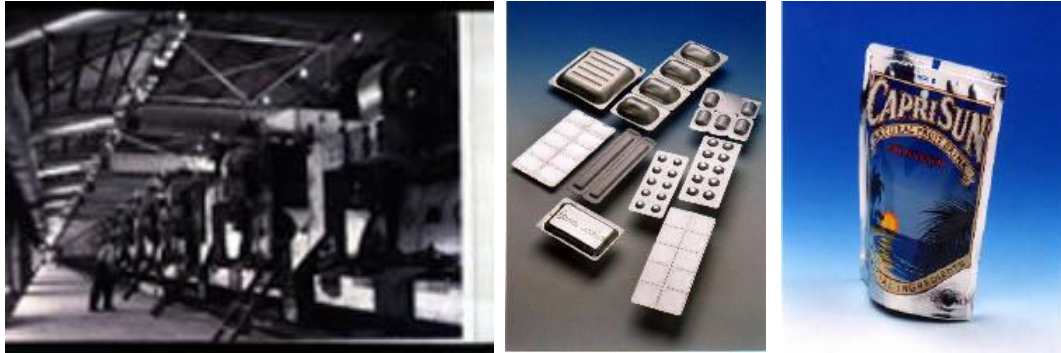
Figure 2.3 a) Aluminum electrical bus bar installation with 1350 bus bar, b) Food packaging trays, c) Decorated foil pouches for food and drink [AA].

Campbell (2006), Engineersedge (n.d.) and Efunda (n.d.) explained stress relieving tempers for aluminum alloys such as by stretching, compressing and combination of stretching and compressing. They also gave details about third a fourth suffix usage. For example;

T5- Cooled from hot working and artificially aged (at elevated temperature)

-**T51** Stress relieved by stretching

-**T510** No further straightening after stretching

-**T511** Minor straightening after stretching

-**T52** Stress relieved by compressing (thermal treatment)

-**T54** Stress relieved by stretching and compressing

T7- Solution heat treated and then stabilized/over-aged

-**T73** Solution heat treated and especially artificially aged. Applies to 7075 alloys which have been specially aged to make the material resistant to stress-corrosion

-**T7351** Solution heat treated and specially artificially aged. Applies to 7075 alloy sheet and plate which have been specially aged to make the material resistant to stress-corrosion

-**T73511** Solution heat treated and specially artificially aged. Applies to 7075 alloy extrusions which have been specially aged to make the material resistant to stress-corrosion

-**T7352** Solution heat treated and specially artificially aged. Applies to 7075 alloy forgings which have both compression-stress relief and special aging to make the material resistant to stress-corrosion

The chemical compositions of the some wrought aluminum alloys are given Table 2.4.

2.1.1 Wrought Aluminum Alloys

2.1.1.1 Al-1000 Alloys

1XXX: Pure AI. Some of the important properties of each of the aluminum alloy 1XXX series can be classified as follows:

- Strain hardenable
- Typical ultimate tensile strength range: 70-185MPa
- Exceptionally high formability, corrosion resistance and electrical conductivity
- Readily joined by welding, brazing, soldering
- Representative designations: 1100, 1350

According to Aluminum Association [AA], the 1xxx series represents the industrially pure aluminum, ranging from the baseline 1100 (99.00% min. Al) to relatively purer 1050/1350 (99.50% min. Al) and 1175 (99.75 % min. Al). Some of them are used especially for electrical applications, like 1350 which have relatively tight controls on those impurities that might lower electrical conductivity.

The 1xxx series are strain-hardenable, although they would not be used where strength is a main factor. Quite importance would be on those applications where extremely high corrosion resistance, formability and/or electrical conductivity are required, e.g., foil and strip for packaging, chemical equipment, tank car or truck bodies, spun hollowware, and elaborate sheet metal work. Some of the specific

industrial applications are aluminum electrical bus bar installation with 1350 bus bar as shown in Figure 2.3a, food packaging trays of pure aluminum (1100) as shown in Figure 2.3b and decorated foil pouches for food and drink (1060 or 1100) as shown in Figure 2.3c.

2.1.1.2 Al-2000 Alloys

2XXX: AI-Cu Alloys. Some of the important properties of each of the aluminum alloy 2XXX series can be classified as follows:

- Formerly named as duralumin
- Heat treatable
- High strength, at room and elevated temperatures
- Typical ultimate tensile strength range: 185-430MPa
- Usually joined mechanically but some alloys are weldable
- Not as corrosion resistant as other alloys
- Aircraft, transportation applications
- Representative alloys: 2014, 2017, 2024, 2219, 2195

The 2xxx series are heat-treatable, and especially at elevated temperatures this series possess in individual alloys good combinations of high strength, toughness, and, in specific cases, weldability; they are not resistant to atmospheric corrosion, therefore they are usually painted or clad in such exposures. The higher strength 2xxx alloys are commonly used in bolted or riveted construction applications such as mainly utilized for aircraft (2024) and truck body (2014). As shown in Figure 2.4a, aircraft internal structure includes extrusions and plate of 2xxx and 7xxx alloys like 2024, 2124 and 2618. External sheet skin may be alclad 2024 or 2618; the higher purity cladding provides corrosion protection to the Al-Cu alloys that will darken with age otherwise. As shown in Figure 2.4b, heavy dump and tank trucks and trailer trucks employ 2xxx extrusions for their structural members. Specific members of the

series (e.g. 2219 and 2048) are used for aerospace applications because of readily weldable, where that is the preferred joining method.

Figure 2.4 a) Aircraft internal structure includes extrusions and plate of 2xxx and 7xxx alloys, b) Heavy dump and tank trucks and trailer trucks [AA].

Figure 2.5 The fuel tanks and booster rockets of the Space Shuttle.

Alloy 2195 is a new Li-bearing alloy for space applications offering extremely high modulus of elasticity along with high strength and weldability. Moreover, some of the aluminum alloys like 2124, 2324, 2419 are high-toughness versions which have tighter control on the impurities that may diminish resistance to unstable fracture, all of the alloys developed specifically for the aircraft industry. Generally, alloys 2011, 2017 and 2117 are preferred to use for fasteners and screw-machine stock. Another applications for the 2xxxx series alloys is as shown in Figure 2.5, the

fuel tanks and booster rockets of the Space Shuttle are 2xxx alloys, originally 2219 and 2419, now sometimes Al-Li "Weldalite"alloy 2195.

2.1.1.3 Al-3000 Alloys

3XXX: AI-Mn Alloys. Some of the important properties of each of the aluminum alloy 3XXX series can be classified as follows:

- High formability, corrosion resistance and joinability with medium strength
- Typical ultimate tensile strength range: 110-280MPa
- Heat transfer, packaging, roofing-siding applications
- Readily joined by all commercial procedures
- Hardened by strain hardening
- Representative alloys: 3003, 3004, 3005
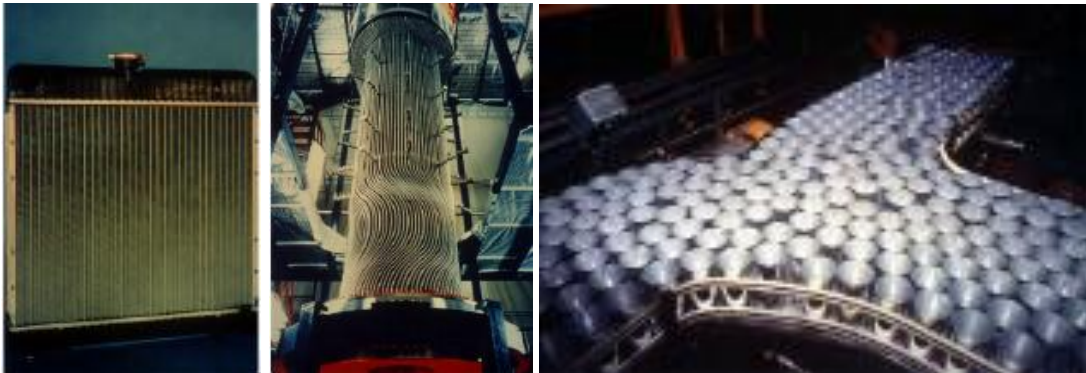
Figure 2.6 a) Automotive radiator heat exchangers are of alloys like 3002, b) Alloy 3003 tubing in commercial power plant heat exchanger, c) The bodies of beverage cans are alloys 3004 or 3104, making it the largest volume alloy combination in the industry [AA].

The 3xxx series have excellent corrosion resistance and are strain-hardenable, quickly welded, brazed and soldered. Alloy 3003 is commonly used in cooking utensils and chemical equipments due to its superiority in usage many foods and chemicals, and in builders' hardware. Main application of alloy 3105 is for roofing and siding. Variations of the 3xxx series are used in sheet and tubular form for heat

exchangers in vehicles and power plants as shown in Figure 2.6a and Figure 2.6b. The largest volume alloy combination in the industry usage of aluminum alloys are 3004 and its modification 3104 since they are drawn and ironed into the bodies of beverage cans as shown in Figure 2.6c.

2.1.1.4 Al-4000 Alloys

4XXX: AI-Si Alloys. Some of the important properties of each of the aluminum alloy 4XXX series can be classified as follows:

- Also known as silumin
- Some heat treatable
- Good flow characteristics, medium strength
- Typical ultimate tensile strength range: 170-380MPa
- Easily joined, especially pistons, complex-shaped forgings
- Representative alloys: 4032 and filler alloy 4043

The 4xxx series alloys are heat treatable and used principally for forgings in applications such as aircraft pistons are made up of 4032 which is a medium high-strength. On the other hand, the other most widely usage is alloy 4043 as filler alloys for gas-metal arc (GMA) and gas-tungsten arc (GTA) welding 6xxx alloys for structural and automotive applications as shown in Figure 2.7a.

The high silicon content provides good flow characteristic. Therefore, in the case of forgings ensures the filling of complex dies and in the case of welding ensures complete filling of gaps and grooves in the members to be joined. For that reason, other variations of the 4xxx alloys are used for the cladding on brazing sheet, the component that flows to complete the bond. An example for that kind of application is a refrigerator coolant circulation system in brazed unit of high-Si brazing alloy sheet as shown in Figure 2.7b.

Figure 2.7 a) Alloy 4043 is one of the most widely used weld
wires, b) Refrigerator coolant circulation system in brazed unit of
high-Si brazing alloy sheet [AA].

2.1.1.5 Al-5000 Alloys

5XXX: AI-Mg Alloys. Some of the important properties of each of the aluminum
alloy 5XXX series can be classified as follows:

- Named as Magnox
- Strain hardenable
- Excellent corrosion resistance, toughness, weldability, moderate strength
- Building and construction, automotive, cryogenic, marine applications
- Typical ultimate tensile strength range: 125-350MPa
- Representative alloys: 5052, 5083, 5754

Al-Mg alloys of the 5xxx series have moderately high strength, excellent
corrosion resistance even in sea, and very high toughness even at cryogenic
temperatures to near absolute zero and are strain hardenable. They can be easily
welded by a variety of techniques, even at thicknesses up to 20 cm. Thus, in building
and construction applications, highways structures including bridges, storage tanks
and pressure vessels, cryogenic tank and systems for temperatures as low as -270°C

(near absolute zero), and marine applications are wide variety of usage for 5xxx alloys. The Foresmo Bridge in northern Norway is an excellent example of the use of Al-Mg alloys for built up girders systems; Figure 2.8a illustrates a major advantage of replacement aluminum bridges: the ability to pre-fabricate the spans and move them in place quickly, minimizing the disruption to traffic. Rugged coal cars are manufactured by welded 5454 alloy plate construction as shown in Figure 2.8b. It is an interesting example for application of alloy 5083 was used to build a 125-ft diameter spheres for shipboard transport of liquefied natural gas; the all-welded construction was 8-in.thick at the horizontal diameter as illustrated in Figure 2.8c.

Figure 2.8 a) The Foresmo Bridge in northern Norway, b) Rugged coal cars, c) The 125-ft.diameter spheres for shipboard transport of liquefied natural gas [AA].

For structural usage alloys 5052, 5086, and 5083 have increasingly higher strength associated with the increasingly higher Mg content. As an example of the 5083 alloy application as shown in Figure 2.9a and Figure 2.9b, high speed single-hull ships like the Proserio employ 5083- H113/H321 machined plate for hulls, hull stiffeners, decking, superstructure and the internal hull stiffener structure. As marine application of the 5xxx series of alloys, single or multiple hull high-speed ferries, employ several Al-Mg alloys, 5083, and 5454 as sheet and plate which along with 6xxx extruded shapes, with all-welded construction as shown in Figure 2.9c. The 5182 alloy is major alloy in the group, has the largest volume tonnage in the industry because of using the beverage can end alloy as shown in Figure 2.10a. 5754 Alloy is used for automotive body panel and frame applications as shown in Figure 2.10b. 5252, 5457, and 5657 alloys are preferred for bright trim applications, including automotive trim.

Figure 2.9 a) High speed single-hull ships like the Proserio employ 5083- H113/H321 machined plate for hulls, hull stiffeners, decking and superstructure, b) The internal hull stiffener structure of the high-speed yacht Proserio, from the previous figure, c) Single or multiple hull high-speed ferries, employ several Al-Mg alloys, 5083, and 5454 as sheet and plate (along with 6xxx extruded shapes, to be described next) with all-welded construction [AA].

5xxx alloys may become sensitized and susceptible to stress corrosion cracking occur as main problem when they include more than 3% Mg content in applications where they receive continuous exposure to temperatures above 100°C (212°F). 5454 and 5754 are recommended to use to avoid from these problems for applications where high temperature exposure is likely. Some other examples of applications for generally used 5xxx series of alloys as follows; the demands of high-humidity and water exposure in offshore oil rigs are met with 5454, 5086, and 5083 Al-Mg alloy welded construction as shown in Figure 2.10c.

Figure 2.10 a) Aluminum can ends of 5182 make that one of the largest volume alloys in production, b) Automotive structures are likely to employ increasing amounts of 5754-0 formed sheet for parts such as internal door stiffeners or the entire body-in-white, c) The demands of high-humidity and water exposure in offshore oil rigs are met with 5454, 5086, and 5083 Al-Mg alloy welded construction [AA].

2.1.1.6 Al-6000 Alloys

6XXX: AI-Mg-Si Alloys. Some of the important properties of each of the aluminum alloy 6XXX series can be classified as follows:

- Heat treatable

- High corrosion resistance, outstanding extrudability; moderate strength

- Typical ultimate tensile strength range: 125-400MPa

- Readily welded by gas metal arc welding (GMAW) and gas tungsten arc welding (GTAW) methods

- Building & construction, highway, automotive, marine applications

- Representative alloys: 6061, 6063, 6111

Figure 2.11 a) The power of extruded Al-Mg-Si alloys is the "put-the-metal where-you need-it" flexibility that these alloys and the extrusion process provide, b) and c) An integrally stiffened bridge deck shape usually produced in 6063, used to produce replacement bridge decks, readily put in the roadway in hours [AA].

The 6xxx series alloys are heat treatable, readily welded and have moderately high strength together with excellent corrosion resistance. These series alloys are prime selection for architectural and structural members if unusual or particularly strength or stiffness criticality is important, because of their unique feature extrudability. Some of examples of the extruded Al-Mg-Si alloys is the "put-the-metal where-you

need-it" flexibility that these alloys and the extrusion process provide as shown in Figure 2.11a.

Figure 2.12 a) Extruded Al-Mg-Si alloys may make up the entire frame of motorcycles or cars b) Illustration is of the Audi A-8 body, c) Welded 6063 extrusions combined with 5083 tube make up the front and rear axle bodies for the BMW Model 5 [AA].

Maybe, the most widely used in 6xxx series is alloy 6063 since it is outstanding extrudability; an integrally stiffened bridge deck shape usually produced in 6063, used to produce replacement bridge decks, readily put in the roadway in hours as shown in Figure 2.11b and Figure 2.11c. In addition to this, extruded Al-Mg-Si alloys may make up the entire frame of motorcycles or cars are used as the choice for the Audi automotive space frame members as shown in Figure 2.12a and Figure 2.12b. Another automotive manufacturer BMW are also used welded 6063 alloy extrusions along with 5083 alloy tube make up the front and rear axle bodies for the Model 5 as shown in Figure 2.12c.

Figure 2.13 a) Roof structures for arenas and gymnasiums are usually 6063 or 6061 extruded tube, covered with 5xxx alloy sheet, b) Geodesic domes, such as this one made originally to house the "spruce Goose" in Long Beach, CA, the largest geodesic dome ever constructed, at 1000 ft across, 400 ft. high [AA].

One more example for application of the extruded tube of the 6063 or 6061 alloy are used roof structures for arenas and gymnasiums, covered with 5xxx alloy sheet as shown in Figure 2.13a. Geodesic domes, such as this one made originally to house the "spruce Goose" in Long Beach, CA, the largest geodesic dome ever constructed, at 1000 ft across, 400 ft. high as shown in Figure 2.13b.

Furthermore, higher strength 6061 alloy are extensively used in welded structural parts such as truck and marine frames, railroad cars, and pipelines. The new Mag-Lev trains produce bodies with 6061 and 6063 structural parts in Europe and Japan as shown in Figure 2.14a and Figure 2.14b. Among specialty alloys in the series: 6066-T6, with high strength for forgings; 6111 for automotive body panels with high dent resistance; and 6101and 6201 for high strength electrical bus and electrical conductor wire, respectively.
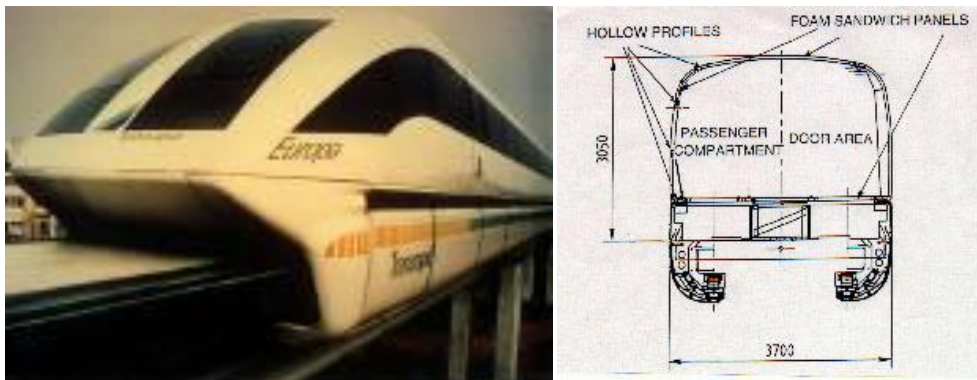
Figure 2.14 a) The new Mag-Lev trains in development in Europe and Japan employ bodies with 6061, b) 6063 Structural members [AA].

2.1.1.7 *Al-7000 Alloys*

7XXX: AI-Zn Alloys. Some of the important properties of each of the aluminum alloy 7XXX series can be classified as follows:

- Heat treatable
- Very high strength; special high toughness versions

- Aerospace, automotive applications
- Typical ultimate tensile strength range: 220-605MPa
- Mechanically joined
- Representative alloys: 7005, 7075, 7475, 7150

The 7xxx alloys have the highest strengths of all aluminum alloys with the Al-Zn-Mg-Cu versions which are named Zamak and are heat treatable. Many alloys in the series are produced especially for their high toughness, remarkably 7150 and 7475, both with controlled impurity level to maximize the combination of strength and fracture toughness. Another main issue to use lightweight 7xxx series such as 7029 or 7129 alloys for bumper structures help to improve gas mileage as shown in Figure 2.15a.

Figure 2.15 a) Lightweight 7029 or 7129 bumper structures help improve our gas mileage, b) Aircraft structures are of 7xxx alloy sheet or extrusion construction; alloys like 7075-T73 or high-toughness alloys like 7050 or 7475 are among the principal choices [AA].

The 7xxx alloys are widely used in the aircraft industry, where fracture-critical design concepts have provided the impetus for the high toughness alloy development. They are accepted as non-weldable alloys for common industrial processes, for that reason, they are preferred to join by riveting.

The 7xxx alloys are usually coated or, for sheet and plate, used in an alclad version due to protect from corrosion. Because, their corrosion resistances a not as

high as that of the 5xxx and 6xxx alloys. For example, the T73- special temper type is required in place of T6-type tempers whenever stress corrosion cracking may be a problem. Likewise, the high-toughness 7050 or 7475 alloys and tempered 7075-T73 alloy sheets or extrusions are mainly selected for aircraft structures as shown in Figure 2.15b.

2.1.1.8 Al-8000 Alloys

8XXX: Alloys with AI-Other Elements (Not Covered by Other Series). Some of the important properties of each of the aluminum alloy 8XXX series can be classified as follows:

- Heat treatable
- High conductivity, strength, hardness
- Electrical, aerospace, bearing applications
- Typical ultimate tensile strength range: 115-415MPa
- Common alloying elements include Fe, Ni and Li
- Representative alloys: 8017, 8176, 8081, 8280, 8090

The 8xxx series comprises alloys in which the major alloying elements such as Fe, Ni and Li are other than for the other series, as well as a number of industrial purity alloys based on Al, Fe and Si which are too concentrated to be classed as 1xxx series. Every element is used for the specific characteristics it provides the alloys: Fe and Ni give strength with little loss in electrical conductivity and so are used in a series of alloys represented by 8017 alloy for conductors which are used today in building wire and service cables. Recently developed Al-Li in alloys 8090, 8091 and 8093 are offered outstandingly high strength and modulus. Lithium has a significantly lower density than aluminum and while its solubility is also relatively high, it can be alloyed with aluminum in sufficient quantities to give a significant reduction in density and as a result of this alloy is used for aerospace applications where increases in stiffness along with high strength reduce component weight.

For example, alloys such as 8011 are based on Al, Fe and Si are used for application as foil and closures as well as heat exchanger finstock. Al, Ni and Fe in alloy 8001 are used in nuclear power generation for applications demanding resistance to aqueous corrosion at elevated temperatures and pressures. Al and Sn in alloys such as 8280 and 8081 included in the 8xxx series are bearing alloys usually used in cars and trucks.

A group of alloys containing about 5 % Calcium and 5 % zinc have superplastic properties.

2.1.2   Cast Alloys

2.1.2.1 Al-100.0 Cast Alloys

1XX.X: Commercially Pure Al: Unalloyed aluminum. They are minimum 99.00% aluminum. These alloys low strength. An application is cast motor rotor.

Figure 2.16 Aircraft components [AA].

2.1.2.2 Al-200.0 Cast Alloys

2XX.X: Al –Cu Cast Alloys: Some of the important properties of each of the aluminum alloy 2XX.X series can be classified as follows:

- Heat treatable

- Copper content between 4% to 4.6%

- Sand and permanent mold castings

- High strength at room and elevated temperatures; some high toughness alloys

- Aircraft, automotive applications/engines

- Representative alloys: 201.0, 203.0

- Approximate ultimate tensile strength range:130-450MPa

The heat-treated 201.0/AlCu4Ti is the strongest of the common casting alloys. But, there are slightly limitations because of microporosity and hot tearing. Its high toughness makes useful for highly stressed components in machine tool construction, in electrical engineering like pressurized switchgear casings, and in aircraft construction. Landing flap mountings and other aircraft components are made in alloys of the 201.0 or in A356.0 types as shown in Figure 2.16.

There are some special alloys for particular components, for instance, for engine piston heads, integral engine blocks, or bearings. Good wear resistance and a low friction coefficient, as well as adequate strength at elevated service temperatures are necessary for these applications. The alloy 203.0/AlCu5NiCo is an example for the highest strength casting alloy at around 200°C.

2.1.2.3 Al-300.0 Cast Alloys

3XX.X: Al-Si+Cu and/or Mg Cast Alloys: Some of the important properties of each of the aluminum alloy 3XX.X series can be classified as follows:

- Heat treatable

- Silicon content between 5% to 17% with added copper and/or magnesium

- Sand, permanent mold, and die castings

- Excellent fluidity, high strength, some high-toughness alloys

- Automotive and applications like pistons, pumps, electric components

- Representative alloys: 356.0, A356.0, 359.0, A360.0

- Approximate ultimate tensile strength range: 130-275MPa
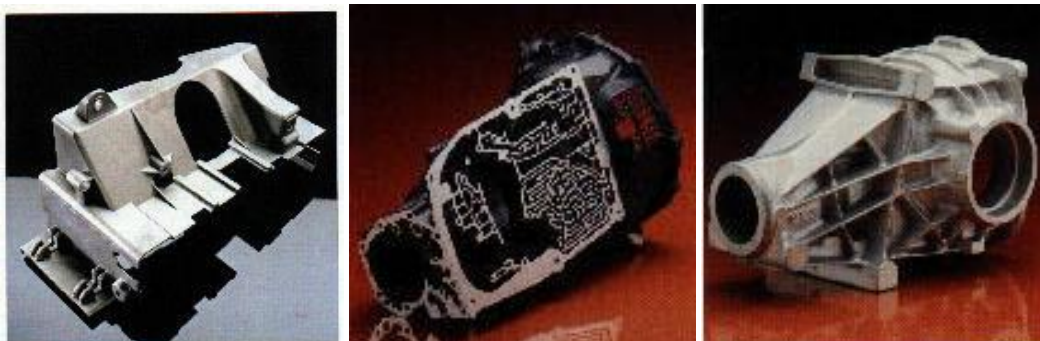
Figure 2.17 a) Inner turbo frame, b) Gearbox casing, and c) Rear axle housing [AA].

One of the most widely are used the 3xx.x series of castings due to the flexibility offered by the high silicon contents and its contribution to fluidity additionally their response to heat treatment which provides a variety of high-strength options.

The most widely used alloys are 319.0 and 356.0/A356.0 for sand and permanent mold casting, 360.0, 380.0/A380.0 and 390.0 for die casting, and 357.0/A357.0 for several type of casting including especially the squeeze/forge cast technologies. Moreover, alloy 332.0 is one of the most frequently used aluminum casting alloys since it can be made almost wholly from recycled scrap.

Some of the industrial applications are 356.0 cast aluminum alloy used inner turbo frame for a Mercedes truck as shown in Figure 2.17a, gearbox casing for a passenger car in alloy pressure die cast 380.0 as shown in Figure 2.17b and rear axle housing of 380.0 alloy sand casting as shown in Figure 2.17c.

The fluidity property of 3xx.x castings offers outstanding detail and complexity by using the lost-foam process as shown in Figure 2.18a. Some other applications in the automotive industry are 357.0 and A357.0 sand and permanent mold castings for automotive components as shown in Figure 2.18b and A356.0 cast wheels as shown in Figure 2.18c.

Figure 2.18 a) 3xxx.x castings made by the lost-foam process, providing exceptional detail and complexity, b) Automotive components of 357.0 and A357.0 sand and permanent mold castings, c) A356.0 cast wheels are now widely used in the US industry [AA].

2.1.2.4 Al-400.0 Cast Alloys

4XX.X: Al-Si Cast Alloys: Some of the important properties of each of the aluminum alloy 4XX.X series can be classified as follows:

- Non-heat treatable
- Silicon content between 5% to12%
- Sand, permanent mold, and die castings
- Excellent fluidity, good for intricate castings
- Typewriter frames, dental equipment, marine, architectural
- Representative alloys: 413.0, 443.0
- Approximate ultimate tensile strength range:115-170MPa

Remarkably, very good castability and excellent weldability in the 4xx.x series is alloy B413.0/AlSi12 due to its eutectic composition and low melting point of 570°C. It has good corrosion resistance with moderate strength and high elongation before fracture. The alloy is proper to use for complicated, thin walled, leak-proof, fatigue resistant castings.

2.1.2.5 Al-500.0 Cast Alloys

5XX.X: Al-Mg Cast Alloys: Some of the important properties of each of the aluminum alloy 5XX.X series can be classified as follows:

- Non-heat treatable
- Magnesium content between 4% to 10%
- Sand, permanent mold, and die
- Tougher to cast but, provides good finishing characteristics
- Excellent corrosion resistance, machinability, surface appearance
- Cooking utensils, food handling, aircraft and highway fittings
- Representative alloys: 512.0, 514.0, 518.0, 535.0
- Approximate ultimate tensile strength range: 115-170MPa

The good corrosion resistance is the common feature of 5xx.x alloys even if in sea water or corrosive environments. Besides, alloys 512.0 and 514.0 have medium strength and excellent elongation. These series alloys are very useful for door and window fittings especially the alloy 520.0, because of ability to decorate by anodized to give a metallic finish or in a wide range of colors. The castability of the series is low-grade because of long freezing range of magnesium content.

2.1.2.6 Al-700.0 Cast Alloys

7XX.X: Al-Zn Cast Alloys: Some of the important properties of each of the aluminum alloy 7XX.X series can be classified as follows:

- Heat treatable
- Zinc content between 6.2% to 7.5%
- Sand and permanent mold cast (harder to cast)
- Excellent machinability and appearance

- Furniture, garden tools, office machines, farm, mining equipment
- Representative alloys: 705.0, 712.0
- Approximate ultimate tensile strength range: 205-380MPa

7xx.x series alloys are preferred to use only where the excellent finishing characteristics and machinability are important owing to the increased difficulty in casting 7xx.x alloys.

2.1.2.7 Al-800.0 Cast Alloys

8XX.X: Al-Sn Cast Alloys: Some of the important properties of each of the aluminum alloy 8XX.X series can be classified as follows:

- Heat treatable
- sand and permanent mold castings (harder to cast)
- Excellent machinability
- Bearings and bushings of all types
- Representative alloys: 850.0, 851.0
- Approximate ultimate tensile strength range:105-205MPa

8xx.x alloys are relatively hard to cast when they are used only where their unique machining and bushing characteristics are necessary.

2.2 Copper

Copper is one of the few metals to occur naturally as an uncompounded mineral. Copper has a history of use that is at least 10,000 years old and was known from some of the oldest civilizations on record. Cupronickel coin is the example of the historical utilization as shown Figure 2.19.

Fig 2.19 Cupronickel coin of king Pantaleon c. 170 BCE (Wikipedia, n.d.).

Table 2.5 Classification of the copper and base alloys.

Classification of copper and its alloys		
Family	**Principal alloying element**	**UNS numbers**
Copper alloys, brass	Zinc (Zn)	C1xxxx–C4xxxx,C66400–C69800
Phosphor bronzes	Tin (Sn)	C5xxxx
Aluminum bronzes	Aluminum (Al)	C60600–C64200
Silicon bronzes	Silicon (Si)	C64700–C66100
Copper nickel, nickel silvers	Nickel (Ni)	C7xxxx

Copper and copper base alloys provide extraordinary combinations of thermal and electrical conductivity, formability, strength and corrosion resistance, and as a result they can be extensively used in variety of engineering applications. Moreover, obtainable in different colors, resistance sparking and nonmagnetic behavior are

beneficial features. The formability or strength can be useful for drawing wire for electrical work as well as its tremendous electrical properties (Mishra & Mahoney, 2007, chap.8).

The resemblance in external appearance of the many alloys, together with the different combinations of elements used when making each alloy, can cause confusion when classifying the different compositions. Around 400 different copper and copper-alloy compositions can be loosely classify into the groups as follows copper, high copper alloy, brasses, bronzes, copper nickels, copper–nickel–zinc (nickel silver), leaded copper, and special alloys. Table 2.5 shows the principal alloying element for four of the more common groups and the name for each group (Copper, Wikipedia).

Alloying coppers have significantly less thermal and electrical conductivity than pure copper. Pure copper does not have phase change after solidification. Zn, Sn, P, Fe, Al, Be, Ni, Pb, Co Mn kind of elements exhibit extraordinary solid solubility in copper. The solubility of zinc is more than 30 wt% in copper at 25°C. The mechanical properties of some common copper alloys are shown in Table 2.6.

Brass is any alloy of copper and zinc. The zinc content can vary between few percent to about 40%. If the zinc content should be kept under 15%, the corrosion resistance of copper does not noticeably decrease. The color of brasses is generally yellow. The most of the compositions exhibit excellent combination of strength and to and toughness at different temperature ranges. Besides, they are easily formed and strength by cold deformation and annealing treatments. Brasses can be responsive to selective leaching corrosion under certain conditions, as a result of this they are leaving behind a spongy copper structure because of dezincification which means zinc is leached from the alloy.

In addition to Table 2.6, brass types and properties of them are below (Copper, Wikipedia):

Table 2.6 Mechanical properties of some common copper alloys.

Name	ASTM Standard	Nominal composition (%)	Form and condition	Y.S. MPa	T.S. MPa	El. %	HD. HB	Comments
Copper	B1, B2, B3, B152, B124, R133	Cu 99.9	Annealed	69	220	45	42	Electrical equip., roofing, screens
			Cold-drawn	275	310	15	90	
			Cold-rolled	275	317	5	100	
Gilding metal	B36	Cu 95.0, Zn 5.0	Cold-rolled	344	386	5	114	Coins, bullet jackets
Cartridge brass	B14, B19, B36, B134, B135	Cu 70.0, Zn 30.0	Cold-rolled	434	524	8	155	Radiators, drawn cartridge cases, electrical, hardware
Phosphor bronze	B103, B139, B159	Cu 70.0, Sn 10.0, P 0.25	Spring Temper	—	841	4	241	High fatigue-strength and spring qualities
Yellow or High brass	B36, B134, B135	Cu 65.0, Zn 35.0	Annealed	124	330	60	55	Good corrosion resistance
			Cold-drawn	379	482	15	115	
			Cold-rolled	413	510	10	180	
Manganese bronze	B138	Cu 58.5, Zn 39.2, Fe 1.0, Sn 1.0, Mn 0.3	Annealed	206	413	30	95	Forgings
			Cold-drawn	344	551	20	180	
Naval brass	B21	Cu 60.0, Zn 39.25, Sn 0.75	Annealed	151	386	40	90	Resistance to salt corrosion
			Cold-drawn	275	448	35	150	
Muntz metal	B111	Cu 60.0, Zn 40.0	Annealed	137	372	45	80	Condenser tubes
Aluminum bronze	B169 A, B124, B150	Cu 92.0, Al 8.0	Annealed	172	482	60	80	—
			Hard	448	723	7	210	"
Beryllium copper	B194, B196, B197	Cu 97.75, Be 2.0, Co or Ni 0.25	Annealed, ST	220	482	45	B60*	Electrical, valves, pumps
			Cold-rolled	104	110	5	B81*	
Free-cutting brass		Cu 62.0, Zn 35.5, Pb 2.5	Cold-drawn	303	482	18	B80*	Nuts, gears, keys, Screws
Nickel silver	B112	Cu 65.0, Zn 17.0, Ni 18.0	Annealed	172	400	40	70	Hardware
			Cold-rolled	482	586	4	170	
Nickel silver	B149	Cu 76.5, Ni 12.5, Pb 9.0, Sn 2.0	Cast	124	241	15	55	Ornaments, plumbing
Cupronickel	B111, B171	Cu 88.35, Ni 10.0, Fe 1.25, Mn 0.4	Annealed	151	303	45	–	Condenser, salt-water pipes
			Cold-drawn tube	393	413	15	–	
Cupronickel		Cu 70.0, Ni 30.0	Wrought	–	–	–	–	Heat-exchange equipment, valves
Ounce metal (Red brass or composition metal)	C83600, B62	Cu 85.0, Zn 5.0, Pb 5.0, Sn 5.0	Cast	17	37	25	60	—
Gun metal (red brass in US)		Varies Cu 80-90%, Zn <5%, Sn ~10%, +other elements @ <1%						

 * Rockwell Scale

Fig 2.20 The firebox of a coal-fired train steam engine (Wikipedia).

- **Admiralty brass:** It consists of 30% zinc and 1% tin which restrains dezincification in most environments.

- **Aich's alloy:** It usually contains 60.66% copper, 36.58% zinc, 1.02% tin and 1.74% iron. Aich's alloy is developed for use in marine industry due to its corrosion resistance, hardness and toughness. A typical application is used for protecting ships' bottoms, but, nowadays, new modern methods make it less common. Its appearance looks like gold.

- **Alpha brass:** It is consists of less than 35% zinc, is malleable, can be worked cold, and is used in pressing, forging, or similar applications. A type of alpha brass **Prince's metal** or **Prince Rupert's metal** is containing 75% copper and 25% zinc. It is used as an imitation of gold owing to its beautiful yellow color.

- **Alpha-beta brass:** It is also called **Muntz metal** or **duplex brass** which contains 35–45% zinc. It is useful for hot working.

- **Aluminum brass:** It contains aluminum, which is used to improve its corrosion resistance. Euro coins (Nordic gold) are made up of aluminum brass as shown Fig 2.21.

- **Arsenical brass:** It contains arsenic substance with usually adding aluminum. It is used for boiler fireboxes as shown in Figure 2.20.

- **Beta brass:** It contains 45–50% zinc. Beta brass can only be worked hot and it is useful for casting with harder and stronger material properties.

- **Cartridge brass:** It contains a 30% zinc brass with good cold working properties.

- **Common brass/Rivet brass**: It is a 37% zinc brass, cheap and standard for cold working.

- **DZR brass:** It is a dezincification resistant brass including a small percentage of arsenic.

- **Gilding metal:** It is usually available the softest type of brass which contains 95% copper and 5% zinc. Gilding metal is commonly used for ammunition components.

- **High brass:** It contains 65% copper and 35% zinc. Besides, it has a high tensile strength. It is suitable to use for springs, screws, and rivets.

- **Leaded brass:** Adding some lead (Pb) to an alpha-beta brass thereby excellent machinability.

- **Lead-free brass:** It contains less than 0.25% lead content.

- **Low brass:** It is containing 20% zinc with excellent ductility and a light golden color. It is used for flexible metal hoses and metal bellows.

- **Manganese brass:** It contains approximately 70% copper, 29% zinc, and 1.3% manganese. It is especially used in making golden dollar coins in the United States as shown in Fig 2.21b.

- **Muntz metal:** It is roughly 60% copper, 40% zinc and a trace of iron. It is used as a lining on boats.

- **Naval brass**: It contains 40% zinc and 1% tin, similar to admiralty brass.

- **Nordic gold:** An alloy brass contains 89% copper, 5% aluminum, 5% zinc, and 1% tin. It used in 10, 20 and 50 cents € coins as shown in Figure 2.21a.

- **Red brass**: It is an alloy of copper-zinc-tin known as **gunmetal**, which is technically not brass, can also called **ounce metal**.

- **Rich low brass (Tombac):** It consists of 15% zinc. It is often preferred in jewelry applications.

- **Tonval brass:** It is also known as CW617N, CZ122 or OT58. Tonval brass is a copper-lead-zinc alloy. It is not suitable for seawater use because of the risk of dezincification.

- **White brass:** It contains more than 50% zinc. White brass is too brittle for general use due to zinc content.

- **Yellow brass:** It is an American term for 33% zinc brass.

Figure 2.21 a) Euro coins, b) Golden dollar coin, c) €1 centre is made up of Cupronickel (Wikipedia).

Bronze is an alloy of copper and other metals, like tin, nickel, lead, phosphor, beryllium, manganese, iron including aluminum and silicon. Aluminum bronzes alloys are consist of copper and aluminum. The content of aluminum ranges is around 5-11%. In the salt water, they have higher strength and corrosion resistance than other bronzes, and have low tendency to sulfur compounds. Some bronze alloy types contain iron, nickel, manganese and silicon.

Figure 2.22 Phosphor bronze propeller from a personal watercraft. Tenor saxophone manufactured from phosphor bronze (Wikipedia).

Table 2.7 Mechanical properties and chemical compositions of CDA standards copper

Name	CDA	Nominal composition %	TS [MPa]		YS [MPa]		El %	HD [HB]	Mac. [YB]
			Min	Typ	Min	Typ			
Red brass	833	Cu 93.0, Sn 1.5, Pb 1.5, Zn 4.0		220		70	35	35	35
	836	Cu 85.0, Sn 5.0, Pb 5.0, Zn 5.0	206	255	96	117	30	50–65	84
	838	Cu 83.0, Sn 4.0, Pb 6.0, Zn 7.0	200	241	82	110	25	50–60	90
Semi-red brass	844	Cu 81.0, Sn 3.0, Pb 7.0, Zn 9.0	200	234	90	103	26	50–60	90
	848	Cu 76.0, Sn 3.0, Pb 6.0, Zn 15.0	172	248	82	96	30	50–60	90
Manganese bronze	862	Cu 64.0, Zn 26.0, Fe 3.0, Al 4.0, Mn 3.0	620	655	310	330	20	170–195[†]	30
	863	Cu 63.0, Zn 25.0, Fe 3.0, Al 6.0, Mn 3.0	758	820	413	572	18	225[†]	8
	865	Cu 58.0, Sn 0.5, Zn 39.5, Fe 1.0, Al 1.0, Mn 0.25	448	490	172	193	30	130[†]	26
Tin bronze	903	Cu 88.0, Sn 8.0, Zn 4.0	275	310	124	144	30	60–75	30
	905	Cu 88.0, Sn 10.0, Pb 0.3max, Zn 2.0	275	310	124	151	25	75	30
	907	Cu 89.0, Sn 11.0, Pb 0.5max, Zn 0.5max	241	303	124	151	20	80	20
Leaded tin bronze	922	Cu 88.0, Sn 6.0, Pb 1.5, Zn 4.5	234	275	110	137	30	60–72	42
	923	Cu 87.0, Sn 8.0, Pb 1.0max, Zn 4.0	248	275	110	137	25	60–75	42
	926	Cu 87.0, Sn 10.0, Pb 1.0, Zn 2.0	275	303	124	137	30	65–80	40
	927	Cu 88.0, Sn 10.0, Pb 2.0, Zn 0.7max	241	289		144	20	77	45
High-leaded tin bronze	932	Cu 83.0, Sn 7.0, Pb 7.0, Zn 3.0	206	241	96	124	20	60–70	70
	934	Cu 84.0, Sn 8.0, Pb 8.0, Zn 0.7max	172	220		758	20	55–65	70
	935	Cu 85.0, Sn 5.0, Pb 9.0, Zn 1.0, Ni 0.5max	172	220	82	758	30	55–65	70
	937	Cu 80.0, Sn 10.0, Pb 10.0, Ni 0.7max	172	241	82	124	20	55–70	80
	938	Cu 78, Sn 7.0, Pb 15.0, Ni 0.75max	172	205	96	758	18	50–60	80
	943	Cu 70.0, Sn 5.0, Pb 25.0, Ni 0.7max	144	186		620	10	42–55	80
Aluminum bronze	952	Cu 88.0, Fe 3.0, Al 9.0	448	551	172	186	35	110–140[†]	50
	953	Cu 89.0, Fe 1.0, Al 10.0	448	517	172	186	25	140[†]	55
	954	Cu 85.0, Fe 4.0, Al 11.0	517	586	205	241	18	140–170[†]	60
	955	Cu 81.0, Ni 4.0, Fe 4.0, Al 11.0	620	100	275	303	12	180–200[†]	50
	958	Cu 81.0, Ni 5.0, Fe 4.0, Al 9.0, Mn 1.0	586	655	241	262	25	150-170[†]	50
Silicon bronze	878	Cu 80.0, Sn 0.25, Pb 0.15, Zn 16.0max, Ni 0.2, Fe 0.15, Al 0.15	551	572	205	255	29	115	40
[†] Brinell scale with 3000 kg load									

Phosphor bronze alloy contains copper with 3.5 to 10% of tin and a significant content of up to 1% phosphorus is added as deoxidizing agent during melting. These alloys are remarkable with their toughness, strength, low coefficient of friction, and fine grain. Moreover, the phosphorus progresses the fluidity of the molten metal and in that way the castability is improved, and mechanical properties are upgraded by cleaning up the grain boundaries. As an example of, phosphor bronze propeller and tenor saxophone manufactured from phosphor bronze as shown in Fig 2.22.

Beryllium copper is an alloy which is also known as copper beryllium, BeCu or beryllium bronze is consists of copper and 0.5 to 3% beryllium, and occasionally with other alloying elements. Combination of high strength with non-magnetic and non-sparking properties of Beryllium Copper makes excellent choice for metalworking, forming and machining qualities. Figure 2.23a shows an example of a non-sparking tool. Beryllium copper is used for springs carrying electrical current because of its low electrical resistance as shown in Figure 2.23b.

Figure 2.23 a) Example of a non-sparking tool, b) Springs made from Beryllium copper, c) The speculum metal mirror from William Herschel's 1.2-meter (49.5-inch) diameter "40-foot telescope", at the Science Museum in London (Wikipedia).

Nickel silver is a metal alloy of copper with nickel and sometimes but not always zinc. General formulation is 60% copper, 20% nickel and 20% zinc. Its appearance resembles silvery.

Cupronickel is an alloy of copper with containing nickel and strengthening elements, such as iron and manganese. Highly corrosion resistant of cupronickel

makes useful in seawater, since its electrode potential is adjusted to be neutral with regard to seawater. €1 is made up of cupronickel as shown in Figure 2.21c.

Bell metal is a form of bronze which is typically about 3:1 ratio of copper to tin (78% copper, 22% tin). It is a hard alloy is preferred for making bells.

Speculum metal is a mixture of around 2:1 ratio of copper to tin making a white brittle alloy when it can be polished to make a highly reflective surface. Mostly, It is used to make different types of mirrors including early reflecting telescope optical mirrors as shown in Fig 2.23c.

Copper Development Association (CDA) also has similar standards for brass and bronze types which are summarized at Table 2.7 including mechanical properties and chemical compositions.

Copper is not commonly considered as weldable by spot and projection welding processes due to its high conductivity, which is 10–100 times higher than that of steels and nickel alloys. Hence, the heat input required for welding is much higher, resulting in quite low welding speeds. 1.5–50 mm thickness copper plates were successfully friction stir welded (Mishra & Ma, 2005).

CHAPTER THREE
APPLICATIONS OF FRICTION STIR WELDING

3.1 Applications of Friction Stir Welding

Friction Stir Welding is a new process, but has been used in production applications since 1995 in Europe and is now being industrialized all over the world. The first commercial applications involved welding of Scandinavian aluminum extruders to form of hollow aluminum panels for deep-freezing of fish and for paneling for marine applications. Since then, friction stir welding (FSW), the name under which it was patented, the process has been commercialized in many other applications, including rail car, railroading, marine, shipbuilding, building decks for car ferries, automotive, automotive hybrid aluminum, aircraft, aerospace industry where it is used to weld the aluminum external tank of the space shuttle, heavy truck, large tank structure assembly, fuel tanks, radioactive waste container manufacturing, medical applications, etc. Now, the FSW process is being moved into fabrication of complex assemblies because of producing yielding significant quality and cost improvements. Designers are taking advantage of the process, by designing the product specifically for the FSW process when the process is maturing (NASA).

Research and development efforts have resulted in improvements in FSW and the follow-up a series of related technologies over the last decade (Arbegast, 2006). FSW can be used to produce lap joint, butt joint, and T-joints in a wide variety of materials.

3.2 Economical Maturing and Expectations of Applications of FSW

Until the end of the 19th century, forge welding was the only welding process known. Arc welding and oxyfuel welding developed at the end of the 19ths. Starting from the beginning of 1920s, rivets have replaced by arc welding as the joining process for pressure vessels. Welding methods moved forward by wars in the

beginning of the 20th century, because of the using more metals daily life. Weld usage enlarged through the 1940s with application to buildings, structures, and ships. Arc welding has evolved into an international industry complete with welder education and certification programs and ruled by extensive specifications, design criteria, and standards, by 2006. The American Welding Society (AWS) made a survey in 2002 about estimating to spend more than \$34.4 billion annually on arc welding of metallic materials with an anticipated growth rate averaging 5 to 15% per year in the U.S. manufacturing industries. By the way, the construction, heavy manufacturing, and light manufacturing industries make up the majority with \$25 billion in annual expenditures. Estimated cost is around \$4.4 billion per yearly, to repair and maintenance of the welded structures joining industry-wide. As a result of this, these industries are a main consumer of energy and a producer of airborne emissions and solid waste (Arbegast, 2006, 'Welding' Wikipedia).

Friction stir welding researchers and producers estimate that if 10% of the U.S. joining market can be replaced by FSW, then 1.28×10^{13} Btu/year (about 3.75×10^9 kWh/year) energy savings and 500 million lb/year (2.28×10^5 ton/year) greenhouse gas emission reductions can be obtained. Arbegast (Mishra & Mahoney, 2007, chap. 13) mentioned hazardous fume emissions were eliminated during the FSW of high-temperature and chromium-containing alloys. As a result of the Rockwell Scientific report, the emission levels of during FSW of ferrous alloys (Cr<0.03, Cu <0.03, Mn <0.02, and Cr+6 <0.01 mg/mm3) considerably lower than those measured during gas tungsten arc weld (GTAW) (Cr 0.25, Cu 0.11, Mn 1.88, and Cr+6 0.02 mg/mm3). Additionally to higher structural strength, increased reliability, and reduced emissions, the annual economic benefit of the FSW in the US industry is more than \$4.9 billion/year (Mishra & Mahoney, 2007, chap.13 and chap.6).

Defalco (2006) compared the production costs of aluminum joints made using FSW and GMAW as shown in Table1.5. Arbegast (Mishra & Mahoney, 2007, chap. 13) pointed out the production costs were reduced from \$2.11/ft for GMAW to \$1.27/ft for FSW by using Table 1.5.

Polt (2004) reported, in conventional welding, rivets and the filler materials add weight to air and space vehicles. At one time it drilled and filled 1.1 million rivet holes a day-at $5 to $10 each, when those holes need to require engineering, drilling, filling and inspecting. Millions of rivets have used Boeing before invention of the FSW. That's one reason Boeing explored friction-stir welding as a replacement for Phantom Works by using no filler materials in 1995.

Annual welding expenditures of the aeronautic and aerospace industries in the total U.S. is less than 1% ($300 million) of because of the joining method of choice of the mechanical fastening. On the other hand, the bulk of FSW development dollars has been spent by these sectors. FSW applications in the broader industrial markets which are automotive, construction, marine, heavy manufacturing and light manufacturing for has been neglected, that's why they have the huge portion of the expenditures (American Welding Society [AWS]).

Arbegast (2006) evaluated that there were only 114 FSW licenses wherein North America were reported 36, Europe were reported 37 and Asia were reported 41, granted by TWI Figure 3.1 as of January 2005. These were no reported licensees in South America. Whereas only 36% of the North America licensees are industrial and the remaining 64% were held by government laboratories, equipment manufacturers, and academic and research institutes, 68% of the licensees were industrial at overseas. This implies that industrial application of the FSW process in the United States was falling behind the overseas industries as indicated by the data Jan'05.

Smith and Lord (2007) reported a study about FSW patents at September, 2007. In this paper, they reviewed the growth in interest in FSW evaluated by both the real applications in industry and the distribution of related patent filings by time and location. TWI had issued 192 FSW licenses to a range of groups including end users, equipment suppliers, universities and R&D institutes and additionally, there have been over 1800 patent applications filed as of September 2007. The Table 3.1 shows the distribution by location and type of group.
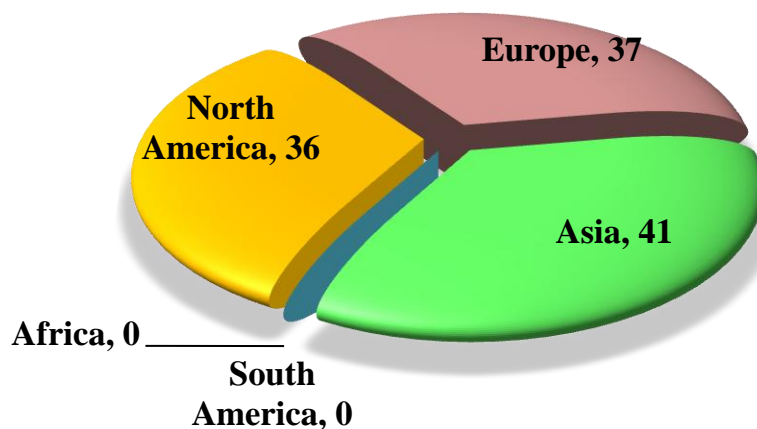
Overseas FSW License Holders by Entity Type
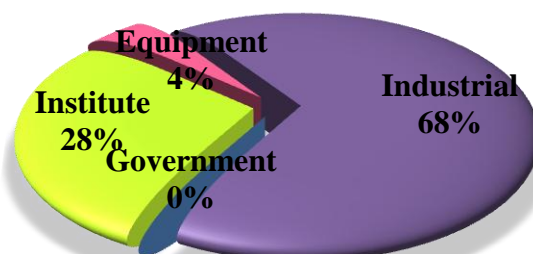
North America FSW License Holders by Entity Type
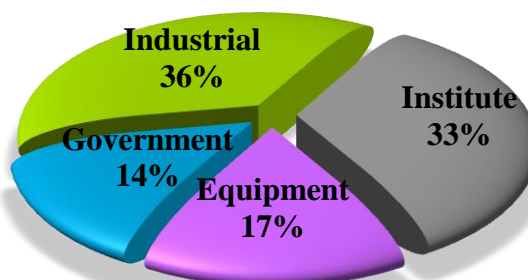
Figure 3.1 Demographics of FSW licensees as of January 2005 (Arbegast, 2006).

Table 3.1 Current licensees as of September 2007.

Region	Industrial End User	Univ. R&D	Equip. Supplier	Total
UK & EU	28	22	6	56
USA & Canada	18	18	6	42
Japan	24	14	1	39
China & SEA	10	23	2	35
Totals	74	70	14	172

Generally, patent application can be categorized five statuses by TWI as shown in Figure 3.2 by using data given in paper Smith and Lord (2007). Moreover, with the same way, these categorizations can be classified by geographically, as follows to three main patent offices, namely European Patent Office (EPO), Japan Patent Office (JPO) and United States Patent & Trademark Office (USPTO) as shown in Figure 3.3.
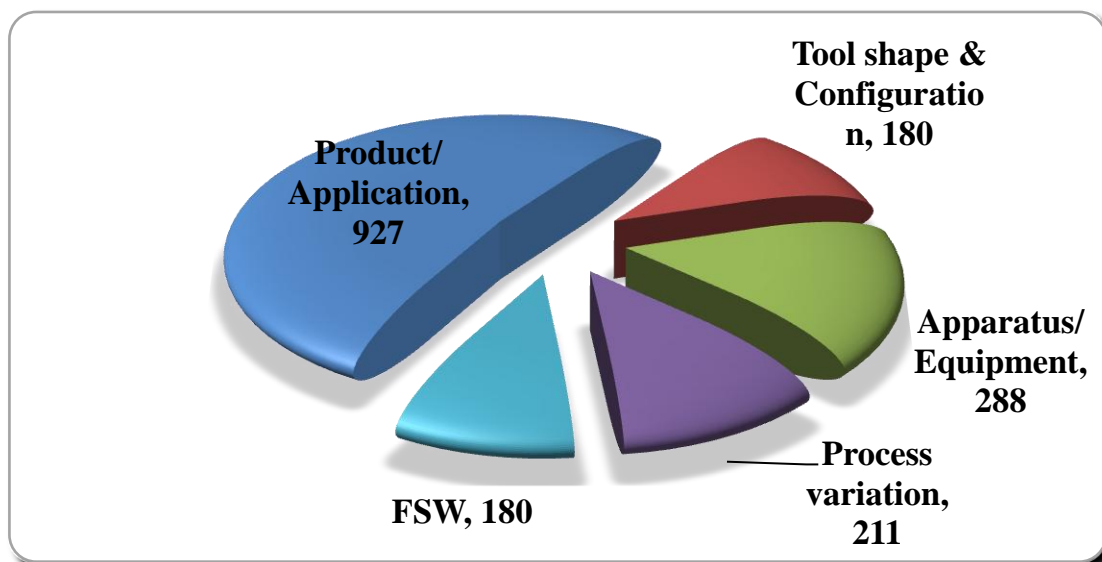
Figure 3.2 Patent applications categorization.

As beginning of January 2010, total patent application filled out around 2380 due to the list of TWI and Figure 3.4 is showing applications by territories is obtained by using this list. When Figure 3.3 and Figure 3.4 are considered, Japanese applicants

have higher successful rate than others. Another result is obtained by using TWI list is the yearly base patent application as shown in Figure 3.5. There is a rapid increase in patent applications over 100-150 each year between 1996 and 1999. Furthermore, the increase continued as around the 200 to 250 between 2000 and 2006. Unfortunately, patent applications for FSW were suddenly decrease after the August 2008 with the global crises. Only 9 applications have been filled out between January and June 2009.

Main Themes in Patent Application Filings

	Product/App lication	Tool shape & Configuratio n	Apparatus/E quipment	Process variation	FSW
EPO	101	21	39	44	27
JPO	569	89	142	115	114
USPTO	210	52	78	38	27
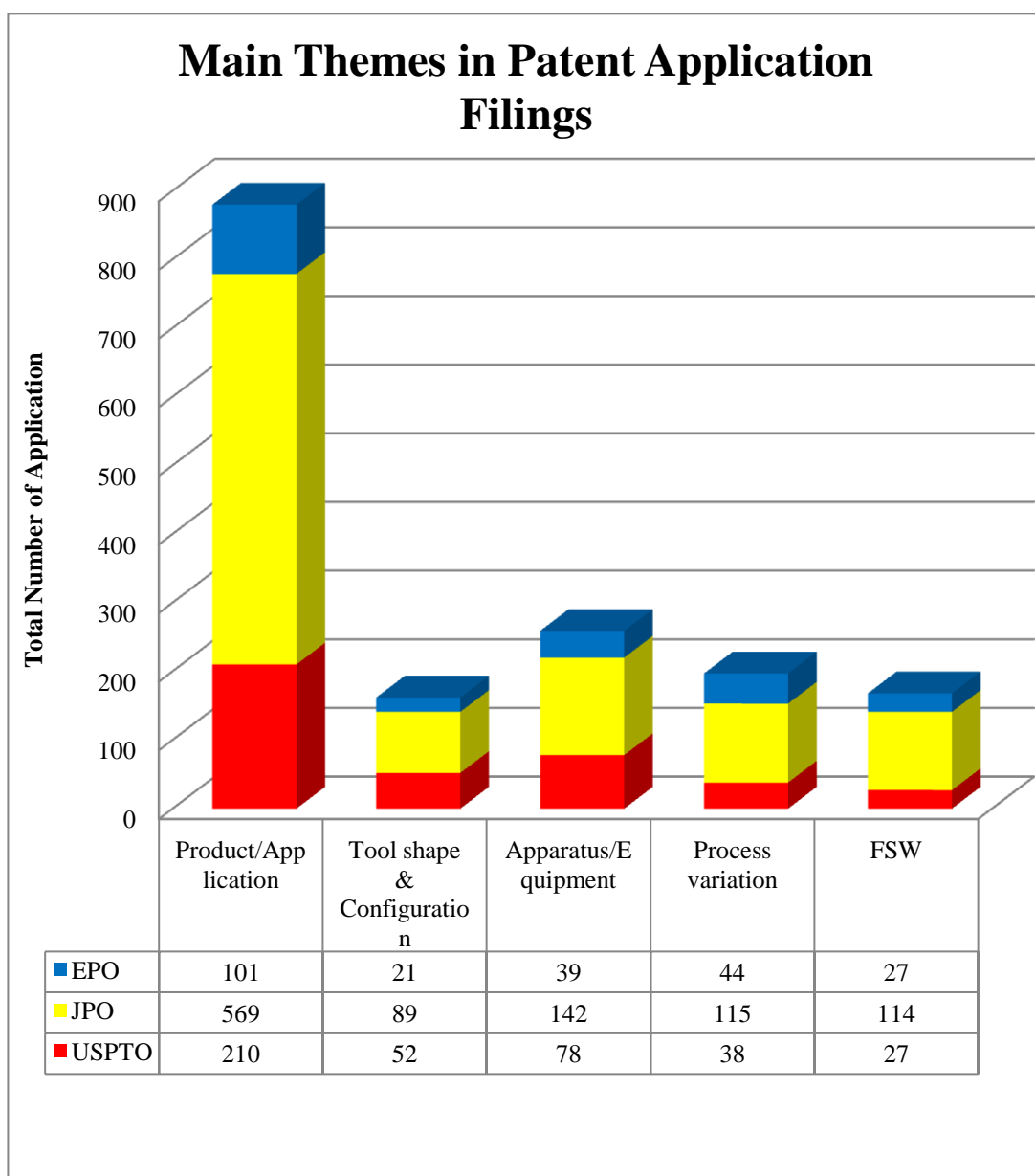
Figure 3.3 Patent applications categorizations classification by geographically.
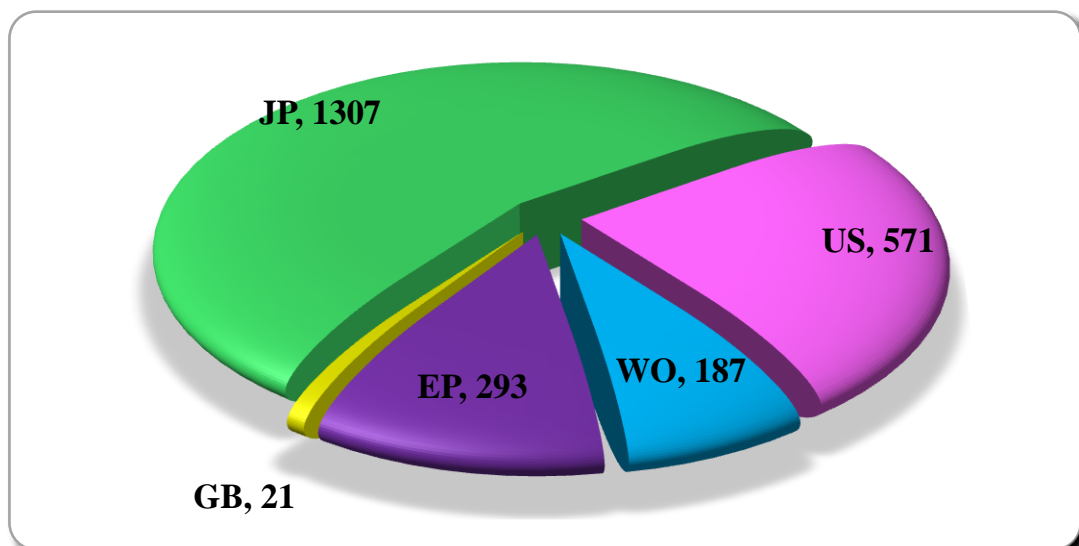
Figure 3.4 Patent applications filled out by territory.
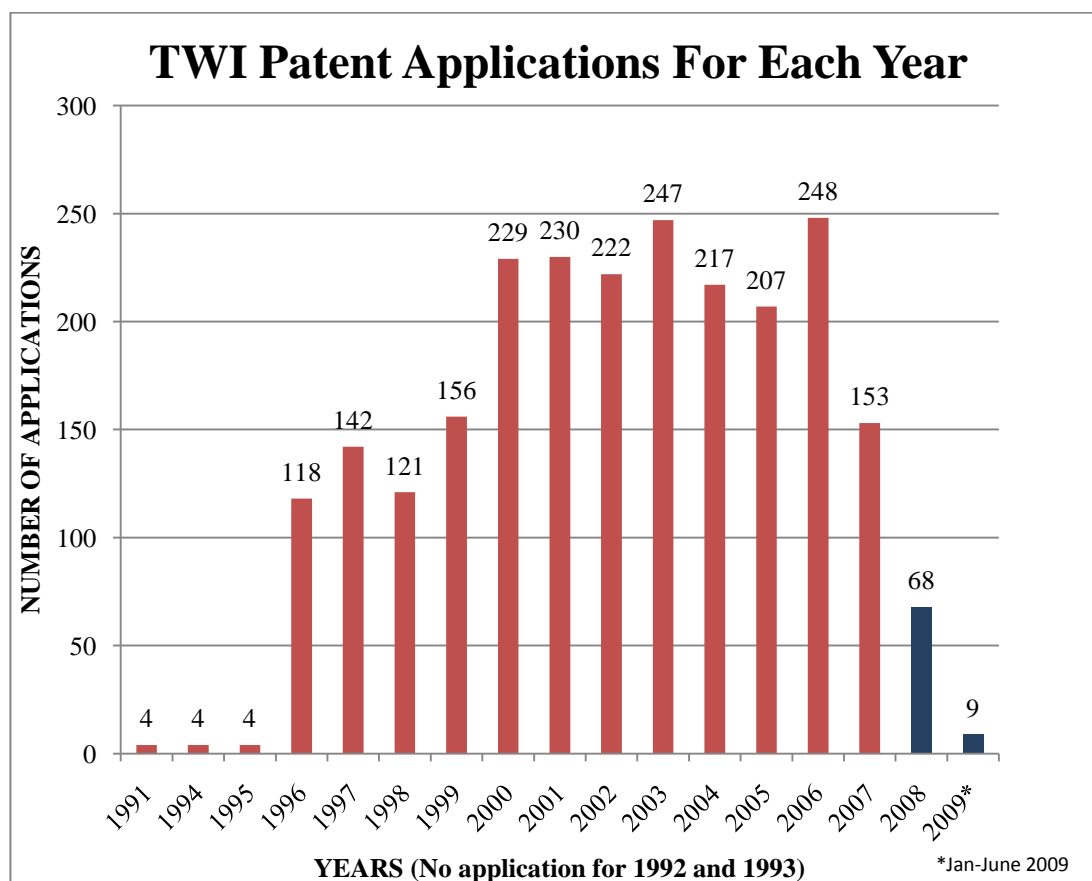
Figure 3.5 TWI patent applications for each year (Data Source TWI)

NUMBER OF PATENT APPLICATION PER COMPANY SINCE 1991
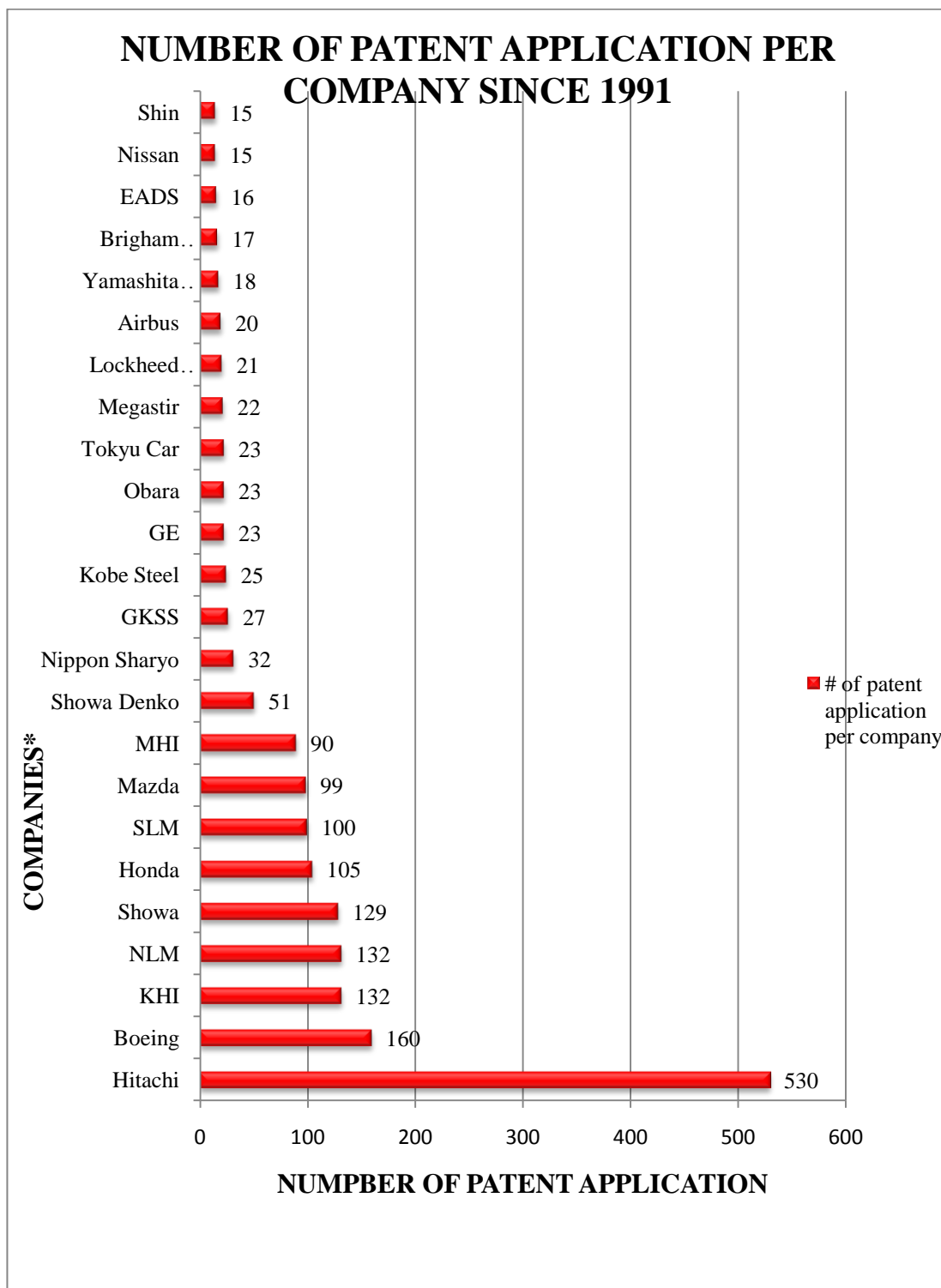
Figure 3.6 Number of patent applications for company wise. (Data source TWI) (*for multi name applications, only the first name is accepted as applicant name)

According to list issued by TWI as beginning of January 2010, the top organizations in terms of number of applications are filled out as shown in Figure 3.6. For Hitachi, Smith and Lord (2007) mentioned why they have huge amount of patent application as like this, the benefits and promises proved so great that they adopted a tactic of filing a wide variety of patent applications covering one particular product type so as to try and 'picket-fence' FSW for their market. They consider FSW as a differentiating technology that allows them to create a global patent portfolio so as to gain new orders and expand global business. Far behind from Hitachi, Boeing, Kawasaki Heavy Industries (KHI), Nippon Light Metal (NLM) and Showa are coming respectively. Four of the first top five organizations are Japanese company. That's why they have more applications than others.

3.3 Industrial Applications of FSW

Friction stir welding has made an increasing impact in the welding of aluminum in many industry sectors, notable shipbuilding, aerospace, and railways, and is growing rapidly in other industries, for example automotive since its invention at TWI in 1991. The fact that for the rapid comprehension of the technology is the basic simplicity and flexibility of the process, and its ability to weld just about any aluminum alloy including non-weldable by most of the fusion processes (Johnson & Threadgill, 2003).

3.3.1 Applications of FSW in Shipbuilding and Marine Industry

- Panels for decks, sides, bulkheads and floors
- Aluminum extrusions
- Hulls and superstructures
- Helicopter landing platforms
- Offshore accommodation
- Marine and transport structures
- Masts and booms, e.g. for sailing boats

- Refrigeration plant

The first commercial application of the FSW were in the marine industry, to manufacture of hollow aluminum panels for deep freezing of fish on fishing boats as shown in Figure 3.7a. These panels were made from friction stir welded 6xxx aluminum extrusions for use in decks, bulkheads, on a variety of vessels. Since then, significant progress has been made in reducing distortion and high reproducibility make FSW both technically and economically a very attractive method to produce these stiff panels. Especially, the naval applications have been growing interest in the friction stir welding of steel. While the process has been successfully operated, more development is needed to improve tool material technology and process control, and to get more data on the performance of welds (Johnson & Threadgill, 2003 and Nicholas & Kallee, 2002).
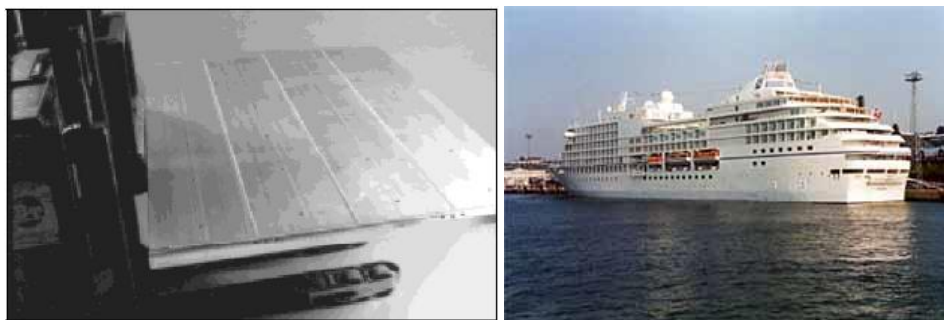
Figure 3.7 a) Sapa FSW aluminum panel for pressing of fish blocks before quick freezing. The panel is welded from both sides (Nicholas & Kallee, 2002), b) 'Seven Seas Navigator', a cruise ship with extensive friction stir welding in the superstructure (Johnson & Threadgill, 2003).

The greatest advantage of the FSW in marine applications for flat structures, such as decks, bulkheads, floors, and superstructures etc. which do not contain complex curves welding long straight welds, as this allows maximum use of the fully mechanized nature of the process. Although early industrial applications welding speed was about 0.7 to 0.8m/min with a joint line thickness of 5 to 6mm friction stir for extrusions such as AA6082-T6, welding speeds are now around 10m/min, and

thus increase of an order of magnitude. Johnson and Treadgill (2003) gave an example of tensile strength and elongation comparison chart for FSW and MIG for AA6082-T6 as shown in Figure 3.8. 'Seven Seas Navigator', is an example of a cruise ship with extensive use of friction stir welding in the superstructure as shown in Figure 3.7b.
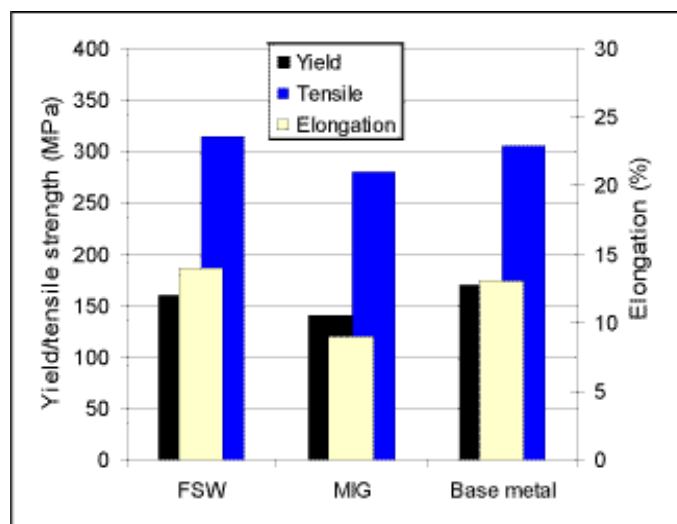
Figure 3.8 Comparison chart for FSW and MIG for AA6082-T6 (Johnson and Treadgill).

A portable prototype FWS machine has developed for flat friction stir welded plates where were explosively formed into hull profiles for a high speed tourist vessel designed for reef viewing in Australia the University of Adelaide in the mid 90's as shown in Figure 3.9a. The machine can be lift up and aligned it above the joint line by using only two operators without a crane. The Research Foundation Institute (RFI) in Cairns where the portable machine has used after university has made six friction stir welds in the bow section of a patented prototype ship using 5 mm thick aluminum alloy 5083 H321 as shown in Figure 3.9b. In spite of the fact that the process was a technical success, the whole vessel development funding was cancelled, and this design has not been restart in another place (Johnson & Threadgill, 2003 and Nicholas & Kallee, 2002).
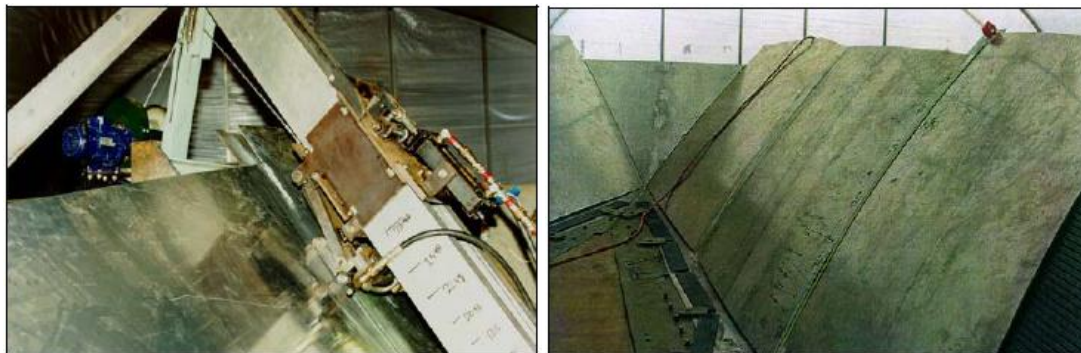
Figure 3.9 a) Portable FSW machine on the shipyard of the Research Foundation Institute in Cairns, Australia, b) Friction stir welds on the star board side of the bow section prior to explosive forming at the Research Foundation Institute (Nicholas & Kallee, 2002).

When the flared shape of the structure welded by high energy rate forming (HERF), the friction stir welded sheets of the bow section were deformed. The aluminum sheets where were placed in a mold have been situated on some explosive plates for explosion after the mold was filled water as shown in Figure 3.10a. Compare to the MIG welded sheets, a much smaller amount of explosive used in FSW welded sheets. The prototype ocean viewer vessel was manufactured by using FSW as shown in Figure 3.10b.

Figure 3.10 a) Detonation of the explosion for high energy rate forming of the bow section, b) Explosively formed bow section of the ocean viewer vessel at RFI in Cairns, c) Large aluminum ship panel made from 5083-H112 aluminum alloy extrusions, made by Sumitomo Light Metal (Nicholas & Kallee, 2002).

Nicholas and Kallee (2002) explained some other marine applications as follows. Seawater resistant aluminum panels were produced from five, 250mm wide 5083 aluminum alloy extrusions for ship cabin walls because of good smoothness of the weld root in Japan as shown in Figure 3.10c.

Commercially, standard size wide aluminum panels with low heat input which results in minimal distortion and reduced thermal stresses can be manufactured by FSW for cruise ships and high-speed ferryboats as shown in Figure 3.11a and Figure 3.11b.
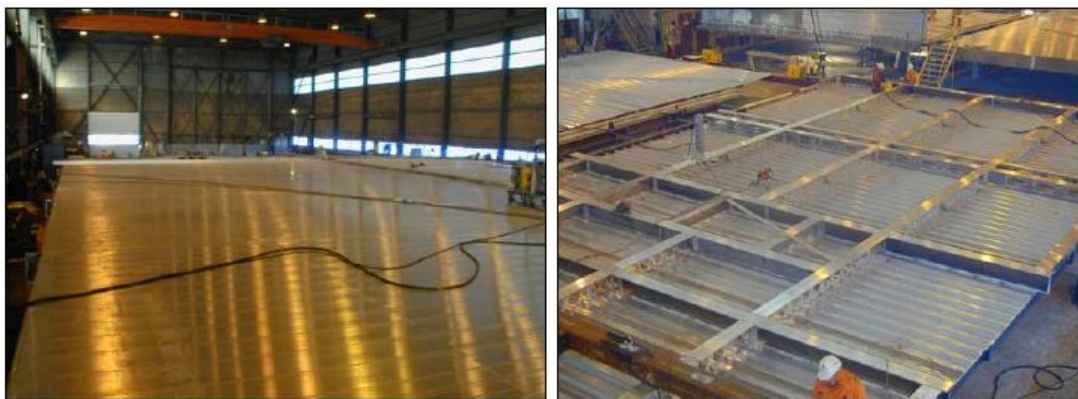
Figure 3.11 a) FSW decks of Hydro Marine Aluminium with a superb surface quality and negligible distortion, b) Hydro Marine Aluminium produced FSW decks for 'The World'' of up to 15x30m (Nicholas & Kallee, 2002).

Hydro Marine Aluminium in Haugesund, Norway produced 285km friction stir welded shipbuilding panels which can be rolled for road transport as shown in Figure 3.12a and Figure 3.12b. Besides were stiffed only in the longitudinal direction.

Generally, aluminums can be friction stir welded around 500°C, but C-Mn steels which are used in shipbuilding is necessary much higher temperatures of between 1000°C and 1200°C for welding, and the options for tool materials are greatly limited, especially when the high forces present are considered. It is important that the tool does not break down by wear, deformation, microstructural weakness, reaction with the workpiece or fracture (Johnson & Threadgill, 2003). Hence, two tool material types which are refractory alloys based on the tungsten - rhenium system that exhibit excellent high temperature strength and toughness without having strength to tend to wear and deformation, and a ceramic solution based on polycrystalline cubic boron nitride (PCBN) that is a very hard material (boron nitride is thought to be the second hardest material known) with low wear rates have given

promising results. On the other hand, the tungsten – rhenium tools which can be machined relatively easily are much cheaper than PCBN. When the tools obtained a very complex manufacturing process, they are slightly expensive.

Figure 3.12 a) Esab SuperStir^{TM} machine at Hydro Marine Aluminium to weld aluminium extrusions for shipbuilding panels, b) Prefabricated FSW panel for catamaran side-wall, rolled for road transport (at Hydro Marine Aluminium) (Nicholas & Kallee, 2002).

One of the biggest advantages of the FSW process in marine industry is no requirement for filler. But it can be a disadvantage, if the weld needs to make filler welds or other geometries where extra material must be added to the weld. However, most aluminum alloys used in marine structures are weldable by a type of processes, and as a result friction stir welding must challenge on technical and economic terms, and demonstrate clear advantages over competing processes.

3.3.2 Applications of FSW in Automotive Industry

- Engine and chassis cradles
- Wheel rims
- Attachments to hydroformed tubes
- Tailored blanks, e.g. welding of different sheet thicknesses
- Space frames, e.g. welding extruded tubes to cast nodes
- Truck bodies
- Tail lifts for lorries
- Mobile cranes
- Armour plate vehicles

- Fuel tankers

- Caravans

- Buses and airfield transportation vehicles

- Motorcycle and bicycle frames

- Articulated lifts and personnel bridges

- Skips

- Repair of aluminum cars

- Magnesium and magnesium/aluminum joints

The automotive industrial applications for FSW represent how big the growing uses of the technology. The first study was started on aluminum tailored blanks for door panels by TWI, in 1998 as shown in Figure 3.13a and Figure 3.13b. Additionally, a confidential group sponsored project involving BMW, DaimlerChrysler, EWI, Ford, General Motors, Rover, Tower Automotive and Volvo have demonstrated new concepts on FSW drive shafts and space frames (Thomas, Kallee, Staines & Oakley, 2006).

Figure 3.13 a) Prototype aluminum car door made from a 3.0 and 1.5mm thick AA6181 tailor welded blank (Nicholas & Kallee, 2002), b) FSW tailor welded blank produced from 6000 series aluminum 1998 TWI, BMW, Land Rover (Thomas, Kallee, Staines & Oakley, 2006).

Ford Motor Co. uses a FSW central tunnel assembly to produce several thousand Ford GT sport automobiles as shown in Figure 3.14. The centre tunnel houses and isolates the fuel tank from the interior compartment and increases the rigidity of the chassis as shown in Figure 3.15a. A linear FSW lap joint has used to join the top aluminum stamping and two hollow aluminum extrusions along the length of the

tunnel. Therefore, dimensional accuracy improved and a 30% increase in strength over similar GMA welded assemblies by using FSW (Arbegast, 2006 and Thomas, Kallee, Staines & Oakley, 2006).
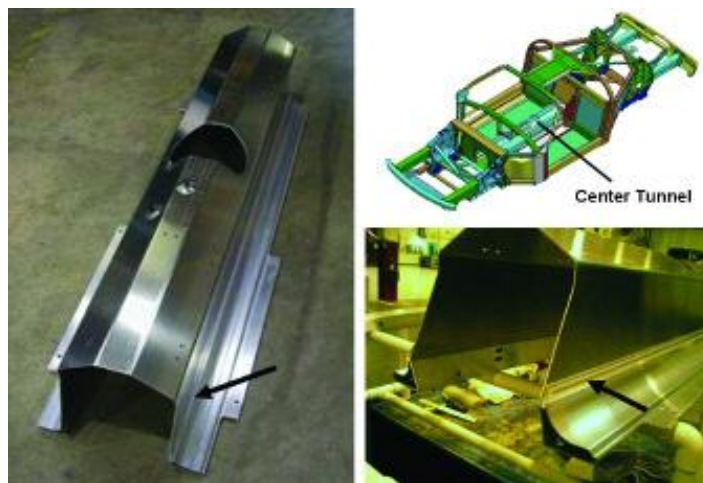
Figure 3.14 The central tunnel assembly of the Ford GT is a FSW assembly made from aluminum stampings and extrusions (Arbegast, 2006).

Figure 3.15 a) Friction stir welding of the centre tunnel of the Ford GT, b) Friction stir welded suspension links for Lincoln stretched limousines (Thomas, Kallee, Staines & Oakley, 2006).

Aluminum suspension links which was made from two identical extrusions, friction stir welded simultaneously with two spindles from both sides were produced for Lincoln Town Cars designated as stretched limousines by Tower Automotive in Grand Rapids (Michigan, USA), as shown in Figure 3.15b. These heavy–duty rear axles have excellent fatigue properties.

Sapa in Finspång (Sweden) is a manufacturer is using FSW for the high-volume production of aluminum automotive components. For that purpose, ESAB SuperStir[TM] machine with two welding heads for welding hollow aluminum extrusions from both sides simultaneously were installed. It has been used to produce foldable rear seats of the Volvo V70 station wagon. Figure 3.16a shows this machine which has a carousel-type loading and unloading station and is automatically loaded by an articulated arm robot.

Figure 3.16 a) Sapa's Esab-SuperStir[TM] machine with two welding heads for welding hollow aluminum extrusions simultaneously from both sides, b) Prototype FSW engine cradle of the Sapa (Nicholas & Kallee, 2002).

Recently, Sapas' another application to produce a friction stir welded prototype for engine cradles. By this way, the cradle weight of the substructure has reduced from 23kg to 16 kg as show in Figure 3.16b (Thomas, Kallee, Staines & Oakley, 2006).

Arbegast (2006) mentioned the industrial application of the rivet technology has started to replace with the friction stir spot welding (FSSW) when it has been developed. Currently, two variations of FSSW were being used. Mazda patented the "plunge" friction spot welding (PFSW) method in 2003 and GKSS-GmbH patented the "refill" friction spot welding (RFSW) method in 2002.

Mazda in Hiroshima (Japan) uses plunge friction stir spot welding (PFSW) for the rear doors and bonnet of the Mazda RX-8 as shown in Figure 3.17a. The metal sheets

were locally plasticized and stirred together by a rotating fixed pin tool similar to that used in linear FSW is plunged and retracted through the upper and lower sheets of the lap jointnd stir the sheets together. Although this application leaves a pull-out hole in the center of the spot, the strength and fatigue life is sufficient to allow application at reduced production costs on the Mazda RX-8 aluminum rear door structure when compared to resistance spot welding as shown in Figure 3.17b. Mazda PFSW doors which have more than 100,000 vehicles provide structural stability against side impact for aiming passenger protection and impart five-star rollover protection since 2003.
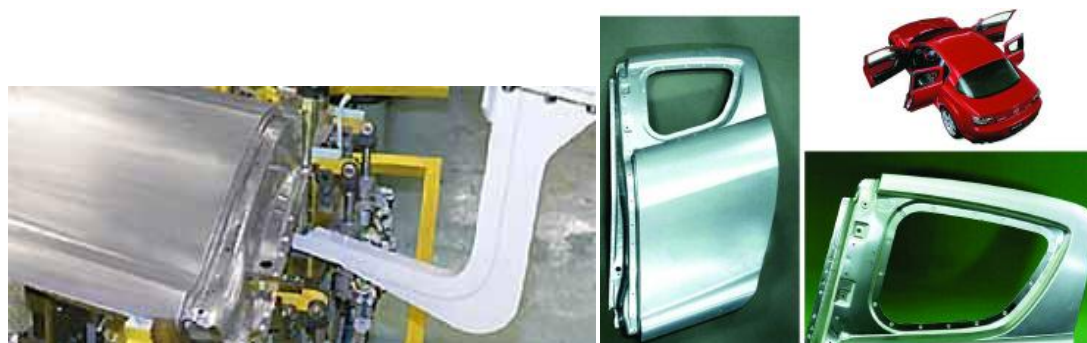
Figure 3.17 a) Friction stir spot welding of rear doors for the Mazda RX-8 (Thomas, et al., 2006), b) Use of the plunge friction spot welding (PFSW) method on the Mazda RX-8 rear door structure provides for structural stability against side impact and five-star rollover protection at reduced production costs (Arbegast, 2006).
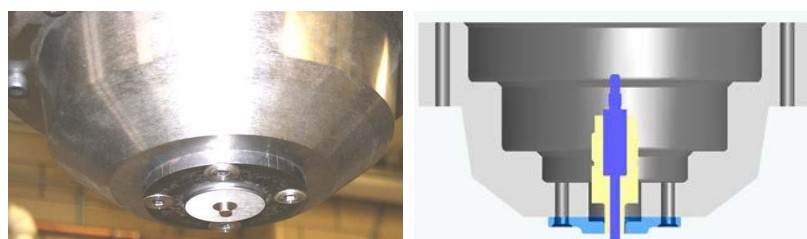
Figure 3.18 AMP FSSW tool and illustration of the tool (Arbegast, 2007).

The GKSS refill friction stir welding (RFSW) is being developed at South Dakota School of Mines & Technology (SDSMT) Advanced Material Processing (AMP) Center under license to RIFTEC-GmbH. RFSW process used a rotating pin tool with a separate pin and shoulder actuation system that allows the plasticized material

initially displaced by the pin to be captured under the shoulder during the first half of the cycle and then reinjected into the joint during the second half of the cycle as shown in Figure 3.18. This type of tool completely refills the joint flush to the surface as shown in Figure 3.19. RFSW is also being used as a tacking method to hold and restrain parts during welding by linear FSW.
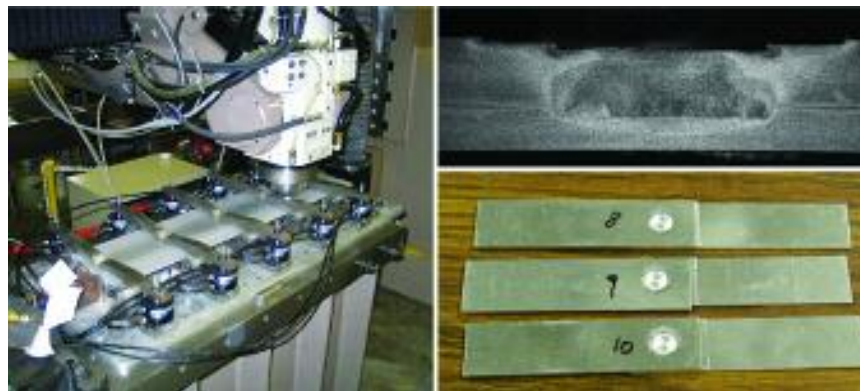
Figure 3.19 Refill friction spot welding (RFSW) using MTS ISTIR 10 system and custom designed head adapter (left). RFSW lap shear coupons (right, bottom), and metallurgical cross section of RFSW showing complete joint penetration in 0.080-in.-thick 7075-T73 aluminum (right, top) (Arbegast, 2006).

Regarding the process variant, basically the tool can penetrate in the plates in two ways, called the pin plunge and the shoulder plunge variants of the process. Schematically, the two process variants sequence of relative movement between tool´s parts during welding is shown in Figure 3.20 (Arbegast, 2007).

Showa Denko in Oyama City (Japan) manufactured suspension arms by joining extruded end-pieces to 20-30 mm diameter tubes. The rubber of the end-pieces of the suspension arms can be vulcanized before welding because of the low heat input of the new assembly method as shown in Figure 3.21a.

Simmons Wheels in Alexandria (Australia) developed a new method of producing a car wheel rim from rolled aluminum 6061-O sheet with a longitudinal friction stir welding. After cutting it into several rim sections they spin form it into the desired

rim profile and in the end this part needed to be heat treatment to the required T6 temper. Moreover, the company was now supporting UT Alloy Works in Guandong (China) during FSW production increase of light alloy wheels as shown in Figure 3.21b (Thomas et al., 2006 and Nicholas & Kallee, 2002).
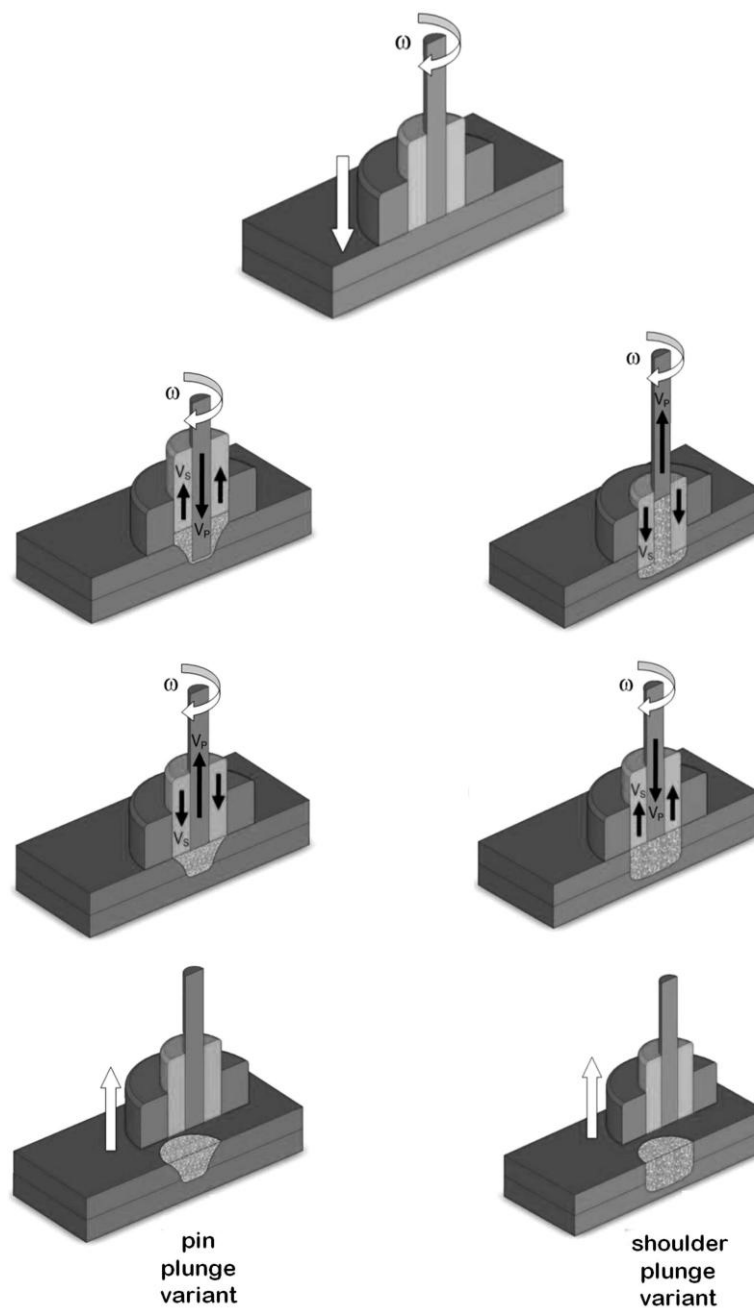
Figure 3.20 Schematic illustration of the FSpW process variants (Mazzaferro, 2009).

Figure 3.21a) FSW suspension struts, b) Aftermarket three-piece wheel made from friction stir welded and spin formed aluminum cylinders (Thomas et al., 2006).

In Norway, a new innovative technique of joining two parts of a car wheel, as shown in Figure 3.22a, has been invented and developed for butt or lap cast or forged centre parts were friction stir welded to rims that were made from wrought alloys successfully demonstrated by Hydro Aluminium in Håvik. DanStir in Copenhagen, Denmark industrialized this concept by reducing the wheel weight by 20-25% (Thomas et al., 2006).

Figure 3.22 a) FSW of a casting to a spin formed wheel rim b) CNC controlled FSSW gun on an articulated arm robot (Thomas et al., 2006)

Friction Stir Link in Waukesha, Wisconsin, USA is a service supplier focusing on the automotive industry for FSW process development, technology transferring, moderate-volume production and friction stir welding system integration services. CNC controlled FSSW gun an articulated arm robot is an example of their application as shown in Figure 3.22b.

In 2004, a collaborative research program by Pacific Northwest National Laboratory (PNNL) and South Dakota School of Mines & Technology (SDSMT) Advanced Material Processing (AMP) Center successfully investigated to improve increasing the wear resistance of heavy vehicle brake rotors by processing TiB2 particles into the surface of Class 40 gray cast iron.
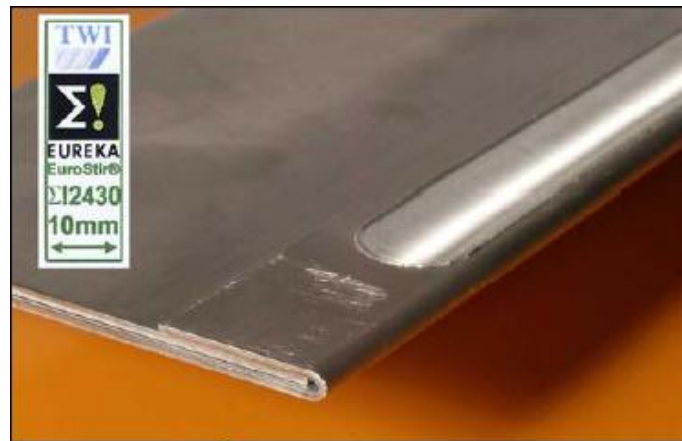
Figure 3.23 EuroStir[TM] study on hem joints as they can be used for joining inner panels to skins of car doors (Nicholas & Kallee, 2002).

In 1998, first ideas of the friction stir welded hem joints and sandwich panels were published. Lately, Eurostir® projected on hem joints as they can be used for joining inner panels to skins of car doors as shown in Figure 3.23.

3.3.3 Applications of FSW in Railway Industry

- High speed trains
- Rolling stock of railways, underground carriages, trams
- Railway tankers and goods wagons
- Container bodies

The FSW process has productivity, cost and joint performance benefits which were first exploited by the Japanese railway industry and Europe is fast reaching up.

Figure 3.24 Commuter train built by Hitachi with full length friction stir welds of double-skin side, and roof panels (welded from one side) (Blignault, Kallee, Thomas & Russell, 2008).

Railcar manufacturers in Japan have designed multi-head machines for longitudinal aluminum extrusions for modern passenger rail cars, in lengths up to 25m (Johnson & Threadgill, 2003). The whole body shell can be manufactured from single wall or hollow double skin extrusions.

Figure 3.25 a) Express train built by Hitachi containing full length friction stir welds of double-skin side and roof panels (Nicholas & Kallee, 2002) b) Hitachi uses FSW for assembling the new Channel Tunnel Rail Link trains (Blignault et al., 2008).

Hitachi was amongst the first train manufacturers to realize the technical and economic benefits of FSW. The single wall or double-skinned designs which are constructed from aluminum extrusions joined along their length by FSW for the vehicles are used. Hitachi remark positively on the low distortion which is one twelfth and excellent mechanical properties of friction stir welding compared to arc welding. Hitachi has delivered a range of friction stir welded vehicles for both

commuter and express trains use. The Commuter Emu Series 20000 for Seibu Railway as illustrated in Figure 3.24, the Express EMU Series 885 for JR-Kyushu as illustrated in Figure 3.25a Channel Tunnel Rail Link (CTRL) in Britain as illustrated in Figure 3.25b. Hitachi uses a number of different FSW joint designs, some of these are illustrated in Figure 3.26a and 3.26b.
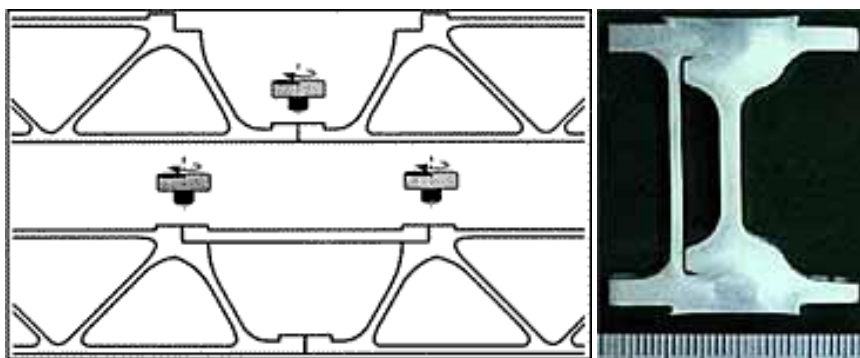
Figure 3.26 a) Hitachi extrusion designs used in manufacture of Series 885 Tilting EMU for JR-Kyushu. Overall panel thickness 40mm b) Section of typical FSW made on aluminum extrusion (Blignault et al., 2008).

Figure 3.27 a) The FSSW robot from Kawasaki, b) Kawasaki uses FSSW for making aluminum roof panels for the Fastech 360Z (Blignault et al., 2008).

Kawasaki Heavy Industries (KHI) is using friction stir spot welding (FSSW) to attach stringers to roof panels by using FSSW robot for the new Fastech 360Z train as shown in Figure 3.27a and Figure 3.27b. A new aluminum car body design has developed by assembling by this method. KHI reported main benefits for the FSW

approach, improving the flatness and visual appearance of the skin panels with the low heat input.
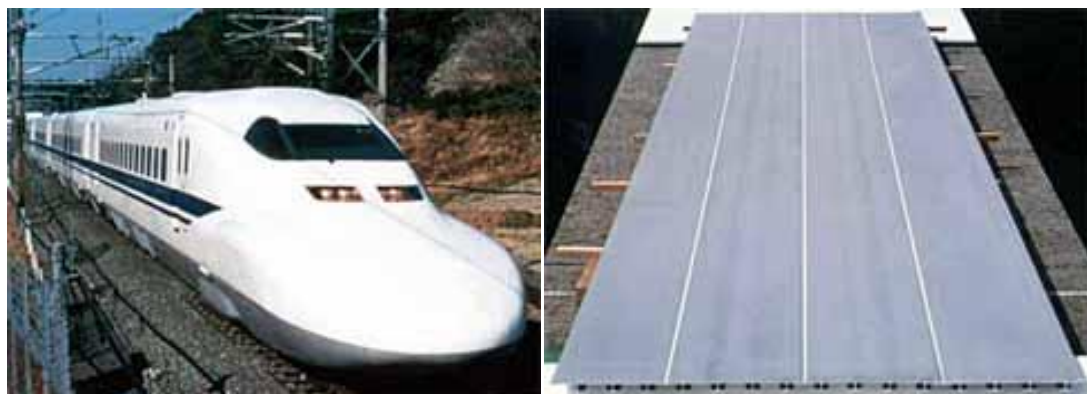
Figure 3.28 a) Trainsets with FSW floor panels of Sumitomo Light Metal operate on the Shinkanen in Japan, b) Friction stir welded floor panel produced by Sumitomo Light Metal for Shinkansen trains (Davenport & Kallee, 2002).

Nippon Sharyo has been using friction stir welded panels produced by Sumitomo Light Metal Industries for the floor panels of the new 700 series Shinkansen operating Taaido Line and Sanyo Line as shown in Figure 3.28a and Figure 3.28b. Some of these trains operate on the Nozomi at speeds up to 285km/hour. Nippon Light Metals have also exploited friction stir welding for subway rolling stock. The weld quality was verified as excellent based on microstructural, X-ray and tensile test results.

Since 1997, Alstom LHB in Salzgitter (Germany) have purchased prefabricated single wall aluminum roof panels from the Scandinavian aluminum extruders Sapa and Hydro Marine Aluminium for Copenhagen suburban trains as shown in Figure 3.29a and Figure 3.29b. Since early 2001 they have used FSW aluminum side walls and since 2002 FSW floor panels for Munich suburban trains. These panels are supplied by Sapa.

In March 1999, TWI presented the benefits of using FSW to Alstom LHB engineers which considered friction stir welding of hollow aluminum profiles for

making floor and side panels, but estimated to achieve a return on approximately €
3.5M investment in an acceptable time span that a three-shift operation would be
necessary. The most significant technical and economic benefits could be
approximated to achieve by applying FSW to aluminum joints of more than 12mm
thickness. The Alstom METROPOLIS underground coaches for the metros in
Singapore, Shanghai and Warsaw have reported to use of Sapa FSW extrusions
(Davenport & Kallee, 2002).

Figure 3.29 a) Alstom LHB trains for DSB Danish State Railways during production. FSW roof
panels for these trains are made at Hydro Marine Aluminium under a contract with Sapa, b) Friction
stir welded roof panel produced at Hydro Marine Aluminium for Sapa for delivery to Alstom LHB
(Davenport & Kallee, 2002).

The use of friction stir welding for the fabrication of aluminum rolling stock
continues to grow around the world and the use of a double-skinned extrusion design
for the construction of rail vehicles is prevalent.

Davenport and Kallee (2002) also concluded the use of FSW for aluminum rail
vehicles in Europe as industry becomes more familiar with the technology and
current developments extend the range of applications. The presence of a strong
specialist European supply chain to the European rail vehicle manufacturers for
friction stir welded sub-assemblies will be an essential part of this growth.

3.3.4 Applications of FSW in Aircraft Industry

- Wings, fuselages, empennages
- Aviation fuel tanks
- External throw away tanks for military aircraft
- Military and scientific rockets
- Repair of faulty MIG welds

The aerospace industry has been pioneers in the application of FSW technology in the world. However, FSW processing is presently used in non-critical aircraft structure.

The FSW process presents incredible potential for low-cost joining of lightweight aluminum airframe structures for large civil aircraft such as the Airbus A380. Researchers at Airbus Deutschland noticed a high capability for joining aluminum alloys by FSW for skin-to-skin fuselage connections. Their studies demonstrated the mechanical and technological properties of these welds approach the properties of the parent material. As a result of this, the cost and weight can be reduced with improving joint quality and the possibility of new design (Nicholas & Kallee, 2002 and Kallee, Nicholas & Thomas, 2001).

The Phantom Works of The Boeing Company are pursuing FSW of thin butt, lap and T-joints and thick butt joints for a variety of aircraft missile and space applications. Joint configurations on curvilinear paths which make welding of complex aircraft parts are more desired for welding. A force actuator patented by Boeing has developed to use curvilinear FSW of a complex aircraft landing gear door. A fighter aircraft fairing manufactured by Boeing has assembled to weld thin T-joints by sandwich type FSW, which has been flight tested. At the end of the 2001, Boeing commercial aircraft scheduled to start no-structural parts production by friction stir welded (Nicholas & Kallee, 2002 and Kallee, Nicholas & Thomas, 2001).

Boeing got approval for a governmental development program under the name of "Joining of Complex Aluminum Assemblies" about a FSW cargo "slipper" pallet and implemented a FSW cargo ramp toenail on the C17 transport due to significant cost and weight savings. The toenail is the only known friction stir welded part flying on a military aircraft. Boeing is also planning to use FSW technique for the 747 freighter barrier beam as next step (Arbegast, 2006 and Polt, 2004).
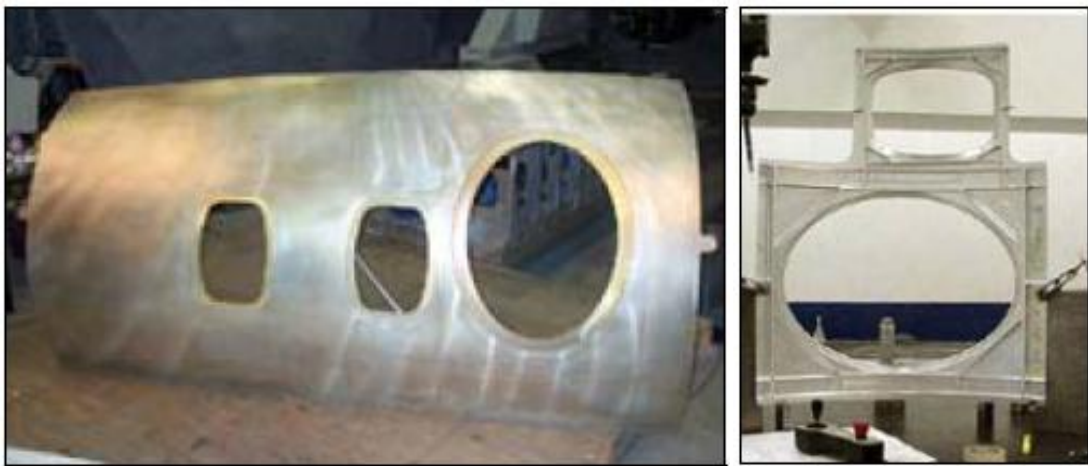
Figure 3.30 a) Eclipse right skin assembly with an oval emergency hatch. FSW results in a smooth and easy to paint surface, b) Single-piece surround frame for the emergency hatch (Nicholas & Kallee, 2002).

Eclipse Aviation Corporation of Albuquerque, New Mexico, has decided to use FSW to replace traditional riveting and bonding processes. By this way, maybe the first time, the application time and cost dramatically lowered for welding process in high-volume aviation applications. At the end of 2001, Eclipse started building structures for scheduling first flights in 2002 as shown in Figure 3.30a and Figure 3.30b (Kallee et al., 2001 and Nicholas & Kallee, 2002).

Eclipse Aviation Corporation are pioneering a new-economy model of air travel which couples the fractional jet business with the new 'dispersed operation' air travel concept using the more than 5,000 small utilization airports in the United States to provide individual air service (Kallee et al., 2001 and Nicholas & Kallee, 2002). In

2002, Eclipse 500 business class jet which was developed the use of friction stir welding (FSW) in aircraft structures received FAA (US Federal Aviation Administration) approval. Friction stir welded lap joints are used as a rivet replacement technology to join the longitudinal and circumferential internal stiffeners to the aft fuselage section and to attach doublers at window and door cutout locations as shown in Figure 3.31. MTS Systems Corp. designed and fabricated the custom FSW equipment and production tooling for Eclipse Aviation to weld complex curvatures over many sections of the fuselage, cabin, and wing structures by using friction stir welding which is about 20 inches per minute is approximately 10 times faster than manual riveting and provides a continuous join for improved structural rigidity as shown in Fig 3.32. The process is faster than more conventional mechanical joining processes, production cycle time is significantly reduced. (Eclipse Aviation, Arbegast, 2006 and Kallee et al., 2001).

Figure 3.31 The Eclipse 500 business class jet is currently in final FAA certification trials (left). The internal longitudinal and circumferential aluminum stiffeners (right, top) and window and door doublers (right, bottom) are attached to the aluminum fuselage section with friction stir welded lap joints (Arbegast, 2006).

Recently, Eclipse Aviation announced that nearly 100 Eclipse 500 buyers have traded in their orders for the new Eclipse 400 single engine personal jet. The main change was to a composite empennage, but most other major feature remain the same, and additionally it will most likely be friction stir welded (Joining News - archive Aerospace industry news, TWI)

Figure 3.32 The friction stir welding equipment used to attach the stiffeners and doublers to the Eclipse 500 fuselage sections was designed and fabricated by MTS Systems Corp. It is capable of welding a variety of component geometries through the use of interchangeable holding fixtures located beneath the multiaxis FSW head and movable gantry frame (Arbegast, 2006).

In 2000, Lockheed Martin completed a governmental development program under the name of "Joining of Traditional Aluminum Assemblies" that replaced the riveted aluminum floor structure of the C130J air transport with a FSW floor structure. High-temperature pin tools for the FSW of steel, titanium, and Inconel® alloys for aircraft engine applications developed by the Edison Welding Institute and the General Electric Corp. (Engines Div.) under the name of another program "Hard Metals Joining Development" (Arbegast, 2006).

Airbus has also announced the use of FSW in selected locations on the Airbus A350 and two new versions of the A340 (A340-500, A340-600) (Arbegast, 2006). Initially, joining the longitudinal fuselage skin joints of production A340-500s and A340-600s aircraft were planning to use friction stir welding (FSW). The use of FSW in place of overlapping and riveting was expected to save 0.9 kg a meter and also removed the need for overlapping panels. The next application of FSW could be

in the production of the A350-800 and A350-900 for the joining of longitudinal fuselage panels. The use of the friction stir welding technique will make possible four fuselage panels being required rather than 8 for an aircraft the size of the A350 (Joining News - archive Aerospace industry news, TWI).

3.3.5 Applications of FSW in Aerospace Industry

- Cryogenic fuel tanks for space vehicles
- Crew Launch Vehicle upper stage
- Repair of faulty MIG welds

Friction stir welding of aluminum alloys has encouraged a lot of interest within aerospace industry. In fall 1995, the first welds were made at NASA. In 1998, friction stir welding studies targeting the external tank (ET) manufacturing program began. The first demonstration of a 27.5-ft-diameter simulated hydrogen tank barrel section which is comprised of eight barrel panels measuring 15 ft tall was completed jointly between NASA and the prime contractor, Lockheed-Martin Engineers.

Fig 3.33 Marshall's Space Center vertical weld tool and detail view of the tool (Nicholas et al., 2006).

Marshall's vertical weld tool (VWT) was used for the welding as shown in Figure 3.33. The weld joints built in 15 ft of constant thickness with thickness tapers from

0.32 to 0.65 in with the first time using retractable pin tool for taper welds. Because, it is important the automatic adjustment is critical when welding material tapering between two thicknesses. NASA's modified circumferential weld tool (CWT) established circumferential welding and clamping techniques for FSW as shown in Figure 3.34a. Approximately one-half mile of weldments used on each ET reduced to approximately 700 ft by using FSW with variable polarity plasma arc (VPPA) welding still used for the remainder of the weldments for joining eight longitudinal weld joints on the 2195 Al-Li liquid hydrogen barrel and four longitudinal welds on the liquid oxygen barrel for Space Shuttle as shown in Figure 3.35. Lockheed Martin Missiles and Fire Control and the South Dakota School of Mines & Technology (SDSMT) have upgraded square box beams for mobile rocket launch systems that are manufactured from thick-wall "C" section extrusions joined by FSW to replace the current hollow, square tube extrusions (Nicholas & Kallee and Ding, Carter, Lawless, Nunes, Russell & Suits, 2006).

Figure 3.34 a) Circumferential welding tool for FSW with recently welded transition rings and dome, b) Horizontal weld tool for FSW.

NASA is focusing on the improvement of this self-reacting tool for circumferential welds in the external tank and Crew Launch Vehicle upper stage hardware. As shown in Figure 3.34b the horizontal weld tool was used with the self-reacting friction stir welding pin tool to weld 27.5-ft-diameter ring test sections located between barrel sections in the Shuttle ET.

Figure 3.35 FSW process development tool at the Marshall Space Flight Center shown with a 27-ft-diameter LH2 barrel segment of the 2195 Al-Li Space Shuttle external tank (left). Fullscale LH2 tank (right) at the NASA Michoud Assembly Facility in New Orleans. (Arbegast, 2006).

Ding, Carter, Lawless, Nunes, Russell & Suits, (2006) reported the acceptable value for structural design criteria for NASA as fracture and structural analysis of the weld mechanical test data results require a 99% confidence level that 90% of the weld strength values. This statistical evaluation process creates margins of safety required to safely support and protect human life in space. The ET has a greater margin of safety using the FSW process because of increased weld strength and the standard deviation of test data is smaller than VPPA weld test data.

NASA selected a Boeing-led team a $515m contract to produce the upper stage of the Ares I crew launch vehicle. Boeing's team included Hamilton Sundstrand, Moog, Northrop Grumman, United Space Alliance and United Launch Alliance, plus a number of small businesses. NASA and Boeing led team's Marshall Center used FSW is the baseline welding process to manufacture major components for the Ares I rocket of the Crew Launch Vehicle upper stage hardware as shown in Figure 3.36. The rocket will launch the Orion crew capsule, six astronauts and small pressurized cargo payloads to the International Space Station no later than 2015. Officially, the first weld on the Ares I took place on 11 August 2008 (Joining News - archive Aerospace industry news).
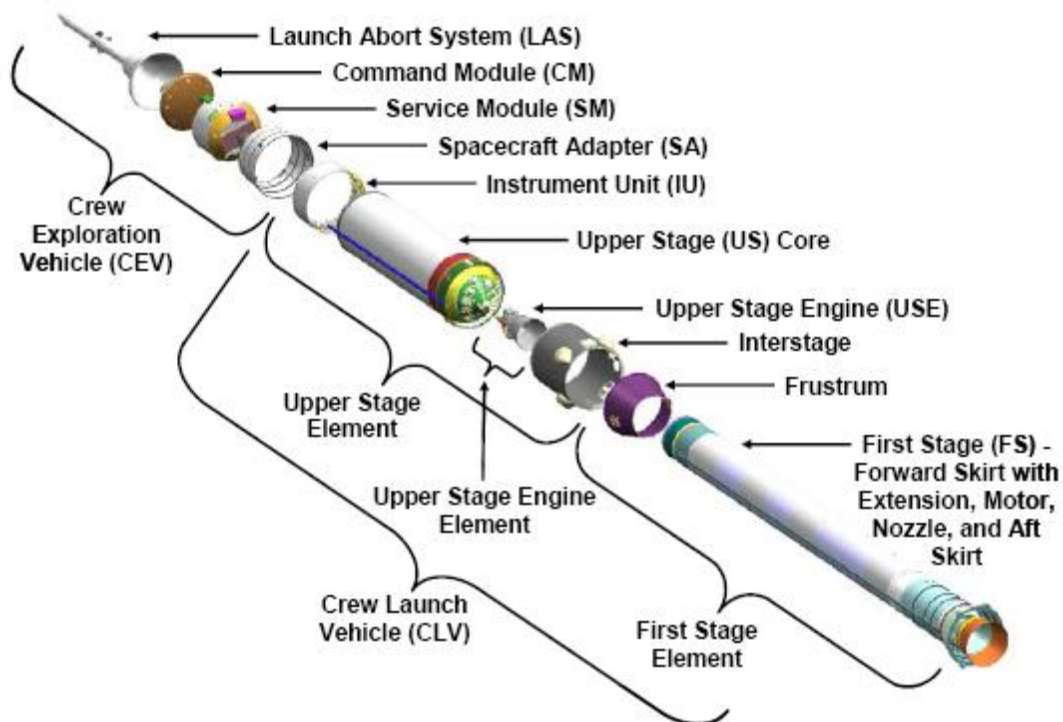
Figure 3.36 Ares I parts.

Assembling the upper stage will required about 18,000 inches of welds. By using the friction stir welding at the upper stage, the materials will join together without melting the components and provides a more reliable, high-strength weld (Space Exploration, Boeing).

The design concepts are ensured compatible with the baselined FSW process by welding representation on the Integrated Product Team. Then, the Crew Exploration Vehicle (CEV) and Cargo Lift Vehicle (CaLV) will be designed for finalization. A new largest robotic friction stir welding system has designed for being capable of welding full-scale man-rated space vehicle hardware comprised of complex geometries such as domes and ogive sections as shown in Figure 3.37a and Figure 3.37b. Solid-state FSW makes indispensable for elimination of the safety and porosity concerns (Ding et al., 2006).

Figure 3.37 a) NCAM's Friction Stir Welding System produces a uniform weld as it joins the panels of an elliptical dome structure (LMSSC-MO) (National center for advance manufacturing, NASA, 2007), b) Robotic Weld Tool which has Capable of circumferential and complex curvature welds in structures up to 36 feet in diameter (Ding, 2008).

Figure 3.38 High-speed friction stir weld system (Ding et al., 2006).

High-speed FSW (HS-FSW) is under investigation by NASA for in-space welding and weld repair as a potential basis for handheld manual welding. The idea behind HS-FSW is based on the principle that high spindle speeds (tens or hundreds of thousands of revolutions per minute) in FSW reduce the forces essential to produce sound welds to a level permitting manual hand-held devices. As shown in Figure

3.38 the machine is capable of 30,000 rpm, with a travel speed up to 200 in/min and used to investigate welding 0.060-in. GRCop-84, a copper alloy for thrust chambers (Ding et al., 2006).

Figure 3.39 a) Boeing's FSW Machines in Decatur for the tanks of Delta IV rockets. b) Boeing's liquid-oxygen and liquid-hydrogen tanks for the 42m (125ft) long Common Booster Cores (Nicholas & Kallee, 2002).

An increasing number of fuel tanks for spacecraft are now being manufactured from difficult-to-weld aluminum alloys. In August 1999, Boeing has applied FSW to the Interstage Modules of a Delta II rockets successfully launched. In April 2001, the Mars Odyssey spacecraft which has utilized the first pressurized structures lifted off on a Delta II rocket, which demonstrated the strength and quality of longitudinal friction stir welded joints on all three cylindrical tank components .The weld strength of the Delta IV common booster core tanks increased from 30 to 50% and cycle time lowered to nearly 80% by using friction stir welding technology (Kallee et al., 2001 and Nicholas & Kallee, 2002).

Boeing used ESAB production machine to produce FSW 2014 aluminum propellant tanks successfully as shown in Figure 3.39a and Figure 3.39b. 2100m of defect free friction stir welds have been produced for Delta II rockets, and 1200m for the larger Delta IV rocket. Moreover, 60% cost saved, and reduced the manufacturing time from 23 to 6 days by changing specifically design of Delta IV and Delta II for FSW.
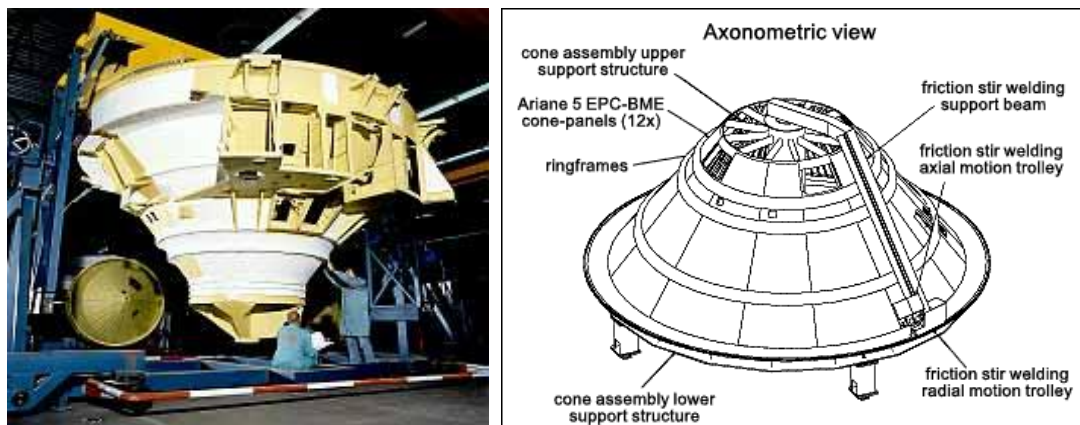
Figure 3.40 a) Assembly of Ariane 5 main motor thrust frame from 12 integrally machined, blade stiffened, flat, b) Fokker's concept for the new cone sub-assembly jig, which is multifunctional, i.e. for both Hi-lok riveting and FSW panels (Nicholas & Kallee, 2002).

Fokker Space that was a Dutch aircraft manufacturer developed Ariane 5 motor thrust frames by using FSW as shown in Figure 3.40a. Booker, van Deudekom, Kallee & Sketchley (2000) the FSW can be easily applied to lap joint in aluminum alloy 7075-T7351 of the Ariane 5 as shown in Figure 3.40b. Even though the tensile strengths measured in this study are lower than those that can be obtained with friction stir welded butt joints, the results are at an acceptable level to replace bolted lap joints. The lap joints in the unpressurised structures presented the significant advantages of generous tolerances at interfaces between components and ease of assembly (Nicholas & Kallee, 2002 and Kallee et al., 2001).

3.3.6 Applications of FSW in Pipeline Industry

- Pipe fabrication
- Aluminum pipelines

Until recently, FSW technique has been typically used in linear butt and lap joints as a one sided welding process. Thomas & Dolby (2002) studied tubular applications of FSW. The some examples of positional friction stir welding applications provide

all-positional welding capability as shown in Figure 3.41 a-e, which have difficulty with fusion welding.
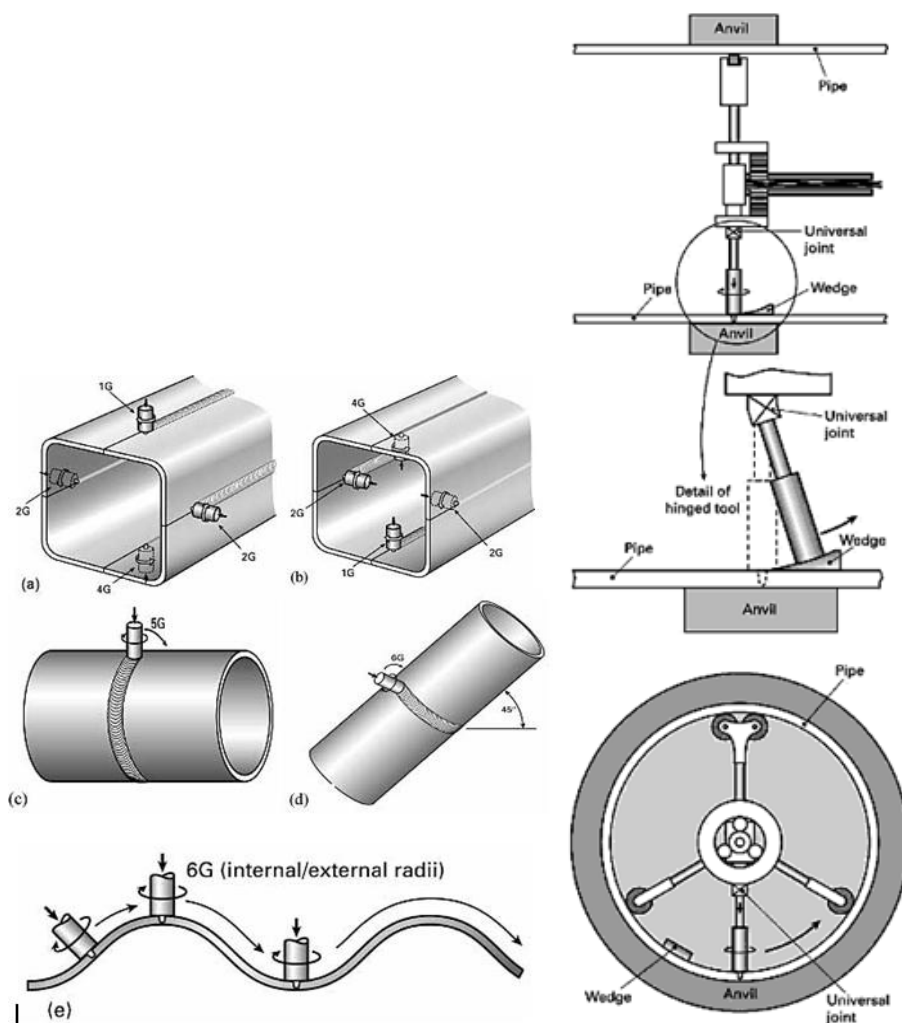
Figure 3.41 a) External Welding of hollow component, b) Internal Welding of hollow component, c) Welding stationary horizontal pipe, d) Welding stationary 45° angled pipe, e) Welding a corrugated component, f) FSW design concept facility for butt welding of line pipe. Comprising a hinged flexible drive head together with a longitudinal positioned 'run off' wedge plate, designed to eliminate any end of run hole filing requirements. Side view and end view (Thomas & Dolby, 2002).

Tubular components the design of the shoulder depends upon whether the tool is operated to the outside or inside of the tube, when welding comparatively small radii as shown in Figure 3.41a and Figure 3.41b. Besides, the tool can be traversed around

the tube or the tool is stationary and the tube is rotated, when welding tubular components as shown Figure 3.41c and Figure 3.41d. Single or multi-headed frictions stir welding machine can be used to internally butt weld line pipe and carry out remote down hole-repairs as illustrated in Figure 3.41f.
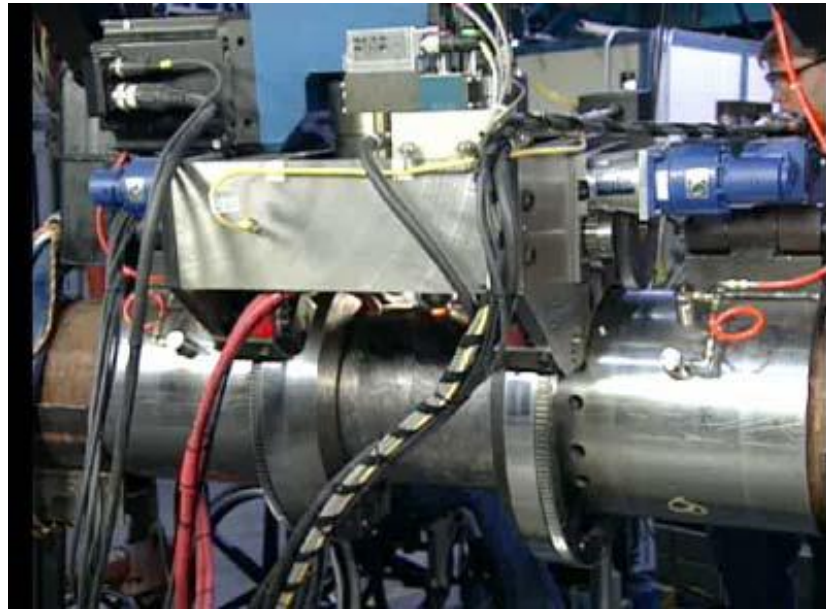
Figure 3.42 Prototype pipe welding system showing external FSW head (Feng, Steel, Packer & David, 2005).

Although the actual number would depend on the flexibility of the tubular component being welded, a minimum of three centralizing roller supports is necessary and also additional roller supports would act as an extension device to force the tube against the external anvil. The required pressure of the tool on the inside tubular workpiece should be kept constant through the welding operation. Furthermore, the technique could also be applied to the manufacture of helical welded pipe and to the repair of defects encountered in pipelines (Thomas & Dolby, 2002).

After giving the brief information about the FSW for pipes, the technology applicable for on-site applications can be easily comprehensible such as pipeline welding, a portable, rotating machine needed to be developed. Besides, the

advantages stated previous chapter, FSW on pipe can be completed in a single out-of-position pass that is not affected by gravity (Defalco & Steel, 2009)

Figure 3.43 Hydraulic internal support/fixture (Feng, Steel, Packer & David, 2005).

In 2004, MegaStir, Inc., completed a prototype oil and gas field pipeline FSW demonstration program which is named under Industrial Technologies Program and sponsored in part by the U.S. Department of Energy, Office of Energy Efficiency and Renewable Energy. This standalone portable pipe welding machine was designed to use as a field-ready and single-pass machine that was capable of friction stir welding stationary pipe typical of that found in the assembly of a pipeline. It successfully joined 12in (305 mm) ID pipe with a wall thickness which was 0.25in (6.35mm) in the beginning of the design were increased up to 0.5in (13 mm) of X-65 steel pipe segments using an automated external mandrel FSW tooling system as shown in Figure 3.42. Moreover, the machine is designed to weld butt joints in pipe segments using a spindle head that traverses the joint with the FSW tool on the outside as an expandable mandrel supports the rear side of the weld on the inside of the pipe (Feng, Steel, Packer & David, 2005 and Defalco & Steel, 2009 and Arbegast, 2006).

The portable orbital welding machine has a radial axis to drive the spindle and FSW head assemblies circumferentially around the pipe. A clamping fixture clamps and holds the two segments of pipe together for butt joint welding as shown in Figure 3.43. An internal, expandable anvil was designed to provide the internal pipe support

to prevent wall collapse because of the high pressures exerted by the FSW process. Figure 3.44a shows example of the fiction stir welding pipes (Defalco & Steel, 2009).

Figure 3.44 a) FSW finished pipes, b) Run-off tab solution for exit hole of the FSW pipes (Feng et al., 2005).

Defalco and Steel (2009) mentioned an inherent problem with FSW is the presence of an extract hole after the weld is completed. On linear joints such as in plate, a run-off tab is often used to remove after the weld is completed, if retractable pin tool is not used. The similar solution was used for removing the exit hole for pipe welding. A run-off tab was fixture over a joined portion of the pipe near the starting point of the weld after the weld had begun for a full circumferential weld. The joint consists of the weld overlapping at the beginning and then moving off-axis on a run-off tab to complete the weld as shown in Figure 3.44b. Then, run-off tab is removed from the finished weld joint.

The NASA Marshall Space Flight Center has developed an apparatus for joining two cylindrical (i.e., pipe-shaped) sections together by friction stir welding. The Orbital Friction Stir Weld System is made up of a structural base frame, a cylindrical clamping mechanism for securing two sections of cylindrical work piece to be welded, a weld head, a reaction support, a means for transmitting load from the weld head to the reaction support, and a means for rotating the weld head in conjunction

with the reaction support around the longitudinal axes of the clamping mechanisms as shown in Figure 1.94 at section 1.5.7.

Figure 3.45 a) Pipe sample made at TWI for Framatome, b) Welding head of Framatome's orbital FSW machine for pipelines, c) Framatome's orbital friction stir welding machine (Nicholas & Kallee).

Framatome ANP Inc. and Siemens PTD (Power Transmission & Distribution) conducted a project on orbital friction stir welding of 5083 aluminum alloy pipelines for the site assembly of gas insulated power transmission lines (GIL). These pipes are used for transferring high electrical currents underground. The first feasibility and other development parameters of circumferential welds were investigated by TWI for Framatome as shown in Figure 3.45a. Moreover, orbital FSW system which is a transportable, hydraulic actuated developed by Framatome as shown in Figure 3.45b and Figure 3.45c (Nicholas & Kallee).

The orbital FSW equipment is comprised of a hydraulic unit, control panel, FSW head with steel wire rope and a guide ring which is clamped onto the pipe. The orbital track is fixed onto the guide ring. Before fixing the pipe a backing ring is installed in the pipe. Once the initial contact of the shoulder, the traversing rate is started and traverse rate and tool rotation speed is kept constant during the welding process. The proper downward pressure on the tool should be also constant during the orbital weld length. FSW Orbital technique offers certain benefits pertaining to time and quality.

3.3.7 Applications of FSW in Electrical Industry

- Electric motor housings

- Busbars

- Electrical connectors

- Encapsulation of electronics

Another commercial application of the FSW is for electrical industry. Hydro Marine Aluminium in Magnor, Norway is producing the aluminum electrical motor housings by using ESAB SuperStir^{TM} machine which is weld thickness up to 8mm, longitudinal welds in diameters from 320 up to 420 mm and also possible to weld longitudinal welds on a table up to 3 m as shown in Fig 3.46. Nicholas and Kallee (2002) mentioned two German companies that are licensed for attaching brackets to electrical motors or to encapsulate electronics by using FSW.

Figure 3.46 ESAB SuperStirTM machine for welding housings for electrical motors at Hydro Aluminium in Magnor (Norway) (Nicholas & Kallee, 2002).

PDC Teknik in Helsinge, Denmark manufacture loudspeaker housings for Bang & Olufsen.by joining two hemispherical aluminum casting using FSW as shown in Figure 3.47a and Figure 3.47b (Nicholas & Kallee, 2002)

Figure 3.47 a) Run-on and run-off-tabs on PDC Teknik's loudspeakers, b) PDC Teknik uses FSW for joining cast aluminum loudspeaker housing for Bang and Olufsen (Nicholas & Kallee, 2002).
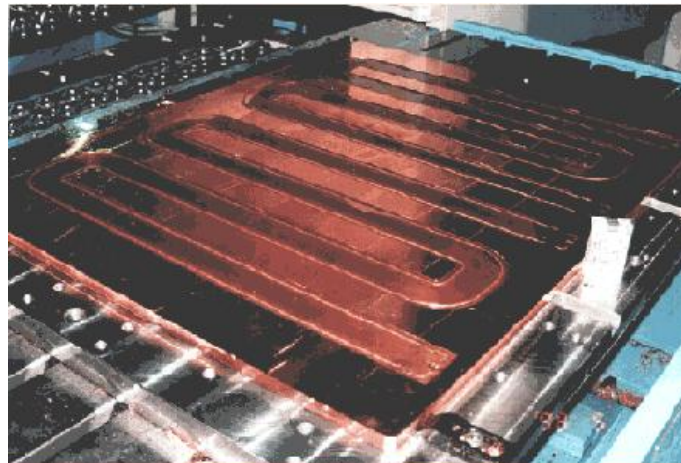
Figure 3.48 Copper backing plate for sputtering. (Haver, n.d.).

Hitachi Cable, Ltd is using FSW OFHC copper backing plate as shown in Figure 3.48 for sputtering (LCDs, semiconductors) with thicknesses 10mm though 70 mm (Haver, n.d.).
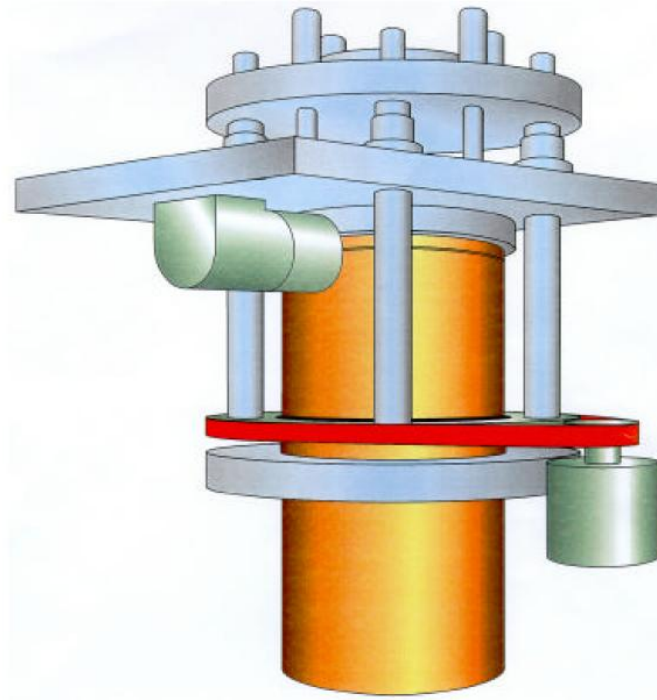
Figure 3.48 Illustration of experimental canister base welding machine (Andersson & Andrews, 1999).

3.3.8 Applications of FSW in Nuclear Industry

In 1997, Canister Laboratory in Oskarshamn, Sweden owner the Swedish Nuclear Fuel and Waste Management Co. (SKB) commissioned TWI to develop FSW for thick section copper, and specifically to aim at applying the process to welding bases onto canisters. A prototype machine was built in 1999 as schematically illustrated in Figure 3.49, Andersson & Andrews (1999), compared the fabrication of copper canister by electron beam and friction stir processes. They explained the preferred mode of operation involves rotating the canister, which is mounted in the vertical position, past the rotating FSW tool. A hydraulically actuated radial clamping system grips the canister body which is rotated using a small electric motor; on the contrary they do not damage the surface. The base in contact with the canister by using another hydraulic actuator keeps during welding. It is necessary to apply sufficient

amount of force for preventing the canister and the base from being pushed apart as the FSW tool passes along the weld interface (Andersson et al., 2000).

Figure 3.49 a) One of the trial manufactured full size canisters together with some exhibits (Andersson & Andrews, 1999), b) Canister for spent nuclear fuel. ~5m length (Andersson et al., 2000).

Andersson & Andersson (1999) investigated the fabrication of containment canisters for nuclear waste by friction stir welding. Before the FSW, full-size copper canisters have been manufactured using three different methods, roll forming of tube halves that are welded together by electron beam welding and seamless tubes produced by extrusion or pierce and draw processing as shown in Figure 3.50a. SKB designed canisters which is consisting of an outer corrosion barrier of 50mm thick copper and a nodular cast iron insert to provide the necessary mechanical strength and matching with other requirements. It has been shown that a canister of this type, 1050mm diameter and 4830mm long, will remain intact for 100,000 years, by which time the radioactivity will have decayed to an acceptable level as shown in Figure 3.50b. However, the canister design needed that the copper base and lid be sealed to the cylindrical body using a method that manufactures extremely high joint integrity. The friction stir welding of 50mm thick copper material has obtained a solution for nuclear encapsulation of radioactive waste.

Furthermore, when nuclear plants around the world grow older, incidences of stress corrosion cracking (SCC) problems are increased. In pressurized water reactors (PWRs) such cracking is well known and often associated with reactor pressure vessel parts e.g. primary water SCC at reactor nozzle locations. On the other hand, SCC also occurs in the secondary circuit and supplementary parts of the plant which are also most important for safety. This repair method is used to fix at relatively thin-walled Type 304 stainless steel water storage tanks which have experienced SCC cracks at the outer surface.

Friction stir processing is a technique fundamentally provides a high integrity smooth repair of thin surface breaking defects. FSW is attractive for the utility customers, when compared with conventional weld repair methods FSW has advantages for on-line application of nuclear plant with its controllability and lower risk of through-wall penetration (TWI).

3.3.9 Applications of Friction Stir Welding in Construction Industry

- Aluminum bridges
- Facade panels made from aluminum, copper or titanium
- Window frames
- Aluminum reactors for power plants and the chemical industry
- Heat exchangers and air conditioners

Generally, the portable FSW equipment is used in construction industry applications.

3.3.10 Other Industries

- Refrigeration panels
- Cooking equipment and kitchens
- White goods

- Gas tanks and gas cylinders
- Connecting of aluminum or copper coils in rolling mills
- Furniture
- Many other applications

CHAPTER FOUR
EXPERIMENTAL STUDY OF MICROSTRUCTURAL CHARACTERIZATION AND MECHANICAL PROPERTY DETERMINATION OF OVERLAP FRICTION STIR WELDING OF ALUMINUM AND COPPER

4.1 Introduction

One of the reasons for attempting to weld aluminum and copper, is that there is limited study on joining aluminum and copper, most of the research and industrial applications are about joining aluminum alloys by Friction Stir Welding (FSW).

A few reports have been made on the weldability of copper to copper and aluminum to copper. Murr et al (1998) investigated welding of 6061-T6 aluminum alloy and copper by using FSW, but could not obtain porosity-free welds as aluminum alloys. Moreover, they have mentioned that to achieve reasonable welds, the 6061-T6 aluminum should be on the left side for a clockwise rotation of the head pin tool and higher rotation speeds and slower traverse speeds were also required in contrast to the monolithic aluminum alloy work pieces. Lee and Jung (2003) reported to obtain defect-free welds by using FSW for joining commercially pure copper. Park et al (2003) also claimed successful joining as the defect-free welds for 60% Cu - 40% Zn alloy (60/40 brass). Nakata (2005) researched friction stir weldability of oxygen-free copper and 60/40 brass, and he emphasized the importance of the suitable tool for copper alloy applications. Ouyang et al (2005) revealed that the direct FSW of 6061 aluminum alloy to copper has proved difficult due to the brittle nature of the intermetallic compounds formed in the weld nugget. Meran and Kovan (2008) investigated the microstructures and mechanical properties of FS welded dissimilar copper and CuZn30 brass joints and affects of axial force. Abdollah-Zadeh et al (2007) obtained successful results for aluminum alloy 1060 and pure copper by using FSW lap joints. They also reported that higher rotational speeds increase the amount of intermetallic compound formed at the aluminum/copper interface.

The purpose of this study is to join1050 aluminum alloy and commercially pure copper by using overlap friction stir welding for three different tools with constant rotational and welding speed. The aim is to determine the optimum welding tool parameter. Microstructural examination, hardness measurements and room temperature tensile tests have been carried out in order to determine the optimum tool. Unfortunately, some changes had to be made in experimental schedule due to physical conditions of the friction stir welding machine capacity used. Before making this decision, some preliminary experiments have been conducted.

The study was carried out as three different welding speeds with a constant rotational speed and a triangular tool to be used to join aluminum alloy 1050 and pure copper by friction stir welding for overlap joint. From time to time some problems were faced again due to machine capacity. When axial force had to be increased for suitable contact force, the machine stared to shake. Without damaging the machine, some friction stir spot welding joints were tried. Finally, when joints wre compared visually, the friction stir spot welding joints looked better than friction stir welding and the study was altered in order to investigate microstructural characterization and mechanical property determination of overlap friction stir spot welding joints instead of friction stir welding.

4.2 Material Properties

The materials used in this study are 1050 aluminum alloy rolled plate and commercially pure copper with thicknesses of 4 and 3 mm, respectively. The chemical compositions of both materials are listed in Table 4.1.

Aluminum alloy 1050 is a common grade of aluminum for regular sheet metal work where moderate strength is required. Aluminum alloy 1050 is known for its outstanding corrosion resistance, high ductility and highly reflective finish. Copper is malleable, ductile and has good heat and electrical conductivity. The physical and mechanical properties of both materials are listed in Table 4.2.

Table 4.1 Chemical composition of aluminum alloy 1050 and commercially pure copper.

	Cu	Mn	Mg	Fe	Si	Ti	Zn	Pb	Ni	Al
Commercially pure copper	Balance	-	-	0.05	0.009	-	0.69	0.03	0.03	0.02
Al (1050)	0.05	0.05	0.05	0.4	0.25	0.05	0.07	-	-	Balance

Table 4.2 Physical and mechanical properties of aluminum alloy 1050 and commercially pure copper.

Properties	Al 1050	Pure Copper
Density ($\times 1000$ kg/m^3)	2.6-2.8	8.8-8.94
Melting Point (°C)	650	1085
Modulus of Elasticity (GPa)	71	110-128
Poisson's Ratio	0.33	0.34
Elastic Modulus (GPa)	70-80	117
Tensile Strength (Mpa)	110	221-455
Yield Strength (Mpa)	105	69-365
Elongation (%)	42	55
Shear Strength (MPa)	69	48

Aluminum alloy 1050 is typically used for chemical process plant equipment, food industry containers, pyrotechnic powder, architectural flashings, lamp reflectors and cable sheathing. Copper is normally too soft for its applications, as a result it is incorporated in numerous alloys such as brass and bronze. Copper alloys have wide variety of applications.

4.3 Experimental Procedures

The materials used in the experiments are commercially pure copper and aluminum alloy 1050. The dimensions of the plates were 200x150x3mm for aluminum alloy and 200x150x2mm pure copper. The surfaces of both plates were cleaned by acetone before welding procedure. All welds were made in lap configuration. A rotating tool was made of SPK quenched and tempered tool steel and had a shoulder of 20mm diameter with a triangular pin of 1mm pitch and 6.5mm long. The tilted angle of the rotating tool with respect to Z-axis of welding machine

was 3˚. Rotating tool was plunged from the aluminum alloy 1050 surface into the surface of copper and lap joints were produced by welding speeds of 80, 106 and 130 mm/min and constant rotational speed of 1600 rpm. Other parameters were kept constant. The welding tool was rotated in the counter clockwise direction and plates were tightly fixed at the backing plate. Temperature measurements were obtained by using thermocouples at various parts of the aluminum and copper plates, from the welding center to outer sides, during welding as shown in Figure 4.1.
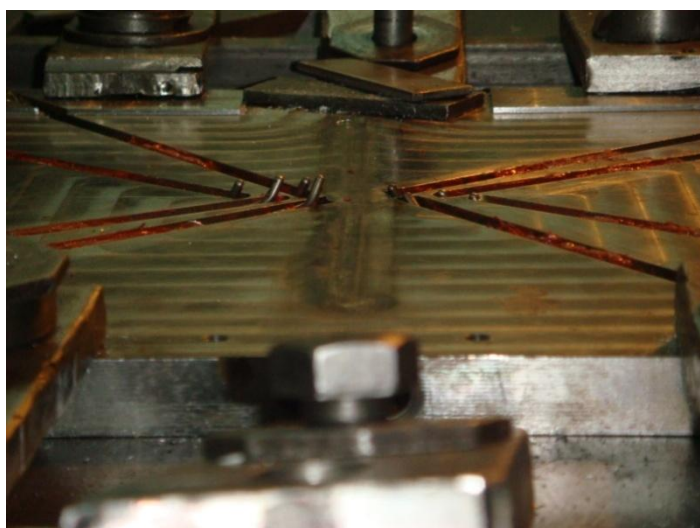
Figure 4.1 Location of thermocouples.

Fig ure 4.2 Placing aluminum plate over the copper.

In the first try, the aluminum plate was placed over the copper plate as shown in Figure 4.2. First attempt was not enough to obtain a successful joint as shown in

Figure 4.3, and next attempt was started good but finally, no successful friction stir welding were obtained as shown in Figures 4.4.
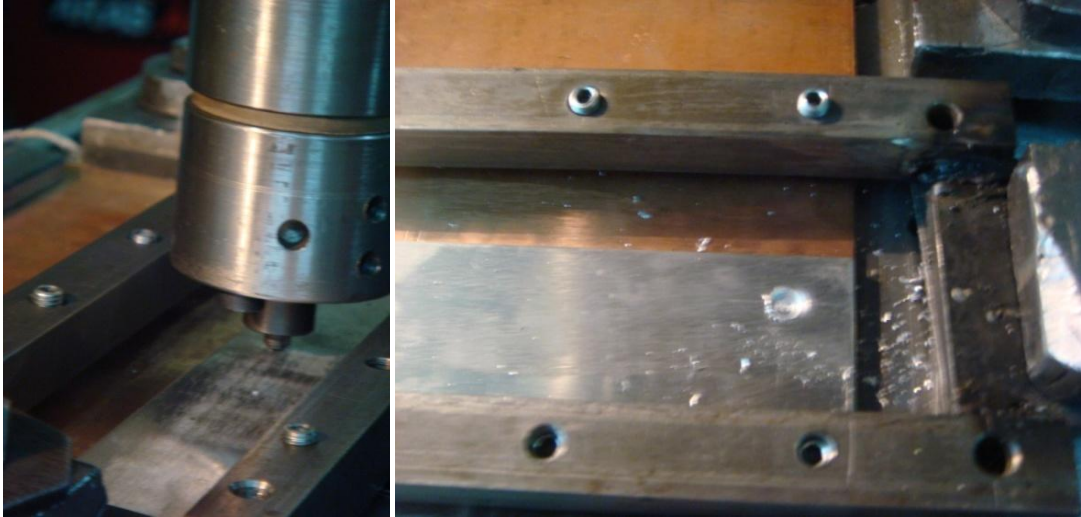
Figure 4.3 Unsuccessful process at first try.

Figure 4.4 Unwelded joint structure.

In the second try, the copper and aluminum plates were swapped, the aluminum plate was put down and the copper plate was overlapped on the aluminum plate as shown Figure 4.5. The experiment started, and after a while reaching the friction stir welding temperature, the tool was tried to move welding direction as shown in Figure 4.6. Unfortunately, the welding machine started to shake and some sparkling came out due to the welding machine capacity and its obsolete were not allow to obtain for additional contact force, thus machine was stopped for safety. On the other hand, an acceptable joint was eventually obtained by using friction stir welding as friction stir spot welding as shown in Figure 4.7.

Figure 4.5 Copper plate is overlapped on aluminum plate.

After at that point, the experiments were continued as the purpose of the joining by friction stir spot welding, for not damaging welding machine. Friction stir spot welding was produced for three speed levels which are 80, 106 and 130 mm/min by keeping other parameters constant. Samples of the produced joints are as shown in Figure 4.8.

The cross sectioned samples were prepared using standard metallographic procedure, for microstructural analysis. Microstructural examinations were carried out by using optical microscope.

Figure 4.6 Machine started to shake.
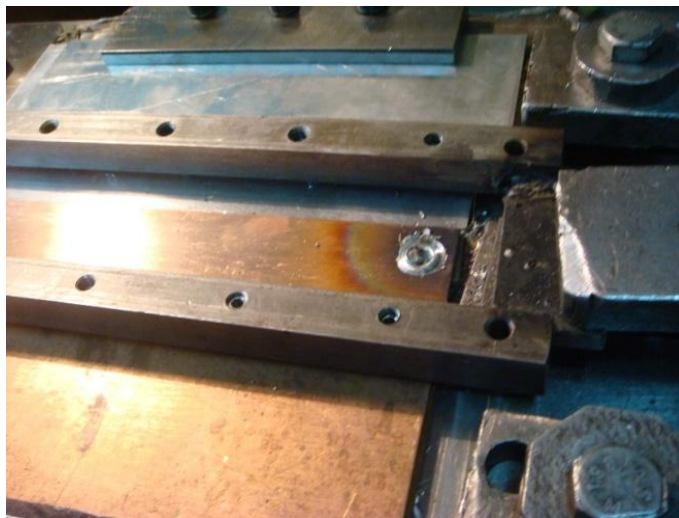
Figure 4.7 Eventually obtained friction stir spot welding.

Figure 4.8 Examples of friction stir spot welding joints.

The tensile shear test was used to estimate the tensile shear load of the joint. The welded area was positioned in the center of the tensile specimen.

4.4 Experimental Results

The tensile shear test results are given in Table 4.3 and shear stress-strain diagrams of specimens in Appendices indicating the failure load and failure location of the joints. The failure loads are ranged from 1746 to 3325 N. There are some conditions in which failure has occurred in the base metal, sufficiently far from the jointed area, and therefore, it is possible to achieve the optimum shear tensile

strength of joint (3325 N) by adjusting the welding speed. On the other hand, most of the specimens failed on the advancing side. From microstructural point of view, formation of intermetallic compounds is likely to occur in advancing side because of higher amount of temperature and strain at this side (Abdollah –Zadeh et al., 2007). Ouyang et al., (2005) suggested that the intermetallic compounds of Al4Cu9, AlCu and Al2Cu are responsible for preferential development of the crack on the tensile shear test.

Table 4.3 The tensile shear test results.

Specimen #	Shear Force	Average	
9-2	3178 N	2043 N	
9-4	3325 N		
10-3	3502 N	2746.5 N	
10-4	1991 N		
11-1	3315 N	3168 N	2813 N
11-3	3129 N		
11-4	3061 N		
11-5	1746 N		

Increasing the welding speed of the tool for a constant rotational speed of 1500 rpm resulted in increasing of the failure load up to a maximum and then a decrease in failure load has appeared.

CHAPTER FIVE
SUMMARY AND DISCUSSION

1. Friction stir spot welding overlap joint has been successfully obtained between aluminum alloy 1050 and pure copper by using FSW.

2. For future studies; the pin geometry could be changed, different rotational speeds could be applied, modern welding machines could be used, copper alloys could be used instead of pure copper, different aluminum alloys could be used instead of aluminum1050.

3. Alloys with similar melting points could be a better choice for optimum joint when choosing dissimilar alloys.

4. Preheating could be a solution for high melting point materials.

5. Friction stir welding needs to be used more in industrial applications, especially automotive, marine, aircraft, pipelines industries and military implementations.

REFERENCES

Abdollah-Zadeh, A., Saeid, T., & Sazgari, B. (2008). Microstructural and mechanical properties of friction stir welded aluminum/copper lap joints. *Journal of Alloys and Compounds, 460*, 535-538. Retrieved June 25, 2009, from Elsevier database.

Aluminum Association [AA]. *Selection and applications*. Retrieved December 2, 2009, from http://www.aluminum.org/Content/NavigationMenu/TheIndustry/ TechnologyResources/TechnologyArticles/applications.pdf.

American Welding Society [AWS]. Welding-Related Expenditures and Productivity Measurement in U.S. Manufacturing, Construction, and Mining Industries, *Welding Journal*, May 2002. Retrieved December 2, 2009, from http://files.aws.org/research/HIM.pdf.

Anderson, C.-G., & Andrews, R. E. (1999). *Fabrication of containment canisters for nuclear waste by friction stir welding*. Retrieved December 29, 2009, from http://www.twi.co.uk/content/spcgajun1999.pdf.

Anderson, C.-G., & Andrews, R. E., Dance, B. G. I., Russell, M. J., Olden, E. J., & Sanderson, R. M (2000). *A comparison of copper canister fabrication by the Electron beam and friction stir processes*. Retrieved December 29, 2009, from http://www.twi.co.uk/content/spcgjun2000.pdf.

Arbegast, W. J. (2003). Modeling Friction Stir Joining as a Metalworking Process. *Hot Deformation of Aluminum Alloys III, TMS*, 313-327.

Arbegast, W. J. (2006). Friction Stir Welding After a Decade of Development. *Welding Journal, 85*, 28-35. Retrieved July 19, 2009, from Welding Journal database.

Arbegast, W. J. (August 27-30, 2007). *Friction Stir Welding and Processing – Current State of the Art and Needs for the Future*. Retrieved July 29, 2009, from http://ampcenter.sdsmt.edu/2000/presentation_files/Arbegast%20Keynote%20Brazil%20ABS%20200728092008.pdf.

Aydın, H., Bayram, A., Uğuz,, A., & Akay, K. S. (2008). Tensile properties of friction stir welded joints of 2024 aluminum alloys in different heat-treated-state. *Materials and Design, 30*, 2211-2221. Retrieved June 25, 2009, from Science Direct database.

Babu, S., Elangovan, K., Balasubramanian, V., & Balasubramanian, M. (2008). Optimizing Friction Stir Welding Parameters to Maximize Tensile Strength of AA2219 Aluminum Alloy Joints. *The Korean Institute of Metals and Materials, Vol 15, No. 2*, 321-330. Retrieved June 25, 2009, from SpringerLink database.

Balasubramanian, N., Mishra, R.S., & Krishnamurthy, K. (2008). Friction stir channeling: Characterization of the channels. *Journal of Materials Processing Technology, 209*, 3696-3704. Retrieved June 25, 2009, from Science Direct database.

Balasubramanian, V. (2007). Relationship between base metal properties and friction stir welding process parameters. *Materials Science & Engineering A, 480*, 397-403. Retrieved June 25, 2009, from Elsevier database.

Benavides, S., Li, Y., Murr, L.E., Brown, D., & McClure, J.C. (1999). Low-temperature friction-stir welding of 2024 aluminum. *Scripta Materialia, 41*, 809-815. Retrieved December 24, 2009, from Elsevier database.

Biallas, G., Braun, R., Donne, C.D., Staniek, G., & Kaysser, W.A. (1999). Mechanical properties and corrosion behavior of friction stir welded 2024-T3. The First International Conference on Friction Stir Welds.

Blignault, C., Kallee, S. W., Thomas, W. M., & Russell, M. J. (May 28-29, 2008). *Friction stir weld integrity and its importance to the rolling stock industry*. Retrieved December 29, 2009, from www.twi.co.uk/content/spcbmay08.html.

Boeing . Space exploration Ares I upper stage backgrounder. Retrieved December 29, 2009, from www.boeing.com/defense-space/space/constellation/docs/ Ares_I_ USP.pdf.

Boz, M. & Kurt, A. (2003). The influence of stirrer geometry on bonding and mechanical properties in friction stir welding process. *Material & Design, 25*, 343-347. Retrieved June 25, 2009, from Science Direct database.

Brooker, M. J.,van Deudekom, A. J. M., Kallee, S. W., & Sketchley, P. D. (June 26-28, 2000). *Applying Friction Stir Welding to the Ariane 5 Main Motor Thrust Frame.* Second International Symposium on Friction Stir Welding. Retrieved December 29, 2009, from http://articles.adsabs.harvard.edu//full/2001ESASP. 468..507B/0000507.000.html.

Buffa, G., Campanile, G., Fratini, L., & Prisco, A. (2009). Friction stir welding of lap joints: Influence of process parameters on the metallurgical and mechanical properties. *Materials Science and Engineering A, 519*, 19-26. Retrieved June 25, 2009, from Elsevier database.

Campbell, F. Jr. (2006). *Manufacturing Technology for Aerospace Structural Materials* (Chapter 2 Aluminum). Retrieved June 25, 2009, from Elsevier database.

Chao, Y. J. & Qi, X., (June 14-16, 1999). *Heat Transfer and Thermo-Mechanical Analysis of Friction Stir Joining of AA6061-T6 Plates*. The First International Symposium on Friction Stir Welding.

Chao, Y. J., Qi, X., & Tang, W. (2002). Heat Transfer in Friction Stir Welding—Experimental and Numerical Studies. *Journal of Manufacturing Science and Engineering, 125*, 138-145. Retrieved December 19, 2009, from http://www.me.sc.edu/fs/pdf/ASME%20JMSE%20Chao-Qi-Tang.pdf.

Chen, C.M., & Kovacevic, R. (2003). Finite element modeling of friction stir welding—thermal and thermomechanical analysis. *Machine Tools & Manufacture, 43*, 1319-1326. Retrieved December 19, 2009, from Science Direct database.

Chen, Y.C., Feng, J.C., & Liu, H.J. (2008). Precipitate evolution in friction stir welding of 2219-T6 aluminum alloys. *Materials Characterization, 60*, 476-481. Retrieved June 25, 2009, from Science Direct database.

Chen, Y.C., & Nakata, K. (2007). Friction stir lap joining aluminum and magnesium alloys. *Scripta Materialia, 58*, 433-436. Retrieved June 25, 2009, from Science Direct database.

Chen, Y.C., & Nakata, K. (2008). Microstructural characterization and mechanical properties in friction stir welding of aluminum and titanium dissimilar alloys. *Materials & Design, 30*, 469-474. Retrieved February 27, 2009, from Science Direct database.

Chen, Z.W., Pasang, T., & Qi, Y. (2007). Shear flow and formation of Nugget zone during friction stir welding of aluminium alloy 5083-O. *Materials Science & Engineering A, 474*, 312-316. Retrieved December 22, 2009, from Science Direct database.

Colegrove, P., Painter, M., Graham, D., & Miller, T. (2000). *3 dimensional flow and thermal modeling of the friction stir welding process*. The Second International Symposium on Friction Stir Welding.

Colegrove, P. A., & Shercliff, H. R. (2003). Two-dimensional CFD modelling of flow round profiled FSW tooling. *Science and Technology of Welding and Joining, 9*, 483-492. Retrieved December 17, 2009, from http://web.ebscohost.com/ehost/pdf?vid=2&hid=12&sid=e521cf8e-ae78-482f-bc56-5c986808afb1%40sessionmgr14.

Colegrove, P. A., & Shercliff, H. R. (2005). 3-Dimensional CFD modelling of flow round a threaded friction stir welding tool profile. *Journal of Materials Processing Technology, 169*, 320-327. Retrieved June 25, 2009, from Elsevier database.

Colligan, K. (1999). Material Flow Behavior during Friction Stir Welding of Aluminum. *Welding Journal, 78*, 229-237. Retrieved February 27, 2009, from http://12.176.97.197/wj/supplement/july99/COLLIGAN.pdf .

Copper, Wikipedia (n.d.). Retrieved December 2, 2009, from http://en.wikipedia.org/wiki/List_of_copper_alloys.

Defalco, J. (2006). Friction Stir Welding vs. Fusion Welding. *Welding Journal, 85*, 42-44. Retrieved December 2, 2009, from Welding Journal database.

Defalco, J. & Steel, R. (2009). *Friction Stir Process Now Welds Steel Pipe.* Welding Journal, May 2009, 44-48. Retrieved December 29, 2009, from http://research.vuse.vanderbilt.edu/vuwal/Research/PipeDocs/wj0509-44.pdf.

Davenport, J., & Kallee, S. W. (2002). *Friction stir welding - a competitive new joining option for aluminium rolling stock manufacturers*. Retrieved December 29, 2009, from http://www.twi.co.uk/content/spjdoct2002.html.

Ding, J. (October 8, 2008). *NASA'S MSFC Welding Development for Ares I*. NASA. Retrieved December 29, 2009, from http://ntrs.nasa.gov/archive/nasa/casi.ntrs.

nasa.gov/20090015019_2009013964.pdf.

Ding, J., Carter, R., Lawless, K., Nunes, A.,Russell, C. & Suits, M (2006). *Friction Stir Welding Flies High at NASA*. Welding Journal, 55-59. Retrieved December 29, 2009, from http://files.aws.org/wj/2006/03/wj200603/wj200603-54.pdf.

Donne, C. D., Lima, E., Wegener, J., Pyzalla, A., & Buslaps, T. (September 27-28, 2001). Investigations on Residual Stresses in Friction Stir Welds. *Third International Symposium on Friction Stir Welding*.

Eclipse Aviation. Friction stir welding. Retrieved December 29, 2009 from http://www.eclipseaerospace.net/company/about/innovations.php.

Efunda. Temper designations (n.d.). Retrieved December 2, 2009, from http://www.efunda.com/materials/alloys/aluminum/temper.cfm.

Elangovan, K., & Balasubramanian, V. (2006). Influences of pin profile and rotational speed of the tool on the formation of friction stir processing zone in AA2219 aluminium alloy. *Materials Science & Engineering A, 459*, 7-18. Retrieved August 2, 2009, from Elsevier database.

Engineersedge. Aluminum tempers (n.d.). Retrieved December 2, 2009, from http://www.engineersedge.com/aluminum_tempers.htm.

Etter, A.L., Baudin, T., Fredj, N., & Penelle, R. (2006). Recrystallization mechanisms in 5251 H14 and 5251 O aluminum friction stir welds. *Materials Science & Engineering A, 445-446*, 94-99. Retrieved December 26, 2009, from Science Direct database.

Feldman, K., Kohn, G., & Stern, A. (2006). On laser assisted - Friction stir welding. Retrieved July 10, 2009, from www.engineers.org.il/_Uploads/1636feldmanandkohnandstern0206.pdf.

Feng, Z, Santella, M. L., David, A., Steel, R.J., Packer, S. M., Pan, T., Kuo, M., & Bhatnagar, R. S. (2005). *Friction stir spot welding of advanced high-strength steels- A feasibility Study*. SAE International. Retrieved July 6, 2009, from http://www.ornl.gov/~webworks/cppr/y2001/pres/122418.pdf.

Feng, Z., Steel, R., Packer, S., & David, S. A. (April 2005). *Friction Stir Welding of API Grade X65 Steel Pipes*. Retrieved December 29, 2009, from http://www.et.byu.edu/groups/fsw/presentations/X65%20Steel%20Pipes.pdf.

Field, D. P., Nelson, T. W., Hovanski, Y., & Jata K. V. (2001). Heterogeneity of Crystallographic Texture in Friction Stir Welds of Aluminum. *Metallurgical and Materials Transactions A, 32A*, 2869-2877. Retrieved December 27, 2009 from Springer Link database.

Fonda, R.W., & Bingert, J.F. (2007). Texture variations in an aluminum friction stir weld. *Scripta Materialia, 57*, 1052-1055. Retrieved June 25, 2009, from Science Direct database.

Friction Stir Link, Inc., *Friction stir welding (FSW) description*, (n.d.). Retrieved June 23, 2009, from http://www.frictionstirlink.com/fslfswdescription.html.

Friction stir welding technology (n.d.). NASA. Retrieved June 25, 2009, from http://techtran.msfc.nasa.gov/new/FSW.html.

Friction stir welding technology: adopting NASA's retractable pin tool (n.d.). Retrieved June 23, 2009, from http://rebar.ecn.purdue.edu/ECT/links/technologies/mechanical/fsw.aspx.

Frigaard, Ø., Grong, Ø., & Midling, O.T. (2001). A Process Model for Friction Stir Welding of Age Hardening Aluminum Alloys. *Metallurgical and Materials Transactions A, 32*, 1189-1200. Retrieved December 29, 2009 from Springer Link database.

Fujii, H., Cui, L., Maeda, M., & Nogi, K. (2005). Effect of tool shape on mechanical properties and microstructure of friction stir welded aluminum alloys. *Materials Science & Engineering A, 419*, 25-31. Retrieved June 25, 2009, from Elsevier database.

Google Images (n.d.).Retrieved June24, 2009, from http://www.fluent.com/solutions/ metals/img/frweild1_lg.gif.

Guerra, M., Schmidt, C., McClure, J.C., Murr, L.E., & Nunes, A.C. (2002). Flow patterns during friction stir welding. *Materials Characterization, 49*, 95-101. Retrieved February 27, 2009, from Elsevier database.

Hamilton, C., Dymek, S., & Sommers, A. (2008). A thermal model of friction stir welding in aluminum alloys. *International Journal of Machine Tools & Manufacture, 48*, 1120-1130. Retrieved December 29, 2009, from Science Direct database.

Hamilton, C., Sommers, A., & Dymek, S. (2008). A thermal model of friction stir welding applied to Sc-modified Al–Zn–Mg–Cu alloy extrusions. *International Journal of Machine Tools & Manufacture, 49*, 230-238. Retrieved February 27, 2009, from Science Direct database.

Hartawan, A., Thoe, T. B., Ng, S. T., Wu, H. & Liu K. (2009). Initial investigation into friction stir welding. *SIMTech Technical Reports, 10*, 5-9. Retrieved December 22, 2009, from http://www.simtech.a-star.edu.sg/Research/Technical Reports/STR_V10_N1_CD_Version/STR_V10_N1_02_MTG.pdf.

Hatamleh, O. (n.d.). *Laser peening of friction stir welds*, Johnson Space Center. Retrieved June 25, 2009, from http://research.jsc.nasa.gov/BiennialResearch Report/PDF/Eng-19.pdf.

Haver, W. V. (Belgium Welding Institute [BWI]) (n.d.). *Friction stir welding*. Retrieved December 29, 2009, from http://www.bil-ibs.be/nl/onderzoek/pdf/FSW. pdf.

Hwang, Y.-M., Kang, Z.-W., Chiou, Y.-C., & Hsu, H.-H. (2007). Experimental study on temperature distributions within the workpiece during friction stir welding of aluminum alloys. *International Journal of Machine Tools & Manufacture, 48*, 778-787. Retrieved June 25, 2009, from Science Direct database.

James, M., Mahoney, M., & Waldron, D. (June 14-16, 1999). Residual stress measurements in friction stir welded aluminium alloys. *The First International Symposium on Friction Stir Welding.*

Jata, K. V., Sankaran, K. K., & Ruschau, J. J. (2000). Friction-Stir Welding Effects on Microstructure and Fatigue of Aluminum Alloy 7050-T7451. *Metallurgical and Materials transactions A, 31A*, 2181-2192. Retrieved December 27, 2009, from Springer Link database.

Kallee, S. W., Nicholas, E. D., & Thomas, W. M. (2001). Industrialisation of friction stir welding for aerospace structures. Retrieved December 29, 2009, from http://www.twi.co.uk/content/spswkdec2001.html.

Khaled, Terry. (July 2005). *An outsider looks at friction stir welding*. Retrieved July 3, 2009, from http://www.faa.gov/aircraft/air_cert/design_approvals/csta/ publications/media/friction_stir_welding.pdf.

Khandkar, M. Z. H., Khan, J. A. & Reynolds, A. P. (2002). Prediction of temperature distribution and thermal history during friction stir welding: input torque based model. *Science and Technology of Welding and Joining, 8 (No.3)*, 165-174. Retrieved December 12, 2009, from http://web.ebscohost.com/ehost/pdf?vid= 2&hid=4&sid=2d471c54-a1ef-4f42-bf61-5d4a41c56403%40sessionmgr10.

Kohn, G., Greenberg, Y., Makover, I., & Munitz, A. (2002). Laser-assisted Friction Stir Welding. *Welding Journal, February (2002)*, 46-48. Retrieved July 10, 2009, from http://www.aws.org/wj/2002/02/feature2/.

Krishnan, K.N. (2001). On the formation of onion rings in friction stir welds. *Materials Science and Engineering A, 327*, 246-251. Retrieved June 25, 2009, from Elsevier database.

Kumar, K., & Kailas, S. V. (2007). On the role of axial load and the effect of interface position on the tensile strength of a friction stir welded aluminium alloy. *Materials & Design, 29*, 791-797. Retrieved February 27, 2009, from Science Direct database.

Kwon, Y. J., Saito, N., & Shigematsu, I. (2002). Friction stir process as a new manufacturing technique of ultrafine grained aluminum alloy. *Journal of Materials Science Letters, 21*, 1473-1476. Retrieved December 24, 2009, from Springer Link database.

Johnson, R., & Threadgill, P. L. (2003). *Progress in friction stir welding of aluminium and steel for marine applications*. Retrieved December 29, 2009, from http://www.twi.co.uk/content/sprjoct2003.html.

Joining News - archive Aerospace industry news. TWI. Retrieved December 29, 2009, from http://www.twi.co.uk/content/nfaero_archive.html.

233

Lee, W. B., & Jung, S. B. (2003). The joint properties of copper by friction stir welding. *Materials Letters, 58*, 1041-1046. Retrieved June 25, 2009, from Science Direct database.

Li, Y., Murr, L.E., & McClure, J.C. (1999). Solid-State Flow Visualization in the Friction-Stir Welding of 2024 Al to 6061 Al. *Scripta Materialia, 40*, 1041-1046. Retrieved December 7, 2009, from Science Direct database.

Li, Y., Trillo, E. A., & Murr, L. E. (2000). Friction-stir welding of aluminum alloy 2024 to silver. *Journal of Materials Science Letters, 19*, 1047-1051. Retrieved December 25, 2009, from Springer Link database.

Liu, P., Shi, O., Wang, W., Wang, X., & Zhang, Z. (2008). Microstructure and XRD analysis of FSW joints for copper T2/aluminium 5A06 dissimilar materials. *Materials Letters, 62*, 4106-4108. Retrieved June 25, 2009, from Science Direct database.

London, B., Mahoney, M., Bingel, W., Calabrese, M., Bossi, R. H., & Waldron, D. (2003). Material Flow in Friction Stir Welding Monitored with Al-SiC and Al-W Composite Markers. *Proceedings of the Symposium on Friction Stir Welding and Processing II, Warrendale, PA, TMS*, p.3-10.

Loxin2002, (n.d.). Retrieved June 24, 2009, from http://www.loxin2002.com/imgs/ FSW-Imagen1-Resized.jpg.

Ma, Z.Y., Mishra, R.S., & Mahoney, M.W. (2002). Superplastic deformation behaviour of friction stir processed 7075Al alloy. *Acta Materialia, 50*, 4419-4430. Retrieved December 24, 2009, from Elsevier database.

Mahoney, M.W. & Lynch, S.P. (n.d.). Friction-Stir Processing. Retrieved June 25, 2009, from http://www.darpa.mil/dso/thrusts/matdev/fsp/pdfs/fspsem_a1.pdf.

Mahoney, M.W., Rhodes, C.G., Flintoff, J.G., Spurling, R.A., & Bingel, W.H. (1998). Properties of Friction-Stir-Welded 7075 T651 Aluminum. *Metallergical and Materials transactions A, 29A*, 1955-1964. Retrieved December 27, 2009, from Springer Link database.

Mazzaferro, J. A. E., Rosendo, T. de S., Mazzaferro, C. C. P., Ramos, F. D., Tier, M. A. D., Strohaecker, T. R., & dos Santos, J. F. (2009). *Preliminary Study on the Mechanical Behavior of Friction Spot Welds*. Retrieved December 29, 2009, from http://www.scielo.br/pdf/si/v14n3/v14n3a07.pdf.

McLean, A.A., Powell, G. L. F., Brown I. H., & Linton, V.M. (2003). Friction stir welding of magnesium alloy AZ31B to aluminium alloy 5083. *Science and Technology of Welding & Joining, 8*, 462-464. Retrieved December 9, 2009, from IngentaConnect database.

McNelley, T.R., Swaminathan, S. & Su, J.Q. (2007). Recrystallization mechanisms during friction stir welding/processing of aluminum alloys. *Scripta Materialia, 58*, 349-354. Retrieved December 26, 2009, from Science Direct database.

Meran, C., & Kovan, V. (2008). Microstructures and mechanical properties of friction stir welded dissimilar copper/brass joints. *Mat.-wiss. U. werkstofftech, 39*,521-530.

Micro friction stir welding (n.d.). Retrieved June 25, 2009, from http://www.twi.co.uk/content/tfmicrofsw.html.

Mishra, R.S., & Ma, Z.Y. (2005). Friction stir welding and processing. *Materials Science and Engineering R, 50*, 1-78. Retrieved February 27, 2009, from Science Direct database.

Mishra, R. S., & Mahoney, M. W. (2007). *Friction stir welding and processing* (2ⁿᵈ ed.). Materials park, Ohio: ASM International.

Murr, L.E., Flores, R.D., Flores, O.V., McClure, J.C., Liu, G., & Brown, D. (1998). Friction-stir welding: microstructural characterization. *Materials Research Innovations, 1*, 211-223. Retrieved August 2, 2009, from SpringerLink database.

Murr, L. E., Liu, G., & McClure, J. C. (1998). A TEM study of precipitation and related microstructures in friction-stir-welded 6061 aluminium. *Journal of Materials Science, 33*, 1243-1251. Retrieved December 24, 2009, from SpringerLink database.

Nakata, K. (2005). Friction stir welding of copper and copper alloys. Welding International,19, 929-933. Retrieved July 24, 2009, from TUBTAK EKUAL.

NASA (March 2001). Friction stir welding, *Space Shuttle Technology Summary*. Retrieved June 24, 2009, from http://www.nasa.gov/centers/marshall/pdf/104835 main_friction.pdf.

NASA's ultrasonic stir welding process for handheld solid state welding (n.d.). Retrieved June 25, 2009, from http://techtran.msfc.nasa.gov/tech_ops/TOA_ Ultrastir_9web.pdf.

National center for advance manufacturing (2007). NASA facts. Retrieved December 29, 2009, from http://www.nasa.gov/centers/marshall/pdf/167063main _MSFC%20NCAM%20FS%20copy.pdf.

Orbital Friction stir weld system (n.d.). NASA. Retrieved June 25, 2009, from http://techtran.msfc.nasa.gov/Patents/(54).html.

Ouyang, J.H., & Kovacevic, R. (2001). Material Flow and Microstructure in the Friction Stir Butt Welds of the Same and Dissimilar Aluminum Alloys. *Journal of Materials Engineering and Performance, 11*, 51-63. Retrieved August 2, 2009, from SpringerLink database.

Ouyang, J. H., Yarrapareddy, E., & Kovacevic, K. (2005). Microstructural evolution in the friction stir welded 6061 aluminum alloy (T6-temper condition) to copper. *Journal of Materials Processing Technology, 172*, 110-122. Retrieved August 2, 2009, from Science Direct database.

Padmanaban, G., & Balasubramanian, V. (2008). Selection of FSW tool pin profile, shoulder diameter and material for joining AZ31B magnesium alloy − An experimental approach. *Materials and Design, 30*, 2647-2656. Retrieved June 25, 2009, from Elsevier database.

Park, H. S., Kimura, T., Murakamic,T., Naganod, Y., Nakata, K., & Ushio, M. (2003). Microstructures and mechanical properties of friction stir welds of 60% Cu–40% Zn copper alloy. *Materials Science & Engineering A, 371*, 160-169. Retrieved December 26, 2009, from Science Direct database.

Payton, L. N. (2002). *Metal cutting theory and friction stir welding tool design*. Retrieved June 24, 2009, from http://ntrs.nasa.gov/archive/nasa/casi.ntrs.nasa. gov/20030093619_2003101304.pdf.

Peel, M., Steuwer, A., Preuss, M., & Withers, P. J. (2003). Microstructure, mechanical properties and residual stresses as a function of welding speed in aluminium AA5083 friction stir welds. *Acta Materialia, 51*, 4791-4801. Retrieved February 27, 2009, from Science Direct database.

Prangnell, P.B., & Heason, C.P. (2005). Grain structure formation during friction stir welding observed by the stop action technique. *Acta Materialia, 53*, 3179-3192. Retrieved December 26, 2009, from Science Direct database.

Polt, W. (September, 2004). A little friction at Boeing. Retrieved December 2, 2009, from http://www.boeing.com/news/frontiers/archive/2004/september/i_tt.html.

Rajesh S.R., Bang, H. S., Chang, W. S., Kim, H. J., Bang, H. S., Oh, C. I., & Chu, J. S. (2007). Numerical determination of residual stress in friction stir weld using 3D-analytical model of stir zone. *Journal of Materials Processing Technology, 187-188*, 224-226. Retrieved August 2, 2009, from Science Direct database.

Reynolds, A.P. (2000). Visualisation of material flow in autogenous friction stir welds. *Science and Technology of Welding & Joining, 5*, 120-124.

Reynolds, A. P., Tang, W., Gnaupel-Herold, T., & Prasket, H. (2003). Structure, properties, and residual stress of 304L stainless steel friction stir welds. *Scripta Materialia, 48*, 1289-1294. Retrieved December 29, 2009, from Science Direct database.

Rhodes, C.G., Mahoney, M.W., Bingel, W.H., & Calabrese, M. (2003). Fine-grain evolution in friction-stir processed 7050 aluminum. Scripta Materialia, 48, 1451-1455. Retrieved June 25, 2009, from Science Direct database.

Rhodes, C. G., Mahoney, M. W., Bingel, W. H., Spurling R. A., & Bampton, C. C. (1997). Effects of friction stir welding on microstructure of 7075 aluminum. *Scripta Materialia, 36*, 69-75. Retrieved December 29, 2009, from Springer Link database.

Sato, Y. S., & Kokawa, H. (2001). Distribution of Tensile Property and Microstructure in Friction Stir Weld of 6063 Aluminum. *Metallurgical and*

Materials Transactions A, 32A, 3023-3031. Retrieved December 30, 2009, from Springer Link database.

Sato, Y. S., Kokawa, H., Enomoto, M., & Jogan, S (1999). Microstructural evolution of 6063 aluminum during friction-stir welding. *Metallurgical and Materials Transactions A, 30*, 2429-2437. Retrieved February 27, 2009, from Springer Link database.

Sato, Y. S., Kokawa, H., Ikeda, K., Enomoto, M., Jogan, S., & Hashimoto, T. (2001). Microtexture in the friction-stir weld of an aluminum alloy. *Metallurgical and Materials Transactions A, 32A*, 941-948. Retrieved December 27, 2009, from Springer Link database.

Sato, Y. S., Urata ,M., & Kokawa, H. (2001). Parameters Controlling Microstructure and Hardness during Friction-Stir Welding of Precipitation-Hardenable Aluminum Alloy 6063. *Metallurgical and Materials Transactions A, 33A*, 625-635. Retrieved December 24, 2009, from Springer Link database.

Schmidt, H.B. & Hattel, J.H. (2007). Thermal modelling of friction stir welding. *Scripta Materiala*, 58, 332-337. Retrieved June 25, 2009, from Elsevier database.

Schneider, J.A. & Nunes, Jr. A.C. (2004). Characterization of plastic flow and resulting microtextures in a friction stir weld. *Metallurgical and Materials Transactions B, 35B*, 779-783. Retrieved December 17, 2009, from Springer Link database.

Scialpi, A., De Filippis, L.A.C., & Cavaliere, P. (2006). Influence of shoulder geometry on microstructure and mechanical properties of friction stir welded 6082 aluminium alloy. *Materials & Design, 28*, 1124-1129. Retrieved August 2, 2009, from Science Direct database.

Seidel, T.U., & Reynolds, A.P. (2001). Visualization of the Material Flow in AA2195 Friction-Stir Welds using a Marker Insert Technique. *Metallurgical and Materials Transactions A, 32*, 2879-2884. Retrieved December 7, 2009, from Springer Link database.

Seidel, T.U., & Reynolds, A.P. (2002). Two-dimensional friction stir welding process model based on fluid mechanics. *Science and Technology of Welding and Joining, 8*, 175-183. Retrieved December 17, 2009, from http://web.ebscohost.com/ehost/pdf?vid=2&hid=12&sid=c6d1a871-24a2-487a-95f9-b124c1b81daa%40sessionmgr12.

Smith, I. J & Lord, D. D. R. (2007). FSW patents - a stirring story. Retrieved December 17, 2009, from http://www.twi.co.uk/content/spijssept2007.html.

Soundararajan, V. (December, 9 2006). *Thermo-mechanical and microstructural issues in joining similar and dissimilar metals by friction stir welding*. Retrieved December 7, 2009, from http://gradworks.umi.com/32/45/3245931.html.

Stewart, M. B., Adams, G. P., Nunes, A. C. Jr., & Romine, P. (1998). A combined experimental and analytical modeling approach to understanding Friction Stir Welding. *Developments in Theoretical and Applied Mechanics*, 19, 472-484.

Su, J.-Q., Nelson, T.W., Mishra, R., & Mahoney, M. (2002). Microstructural investigation of friction stir welded 7050-T651 aluminium. *Acta Materialia, 51*, 713-729. Retrieved December 24, 2009, from Science Direct database.

Thermal stir welding (n.d.). NASA. Retrieved June 25, 2009, from http://research.jsc.nasa.gov/BiennialResearchReport/PDF/Eng-19.pdf.

Thomas, W. M., & Dolby, R. E. (April 15-19 2002). *Friction Stir Welding Developments*. Retrieved June 24, 2009, from http://www.twi.co.uk/content/

spwmtapril2002.html.

Thomas, W. M., Kallee, S. W., Staines, D. G., & Oakley, P. J. (2006). Friction Stir Welding - Process variants and developments in the automotive industry. Retrieved December 29, 2009, from http://www.twi.co.uk/content/spwmtapr2006 .html.

Thomas, W. M., Nicholas, E. D., & Smith, S. D. (February 11-15, 2001). *Friction stir welding - tool developments*. Retrieved June 24, 2009, from http://www.twi.co.uk/content/spwmtfeb2001.html.

Thomas, W., Nicholas, D., Staines, D., Tubby, P. J., & Gittos, M. F. (June 17, 2004). FSW Process Variants and Mechanical Properties. Retrieved June 24, 2009, from http://www.twi.co.uk/content/spwmtjuly2004a.html.

Thomas, W. M., Staines, D. J., Watts, E. R., & Norris, I. M. (2005). The simultaneous use of two or more friction stir welding tools. Retrieved July 4, 2009, from http://www.twi.co.uk/content/spwmtjan2005.pdf.

Threadgill, P. L. (1999). Friction stir welding - state of the art. *TWI*, report-678/1999. Retrieved August 2, 2009, from http://www.twi.co.uk/content/tb678-99.html.

Ulysse, P. (2002). Three-dimensional modeling of the friction stir-welding process. *International Journal of Machine Tools & Manufacture, 42*, 1549-1557. Retrieved February 27, 2009, from Science Direct database.

Uzun, H., Donne, C. D., Argagnotto, A., Ghidini, T., & Gambaro, C., (2004). Friction stir welding of dissimilar Al 6013-T4 To X5CrNi18-10 stainless steel. *Materials & Design, 26*, 41-46. Retrieved December 9, 2009, from Science Direct database.

Watanabe, T., Takayama, H., Kimapong, K., & Hotta, N. (2003). Joining of Steel to Aluminum Alloy by Interface-Activated Adhesion Welding. *Materials Science Forum, 426-432*, 4129-4134.

Welding (n.d.). Wikipedia. Retrieved June 25, 2009, from http://en.wikipedia.org/ wiki/Welding.

William, S. W. (2001). Welding of Airframes using Friction Stir. *Air & Space Europe, 3*, 64-66. Retrieved June 25, 2009, from Science Direct database.

Xie, G.M., Ma, Z.Y., & Geng, L. (2007). Development of a fine-grained microstructure and the properties of a nugget zone in friction stir welded pure copper. *Scripta Materiala*, 57, 73-76. Retrieved June 25, 2009, from Science Direct database.

Xu, S., Deng, X., Reynolds, A.P., & Seidel, T.U. (2001). Finite element simulation of material flow in friction stir welding. *Science and Technology of Welding & Joining, 6*, 191-193.

Yeni, C. (2008). The effect of welding parameters on the microstructure and mechanical properties of friction stir welded AA7075. *Praktische Metallographie, 45*, 479-494.

Zahedul, M., Khandkar, H. & Kahn, J.A. (2001). *Journal of Material Processing and Manufacturing Science, 10*, 91-105.

Zhang, Z., & Zhang, H. W. (2008). Numerical studies on controlling of process parameters in friction stir welding. *Journal of Materials Processing Technology, 209*, 241-270. Retrieved June 25, 2009, from Elsevier database.

APPENDICES

Shear stress-strain diagrams of the each specimen are given below as MPa vs. % elongation.